Applications of Continuous Spatial Models in Multiple Antenna Signal Processing

Glenn Dickins

B.Sc.(ANU) B.Eng.(Hons) (ANU) M. Eng.(ANU) MBA (LaTrobe)

July 2007

A THESIS SUBMITTED FOR THE DEGREE OF DOCTOR OF PHILOSOPHY
OF THE AUSTRALIAN NATIONAL UNIVERSITY

THE AUSTRALIAN NATIONAL UNIVERSITY

Department of Information Engineering
Research School of Information Sciences and Engineering
The Australian National University

Declaration

The contents of this thesis are the results of original research and have not been submitted for a higher degree to any other university or institution.

Much of the work in this thesis has been published or submitted for publication as journal papers or conference proceedings. These papers are:

- G. Dickins and L. W. Hanlen, "Fast calculation of singular values for MIMO wireless systems," in *Proceedings of the 5th Australian Communications Theory Workshop*, (Newcastle, Australia), pp. 185–190, 2004.
- G. Dickins and L. W. Hanlen, "On finite dimensional approximation in MIMO," in *Proceedings of the 11th Asia-Pacific Conference on Communications APCC2005*, (Perth, Australia), pp. 710–714, 2005.
- M. I. Y. Williams, G. Dickins, R. A. Kennedy and T. D. Abhayapala, "Spatial Limits on the Performance of Direction of Arrival Estimation", in *Proceedings of the 6th Australian Communications Theory Workshop*, (Brisbane, Australia), pp. 189–194, 2005.
- G. Dickins, M. I. Y. Williams and L. W. Hanlen, "On the dimensionality of spatial fields with restricted angle of arrival," in *Proceedings of the IEEE International Symposium on Information Theory*, (Adelaide, Australia), pp. 1033–1037, 2005.
- M. I. Y. Williams, G. Dickins, R. A. Kennedy, T. S. Pollock and T. D. Abhayapala, "A Novel Scheme for Spatial Extrapolation of Multipath," in *Proceedings of the 2005 Asia-Pacific Conference on Communications*, (Perth, Australia), pp. 784–787, 2005.
- G. Dickins, T. Betlehem and L. W. Hanlen, "A Stochastic MIMO Model Utilising Spatial Dimensionality and Modes," in *Proceedings of the IEEE Vehicular Technology Conference*, (Melbourne, Australia), 2006.

- G. Dickins and R. A. Kennedy, “Angular Domain Representation of a Random Multipath Field,” Submitted to *EURASIP Journal on Wireless Communications and Networking*, 2006.
- G. Dickins, M. I. Y. Williams and R. A. Kennedy, “Spatial limits to direction of arrival estimation,” *Submitted to IEEE Signal Processing Letters*, 2006.

The research represented in this thesis has been performed jointly with Professor Rodney A. Kennedy, Dr. Leif W. Hanlen, Dr. Terence Betlehem and M. I. Y. Williams. The substantial majority of this work is my own.

Glenn Dickins
The Australian National University
July 2007

Acknowledgments

During the time of my studies and research under the supervision of Professor Rodney Kennedy, I have been able explore a diverse range of theoretical and philosophical considerations related to spatial information theory. With a thirst for knowledge and understanding, I have been able to seek out and receive expert tuition whilst sharing many discussions and musings with experts in the field. I give thanks to all those who have gone before me and continue to clarify and distill the essence of research in this area. It is only now that I have moved into a different area of research that I fully realise the value and depth of the expertise I was exposed to in this field.

The pursuit of a PhD can be a long, arduous and largely solitary process, especially when it comes to writing the thesis. In my experience, there were two key factors which kept me going. The first was the time expended during the process of research and the desire to complete the degree. The second and by far the most important was the support, compassion, understanding, faith and gentle prodding of those around me towards submission.

First and foremost I would like to thank my wife Karen, without whom I would have been lost in despair more times than I care to admit. Karen, you are my one true companion through life and I thank you for always being there to help me maintain perspective and find the special moments in life. To my friends and family and parents who have stood by me through the highs and lows of the process, I thank you for being there and for believing in me. I am especially grateful for the time and encouragement given to me by Peter Fyfe, James Galloway and Jodi Steel. Thank you for providing the perspective to see beyond the doctoral process and not take it too seriously.

To my research colleagues at the Australian National University, I am grateful for the opportunity to have worked with you and thank you for your input into this work. In particular I would like to thank Michael Williams for helping to shape many of the ideas in this thesis, Tony Pollock for his support and early research directions in this area and Dino Miniutti for the many lunch room and research conversations over the last four years. I would also like to give thanks to Terence Betlehem, Parastoo Sadeghi, Thushara Abhayapala and Tharaka

Lamahewa for their contributions and collaboration. I would also like to note and give thanks for the enjoyable time at the University of Uppsala and the chance to work with Professors Anders Ahlén and Mikael Sternad.

Finally to my supervisors. I would like to give special thanks to Professor Rodney Kennedy for his wise and flexible supervision which fostered the exploration of far greater subject matter than is contained in this thesis. I would like to also thank Dr. Leif Hanlen for his supervision and contribution to the development of this thesis. I appreciate the assistance from my supervisors to help identify the key research results, develop the thesis structure and review the thesis content.

I have been privileged to have the unwavering support of the people listed above and many others without whom I would have lacked the perseverance to complete this task. I thank you for helping to draw together a selection of my work from the last four years and present it as this thesis. To those who have known me during this time, I acknowledge your friendship and submit this thesis in thanks for all of your encouragement.

Abstract

This thesis covers the investigation and application of continuous spatial models for multiple antenna signal processing. The use of antenna arrays for advanced sensing and communications systems has been facilitated by the rapid increase in the capabilities of digital signal processing systems. The wireless communications channel will vary across space as different signal paths from the same source combine and interfere. This creates a level of spatial diversity that can be exploited to improve the robustness and overall capacity of the wireless channel. Conventional approaches to using spatial diversity have centered on smart, adaptive antennas and spatial beam forming. Recently, the more general theory of multiple input, multiple output (MIMO) systems has been developed to utilise the independent spatial communication modes offered in a scattering environment.

Underlying any multiple antenna system is the basic physics of electromagnetic wave propagation. Whilst a MIMO system may present a set of discrete inputs and outputs, each antenna element must interact with the underlying continuous spatial field. Since an electromagnetic disturbance will propagate through space, the field at different positions in the space will be interrelated. In this way, each position in the field cannot assume an arbitrary independent value and the nature of wave propagation places a constraint on the allowable complexity of a wave-field over space. To take advantage of this underlying physical constraint, it is necessary to have a model that incorporates the continuous nature of the spatial wave-field.

This thesis investigates continuous spatial models for the wave-field. The wave equation constraint is introduced by considering a natural basis expansion for the space of physically valid wave-fields. This approach demonstrates that a wave-field over a finite spatial region has an effective finite dimensionality. The optimal basis for representing such a field is dependent on the shape of the region of interest and the angular power distribution of the incident field. By applying the continuous spatial model to the problem of direction of arrival estimation, it is shown that the spatial region occupied by the receiver places a fundamental limit on the number and accuracy with which sources can be resolved. Continuous spatial models also provide a parsimonious representation for modelling the spatial communications channel independent of specific antenna array configurations. The continuous spatial model is also applied to consider limits to the problem of wireless source direction and range localisation.

Contents

List of Figures

List of Tables

Notation, Symbols and Acronyms

Symbol	Definition
a_p	source amplitude
$\boldsymbol{a}(\theta)$	array response vector for direction θ
$\mathbf{A}$ $\mathbf{A}(\boldsymbol{\theta})$	array response matrix
$\mathbb{B}_R^2$	two-dimensional ball (disc) of radius R
$\mathbb{B}_R^3$	three-dimensional ball (sphere) of radius R
C_m	array response scaling constant for mode m
$ds(\widehat{\boldsymbol{\theta}})$	surface area element of $\mathbb{S}^2$
D	essential dimensionality
$\mathbf{D}(\boldsymbol{\theta})$	derivative of array response matrix
$e^{\cdots}$	exponent function
$E\{\cdots\}$	expectation of a random process
$\mathcal{F}$	space of far-field angular distributions
$g(\widehat{\boldsymbol{\theta}})$ $g(\theta)$	angular domain representation function
$g_n(\widehat{\boldsymbol{\theta}})$ $g_n(\theta)$	angular domain basis function
$g_N(\widehat{\boldsymbol{\theta}})$ $g_N(\theta)$	truncated finite dimensional angular domain representation
$\mathbf{H}$	MIMO channel matrix
$\mathbf{H}_S$	modal channel matrix
$H_n(\cdot)$	Hankel function of order n
$\mathbf{I}$	identity matrix
$j = \sqrt{-1}$	imaginary number
$j_n(\cdot)$	spherical Bessel function of order n
$J_n(\cdot)$	Bessel function of order n
$\mathbf{J}_R$	receiver modal configuration matrix
$\mathbf{J}_T$	transmitter modal configuration matrix
$k = 2\pi/\lambda$	wave number
$\log(\cdot)$	logarithm

Symbol	**Definition**
m	mode or other integer index
M	maximum mode or truncation order
M_R	mode truncation for receiver region
M_T	mode truncation for transmitter region
n	time sample or other integer index
N	number of time samples or max integer index
N_R	number of receive antennas
N_T	number of transmit antennas
p	source number integer index
P	number of sources
$P(\widehat{\boldsymbol{\theta}})$	angular power spectrum
q	sensor number integer index
Q	number of sensors
r	radius
R	maximum radius of region
$\mathbf{R}$	covariance matrix
$\mathbb{R}$	real numbers
$\mathbb{R}^2$	two-dimensional space
$\mathbb{R}^3$	three-dimensional space
$\mathrm{sinc}(\cdot)$	sinc function $= \sin(z)/z$
$s_p(n)$	source signal sample
$\boldsymbol{s}(n)$	vector of source signal samples
S	minimum radius of sources
$\mathbb{S}^1$	unit sphere in $\mathbb{R}^2$, equivalent to $[0, 2\pi]$
$\mathbb{S}^2$	unit sphere in $\mathbb{R}^3$
$\mathcal{S}$	space of spatial fields
t	continuous time
T	maximum time
$u(\boldsymbol{x})$	spatial field
$u(\boldsymbol{x}, n)$	spatial field at time sample n
$\mathcal{U}$	general functional space
$w_q(n)$	sensor noise sample
$\mathbf{W}$	modal coupling weight matrix
$\boldsymbol{w}(n)$	sensor noise vector
$\boldsymbol{x}$ $\boldsymbol{x}'$	position vector

Symbol	Definition
$y \;\; y_q$	output signal
$\boldsymbol{y} \;\; \boldsymbol{y}(n)$	vector of output signals
Y_n	Neumann function of order n
z	arbitrary argument
$z_m(n)$	modal output signal
$\boldsymbol{z}(n)$	vector of modal output signals
α_n	coefficient of expansion
β_n	basis function
$\Gamma(\cdot)$	Gamma function
$\delta(\cdot)$	Dirac delta function
δ_{mn}	Kronecker delta function
ε	error or small perturbation
σ^2	noise variance
λ	wavelength
λ_n	eigenvalue
Λ	spatial region of interest
Ω	range of angular domain $P(\widehat{\boldsymbol{\theta}}) \neq 0$
$\rho(\boldsymbol{x}, \boldsymbol{y})$	spatial correlation function
θ	angle in $[0, 2\pi]$
$\theta_{\boldsymbol{x}}$	polar co-ordinate angle for point $\boldsymbol{x}$
θ_p	direction of source p
$\widehat{\boldsymbol{\theta}}$	unit vector on $\mathbb{S}_2$
$\widehat{\boldsymbol{\theta}}_{\boldsymbol{x}}$	unit vector in direction of point $\boldsymbol{x}$
ϕ	angle in $[0, 2\pi]$
$\widehat{\boldsymbol{\phi}}$	unit vector on $\mathbb{S}_2$
$\triangle$	Laplacian operator
$\|\cdot\|_{\mathcal{U}}$	norm of element in indicated space
$\|\cdot\|$	absolute value of argument
$\langle \cdot, \cdot \rangle_{\mathcal{U}}$	inner product of elements in indicated space
$[a, b] \;\; (a, b)$	closed / open interval from a to b
$\odot$	Schur-Hadamard elementwise matrix product
$\otimes$	Kronecker matrix product
$.^T$	transpose of matrix or vector
$.^H$	Hermetian (conjugate) transpose of matrix
$.^{-1}$	matrix inverse
$\overrightarrow{\cdot}$	vectorise operation – stack matrix columns

Acronym	Meaning
APS	Angular Power Spectrum
AWGN	Additive White Gaussian Noise
BLAST	Bell Labs Layered Space Time communications system
CRB	Cramér-Rao Bound for variance of parameter estimation
DOA	Direction of Arrival
ESPRIT	Estimation of Signal Parameters via Rotational Invariance Techniques
MIMO	Multiple-Input, Multiple-Output communications system
MMSE	Minimum Mean Squared Error
MUSIC	Multiple Signal Classification algorithm
RMS	Root Mean Squared average
SNR	Signal to Noise Ratio
UCA	Uniform Circular Array
ULA	Uniform Linear Array
WSSUS	Wide Sense Stationary Uncorrelated Scatter statistical model

Chapter 1

Introduction

Any sufficiently advanced technology is indistinguishable from magic.
Arthur C. Clarke, 1961.

1.1 History and Background

For most of history, the ability of people to communicate without any physical connection was nothing but a magical fantasy. In 1865, James Clerk Maxwell published a seminal work showing that "*an electromagnetic disturbance in the form of waves*" could propagate through space [1]. This inspired work by Hertz, Marconi and Tesla that lead to the demonstration of wireless communication over significant distances at the dawn of the twentieth century.

The concept of the mobile telephone emerged in 1947, with commercial systems becoming available in the early 1980s and rapid consumer uptake in the 1990s [2]. Now mobile phones are ubiquitous and an accepted part of our culture. The demand for wireless communications continues to increase, driven by the high data rate connectivity requirements of mobile computing and multimedia devices.

A wireless device must be designed to meet the regulatory emission and bandwidth constraints whilst also maximising battery life through low power usage. Such constraints motivate the search for ways to improve the efficiency of wireless communications systems – to send more with less. Understanding the wireless communications channel and how to fully and efficiently exploit it is an important area of research and development.

In 1948, Claude Shannon [3] introduced a mathematical theory for understanding communications and the field of Information Theory was born. Among other things, this work

established the notion of capacity for a continuous communications channel in the presence of noise. For a channel with additive white Gaussian noise, the capacity is related to the logarithm of the signal to noise ratio η. For a channel of bandwidth B, the capacity is given by

$$C = B \log(1 + \eta) \tag{1.1}$$

in bits per second using a logarithm of base 2. This represents an upper bound on the information that can be passed through the channel without error and is known as the "Shannon Limit".

When multiple transmitters use the same frequency spectrum, the signal detected by a receiver will be a combination of all the transmissions. For this reason, conventional systems were developed with each independent broadcaster occupying a unique spectral band or spreading code[1] within the range of radio coverage. Cellular systems were designed to achieve some level of spectral reuse over large distances. With this approach, the Shannon Limit implies that the only way to increase capacity is to increase the signal to noise ratio, or increase the signal bandwidth. The noise floor is not easily reduced and increasing the transmitted power results only in a logarithmic growth in capacity. Increasing the spectrum usage is generally not possible due to practical or regulatory constrains. For much of the twentieth century, this was thought to fundamentally limit the capacity of the wireless communication channel.

For mobile wireless communications, the variation of the channel characteristics over time and space presents many challenges [4]. There has been much research into ways of mitigating or dealing with the effects of the fading wireless channel. The variation of the wireless channel over space is known as spatial diversity Recently there has been a significant shift in the research community toward the idea of spatial diversity as an advantage rather than a problem for wireless communications. The basic principle centres around taking advantage of this spatial diversity in the communications channel by using multiple receiver and transmitter antennas.

Early work by Winters [5] hinted at the possibility of sending multiple streams of data simultaneously using multiple antennas. Further research cemented the theoretical results [6] and practical architectures for achieving them [7]. Experiments at Bell Labs demonstrated these techniques in practice [8, 9], creating great excitement by effectively shattering the single channel Shannon Limit for communications spectral efficiency. The theory and practice

[1] Spread spectrum systems or code division multiple access systems utilise different spreading codes to create signal diversity over the same spectrum.

suggested a capacity limit of the wireless channel that would increase linearly with the number of antenna elements used. These events spawned the area of research and development known as MIMO (multiple input, multiple output) communications.

MIMO is now becoming accepted in practice with the recent IEEE standards 802.11n and 802.16e both providing for higher data rates using spatial multiplexing. Despite the extensive research and practical implementations of MIMO systems, there are some important questions that do not yet have satisfactory answers. The development of MIMO communications theory, reviewed in the following section, stems from strong mathematical results for a general system with multiple inputs and outputs. Whilst the mathematical results are well established, there remains open questions regarding the applicability of such results to practical systems of multiple antennas. A critique of much of the research in this area is that the assumptions follow mathematical convenience rather than arising from a study of the physical MIMO communications system.

The underlying physical process responsible for wireless communications is the propagation of electromagnetic waves. A suitable model of this must be able to represent the associated physical value of the electric and magnetic fields continuously across a region of space. However, by construction, the central ideas in MIMO theory rest on the assumption that there is only a discrete set of input and output signals. The work of this thesis seeks to develop the ideas central to multiple antenna signal processing from the underlying perspective of a continuous spatial field. The development of the continuous spatial models to represent a wave-field is proposed as a way forward to improve the theoretical understanding and development of signal processing algorithms.

The use of a continuous spatial model permits the constraints inherent in electromagnetic radiation to be implicitly embodied in the signal processing frameworks developed. Research in this area will help to illuminate the physical processes and fundamental limitations critical to the performance of MIMO communications systems. The development of a continuous spatial framework will facilitate the effective representation, detection and signal processing for the physical electromagnetic fields that carry information. The goal is to extend the theory of MIMO communications systems beyond that of a discrete set of inputs and outputs, and to elegantly incorporate relevant aspects of spatial wave propagation.

This thesis develops a framework for continuous spatial models and considers their application to several problems in multiple antenna signal processing. The work will consider optimal finite dimensional approximations, intrinsic limits and efficient statistical signal models for the continuous spatial field associated with wireless communications. In covering a fairly broad range of areas, the results vary in depth from observations and conjectures through to

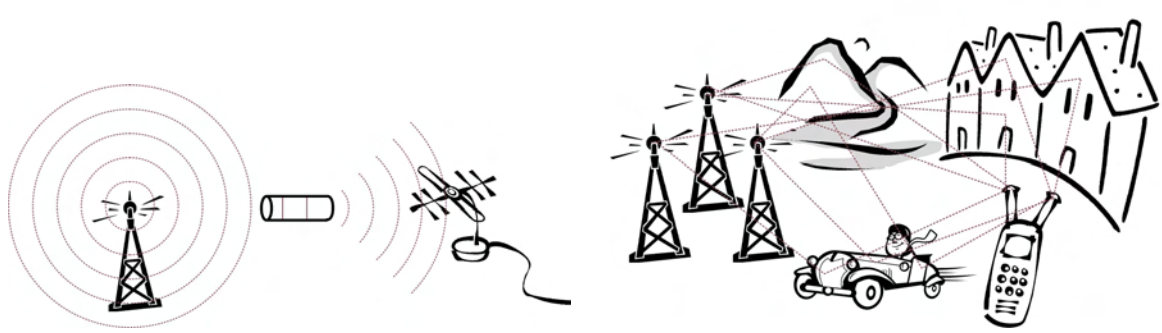

(a) Conventional view of wireless communications. Space is filled by a broadcast as if it were a single dimensional pipe for information.

(b) MIMO wireless communications. Different spatial paths create spatial diversity at receiver and transmitter and allow re-use of the spectrum.

Figure 1.1: Conceptual comparison of conventional and MIMO systems. To the extent that each received signal is a linearly independent combination of the transmitted signals, it is possible to exploit the channel as if it were multiple independent communications channels. Spectral reuse is facilitated by the spatial diversity of the transmitter and receiver antennas, along with the multiple propagation paths introduced by the scattering environment.

well developed frameworks, theorems and proofs. It provides a contribution to communications theory to better reflect the medium over which the signal is being transmitted – in this case the spatial dimension.

1.2 Multiple Antenna Communications

The fundamental premise of multiple antenna (MIMO) systems is that the physical environment in which the wireless signal is transmitted provides a degree of diversity through the existence of independent signal paths. With such spatial diversity, and through appropriate signal processing and detection, it is possible to achieve the transmission of multiple symbols using the same time and spectrum resource within a single wireless communications cell. To the extent that the received signal combinations are linearly independent, the channel can be utilised as if there were multiple independent channels. A conceptual comparison between the conventional view, and that adopted in MIMO systems, is shown in Figure 1.1.

1.2.1 Multiple Antenna Channel Framework

This section presents the conventional framework for modelling and representation of the MIMO communications channel Consider a system with n_T transmitter antennas and n_R

receiver antennas. We define $\boldsymbol{s}(t) = [s_1(t) \cdots s_{n_T}(t)]^T$ as the vector of signals transmitted at time t. Assuming a linear system, the received signal $\boldsymbol{y}(t) = [y_1(t) \cdots y_{n_R}(t)]^T$ is constructed by the convolution of the input signal with a set of channel impulse responses,

$$y_m(t) = \sum_{n=1}^{n_T} \int_{-\infty}^{\infty} h_{mn}(t,\tau) s(t-\tau) d\tau + w_m(t) \quad m = 1, \ldots, n_R \tag{1.2}$$

$$\boldsymbol{y}(t) = \int_{-\infty}^{\infty} \mathbf{H}(t,\tau) \boldsymbol{s}(t-\tau) d\tau + \boldsymbol{w}(t), \tag{1.3}$$

where $\mathbf{H}$ is a matrix of channel impulse responses $h_{mn}(t,\tau)$ representing the contribution at time t of the signal at receive element n from transmit element m at time $t-\tau$. The vector $\boldsymbol{w}(t) = [w_1(t) \cdots w_{n_R}(t)]^T$ represents an additive noise process.

Depending on the signalling bandwidth, we need only consider samples of the baseband signals at an appropriate interval, T, such that $\boldsymbol{y}[n] = \boldsymbol{y}(nT)$. The other signal vectors $\boldsymbol{s}[n] = \boldsymbol{s}(nT)$ and $\boldsymbol{w}[n] = \boldsymbol{w}(nT)$ and sampled channel matrix $\mathbf{H}[n,k] = \mathbf{H}(nT, kT)$. Assuming the channel is causal, we obtain a discrete time representation of the channel

$$\boldsymbol{y}[n] = \sum_{k=0}^{\infty} \mathbf{H}[n,k] \boldsymbol{s}[n-k] + \boldsymbol{w}[n]. \tag{1.4}$$

In the case of frequency flat fading, or where appropriate equalisation has been performed to eliminate inter-symbol interference, we can simplify the model to consider the transmission of a single symbol,

$$\boldsymbol{y} = \mathbf{H}\boldsymbol{s} + \boldsymbol{w}, \tag{1.5}$$

where $\boldsymbol{s}$ is the transmitted symbol on the n_T antenna, $\boldsymbol{y}$ is the received symbol on the n_R antenna, $\mathbf{H}$ is the instantaneous $n_R \times n_T$ channel transfer matrix and $\boldsymbol{w}$ is the noise vector. This equation represents the effect of each "channel use" and is the general signal framework adopted in works investigating the multiple antenna communication link such as [10].

For a given channel realisation $\mathbf{H}$ we can calculate the theoretical channel capacity by considering the number and strength of independent single dimensional channels supported by $\mathbf{H}$. This is dependent on the rank and the eigenvalues of $\mathbf{H}$ with a value related to the logarithmic determinant of the system matrix [11]. The capacity will be

$$C = B \log \det \left[\mathbf{I}_{n_R} + \frac{\eta}{n_T} \mathbf{H}\mathbf{H}^H \right] \tag{1.6}$$

bits per second for a base 2 logarithm, where $\mathbf{I}_{n_R}$ is the $n_R \times n_R$ identity matrix, and $\mathbf{H}^H$ is the Hermitian or complex transpose of $\mathbf{H}$. The signal to noise ratio η is interpreted in the

context of the components of $\mathbf{H}$ having unity expected power. Provided there is sufficient transmitter diversity, the capacity can scale linearly with the number of antenna n_R. This can be compared to the the single antenna case, (1.1), which would only allow a logarithmic increase in capacity as the addition of receiver antennas increased the effective signal to noise ratio.

1.2.2 Statistical Model of Channel Matrix

At typical radio frequencies, the presence of multiple signal paths and their subtle time variations will cause random fluctuations in the individual antenna coupling parameters of $\mathbf{H}$ [4]. For such situations, it is expected that the value and statistics of the channel capacity will be of interest in a system design context.

Significant interest in the use of multiple antennas to achieve higher spectral efficiency in the wireless channel commenced around 1995. The mathematical results of Telatar and Foschini were key to demonstrating the potential for capacity gains when the channel $\mathbf{H}$ was considered as a statistical process [6, 12–14]. Some practical demonstrations soon followed that demonstrated such potential in laboratory environments [7–9]. These activities catalysed an explosion of research investigating the potential and realisable capacities for various classes of random matrix $\mathbf{H}$. With a relatively simple channel model, (1.5), and armed with decades of statistical, matrix, and information theory many capacity results were presented as being informative of the practical MIMO communications problem [15].

Prior to the increased interest in MIMO, the statistics of a single antenna wireless channel were well studied. However, the statistics of the channel ensemble between two antenna arrays was a challenging and open problem. The application of a complete physical and electromagnetic propagation model had been considered for somewhat similar problems in optics [16] and introduced to communications [17]. In the case of a complex scattering environment such an approach becomes unwieldy and is best suited to specific geometrical investigations [18].

The characteristic behaviour and statistics of the channel model $\mathbf{H}$ depends on an array of physical properties and environmental characteristics: the antenna properties, radiation patterns, array geometry, orientation, scattering environment, movement and the overriding laws of electromagnetic radiation. As depicted in Figure 1.2, the matrix equation conceals the complexity and often abstracts the spatial aspects of the multiple antenna channel.

At the outset of the MIMO developments, it was realised that as antenna separation decreased, signals would become correlated, impacting system performance [19]. This

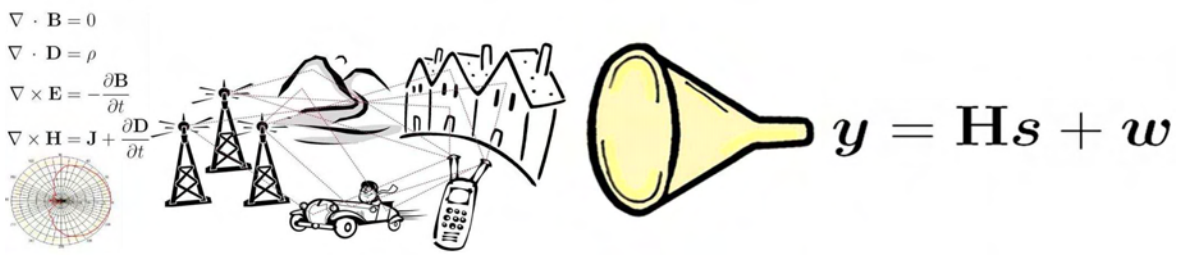

Figure 1.2: The compact form of the MIMO matrix equation. The discrete MIMO matrix equation represents the effects of a broad range of complex physical properties and processes.

prompted work to introduce additional models for correlation between the channel components of $\mathbf{H}$ [19–25]. There has also been significant interest in conducting measurement campaigns to fit empirical distributions to observed data [26–29]. Other efforts have sought to adopt convenient statistical distributions for analytic purposes [30–32]. A further review of MIMO channel models is presented in Section 1.2.5.

Such models provide a numerical framework to characterise antenna correlation, without reference to the physical processes that cause it [25, 33–36]. Since these models are not directly related to the physical propagation, they can be misleading. For example, the framework permits degenerate "keyhole" channels [22, 37, 38], however in practice these are rare [39] and even difficult to reproduce in artificial situations [40]. The development of MIMO theory around statistical channel distributions became an independent research field, and arguably some results were of little practical significance.

1.2.3 Introducing Space into MIMO Channel Models

Around 2003, there was movement toward incorporating the spatial constraint of the MIMO arrays into the channel modelling. Some results suggested a finite dimensionality of a multipath field over a region of space [41–43] and discuss the impact of this on channel modelling [44]. It was recognised that discrete statistical channel models ignored the fundamental aspects of wave propagation inherent in the problem [39, 45, 46].

The performance of a MIMO system will be directly related to the degree of spatial diversity available. However, for much of the MIMO literature, the spatial diversity and correlation of antenna channels was assumed or approximated. Ironically, to address this, the concept of "space" needed to be introduced in to the MIMO framework [47, 48].

This work is a continuation of the development of a spatial theory intended to model, analyse and design optimal signal processing for multiple antenna systems. Rather than being

specific to a particular antenna configuration, the use of a continuous spatial model moves closer to understanding the underlying dimensionality and appropriate representation of the spatial field.

1.2.4 Suggested MIMO Review Articles

Since the explosion in the level of research interest in MIMO systems, there has been numerous publications on the subject. This section presents briefly some of the more useful review and summary articles available.

One particular work [49] developed a wider interest in the field early on. A review by Gesbert et al. addresses theoretical and practical aspects of MIMO systems [50] with explanations and useful interpretations. Paulraj et al. present an overview of MIMO as the solution to meet the needs of high data rate links [51].

Special issues of the Journal of Wireless Communications and Mobile Computing [52, 53], EURASIP Journal on Applied Signal Processing [54], IEEE Transactions on Signal Processing [55] and IEEE Journal on Selected areas in Communications [56, 57] contain a collection of relevant articles. Some key books on the subject have been compiled by Durgin [58], Jankiraman [59], Paulraj et al. [60], Gershman and Sidiropoulos [61] and Tsoulos [62].

1.2.5 Review of MIMO Channel Models

A fairly central theme of this work is the representation and modelling of the MIMO channel using the continuous spatial fields. Whilst there is some work in this area, the majority of MIMO channel models present a statistical model for the the discrete channel matrix specific to a given antenna configuration. This section presents a review of the literature in this area.

The purpose of a channel model is to provide a way of capturing and simulating the behaviour of the channel matrix $\mathbf{H}$. A good channel model should allow for the development and testing of systems to work in real practical situations. The quality and utility of a model depends on the intended application of the model and how well the model captures the parameters of the channel critical to the application [63]. A comprehensive review of the various MIMO channel models developed can be found in the work by Yu and Ottersen [64] and Jensen and Wallace [65].

The models that have been developed can be grouped into two main categories. Statistical or non-physical models directly model the statistics of the entries in the channel matrix $\mathbf{H}$

with statistics based on experimental measurements or convenient probability distributions [22, 35, 36]. Given a system with n_T transmitters and n_R receivers, characterising the correlations between the elements of $\mathbf{H}$ requires $(n_T n_R)^2$ parameters. Various models reduce this by assuming certain structures of the correlations. For example, the Kronecker model [23] assumes the overall correlation is separable as a product of receive side and transmitter side correlation. The virtual channel model [66] assumes a Fourier structure and the Weichselberger model [67] assumes a Kronecker style eigenbasis. Simple statistical models, such as the Kronecker, can provide satisfactory results for small numbers of antenna elements but will fail with more complex configurations [27, 68, 69]. Statistical models are easy to implement and can provide adequate modelling for some purposes. The effects of the propagation channel and the transmit and receive arrays are coupled together in the resultant model.

Geometrical or physical models characterise the spatial propagation aspects of the channel in terms of the directions of arrival and directions of departure [70]. Developed from early work on the nature of the time response of radio channels [71], the models incorporate the idea of distributed scatterers and clusters of scatterers interacting with the wireless signal. Models for the distribution and effect of scatterers can be based on geometric models, such as the one-ring and two-ring and other arrangements [72]. Alternately, the angular characteristics can be modelled as statistical processes [73]. Distributions such as the Laplacian [74] and Von-Mises [31] are used to characterise the angular spread of a scattering cluster. Such models can be fitted to experimental data by identifying scattering paths in array measurement data. This is typically achieved using subspace techniques for estimating direction of arrival.

For specific physical scenarios, it is possible to use point wise ray tracing methods to model the channel [75]. With sufficient model detail, these have been shown to provide a good match to the physical measurements [76]. The experimental validation of channel models is an important area of research [29]. Complex models have been developed that incorporate many of the attributes discussed above and play a role in the development of future wireless standards [77].

An alternative to direct modelling of $\mathbf{H}$ or an angular representation is provided by considering a modal spatial decomposition of the channel [41, 42, 44, 48, 78–81]. The coupling between the receive and transmit volume is described in terms of modes related to the essential dimensionality and degrees of freedom of the spatial field. It is these classes of models that are further developed and investigated in Chapter 2, Chapter 4 and Chapter 6. The estimation of direction of arrival is also an important topic for the development and validation of MIMO channel models. This is investigated in Chapter 5.

1.3 Motivation and Scope of Thesis

There is an extensive amount of existing research on antennas and electromagnetic propagation. The direct application of such results to the field of multiple antenna signal processing can create an onerous and often unnecessary level of complexity. The statistical models for MIMO analysis can provide an over simplification and be guided by mathematical elegance rather than practical correspondence. The motivation of this work is to develop the idea of continuous spatial model in a signal processing context in order to introduce a more appropriate level of complexity and physical correspondence to the MIMO problem. It is anticipated that this will be advantageous in the pursuit of understanding fundamental limits and achieving optimal system design.

In many practical applications, system design will be based on approximation or heuristics. While conventional designs may adopt a half wavelength antenna spacing, it is important to understand if this is efficient and optimal, or if there is room for improvement. Furthermore, as the antenna array is extended in three-dimensional space, a single antenna cannot completely characterise the array geometry.

The motivation of this thesis is to understand spatial fields and multipath diversity to better inform system design, antenna geometries and signal processing used for multiple antenna communications systems.

Pioneering work in this area [41, 42, 44, 47, 78, 79, 82–84] has considered the limits of dimensionality of a multipath field. The electromagnetic wave equation imposes a structure and constraint on the permissable wave-fields over a region of space. This work further develops the proposal of continuous spatial models to naturally incorporate this constraint into the problem formulation. The scope of the topics vary across optimal representations, parameter estimation and statistical modelling in the area of multiple antenna systems. Since the work is largely exploratory, the contributions of the thesis vary in strength from reviews and observations through to detailed frameworks and theorems.

The structure and main ideas of the thesis are arranged as follows:-

- The remainder of this chapter provides some further background material related to electromagnetic fields and multiple antenna communications.
- Chapter 2 provides a review of the key results regarding the spatial dimensionality and the impact it has on the multiple antenna systems. Some developments and conjectures are provided towards improving the bounds and limits in this area.

- Chapter 3 considers the specific problem of modelling a field with restricted direction of arrival. Formal proof of the relationship between dimensionality and angular spread is provided along with a constructive approximation for the optimal representation.

- Chapter 4 contains a significant technical contribution of the thesis in the formal development of the framework required to determine the optimal representation of a spatial field. It is shown clearly how the optimal basis depends on the angular power spectrum and the shape of the region of interest. Several examples are solved and investigated numerically.

- Chapter 5 presents a detailed derivation of a fundamental bound for system performance of direction of arrival estimation. This is a contribution in that the bound is independent of the specific sensor geometry and has been derived for multiple sources. It is shown that the number of sources that can be resolved is directly related to the essential dimensionality of the spatial field independent of the algorithm employed.

- Chapter 6 presents a new continuous space statistical channel model. This model is validated against experimental and simulated data and is shown to provide a more efficient representation of experimental data than existing models. By using the spatial model, this approach facilitates the prediction and optimisation of alternate antenna array geometries from measurement data.

- Chapter 7 presents an exploratory investigation of the implications of the continuous spatial model in the resolution of source location. Some new approaches are developed leading to some useful bounds for the problem defined.

- Chapter 8 offers concluding remarks and provides a set of open areas of research and conjectures that have been identified through this research work.

Understanding the wave equation and how it constrains the signal subspace and thus performance of an antenna array is not a simple matter. It bears a strong resemblance to the issues of sampling and understanding the dimensionality of bandlimited functions [85], an issue which was prevalent for several decades in the middle of last century. Similar developments in relation to multiple antennas and spatial fields will lead to a body of research to guide engineering developments in the area.

1.4 Space, Waves and Intrinsic Limits

Electromagnetic wireless communication requires the creation and detection of an electromagnetic field. By controlling a current distribution across a region of space, the transmitter is able to generate or excite the field. The strength and direction of the electromagnetic field is a physical quantity that varies over space and time, extending beyond the region occupied by the transmitter. The continuous electromagnetic field, defined over the constrained region of the receiver, carries information about the transmitted signal. The interaction of the electromagnetic field with antenna elements at the receiver will generate current and voltage signals.

Complete electromagnetic modelling of a MIMO system is generally prohibitive due to the scope of the propagation environment. A review by Jensen and Wallace [86] lists the physical parameters that are relevant to system performance:

- antenna sensitivity and impedance matching,
- array size and configuration,
- element radiation patterns,
- polarisation,
- mutual coupling, and
- multipath propagation.

Modelling such parameters will increase the accuracy and applicability of the MIMO channel representation. This will provide a benefit when the increase in complexity is justified by a valuable improvement to matching and prediction of the model.

The first three of these items relate to the configuration of the sensor array. In practice, arrays should be designed to maximise their ability to transmit or receive information from the region of the electromagnetic field with which they interact. Jensen and Wallace suggest that the "average capacity is relatively insensitive to array configuration" [86], which leads to the concept of considering the intrinsic capacity of a region of space.

This section reviews literature covering the aspects of electromagnetic radiation relevant to MIMO systems. Some recent ideas and results relating to the essential dimensionality of a spatial field and resultant intrinsic limits are also reviewed. These works represent a foundation and motivation for much of the work in this thesis regarding the study of continuous spatial models for multiple antenna communication and signal processing.

1.4.1 Wave Equation

The physics and associated mathematics of wave propagation and wave motion is an area that has received a significant amount of attention [87, 88] and is accepted as a general engineering principle [89]. A similar theory can be applied across a wide range of physical waves, such as acoustic waves and electromagnetic radiation [90]. A central relationship is known as the reduced wave equation, or Helmholtz equation [91],

$$\triangle u(\boldsymbol{x}) + k^2 u(\boldsymbol{x}) = 0, \tag{1.7}$$

where $u(\boldsymbol{x})$ is a scalar valued field representing some spatial property of the medium, $k = 2\pi/\lambda$ is the wave-number related to the wavelength, λ, of waves in that medium and $\triangle$ is the Laplacian operator equal to the sum of second order partial derivatives of $u(\boldsymbol{x})$ on a unitary orthogonal co-ordinate system. For three-dimensional cartesian coordinates

$$\triangle = \frac{\partial^2}{\partial x^2} + \frac{\partial^2}{\partial y^2} + \frac{\partial^2}{\partial z^2}. \tag{1.8}$$

The second order differential equation (1.7) characterises the spatial distribution of a narrow-band wave-field across a region free of any sources. The time varying physical parameter is obtained from considering

$$U(\boldsymbol{x}, t) = \mathrm{Re}\left\{u(\boldsymbol{x})e^{-j\omega t}\right\} \tag{1.9}$$

where $\mathrm{Re}\{\cdot\}$ is the real component, $j = \sqrt{-1}$ and $\omega = 2\pi f$ is the angular frequency of the waves.

This equation is widely studied in acoustics where it is derived from a linearisation of Eulers's equation and the equation of continuity for a compressible medium [91, 92]. The scalar field, $u(\boldsymbol{x})$, is related to the velocity potential or localised pressure of the medium.

In considering electromagnetic radiation, we have the additional complexity of considering a vector field. The field at a point is fully characterised by six components – the electric field vector $\boldsymbol{E}(\boldsymbol{x})$ and the magnetic field vector $\boldsymbol{H}(\boldsymbol{x})$. These fields must satisfy the vector Helmholtz equations,

$$\triangle \boldsymbol{E}(\boldsymbol{x}) + k^2 \boldsymbol{E}(\boldsymbol{x}) = 0 \qquad \triangle \boldsymbol{H}(\boldsymbol{x}) + k^2 \boldsymbol{H}(\boldsymbol{x}) = 0. \tag{1.10}$$

Where the region is free of sources, the fields will also be divergence free [91]. The magnetic field and electric field are not independent; each field can be derived from the other. The

complete constraint on the field can be expressed

$$\triangle \boldsymbol{E}(\boldsymbol{x}) + k^2 \boldsymbol{E}(\boldsymbol{x}) = 0 \qquad \nabla \cdot \boldsymbol{E}(\boldsymbol{x}) = 0 \qquad \boldsymbol{H}(\boldsymbol{x}) = \frac{\nabla \times \boldsymbol{E}(\boldsymbol{x})}{ik} \quad \text{or} \tag{1.11}$$

$$\triangle \boldsymbol{H}(\boldsymbol{x}) + k^2 \boldsymbol{H}(\boldsymbol{x}) = 0 \qquad \nabla \cdot \boldsymbol{H}(\boldsymbol{x}) = 0 \qquad \boldsymbol{E}(\boldsymbol{x}) = \frac{-\nabla \times \boldsymbol{H}(\boldsymbol{x})}{ik} \tag{1.12}$$

where ∇ is the vector differential operator

$$\nabla = \frac{\partial}{\partial x}\mathbf{i} + \frac{\partial}{\partial y}\mathbf{j} + \frac{\partial}{\partial z}\mathbf{k} \tag{1.13}$$

for three-dimensional space with orthogonal unit vectors $\mathbf{i}, \mathbf{j}$ and $\mathbf{k}$ and respective cartesian coordinates (x, y, z). The divergence and curl operations on the vector field $\boldsymbol{E}(\boldsymbol{x})$ are then defined by the scalar or dot product and the cross product as $\nabla \cdot \boldsymbol{E}(\boldsymbol{x})$ and $\nabla \times \boldsymbol{E}(\boldsymbol{x})$.

The divergence constraint implies that the electric or magnetic field has only two degrees of freedom. From this it is apparent that the complete electromagnetic field can be characterised by a two-dimensional scalar field satisfying the wave equation. A similar case for the importance of the wave equation was made in [93] where it was shown that the Green's function for radiating waves satisfying Maxwell's equations has two degrees of freedom.

This brief analysis demonstrates why the properties of scalar fields satisfying the wave equation (1.7) are central to understanding the limits of wireless communications. To facilitate the analysis, we will investigate the single dimensional scalar field. This approach matches physical implementations that make use of unpolarised antennas to interact with the field. The issue of polarisation will be discussed further in the next section.

1.4.2 Polarisation

Early work in the field demonstrated that different polarisation modes of the radio channel could exhibit uncorrelated amplitudes [94]. The complete electromagnetic field has six components, suggesting that six communication modes are theoretically available [95, 96], however simple antenna designs will generally only excite or detect three modes [97]. Where the polarisation modes are independent, the use of polarisation will offer improved system performance in the form of a diversity gain [98].

For scatterers in the far-field, the electric and magnetic fields are not independent. The rank of the far-field array response matrix is only two [84]. In practice, compact trimode antenna have been proposed [99] and performance approaching three [100] or four [101] independent Rayleigh fading channels have been observed. Whilst such antenna offer multiple signals

from one antenna location, the antenna itself must have some spatial extent to couple with the component modes of the electromagnetic field. It is likely that such results arising from the array may also affect the pattern or directional diversity [102].

In this work we consider scatterers to be a reasonable distance from the array and thus in the far-field. It is the far-field excitation and response of the transmitter and receiver array which are of interest. In addition to satisfying the wave equation, these response matrices will have two degrees of freedom. The use of polarisation could increase the available degrees of freedom by a factor of 2. In this way, limits of capacity or system performance utilising polarisation would be increased by a factor between 1 and 2 depending on the amount of cross polarisation diversity. This approach has also been followed by others to develop a MIMO spatial channel model incorporating polarisation [103].

1.4.3 Mutual Coupling

Practical antennas will exhibit coupling between the elements as they are brought close together. This effect is known as mutual coupling. Initial studies of this effect [104–107] suggested a small improvement in system performance since mutual coupling would introduce antenna pattern diversity, decorrelating the antenna signals. Other works suggested the coupling would be detrimental [108] with a loss in signal to noise ratio degrading capacity [109]. Practical measurements showed that degradation in radiation efficiency would outweigh any increase in pattern diversity leading to a loss in performance [110].

Conflicting views in the existing research literature on this topic are largely due to different scopes and underlying assumptions [111]. Careful analysis shows a tradeoff between any diversity enhancement and the directional characteristics of the channel [112]. It is not possible to make definite predictions without considering the complete impedance network model of the antennas [113] and resultant changes in response and efficiency [114]. A rigourous approach and framework for investigating the effects of mutual coupling was proposed in [115]. With appropriate matching networks it has been shown that it is possible to decrease correlation without loss in gain [116], however the system bandwidth is significantly reduced.

Most approaches to mutual coupling consider the main source of noise to be that generated in the receiver amplifiers. When this is combined with power constraints based on the radiated power rather than any internal element currents, it is possible to benefit from “super directivity” with multiple antennas [117]. However, it is known that when circuit elements are coupled, the thermal noise components generated within them generate correlated noise at the network outputs [118]. This should be considered when analysing the effects of mutual coupling [119, 120].

Whichever approach to mutual coupling is considered, the underlying field incident on the antenna array must satisfy the wave equation constraint. The mutual coupling effects and antenna impedance matching network can be considered to perform a processing operation on the wave-field. This can be well modelled by a linear transformation and consequently cannot increase the information content of the underlying spatial field [121]. Thus mutual coupling is a factor related to the efficiency of a particular antenna configuration, rather than having an impact on the fundamental limits for spatial communication.

1.4.4 Dimensionality

We define a continuous spatial field, $u(\boldsymbol{x})$, to be a scalar function varying over three-dimensional space $\boldsymbol{x} = (x, y, z)$. We are interested in modelling the field over some domain of interest $\Lambda \subset \mathbb{R}^3$ which we require be bounded in extent such that $\boldsymbol{x}, \boldsymbol{y} \in \Lambda$ implies that $\|\boldsymbol{x} - \boldsymbol{y}\| < \infty$. We also require that Λ is not a set of measure zero, and thus contains at least some open interval. We assume the field, $u(\boldsymbol{x})$, is continuous, bounded and integrable over this domain. With these assumptions we can define an inner product and induced norm

$$\langle u, v \rangle = \int_\Lambda u(\boldsymbol{x})\overline{v(\boldsymbol{x})}d\boldsymbol{x} \qquad\qquad \|u\|_\Lambda = \int_\Lambda |u(\boldsymbol{x})|^2 d\boldsymbol{x}. \tag{1.14}$$

Define $\mathcal{S}$ as the space of fields $u(\boldsymbol{x})$ created from this inner product and norm. The space $\mathcal{S}$ is isomorphic to a separable Hilbert space with countable basis. For example, a Fourier basis of spatial complex sinusoids can be easily constructed for an arbitrary region. Since the fields are continuous, the dimensionality of the space of fields $\mathcal{S}$ over the bounded region Λ will be countably infinite.

If the field $u(\boldsymbol{x})$ is required to satisfy the narrow-band wave equation, (1.7), this implies an additional second order differential constraint. Define $\mathcal{S}'$ as the space of functions satisfying the wave equation (1.7) on the bounded region Λ. The space $\mathcal{S}'$ is a strict subspace of the space $\mathcal{S}$ and is again isomorphic to a countably infinite Hilbert space.

Consider a finite region $\Lambda' \subset \Lambda$ whose closure lies in the interior of Λ. A similar norm can be defined on Λ' as in (1.14). Any member of $\mathcal{S}'$ with unit norm $\|u\|_\Lambda$ can be approximated on the region Λ' with arbitrary precision with a fixed basis $\beta_m(\boldsymbol{x})$ for $m = 1, \ldots, M$ for some $M < \infty$. That is, given an arbitrary ϵ, there exists a number M and set of basis functions β_m such that

$$\min_{\alpha_m} \left\| u - \sum_{m=1}^{M} \alpha_m \beta_m \right\|_{\Lambda'} < \epsilon \qquad \forall \quad u(\boldsymbol{x}) : \|u\|_\Lambda = 1. \tag{1.15}$$

This result implies that provided a spatial field satisfies the wave equation over some larger region Λ, an arbitrary field over a bounded finite volume $\Lambda' \subset \Lambda$ is essentially finite dimensional. The combination of the wave equation constraint, a bounded domain of interest, and a finite precision representation leads to a fixed number of degrees of freedom. This is investigated further in Chapter 2 and forms an underlying theme for this thesis. The notion that a field is essentially finite dimensional leads to results regarding the efficient representation of fields and fundamental limits to system performance.

The idea of dimensionality for the multipath spatial field in wireless communications was developed recently [41], leading to a string of results regarding capacity limits [82, 122–124], modelling [44, 48, 78, 125], extrapolation [126, 127] and direction of arrival estimation [128, 129]. Similar ideas were developed by considering a suitable basis representation for the signals observed by a spherical antenna array [43, 84, 130].

The idea of dimensionality and degrees of freedom has been investigated for a scattered field resulting from objects in a finite volume [131–133]. This problem can be thought of as the dual of that considered in this work, where we are interested in the dimensionality of the electromagnetic field itself in a finite volume.

1.4.5 Intrinsic Limits

In wireless communications systems, transmission is achieved by means of a modulated narrow-band radio frequency transmission sent from a finite transmitter region and received in a finite receiver region. It follows then that the concept of the essential dimensionality of a wave-field developed in Section 1.4.4 will be related to the intrinsic ability to send information between the two regions. In the field of Wireless Communications and Information Theory there have been several results presented towards understanding these limits. This section presents a brief literature review of that area.

The assumption of independently fading channel coefficients must be examined in the context of the wave equation [46]. The intrinsic limit can be related to the properties of a continuous operator describing the electromagnetic coupling between the two spatial regions [134, 135]. The laws of electromagnetism will have an effect on the maximum achievable spatial capacity [136, 137].

The interaction with the electromagnetic field through a continuous or distributed sensor, across the receiver and transmitter spatial region, suggests an intrinsic upper bound on the capacity of a wireless channel [138, 139]. A similar result is obtained by taking the limit

of a finite element approximation of the spatial channel [140]. The essentially finite dimensionality of the spatial field can be used to derive bounds for the scaling of the capacity of a constrained antenna array [79, 82]. An extensive numerical investigation has been presented with similar conclusions [121].

A recent detailed work by Jensen and Wallace reviewed the capacity saturation that results from considering the laws of electromagnetism [141]. A more mathematical approach based on the dimensionality of the spatial field is presented in [81].

Whilst this thesis will consider the application of continuous spatial models to several specific problems, it does not extend to incorporate the capacity limits established above. The review in this section has presented the works that have taken the notion of the field dimensionality and applied it to the communications capacity problem. However, since some of the elements and aspects of the continuous spatial model remain poorly established, most of these results sit on tenuous foundations. The motivation of this research and thesis has been to provide a more systematic development of some of the aspects and applications of continuous spatial models.

The following chapter leads into this work by a more thorough review of the dimensionality results and analysis of their application to two-dimensional multipath fields.

Chapter 2

Dimensionality of Multipath Fields

2.1 Introduction

In engineering terms, the dimensionality of a system relates to the degrees of freedom or the number of intrinsic variables required to describe the state of a system. In practice, it is only possible to observe or control a system with a finite dimensionality. Provided such systems are also bounded in energy, they present a manageable level of complexity. We expect this to be the case for most physical systems over a bounded domain of interest.

When we lend mathematical models to physical quantities, it is possible to create a framework that permits unbounded dimensionality and complexity. For example, if we consider a simple continuous function $g(t)$ defined on the real interval $t \in [0, T]$, mathematically it can be bounded in both magnitude and energy and still exhibit a countably infinite complexity:

$$g(t) = \sum_{n=-\infty}^{\infty} \alpha_n e^{j2\pi nt/T} \qquad \sum_{n=-\infty}^{\infty} |\alpha_n| \leq 1 \quad \Rightarrow \quad g(t) \leq 1$$
$$\sum_{n=-\infty}^{\infty} |\alpha_n|^2 \leq 1 \quad \Rightarrow \quad \int_0^T |g(t)|^2 \leq T. \tag{2.1}$$

A useful signal description requires a finite set of coefficients α_n selected from a countably infinite possible set. There is generally some additional constraint or critical parameter that will constrain the dimensionality. For example, any interaction with a physical system will have some constraint on the resolution or scale of observation and control. Intuitively we expect such a constraint to reduce the system model to a finite number of terms and thus a finite dimensionality. For some applications a conservative estimate of this limit is adequate. However, for telecommunications systems, we are interested in the ability to transmit and

capture information. The number of terms and their relative strength are directly related to the information theoretical limits of the system.

An understanding of the relationship between physical constraints and system dimensionality is an important problem. Consider the problem of a signal constrained to a duration of T seconds and a spectral bandwidth of W Hz. The dimensionality of such a signal of $2WT$ time is an accepted result that underpins much of communications and digital signal processing theory. Yet this result has a rich history and an extensive theoretical treatment with the key result presented by Slepian as the second Shannon Lecture in 1974 [85]

> The approximate dimension of the set of bandlimited and time limited functions is asymptotically $2WT$ as W or T becomes large.

For most applications, $2WT \gg 1$ and the asymptotic relationship is appropriate. Whilst the signal space is still infinite in dimensionality, any signal constrained in duration and bandwidth can be well approximated by a finite dimensional representation. The error in a representation decreases rapidly beyond the critical dimensionality. However, rather than this being an absolute threshold, it occurs across a span of the order of $\log 2WT$ [142–145]. Thus for small $2WT$ the required accuracy can have a significant impact on the required number of dimensions.

The recent interest in using multiple antennas for communications has created an active area of research. Rather than considering a signal over a single dimension, we must consider a signal over three possible spatial dimensions in addition to time. Continuous functions are used to represent the variation of some physical property over the spatial region of the transmitter and receiver. In this work the physical properties considered are the electromagnetic field values. Therefore they have the additional constraint of Maxwell's equations. We are interested in developing an understanding of the dimensionality or degrees of freedom in a continuous spatial field over a region of space. Such work will be fundamental to understanding the limits and optimal approaches for transmitting and receiving information from within a confined spatial region.

There is now a significant amount of literature demonstrating a relationship between the degrees of freedom and the spatial extent of an antenna array. Jones, Kennedy and Abhayapala formalised the concept of dimensionality as it relates to the wireless multipath field in 2002 [41, 42] leading to a series of publications regarding capacity limits [82, 122–124], modelling [44, 48, 78, 125], extrapolation [126, 127] and direction of arrival estimation [128, 129]. Poon, Brodersen and Tse developed similar ideas from a signal subspace approach [43, 84, 130]. Rather than treating the MIMO problem as discrete set of antennas,

the idea of taking a volumetric approach to space has been developed [146] and the notion of an intrinsic capacity of the electromagnetic channel [136–139] has been presented.

Whilst these publications are all relatively recent, the observation of a finite dimensional signal space based on the physical extent of the array, rather than the number of array elements, is not new. The practical approach has been to use antenna spacing no less than half a wavelength. Use of the Bessel expansion and principal terms for small ring arrays was established in the 1960s [147, 148]. The signals representing the principal components of variation across the antenna array were known as phase modes and have been applied to problems of direction of arrival estimation [149–153] and extrapolation [154]. The phase modes can be related to the signal from a virtual linear array [155]. The number of significant phase modes is related to the size of the circular array, not the number of antenna elements. Familiarity with the dimensionality of a spatial field in communications and information theory is still at an early stage. The attempts at creating a fundamental limit for the capacity of a region of space provide apparently conflicting and incomplete results.

This chapter presents an analytical and numerical study of the dimensionality and degrees of freedom of a continuous spatial field and its significance to the MIMO communications channel. It is a collection and extension of several works previously published by the author [156–158]. To provide some background, Section 2.2 reviews the framework for discussing the approximate finite dimensionality of a band-limited function. Section 2.3 extends this framework to consider a truncated representation of a two-dimensional multipath field. A discrepancy between the published results of Kennedy [41, 42] and Poon [43] is highlighted and explained. A numerical investigation of the truncation order and modelling error of a multipath field in Section 2.4 is used to demonstrate the applicability of the finite dimensional approximation and bounds. Section 2.5 presents new work to derive a tighter bound on the error and dimensionality of a multipath field, based on a new constructed bound for the Bessel function. As the bounds are developed under the assumption of far-field sources, Section 2.6 presents an analysis and investigation of the impact of near-field sources on the results.

The contribution of this chapter is to provide context and understanding of the finite dimensional approximation of a multipath spatial field. It is apparent that this is a similar problem to that studied extensively by Slepian [142], however the results are subtly different. Most importantly, however, with the spatial extent often a constraint of the system, the asymptotic limit is of less importance than understanding the behaviour of the truncated approximation around the selected representation dimensionality. In practice, this relates to the problem of the optimal number of antennas to use in a particular system configuration, and highlights the issue of diminishing returns for spatially constrained MIMO systems.

2.2 Dimensionality of a Bandlimited Function

In this section we consider the degrees of freedom or dimensionality of a bandlimited signal with finite duration. It is true that no signal can be simultaneously limited in time and bandwidth. Thus we must consider signals which are effectively contained or almost limited, in some sense, to a given time and bandwidth. Without loss of generality, we assume a time signal $g(t)$ with unity energy,

$$\int_{-\infty}^{\infty} |g(t)|^2 = 1. \tag{2.2}$$

Adopting the approach set out by Slepian [85] we define a function as being "limited to a duration of T at level ϵ" to imply that the fraction of the signal's total energy outside of the interval $[0, T]$ is bounded from above by ϵ,

$$\int_{t \notin [0,T]} |g(t)|^2 dt \leq \varepsilon. \tag{2.3}$$

Similarly, we can define a function as being "bandlimited to [-W,W] at level ϵ" with the bound

$$\int_{|f|>W} |G(f)|^2 df \leq \varepsilon \tag{2.4}$$

where

$$G(f) = \int_{-\infty}^{\infty} e^{-2\pi j f t} g(t) dt. \tag{2.5}$$

Now consider $\mathcal{G}$ as the set of all unit energy functions time limited to $[0, T]$ and bandlimited to $(-W, W)$ both at level ε. Define the approximate dimensionality $N(W, T, \varepsilon, \varepsilon')$ of $\mathcal{G}$ at level ε' as the minimum N for which there exists a fixed collection of functions $\Psi_1, \ldots, \Psi_N$ such that for any $g \in \mathcal{G}$ there exists a set of coefficients α_n such that

$$\int_{|t| \leq T/2} \left| g(t) - \sum_{i=1}^{N} \alpha_n \Psi_n(t) \right|^2 dt \leq \varepsilon'. \tag{2.6}$$

The dimensionality theorem is stated as

$$\lim_{T \to \infty} \frac{N(W, T, \varepsilon, \varepsilon')}{T} = 2W \quad \text{or} \qquad \lim_{W \to \infty} \frac{N(W, T, \varepsilon, \varepsilon')}{W} = 2T. \tag{2.7}$$

The works of Slepian, Pollak and Landau [142–145] derive the optimal set of basis functions Ψ_n related to this problem. In these works they consider two classes of functions – those that are finite in duration with maximum concentration of spectral energy in a given interval, and those that are finite in bandwidth with a maximum concentration of energy in a given time interval. The case of signals concentrated in both a time and spectral interval was covered by Slepian in [85] and elegantly generalised by Franks [159]. These turn out to be a family of functions specified by the parameter $2WT$ and scaled for the appropriate time and frequency intervals. The differential equation involved in this derivation is identical to that which arises in the separation of the wave equation in prolate spheroidal coordinates. As a result, these functions are known as the prolate spheroidal wave functions. It is the properties of these functions that are used to prove the dimensionality theorem.

A comprehensive formal framework representing over a decade of research was required to properly establish the dimensionality theorem for the one-dimensional time bandwidth case. Much of the work for this thesis is related to extending such results to the case of multi-dimensional spatial wave-fields. Despite the complexity underlying the formal results, it is evident that in the limiting case of a large dimensionality $2WT$, the exponential basis functions provide a reasonable approximation. This is consistent with the intuition and practical application of signal processing theory.

Taking the infinite basis expansion from (2.1) and definition (2.5)

$$G(f) = \int_{-\infty}^{\infty} e^{-2\pi jft} g(t)dt = \sum_{n=-\infty}^{\infty} \alpha_n \int_0^T e^{2\pi jnt/T} e^{-2\pi jft} dt \tag{2.8}$$

$$= Te^{-j\pi fT} \sum_{n=-\infty}^{\infty} (-1)^n \alpha_n \text{sinc}\left(\pi(fT-n)\right) \tag{2.9}$$

where $\text{sinc}(x) = \sin(x)/x$. From the maximum of 1 at $f = n/T$, $|\text{sinc}\left(\pi(fT-n)\right)|$ will decrease like $|1/\pi(fT-n)|$ as $n \to \infty$. Thus as T and W become larger, it is evident that the bound (2.4) is approximately satisfied provided that

$$\alpha_n \approx 0 \quad \forall \quad |n| > WT \tag{2.10}$$

which leaves $2WT+1$ coefficients α_n to characterise the signal. Whilst the harmonic exponential basis will be suboptimal for small values of $2WT$, it is evident that in the limit this basis choice is consistent with the theoretical limit. Similar ideas and results will now be explored for continuous spatial fields. These can be considered as continuous functions with a multi-dimensional domain rather than the case of the one-dimensional domain function as reviewed in this section.

2.3 Dimensionality of a Multipath Field

Consider a spatial field represented by a continuous scalar value defined over some domain representing the region of space. To begin with we can consider a field defined over a two-dimensional domain $u(\boldsymbol{x})$ where $x \in \mathbb{R}^2$. Rather than the entire field, we are only interested in modelling, detecting or exciting the field in a restricted domain of interest. A suitable simple domain is the set of points within a fixed radius of the origin

$$\mathbb{B}_R^2 = \left\{ \boldsymbol{x} : \boldsymbol{x} \in \mathbb{R}^2, \|\boldsymbol{x}\| < R \right\} \tag{2.11}$$

where the norm $\|\cdot\|$ is the usual cartesian distance norm. Whilst compact in notation, the representation of a field as $u(\boldsymbol{x})$ for $\boldsymbol{x} \in \mathbb{B}_R^2$ suggests an uncountably infinite set of values, $u(\boldsymbol{x})$, and thus does not lend itself to engineering application. As before in (2.1) of Section 2.1, we propose some countable spatial basis functions, $\beta_n(\boldsymbol{x})$, to represent possible fields

$$u(\boldsymbol{x}) = \sum_{n=-\infty}^{\infty} \alpha_n \beta_n(\boldsymbol{x}). \tag{2.12}$$

Such a representation is only useful provided we can obtain an appropriate basis representation for the problem of interest. In practice we must deal with a finite set of signals or basis functions, and thus limit ourselves to consider the truncated space of fields

$$\left\{ u(\boldsymbol{x}) : u(\boldsymbol{x}) = \sum_{n=-N}^{N} \alpha_n \beta_n(\boldsymbol{x}), \sum_{n=-N}^{N} |\alpha_n|^2 < \infty \right\}. \tag{2.13}$$

Our choice of basis functions $\beta_n(\boldsymbol{x})$ should be constructed such that a truncated space at any order N provides an efficient representation of the desired signal space. The basis will be optimal when a N^{th} order truncated space represents the maximal variation in the underlying signal over all possible basis of order N. Without finite truncation of the signal representation, no sense of optimality exists.

To achieve a particular error in modelling the underlying signal, an optimal basis function set will allow a compact representation of the field through the least number of terms in the expansion (2.12).

As discussed previously, we expect some physical constraints and considerations for the engineering application to impose an effective finite dimensionality. Thus we anticipate being able to consider only a finite set of the basis functions to represent, with some level of approximation error, all of the fields of interest for a given problem. The constraints relevant to wireless communications are the properties of the electromagnetic field, the ability of the

antenna elements to excite and detect it, and the bounded nature of our region of observation.

Here we see a key thread of this thesis:-
Understanding the optimal basis representation and the appropriate truncation order for a continuous spatial field related to electromagnetic radiation is key to understanding the theoretical limits of wireless communication systems utilising spatial diversity.

The term *multipath field* is used to describe a field that is constructed from many different signal arrival paths. It is this multipath diversity that creates the spatial variation in the communications channel that can be exploited for improved performance. Recent works on the multipath field suggest that a field of arbitrary path complexity can be well approximated over a finite domain of interest using a fixed number of signal terms [41, 84]. Beyond some critical threshold, the error in such an approximation is bounded and exponentially decreasing with respect to the order of the approximation. Two approaches from these works will be reviewed and compared.

2.3.1 Representation by Wave Equation Basis Functions

The first approach to be reviewed was presented by Jones, Kennedy and Abhayapala [41, 42]. For communications systems, the signalling bandwidth is small compared to the carrier frequency and we can typically make the assumption of a narrow-band source. In a region free of any sources, $\|\boldsymbol{x}\| < R$, the field must satisfy the narrow-band wave equation [91]

$$\triangle u(\boldsymbol{x}) + k^2 u(\boldsymbol{x}) = 0. \tag{2.14}$$

All solutions to this differential equation can be represented from a set of basis functions. Given a choice of a circular domain of interest, a natural set of basis functions are those obtained by separating the wave equation in polar coordinates. The radial variation of the basis functions is characterised by the Bessel function with the angular variation being the harmonic complex exponentials. We can represent an arbitrary spatial field using this basis,

$$u(\boldsymbol{x}) = \sum_{n=-\infty}^{\infty} \alpha_n \beta_n(\boldsymbol{x}) \qquad \beta_n(\boldsymbol{x}) = J_n(k\,\|\boldsymbol{x}\|) e^{jn\theta_{\boldsymbol{x}}}. \tag{2.15}$$

where $J_n(\cdot)$ represents the n^{th} order Bessel function and $\theta_{\boldsymbol{x}}$ represents the angle of the polar coordinates for the point $\boldsymbol{x}$.

Given this basis function we are interested in the number of terms required to represent an arbitrary multipath field. Consider a field as a superposition of P far-field sources, with amplitude a_p and angle θ_p. The coefficients, α_n, for the expansion of this field can be specified

and bounded,

$$\alpha_n = \sum_{p=1}^{P} a_p e^{jn\theta_p} \leq \sum_{p=1}^{P} |a_p| = a. \tag{2.16}$$

If the representation of the field is truncated at order N, we can determine an upper bound on the representation error across the domain of interest. This error will be bounded by the worst case contribution resulting from the terms discarded in the truncation. Define the truncation error as

$$\varepsilon_N = |u(\boldsymbol{x}) - u_N(\boldsymbol{x})| = \left| \sum_{|n|>N} \alpha_n \, J_n(k \, \|\boldsymbol{x}\|) e^{jn\theta_{\boldsymbol{x}}} \right|. \tag{2.17}$$

Using the bound (2.16)

$$\varepsilon_N \leq 2a \sum_{n=N+1}^{\infty} \left| J_n(k \, \|\boldsymbol{x}\|) \right|. \tag{2.18}$$

The Bessel function can be approximated and bounded from above [160],

$$J_n(kr) = \left(\frac{kr}{2}\right)^n \sum_{m=0}^{\infty} \frac{\left(-\frac{1}{4}k^2r^2\right)^m}{m!\Gamma(n+m+1)} \leq \frac{(kr)^n}{2^n\Gamma(n+1)} \approx \frac{1}{\sqrt{2\pi n}} \left(\frac{ekr}{2n}\right)^n \tag{2.19}$$

using the first term of the alternating series as an upper bound and applying the Stirling approximation for the Gamma function, $\Gamma(\cdot)$. The approximation holds for small kr, whilst the bound holds for all kr. This bound is monotonically increasing with r, and for our domain of interest $\|\boldsymbol{x}\| < R$. The worst case for this error bound on ε_N will occur at the extremity of the domain of interest $\|\boldsymbol{x}\| = R$. The truncation error from (2.18) is bounded from above as

$$\varepsilon_N < \frac{2a\rho^{N+1}}{(1-\rho)\sqrt{2\pi(N+1)}} < \infty \qquad \text{where} \quad \rho = \frac{ekR}{2(N+1)} < 1 \tag{2.20}$$

for all $\|\boldsymbol{x}\| < R$ provided N is sufficiently large. Since the summation will only converge for $\rho < 1$, the critical truncation point above which the bound will exist will be

$$N > ekR/2. \tag{2.21}$$

The dimensionality of the field is then the number of required terms $2N + 1$. A two-dimensional multipath field in a region with radius R has an upper bound on its effective

dimensionality of

$$D_R = 2\left\lceil \frac{e}{2} kR \right\rceil + 1 \approx 17R/\lambda. \tag{2.22}$$

It can also be shown that the error decreases exponentially with additional terms beyond this truncation point [41]. The approach is robust in that the bound is a true upper bound. The contribution from all higher order terms is considered and bounded. A similar result was presented by Rossi et al. [153]. However, as will be seen in Section 2.4 this bound is rather conservative for larger regions.

2.3.2 Representation by Antenna Signal Subspace

Rather than considering the underlying field, an alternative approach is to consider the signal space that would be observed by the antenna array [43, 84, 130]. Rather than considering the dimensionality of the field itself, this approach considers the degrees of freedom in the antenna signals. This comes from the assumption that a uniform circular array at the extent of the two-dimensional region is optimal.

Consider a uniform circular array of radius R and an arbitrary superposition of P far-field sources, with amplitude a_p and angle θ_p. The signal received around the circular array will be

$$u(\theta) = \sum_{p=1}^{P} a_p e^{jkr\cos(\theta-\theta_p)} = \sum_{p=1}^{P} a_p e^{-jn\theta_p} \sum_{n=-\infty}^{\infty} j^n J_n(kR) e^{jn\theta} \tag{2.23}$$

using the Jacobi-Anger summation expansion of a plane wave [91]. The basis functions are the harmonic complex exponentials around the circular array weighted by the Bessel function. This approach is also known as the phase mode signal representation of a circular array [151].

The Bessel function of order $n > 0$ will be zero at the origin, $J_n(0) = 0$ for all $n > 0$. Furthermore, the derivatives of $J_n(z)$ at $z = 0$ will be zero up until $\partial^n J_n(z)/\partial z^n = (1/2)^n$. Thus as the order is increased, the Bessel function will remain small for a larger interval from the origin [161]. This is often referred to as the "high pass" nature of the higher order Bessel functions as they have little contribution around the origin. The assumption made in the work of Poon et al. [43] is that

$$J_n(kR) \approx 0 \quad \text{for} \quad n > kR. \tag{2.24}$$

Although this is only an approximation, it has been used for some time [149] and tends to be an accepted result. Since the high order terms $n > kR$ are small, we can truncate the summation to give a finite dimensional subspace approximation of the circular array signal space

$$u(\theta) \approx \sum_{p=1}^{P} a_p e^{-jn\theta_p} \sum_{n=-N}^{N} j^n J_n(kR) e^{jn\theta}. \tag{2.25}$$

The truncated field representation of order of $N = kR$ has an associated dimensionality,

$$D_R = 2\lceil kR \rceil + 1 \approx 12.57R/\lambda. \tag{2.26}$$

This approach does not consider the cumulative sum of the truncated terms nor does it provide any estimate or bound on the representation error in the resultant truncation.

2.3.3 Comparison of Dimensionality Results

The previous two sections detailed two approaches for creating a finite dimensional representation of the spatial field. Both of the suggested truncation orders, (2.22) and (2.26), show a linear growth with the radius of the region R. Both the approaches suggest that the error in the representation of an arbitrary multipath field decreases rapidly with additional terms beyond the suggested truncation. However, it is noted that the two results suggest a different ratio in the limit of $R \to \infty$.

A notable difference between the two approaches is that the wave equation basis (Section 2.3.1) considers the dimensionality of the complete field over the entire domain of interest $\|\boldsymbol{x}\| \leq R$. The signal subspace approach (Section 2.3.2) considers only the antenna signals at the extent of the region on the circular array $\|\boldsymbol{x}\| = R$. However, in the analysis it was noted that the maximum error of the expansion (2.15) occurs near the edge of the array [41]. Also from Huygen's principle [91] it is known that the field in the interior can be completely characterised from the boundary field conditions. This implies the edge of the field will have a similar dimensionality to the entire field across the domain of interest. Therefore this is not the reason for the differing ratios.

Both approaches are developed from electromagnetic theory. While the first approach directly considers a basis of the wave equation, the second restricts signals incident on the array to plane waves (i.e., far-field sources). Both approaches effectively constrain the possible fields to valid solutions of the wave equation [91]. The Bessel function expansion of a plane wave through the Jacobi-Anger expansion is central to both approaches.

The most significant difference between the two approaches is that of obtaining a bound in comparison to an approximation. The approach of Section 2.3.1 is a formal proof, which considers and bounds all of the truncated terms. The heuristic approach of Section 2.3.2 simply considers the terms to be negligible.

An approximation of $J_n(kR)$ at the critical point $n = kR$ is given by [160, p.366]

$$J_n(n) \approx \frac{2^{1/3}}{3^{2/3}\Gamma(\frac{2}{3})}\frac{1}{n^{1/3}} \approx 0.4473 n^{-1/3} \tag{2.27}$$

which cautions the assumption (2.24) that $J_n(kR) \approx 0$ for $n > kR$. Note that in the case of $kR = 1$ then $J_n(kR) \approx 0.4473$ which indicates that the second basis function of a region with $R = \lambda/2\pi$ has a significant contribution to modelling the field on this region. For this reason the expression for dimensionality developed in 2.3.2 tends to underestimate the contribution from the truncated terms and will be inadequate for small regions.

The bound for the Bessel function (2.19) used in Section 2.3.1 suggests

$$J_n(n) < (e/2)^n/\sqrt{2\pi n} \tag{2.28}$$

which will be much larger than the approximate value (2.27) as the order n increases. Thus for larger regions with $kR \gg 1$ the bound developed in Section 2.3.1 will overestimate the contribution of the error from the truncated terms and thus the bound on dimensionality will be conservative.

An intended outcome of the research work in this area was to develop a better understanding and formal basis for the dimensionality results. This section presents the two starting points for this development: a formal bound that is conservative in the limit of a large region and an approximation that is insufficient for the case of a small region. The subsequent sections in this chapter will present further developments from this point to investigate the existence of an alternate bound which can be used for both small and large regions.

2.4 Numerical Investigation of Dimensionality

This section presents a numerical investigation on the appropriate truncation dimensionality for a multipath field. In the investigation we consider three variants of the error criteria considered on a circular region. As will be seen, the bounds for these three error criteria exhibit similar characteristics, but vary slightly in magnitude.

2.4.1 Bound for Worst Case Error Across Region

First we consider the worst case error possible for a particular field. This is the ratio between the maximum error in the truncated field and the maximum value of the field. This error is similar to the error and upper bound that was considered in Section 2.3.1,

$$\varepsilon_1 = \max_{\|\boldsymbol{x}\|<R} |u(\boldsymbol{x}) - u_N(\boldsymbol{x})| \qquad u_N(\boldsymbol{x}) = \sum_{n=-N}^{N} \alpha_n \beta_n. \tag{2.29}$$

Again, we consider the field constructed from a set of P plane waves, and note that the maximum field amplitude is $\sum_{p=1}^{P} |a_p|$. Without loss of generality, we can normalise this to be unity. Thus from (2.16) we have $|\alpha_n| \leq 1$. Provided that the truncation point N is sufficiently large, $J_n(k\,\|\boldsymbol{x}\|)$ is monotonically increasing for $\|\boldsymbol{x}\| \leq R$ thus

$$\varepsilon_1 = \left| \sum_{|n|>N} \alpha_n\, j^n J_n(k\,\|\boldsymbol{x}\|) e^{jn\theta_x} \right| < 2 \sum_{n=N+1}^{\infty} |J_n(kR)|\,. \tag{2.30}$$

2.4.2 Bound for Mean Error at Edge of Region

Often we are not interested in the error for a particular specific field, but rather the expected error for representing a field generated from a random process. We consider the class of fields generated from a large set of plane waves with independent random amplitudes and random directions of arrivals. The incident waves are scaled by $1/\sqrt{P}$ such that the expected value of the field power is unity. Given a large enough P, the field mode coefficients α_n will

also be independent and unit power:

$$\begin{aligned} a_p &= \frac{1}{\sqrt{P}} a'_p & E\left\{a'_p \overline{a'_q}\right\} &= \delta_{pq} \\ u(\boldsymbol{x}) &= \sum_{p=1}^{P} a_p e^{jkr_p cos(\theta-\theta_p)} & E\left\{u(\boldsymbol{x})\overline{u(\boldsymbol{x})}\right\} &= \sum_{p=1}^{P} a_p \overline{a_p} = \frac{1}{P}\sum_{p=1}^{P} a'_p \overline{a'_p} \approx 1 \\ \alpha_n &= \sum_{p=1}^{P} a_p e^{jn\theta_p} & E\left\{\alpha_m \overline{\alpha_n}\right\} &= \sum_{p=1}^{P} a_p \overline{a_p} e^{j(m-n)\theta_p} \approx \delta_{mn} \end{aligned} \tag{2.31}$$

where the Kronecker delta function $\delta_{mn} = 1$ for $m = n$ and zero otherwise. The final approximation of (2.31) is valid provided that there is a suitable large number of incident waves, $P \gg 1$ and $P \gg \max(|m|, |n|)$. This field has maximum richness or entropy in that the field coefficients are independent random variables prohibiting a representation with a reduced set of variables.

In the limit of $P \to \infty$ this field is wide sense stationary in that the characteristics and statistics of the field are independent of the position $\boldsymbol{x}$. The coefficients α_n are an infinite set of independent random variables of unit variance. This implies

$$\begin{aligned} E\left\{u(\boldsymbol{x})\overline{u(\boldsymbol{x})}\right\} &= E\left\{\sum_{m=-\infty}^{\infty} \alpha_m \beta_m \sum_{n=-\infty}^{\infty} \overline{\alpha_n}\overline{\beta_n}\right\} \\ &= \sum_{m=-\infty}^{\infty}\sum_{n=-\infty}^{\infty} E\left\{\alpha_m \overline{\alpha_n}\right\} J_m(k\left\|\boldsymbol{x}\right\|) J_n(k\left\|\boldsymbol{x}\right\|) e^{j(m-n)\theta_{\boldsymbol{x}}} \\ &= \sum_{n=-\infty}^{\infty} E\left\{\alpha_n \overline{\alpha_n}\right\} J_n^2(k\left\|\boldsymbol{x}\right\|) = 1 \end{aligned} \tag{2.32}$$

using some Bessel identities from [162].

In Section 2.3.1 it was shown that beyond a reasonable truncation order, the bound on the worst case error is largest at the edge of the region $\|\boldsymbol{x}\| = R$. Consider the average error in the truncated representation around this edge

$$\begin{aligned} \varepsilon_2 &= E\left\{\frac{1}{2\pi}\int_0^{2\pi}\left|\sum_{|n|>N} \alpha_n\, J_n(kR) e^{jn\theta}\right|^2 d\theta\right\} \\ &= E\left\{\sum_{|m|>N}\sum_{|n|>N} \alpha_m \overline{\alpha_n} J_m(kR) J_n(kR) \frac{1}{2\pi}\int_0^{2\pi} e^{j(m-n)\theta} d\theta\right\} \\ &\leq \sum_{|n|>N} E\left\{\alpha_n \overline{\alpha_n}\right\} J_m(kr) J_n(kR) = 2\sum_{n=N+1}^{\infty} J_n^2(kR) \end{aligned} \tag{2.33}$$

using the expectation around the circular boundary, changing the order of integration and using the orthogonality of the harmonic exponentials in the basis functions β_n.

2.4.3 Bound for Mean Error Across Region

For the third case we consider the expected error across the entire domain of interest. This involves extending the domain of integration to include all radii $r < R$. The orthogonality of the basis functions is still applicable since the integration is performed in polar coordinates.

$$\begin{aligned}\varepsilon_3 &= E\left\{\frac{1}{\pi R^2}\int_0^R\int_0^{2\pi}\left|\sum_{|n|>N}\alpha_n\, j^n J_n(kr)e^{jn\theta}\right|^2 d\theta r dr\right\} \qquad (2.34)\\ &\leq \frac{2}{R^2}\sum_{|n|>N} E\left\{\alpha_n\overline{\alpha_n}\right\}\int_0^R J_n^2(kr)rdr = 2\sum_{n=N+1}^{\infty} J_n^2(kR) - J_{n-1}(kR)J_{n+1}(kR)\end{aligned}$$

Figure 2.1 shows the locus of points satisfying the three errors, ε_1, ε_2 and ε_3, equal to -20dB and -50dB. The ratio of the truncation order to kR plotted in Figure 2.1(b) indicates that the ratio is asymptotically approaching 1 for large regions. Figure 2.1(a) demonstrates that the truncation at $\lceil kR \rceil$ approximates a -20dB average error in the stochastic case. For radii up to one wavelength, the truncation at $\lceil ekr/2 \rceil$ provides a better match to the -20dB worst case error. This observation matches the successful use of the $\lceil ekr/2 \rceil$ truncation for capacity results [79, 122].

2.4.4 Discussion

The numerical investigation in this section suggests the conjecture that for large regions the dimensionality of a multipath field is asymptotically given by the value $D_R = 2kR + 1$. However, for small regions the representation of a field truncated to match this dimensionality will have a considerably larger error. As a result we must be careful with any use of this expression for the dimensionality of a field when dealing with a small region.

To consider the validity of the conjecture of the ratio asymptotically being unity, we can consider the application of the sampling theorem and Huygen's principle for a large region. The complete field across the region can be characterised by the field on the boundary. This will have length $2\pi R$. Since the field is generated from narrow-band sources, the field variation along a one-dimensional path will be strictly bandlimited, and thus can be represented by a

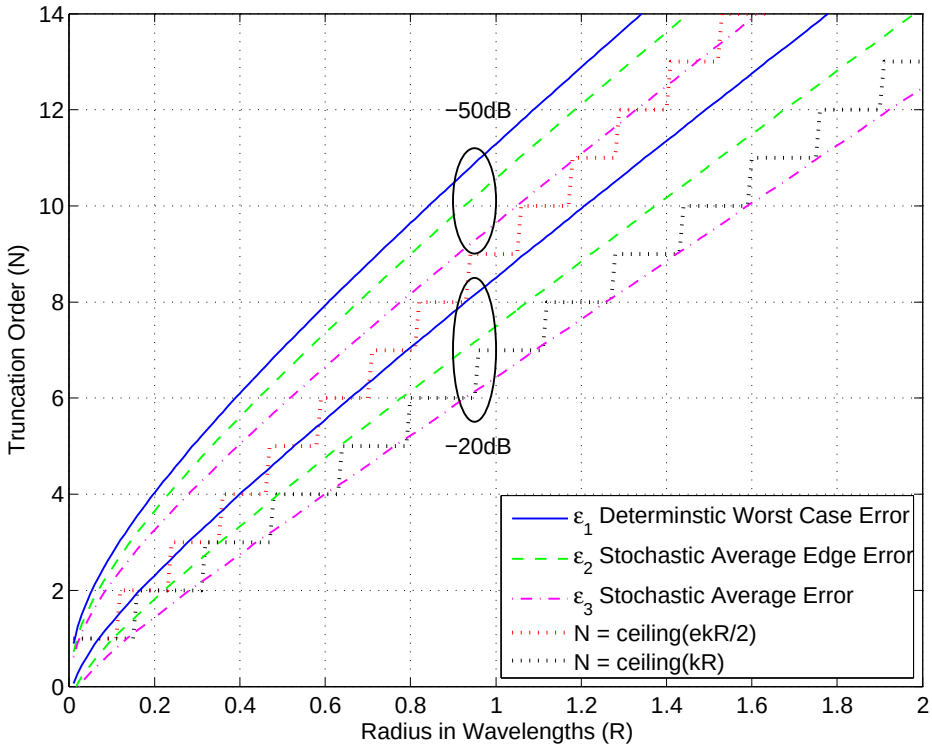

(a) Locus of constant truncation error. The truncation point $N = \lceil kR \rceil$ is closest to the locus for the average error of the stochastic field at -10dB.

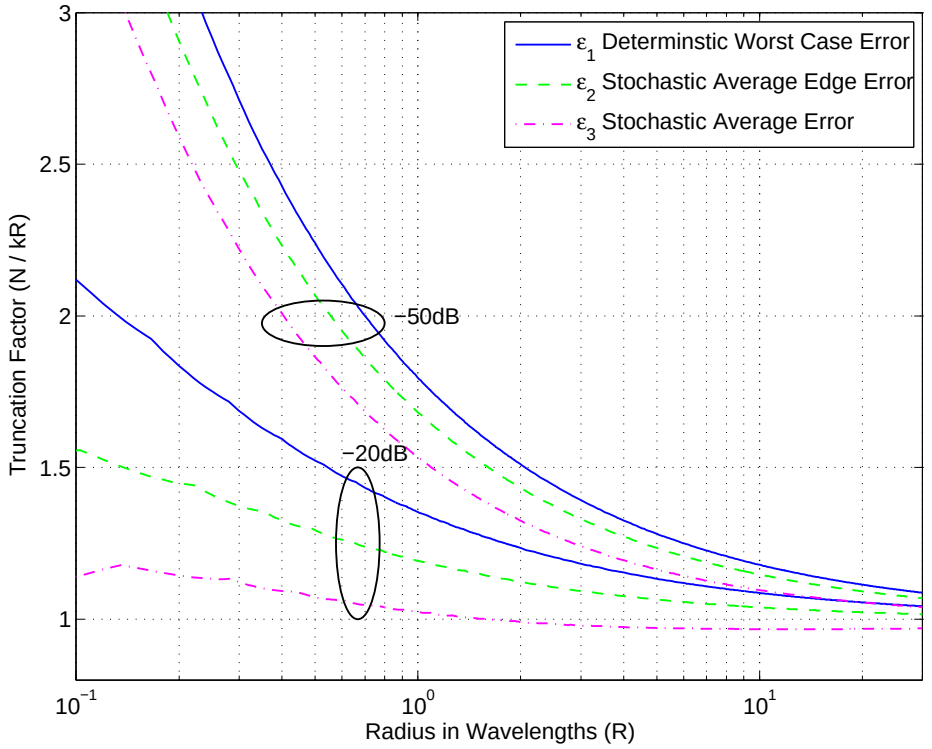

(b) Ratio of the truncation order to kR for a constant truncation error. As the radius increases, the ratio is asymptotic to 1.

Figure 2.1: Numerical investigation of the error in truncated field representation at different radii. Two sets of curves are shown representing modelling error $\varepsilon = -20$dB and $\varepsilon = -50$dB.

set of samples with the critical sampling period of one half wavelength. Thus the number of samples required is

$$D = \frac{2\pi R}{\lambda/2} = 2kR \quad \Rightarrow \quad N = \frac{D-1}{2} \approx kR. \tag{2.35}$$

The use of the sampling theorem for these results highlights the similarity between the dimensionality of a two-dimensional field and the dimensionality of a bandlimited signal as considered in Section 2.2.

The current interest in MIMO communications extends to considering antenna arrays numbering perhaps 8 to 16 elements. This corresponds to the dimensionality of the two-dimensional field in a region of the order of one wavelength. The dimensionality bound of $D_R = ekR+1$ is perhaps a better match for reasonable error contours of truncation at this radius.

From this analysis, it is evident that the dimensionality result as it applies to small regions cannot be simply captured by a single number. It is evident that only a finite number of terms will be required to model a multipath field with a desired accuracy. This has implications for the size of the space of detectable signals for a finite size sensor array. The dimensionality will asymptotically increase linearly with the radius of the domain of interest. However, for regions with a small radius, a more conservative estimate of the dimensionality is warranted. For such small regions the truncated terms will have a greater significance to the represented field.

Following on from this investigation, it would be desirable to have a formal derivation of the asymptotic limit of dimensionality consistent with that suggested from the numerical analysis. It was identified in Section 2.3.3 that the existing bound for the dimensionality is conservative as the result of a conservative bound used for the Bessel function. The following section is presented as a work towards improving this bound and thus the resultant dimensionality bound.

2.5 Development of Tighter Bound on Dimensionality

The framework presented in Section 2.3.1 provides an approach to bounding the error in a finite dimensional field approximation. However, the bound (2.19) used for the Bessel function introduces an overestimation of dimensionality.

Consider the terms of the expansion

$$J_n(kr) = \left(\frac{kr}{2}\right)^n \sum_{m=0}^{\infty} \frac{\left(-\frac{1}{4}k^2r^2\right)^m}{m!\Gamma(n+m+1)} \leq \frac{(kr)^n}{2^n\Gamma(n+1)}. \tag{2.36}$$

The ratio of the magnitude of the term for $m+1$ to that of m will be

$$\frac{(kr)^2}{4(m+1)(n+m+1)}. \tag{2.37}$$

We are interested in bounding the terms for the truncation where $n > kR > kr$. The expression (2.37) suggests that we will need in the order of n terms from the expansion for an accurate approximation. It can also be seen that the bound is asymptotically tight towards the origin as $kr \to 0$.

By using only the first term of the series expansion for the Bessel function as an upper bound, the bound is quite conservative. For large n the bound (2.19) reaches unity at $kr = n2/e$ whilst it is known that the maximum value of the actual Bessel function is upper bounded by 1 and does not occur until $kr > n$. In order to improve this result we seek a tighter bound for Bessel function across $0 < kr < n$. All Bessel functions of positive order are monotonically increasing over this range [163]. We shall name this part the leading edge of the Bessel function as it proceeds the oscillatory wave nature of the Bessel function as $kr \to \infty$.

2.5.1 New Upper Bound for the Bessel Function

The slope of the leading edge of the Bessel function on a log-log scale is monotonically decreasing. The bound (2.19) has a single term in the power series of the argument with exponent n. Whilst this term is a tight bound for the growth of $J_n(z)$ at $z = 0$ it diverges from the Bessel function as z increases.

We can generalise this to have a single term function of the form $f(z) = Az^m$. To extend the bound across the entire leading edge of the Bessel function, we choose to match the value and derivative of this approximation to the value and derivative of $J_n(z)$ at $z = n$,

$$f(n) = An^m \approx J_n(n) \tag{2.38}$$

$$\left.\frac{\partial f(z)}{\partial(z)}\right|_{z=n} = mAn^{m-1} \approx J_n^{'}(n) = J_{n-1}(n) - J_n(n). \tag{2.39}$$

Solving this for the two parameters A and using the recursion relationship for the Bessel

functions and the bound for $J_n(n)$ (2.27) we obtain

$$A = J_n(n)/n^m < \frac{2^{1/3}}{3^{2/3}\Gamma(\frac{2}{3})} n^{-1/3} n^{-m} \leq \frac{1}{2} n^{-1/3} n^{-m} \tag{2.40}$$

$$m = n\left(\frac{J_{n-1}(n)}{J_n(n)} - 1\right) = n\left(1 - \frac{J_{n+1}(n)}{J_n(n)}\right) < n^{2/3}. \tag{2.41}$$

With some additional manipulation and approximations of the Bessel functions, it is possible to show that m will vary in proportion to $n^{2/3}$. A comprehensive numerical investigation was used to verify that this is also an upper bound provided that $n \geq 1$.

Combining the results we conjecture a new single term bound for the Bessel function,

$$J_n(z) < \frac{1}{2} n^{-1/3} \left(\frac{z}{n}\right)^{n^{2/3}} \quad n \geq 1. \tag{2.42}$$

This bound can be verified numerically and provides an improved match to the leading edge of the Bessel function as is shown in Figure 2.2. While this bound remains to be proven analytically, it is an effective and simple expression for modelling the leading edge of the Bessel function. A comparison of this bound with the bound (2.19) is shown in Figure 2.2. By approximating the Bessel function at $J_n(n)$, the new conjectured bound does not diverge from the leading edge of the true Bessel function as the order n is increased. However, since it is a single polynomial term with a power of $n^{2/3}$ it is not as tight as the previous bound towards the origin.

2.5.2 Application of New Bound to Dimensionality

The bound (2.42) provides a fairly compact expression that bounds the Bessel function from above, and is less conservative than the previous bound 2.19 as $z = kR$ approaches n. We can use this new bound to consider the error in the truncation of the Bessel terms. From (2.30) the error bound will be

$$\varepsilon_1 < 2 \sum_{n=N+1}^{\infty} |J_n(kR)| \leq \sum_{n=N+1}^{\infty} n^{-1/3} \left(\frac{kR}{n}\right)^{n^{2/3}} < N^{-1/3} \sum_{n=N+1}^{\infty} \left(\frac{kR}{N}\right)^{n^{2/3}}. \tag{2.43}$$

This becomes more problematic than a simple power series. It is apparent that the terms in the summation will be strictly decreasing provided that $kR < N$. The summation can be

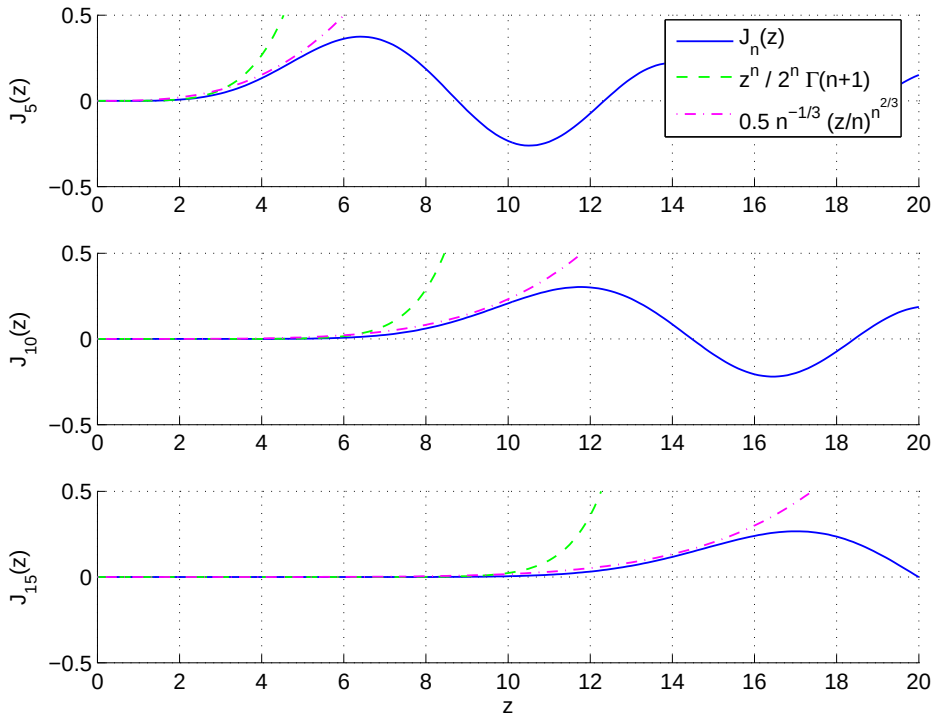

Figure 2.2: Comparison of bounds for the Bessel Function. The new bound provides a better match to the leading edge of Bessel function of higher order.

bounded by an integral,

$$\sum_{n=N+1}^{\infty} \left(\frac{kR}{N}\right)^{n^{2/3}} < \int_{N}^{\infty} \left(\frac{kR}{N}\right)^{n^{2/3}} dn < \int_{0}^{\infty} \left(\frac{kR}{N}\right)^{n^{2/3}} dn$$
$$< \frac{3\sqrt{\pi}}{4\left(-\log\left(\frac{kR}{N}\right)\right)^{3/2}}, \tag{2.44}$$

which exists provided that $kR < N$. This suggests a critical dimension of kR beyond which the error will be bounded and decreasing. However, at this critical dimensionality, the bound (2.43), suggests a relatively large error from the contribution of the truncated terms. The previous bound (2.19) is much tighter on the Bessel function for small argument $kR \ll n$ and as such predicts a lower contribution of the higher order terms beyond the critical threshold.

2.5.3 Discussion

The motivation of this section was to develop a simple tighter bound on the Bessel functions in an effort to improve the dimensionality bound. The conjectured bound (2.42) provides a single term expression that is much tighter around $J_n(n)$ than the existing bound (2.36).

However, when this bound is used to consider the error contribution from the truncated terms in a field representation, a number of problems arise.

The previous bound (2.36) is known to be asymptotically tight at the origin. The new Bessel bound has a lower polynomial order, $n^{2/3} < n$, and will overestimate the value of higher order terms on the region $kR \ll n$. Whilst the bound suggests a tighter truncation threshold for error convergence, it will lead to a conservative estimate of the error.

To bound the error we require an expression for the cumulative sum of all the terms of order $n > N$. The new term $0.5n^{-1/3}(z/n)^{n^{2/3}}$ has a intricate dependence on the order n. Obtaining an expression for the summation of such terms proved to be a challenge. The assumption that $n > N$ simplifies the term, but increases the error bound. A calculation of the expression 2.44 leads to very large values for $N \approx kR$.

The work of this section has provided the step of showing convergence in the error term for $N \approx kR$. It is conjectured that a composite bound for the Bessel function would be required to obtain a tighter bound for the error expression, rather than a single term bound. Given that the efforts to formally bound the dimensionality of single dimensional function spanned over a decade [85, 142], it is to be expected that a similar bound for a multidimensional field would be a challenging endeavour.

2.6 Impact of Near-Field Sources on Dimensionality

The dimensionality results presented and discussed in Section 2.3 are useful for determining the number of variables that would be required to represent or model an arbitrary multipath field across a region of space. However, the two approaches of Section 2.3.1 and Section 2.3.2 both make global assumptions about the spatial field. In particular, the approach of Jones et al. [41] assumes the field is a sum of a finite number of plane waves. Similarly, Kennedy et al. [42] assume a far-field signal model and global bound on the field amplitude. The subspace dimensionality approach [84] rests on a plane wave or far-field source model. The error measures ε_2 and ε_3, presented in Section 2.5.2, were related to a stochastic field assumed to be spatially stationary, again a global property.

In general, we are interested in the problem of describing a multipath field over the finite region of observation. In terms of the spatial field model $u(\boldsymbol{x})$, we are limited to the domain of interest $\|\boldsymbol{x}\| < R$ and desire a framework that is independent of the field properties over the extended domain $\|\boldsymbol{x}\| > R$. The global assumptions of the field in the frameworks presented for dimensionality require some constraint or bounded behaviour on the field for all $\boldsymbol{x} \in \mathbb{R}^2$. However, in practice, this will not be the case.

A practical field must be generated by some distribution of sources. For an ideal point source, the field will increase without bound in the vicinity of the source. Whilst this is not the case in general, it still is apparent that the presence of any real sources near the domain of interest will violate the global assumptions on the field. Any source distribution must be at an effectively infinite distance – this is known as the far-field approximation. Since the basic assumptions of Section 2.3.1 and Section 2.3.2 will not be valid for any sources near the domain of interest, the question naturally arises:
What effects do near-field sources and scattering objects have on the dimensionality of the multipath field?

For a near-field source at position $\boldsymbol{x}'$, the fundamental solution to the wave equation (2.14) in two dimensions is [91]

$$u(\boldsymbol{x}) = H_0^{(1)}(k\left\|\boldsymbol{x}-\boldsymbol{x}'\right\|) = \sum_{n=-\infty}^{\infty} H_n^{(1)}(k\left\|\boldsymbol{x}'\right\|)e^{-in\theta_{\boldsymbol{x}'}} J_n(k\left\|\boldsymbol{x}\right\|)e^{jn\theta_{\boldsymbol{x}}}. \tag{2.45}$$

The angles θ_x and $\theta_{\boldsymbol{x}'}$ are the polar co-ordinate angles of the points $\boldsymbol{x}$ and $\boldsymbol{x}'$. Since the field value at the source $u(\boldsymbol{x}') = H_0^{(1)}(0)$ is not defined, this expansion is convergent for the region from the origin to the source, $\|\boldsymbol{x}\| < \|\boldsymbol{x}'\|$.

From this we note that the coefficients of (2.15) for a point source at $\boldsymbol{x}'$ will be $\alpha_n = H_n^{(1)}(k\left\|\boldsymbol{x}'\right\|)e^{-in\theta_{\boldsymbol{x}'}}$ with $H_n^{(1)}(\cdot) = J_n(\cdot) + iY_n(\cdot)$ being the Hankel function of the first kind and $Y_n(\cdot)$ the Neumann function. The Bessel and Neumann functions are known to have the following asymptotic form for $n \gg z$ [160],

$$J_n(z) \approx \frac{1}{\sqrt{2\pi n}}\left(\frac{ez}{2n}\right)^n \qquad\qquad Y_n(z) \approx \sqrt{\frac{2}{\pi n}}\left(\frac{ez}{2n}\right)^{-n}. \tag{2.46}$$

It can be seen that the Neumann function will be at least exponentially increasing with order n once $n > ez/2$. Thus the terms of the expansion (2.45) multiply a component that is exponentially increasing with one that is exponentially decaying. The rate of convergence of this summation will depend on the relative rates of growth and decay of the components with respect to the summation order n.

Using the asymptotic forms (2.46), it can be shown that the terms of (2.45) will only decay like $(\|\boldsymbol{x}\| / \|\boldsymbol{x}'\|)^n/\pi n$. Given our domain of interest is $\|\boldsymbol{x}\| < R$ this suggests that sources near the boundary $\|\boldsymbol{x}'\| \approx R$ may introduce additional degrees of freedom, or at least worsen the error in the representation of a multipath field. Notably, if $\|\boldsymbol{x}'\| < R$ the field will have an unbound dimensionality. However, in this case we have introduced a singularity and thus a violation of our assumed field constraint within the domain of interest.

A sensible way to formulate the problem would be to confine the sources to the region $\|\boldsymbol{x}'\| > S$ where $S = R + \Delta$. This raises questions regarding the appropriate separation Δ between the observation region and the potential source region. How close can a source be without impacting the essential dimensionality of the field ? Is this buffering distance Δ dependent on the radius of the domain of interest R ?

Consider the average field error defined previously (2.34). We can relax the assumption of $E\{|\alpha_n|^2\} = 1$ for all n to introduce the effect of near-field sources (2.45). Consider a field generated by a source at a radius of S with unit average power, the coefficients will have power related to the squared magnitude of the Hankel function. If the source amplitude is normalised such that the field amplitude at the origin is unity then

$$E\left\{|\alpha_n|^2\right\} = \frac{|H_n^{(1)}(kS)|^2}{|H_0^{(1)}(kS)|^2}. \tag{2.47}$$

It is easily verified that this ratio is asymptotic to unity as $S \to \infty$. This provides a match to the far-field case considered previously. The average field error now becomes

$$\varepsilon_3 = 2 \sum_{n=N+1}^{\infty} \frac{|H_n^{(1)}(kS)|^2}{|H_0^{(1)}(kS)|^2} \left(J_n^2(kR) - J_{n-1}(kR)J_{n+1}(kR)\right). \tag{2.48}$$

Figure 2.3 shows the error contours of ε_3 for four different field radii as the source radius is increased away from the domain of interest. A low truncation error is achieved after sources are separated only a small distance from the domain of interest. The separation required is much less than the radius of the domain of interest. From this investigation it is demonstrated that only sources very close to the domain of interest will increase the dimensionality required to represent the field. Although the required truncation order does grow without bound as the source approaches the edge of the region $\|\boldsymbol{x}'\| \to R^+$, the effect is restricted to a region of the order of one wavelength.

The ability of a near-field source to have an impact on the dimensionality decays rapidly as the distance between the source and the domain boundary increases. This result is analogous to recent results regarding the extrapolation of a multipath field [126, 127]. Regardless of the size of the region of observation, the ability to predict the behaviour of a multipath spatial field decays rapidly based on the distance from the boundary of the observation domain. The duality of the problem here is apparent. If the impact of a source or field singularity diminishes rapidly outside the domain of interest, then given an observed field, it is difficult to ascertain the presence or absence of a singularity, and thus large uncertainty, in the extrapolated field outside the domain of interest.

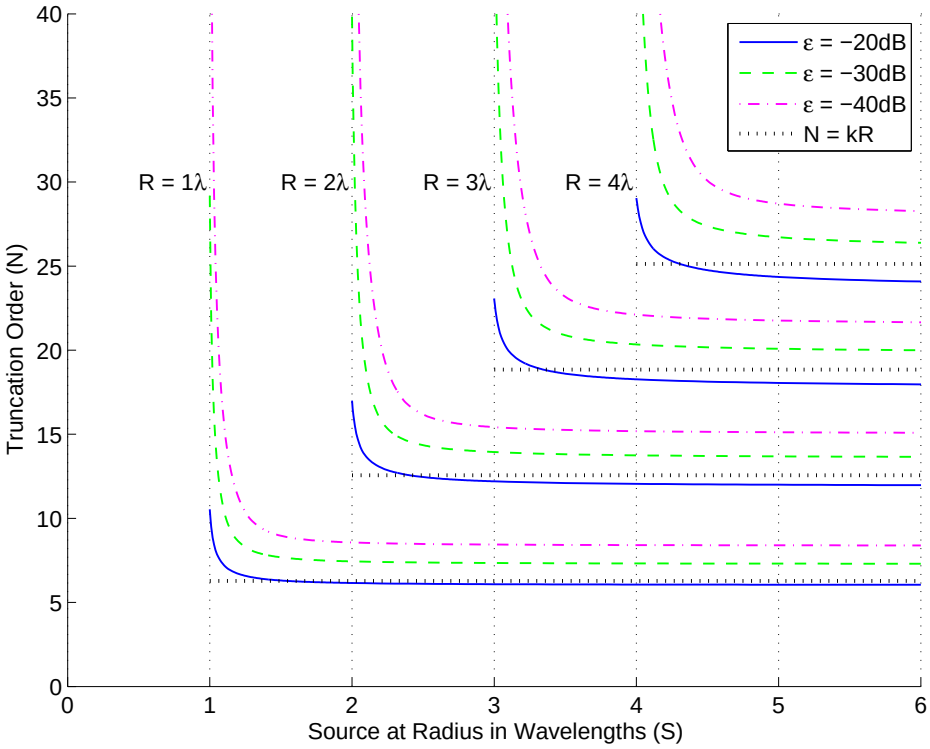

Figure 2.3: Error contours for the truncation of a field generated by near-field sources. For an observation region of radius $R = 1, 2, 3, 5\lambda$, sources are present from the abscissa radius S. The dimensionality approaches the asymptotic value within one wavelength $S - R > \lambda$. The sensitivity to near-field sources increases slightly with increasing observation radius. The lines corresponding to the truncation order $N = kR$ are shown for reference.

In answer to the question posed for the buffer distance between the domain of interest and any sources, the dimensionality reaches its asymptotic value for a buffer distance less than one wavelength. Furthermore, this does not vary significantly as the region size is increased.

2.7 Summary and Contributions

This chapter has developed the framework and clarified some existing results regarding the dimensionality of a multipath field over a finite domain of interest. It has been shown that this problem is important in developing a means of modelling and representation of a multipath field as is required to develop fundamental limits regarding the performance of communications systems using spatial diversity.

Central to this chapter is the result that the dimensionality of an arbitrary two-dimensional multipath field is related to the radial extent of the region of observation scaled by the wave-

length of the narrow-band field,

$$D = 2\lceil kR \rceil + 1 \approx 12.57R/\lambda. \tag{2.49}$$

While a numerical investigation indicates this is asymptotically correct for large regions, it is inappropriate for small regions. While a bound exists, it is conservative for larger radii. This motivated an attempt to create a tighter formal bound. Whilst some progress was made, it remains incomplete and important fundamental difficulties were identified. Through further analysis and numerical investigation it was shown that these dimensionality results can be extended to include fields with sources near the domain of interest, with the influence of sources decaying to insignificance outside a few wavelengths distance from the region boundary.

The following specific contributions were made in this chapter:

1. Provided a comparison of two existing dimensionality results:
   - A dimensionality of $2kR + 1$, although not rigorously derived, appears to be the correct asymptotic expression as $R \to \infty$.
   - The bound on the dimensionality of $ekR + 1$, valid for all R, is conservative by a multiplicative factor of $e/2 \approx 1.35$ for large R, but tighter at small R. In practical MIMO applications, small radii are arguable more relevant.
2. Presented a numerical study to consider the effective dimensionality of regions over a wide range of radii. This supported the use of the bound for small radii whilst the asymptotic dimensionality was $2kR$ as $R \to \infty$.
3. Pursued the path of deriving a bound to obtain a tighter result for the dimensionality bound as $R \to \infty$. This motivated the development of a conjectured bound on the Bessel function $J_n(z)$ in the region $z < n$. Several difficulties were highlighted in the attempt to use this in the development of a tighter dimensionality bound.
4. Considered the impact of near-field sources on the required dimensionality for the field representation. Analysis and numerical investigation demonstrated that the influence of sources need only be considered when within a few wavelengths of the region boundary.

Chapter 3

Impact of Direction of Arrival on Dimensionality

3.1 Introduction

The previous chapter developed the framework for understanding dimensionality of the multipath field. This chapter investigates the effect of restricting the direction of arrival of the multipath field.

Often in wireless communications the directions of arrival are constrained in direction or only span a sector. This restriction on the field can be incorporated into a model to use a more appropriate basis function and more compact parameterisation of the field. It has been noted that the richness, dimensionality or degrees of freedom for a spatial field decrease as the angular diversity is reduced [47, 84, 156]. Whilst such results suggest the dimensionality increases linearly with the angular spread, this has not been rigorously proven for a general region. A formal expression of this relationship is an important tool in better understanding the impact of angular diversity on the upper limits of the capacity of a communications system operating in a finite domain of interest. Conventional works on the limits of the capacity of a multiple antenna communications system rely on specifics of the antenna geometry or spatial correlation models. By capturing the inherent dimensionality of the spatial field, it is possible to show the existence of an upper limit without reference to any specific configuration, thus providing a guide and reference for optimal system design.

The existing results that relate dimensionality to angular diversity are not rigourous and are based on simulation and approximations. Our aim is to provide a tight foundation to these intuitive results. We have seen that the dimensionality varies linearly with the radius of

the domain of interest R. We now introduce a second variable, A, representing the angular diversity. This leads to a spatial analogy of the well known $2WT$ dimensionality of time-bandwidth constrained signals discussed in Section 2.2. In this work we consider the problem of a circular region with the source directions constrained to a single contiguous interval. The effect of different angular distributions is the subject of Chapter 4. The impact of discrete clusters of scatterers was considered in [93].

The work presented in this chapter provides a formal proof of the linear relationship between the dimensionality and angular spread. This key result has been published by the author [157].

3.2 Representation by Wave-Field Basis Functions

A representation for a wave-field based on the basis functions of the wave equation was introduced in Section 2.3.1. Consider a spatial field in two dimensions, $\boldsymbol{x} \in \mathbb{R}^2$. The solutions to the homogenous wave equation can be represented on a countable orthogonal basis, β_n, as shown previously (2.15),

$$u(\boldsymbol{x}) = \sum_{n=-\infty}^{\infty} \alpha_n \beta_n(\boldsymbol{x}) \quad \text{with} \quad \beta_n(\boldsymbol{x}) = J_n(k \left\|\boldsymbol{x}\right\|) e^{jn\theta_{\boldsymbol{x}}}, \tag{3.1}$$

with $J_n(\cdot)$ the Bessel function of order n and $\theta_{\boldsymbol{x}}$ the angle of $\boldsymbol{x}$. Over a domain of interest, $\mathbb{B}_R^2 = \{\boldsymbol{x} \in \mathbb{R}^2 : \|\boldsymbol{x}\| \leq R\}$, define the standard integral inner product, and note that,

$$\langle \beta_n, \beta_m \rangle_R = \int_{\mathbb{B}_R^2} \beta_n(\boldsymbol{x}) \overline{\beta_m(\boldsymbol{x})} dv = 2\pi \delta_{mn} \int_0^R J_n(kr)^2 r dr \tag{3.2}$$

where $\delta_{mn} = 1$ if $m = n$ and 0 otherwise. Using an integration identity from [164] then

$$\left\|\beta_n\right\|_R = \pi R^2 \left(J_n(kR)^2 - J_{n-1}(kR) J_{n+1}(kR) \right) \tag{3.3}$$

which is asymptotic to $2R/k$ as $R \to \infty$.

3.3 Representation by Herglotz Angular Function

The Herglotz representation of a wave-field is described in [91] and was proposed as a generalised framework for source distributions [165]. The concept is introduced here, specific to the two-dimensional case, to provide the machinery for the main result. A standard model

of a multipath field is to represent it as a superposition of plane waves. This can be generalised in two dimensions to a continuous distribution of far-field sources on the interval $\mathbb{S}^1 = [-\pi, \pi)$,

$$u(\boldsymbol{x}) = \int_{-\pi}^{\pi} g(\theta) e^{jk\boldsymbol{x}.\widehat{\boldsymbol{\theta}}} d\theta \tag{3.4}$$

with $\widehat{\boldsymbol{\theta}}$ as the unit vector with direction θ. If the representation of the wave-field $g(\theta)$ is square integrable, that is $g \in L^2(\mathbb{S}^1)$, this is known as the *Herglotz Kernel* and (3.4) is the *Herglotz Wave Function*. A plane wave with direction of arrival θ has coefficients $\alpha_n = j^n e^{-jn\theta}$. Thus the coefficients for the overall field will be

$$\alpha_n = \frac{1}{2\pi} \int_{-\pi}^{\pi} g(\theta) j^n e^{-jn\theta} d\theta \tag{3.5}$$

This relationship is an inverse Fourier transform. The restriction of $g \in L^2(\mathbb{S}^1)$ is equivalent to $\sum |\alpha_n|^2 < \infty$ by Parseval's identity. This slight restriction provides the significant advantage of placing the problem into a Hilbert space. With this space, any bounded field, including a plane wave $g \in L^1(\mathbb{S}^1)$, can be represented to arbitrary precision over a finite domain of interest [80].

We can now define the class of fields represented by a restricted direction of arrival.

Definition 3.1 Multipath field with restricted direction of arrival.
A restricted direction field is represented by a Herglotz Wave Function, $g_A \in L^2(\mathbb{S}^1)$, such that

$$g_A(\theta) = 0 \quad A < |\theta| \leq \pi. \tag{3.6}$$

In this formulation, the angular range of the multipath field is centred around a zero mean without any loss of generality.

The space of Herglotz Wave Functions with restricted angle of arrival is a linear subspace of the full set of Herglotz Wave Functions. It is noted that the restricted direction of arrival field $g_A(\theta)$ represents a distribution of far-field sources. A near-field source could be approximated by a specific far-field distribution, however the associated angular representation would not be strictly restricted in angle. Thus the definition we adopt is specific to restricted direction of arrival far-field wave functions. In practice, this result is appropriate with all sources a small distance beyond the domain of interest, as was demonstrated in Section 2.6.

3.4 Dimensionality of Multipath Field in a Region

It is known that the modal basis (3.1) is optimal under truncation for the representation of a field over a disk of radius R where the source distribution is unconstrained [80]. The truncation,

$$u_N(\boldsymbol{x}) = \sum_{n=-N}^{N} \alpha_n \beta_n(\boldsymbol{x}) \quad \text{with} \quad \beta_n(\boldsymbol{x}) = J_n(k\,\|\boldsymbol{x}\|)e^{jn\theta_{\boldsymbol{x}}} \tag{3.7}$$

provides an approximation of the field with exponentially decreasing error for $N > \pi eR/\lambda$ [42]. This provides a model of the field with $2N+1$ parameters α_n for $n = -N, \ldots, N$.

The general approach to dimensionality was discussed in Section 2.3 where the truncation point was considered so that the error in representation was sufficiently small. Here we present a tighter formal definition. The dimensionality is defined as the point beyond which an exponential improvement in the approximation error can be achieved regardless of the field.

Definition 3.2 Essential Dimensionality of a space of Multipath fields.
Consider a particular space of fields, $\mathcal{U}$, defined on the domain of interest $\mathbb{B}_R^2$. If for some value N_o, and choice of $\{\psi_i\}_{i=0}^{\infty}$, and for any $u \in \mathcal{U}$

$$\left\| u - \sum_{i=0}^{N_o} \langle u, \psi_i \rangle \psi_i \right\|_{\mathbb{B}_R^2} \leq \epsilon < \infty \tag{3.8}$$

and for any $n > N_o$,

$$\left\| u - \sum_{i=0}^{n} \langle u, \psi_i \rangle \psi_i \right\|_{\mathbb{B}_R^2} \leq \epsilon\, e^{-\alpha(n-N_o)} \tag{3.9}$$

for some fixed $\alpha > 0$, then we say the space $\mathcal{U}$ has essential dimension of N_o.

Definition 3.2 is similar in application to the concept of "essential dimension" in operator approximations [166]. Although this definition of dimensionality was not formally adopted in Chapter 2, the bound that was developed in Section 2.3.1 does satisfy this definition [41].

The following lemmas are presented towards the main result.

Lemma 3.3 Equivalence of Multipath field with Restricted Direction of Arrival and a Bandlimited sequence.
The modal coefficients α_n, as determined by (3.5), of a restricted direction field are a bandlimited sequence. Other than the trivial solution $\alpha_n = 0 \; \forall \; n$, the sequence α_n will have infinite support such that given any N there exists $|n| > N$ such that $\alpha_n \neq 0$.

Proof of Lemma 3.3. From (3.5) we can express the modal coefficients of the field

$$\alpha_n = \frac{1}{2\pi} \int_{-\pi}^{\pi} g_A(\theta) j^n e^{jn\theta} d\theta = \int_{-A}^{A} g_A(\theta) j^n e^{jn\theta} d\theta. \tag{3.10}$$

By construction, the sequence α_n will be a bandlimited sequence. A corollary of this is that it will have infinite support. □

Lemma 3.4 Restricted DOA Field on Finite Domain $\equiv$ Finite Bandlimited Sequence.
A restricted direction field can be approximated over a finite domain, $\{\boldsymbol{x} : \|\boldsymbol{x}\| \leq R\}$, by $2N+1$ terms from an infinite bandlimited sequence where $N > \lceil ekR/2 \rceil$. The error resulting from the truncation to $2N+1$ terms will be bounded and will decrease exponentially as N is increased.

Proof of Lemma 3.4. This is immediately apparent from Lemma 3.3 and (3.7) taking a finite truncation of bandlimited sequence. The restricted direction of arrival fields are a subspace of the Herglotz wave-fields. We can use the result from [42] to determine an appropriate truncation. □

A bandlimited sequence that is also confined[1] to a finite length has dimension approximated by the product of its length and fractional bandwidth [167]. Whilst this result is only true asymptotically as the length increases [168] it has been used effectively for small sections of bandlimited sequences that are not confined in time [169, 170]. A variant of the prolate spheroidal functions, the Slepian series [171], provides an optimal basis for representing the $2N+1$ length bandlimited sequence α_n with a reduced number of coefficients.

[1] Here confined is in reference to most of the energy being contained in a finite length. Strictly a bandlimited sequence cannot also be time limited.

3.5 Slepian Series for Representing Bandlimited Sequence

The Slepian series are a family of discrete series basis function, each member of which provides a set of basis functions for a finite length sequence of defined length. Each member of the family is specified by a sequence length, N, and the fractional bandwidth W. The fractional bandwidth is related to the bandlimited process that we infer the sequence of N discrete samples are drawn from. If the sequence of N discrete samples was a section of a larger periodic sequence with a period of N, we could use the standard Fourier transform or complex harmonic exponentials $e^{jnm/N}$ where n is the sample index and m is the index of the basis functions. A bandlimited periodic signal could be represented from only the low order m terms through to the limiting frequency in the series. For such a periodic sequence, it only makes sense to consider discrete steps in the bandwidth of the entire series. In the more general case, where N samples are drawn from a bandlimited process that is not periodic, the Slepian Series is more appropriate. In this case the bandwidth, W, is a continuous parameter.

Define $v_n^m(N,W)$ as the sample index $n = 0,\ldots,N-1$ of the order $m = 0,\ldots,N-1$ Slepian series basis function of length N with an associated scaled bandwidth of $W \in [0,1/2]$. These series are the ordered solutions of the system of equations [167]

$$\sum_{n'=0}^{N-1} \frac{\sin 2\pi W(n-n')}{\pi(n-n')} v_{n'}^m(N,W) = \lambda_m(N,W) v_n^m(N,W)\,. \tag{3.11}$$

The series is orthonormal in that

$$\sum_{n=0}^{N-1} v_n^m(N,W)\, v_n^{m'}(N,W) = \delta_{mm'} \tag{3.12}$$

thus the N sequences, $m = 0,\ldots,N-1$, form a complete basis set for all sequences of length N. The eigenvalues $\lambda_m(N,W)$ are ordered monotonically decreasing between 1 and 0. They represent the maximum ratio of the energy of the signal within the N samples to that of the total energy of a bandlimited extension of that same sequence. Conversely, if we know the N samples are drawn from a bounded and infinite length bandlimited series, the eigenvalues $\lambda_m(N,W)$ are related to the expected energy in the projection of the discrete set of samples onto each of the basis functions.

Figure 3.1 shows the first six Slepian series of length 20 with an associated bandwidth of $W = 0.2$. Also shown in the figure are the bandlimited extrapolations of the basis functions. It can be seen that after the fourth basis function the eigenvalues drop rapidly and the bandlimited extension becomes increased in magnitude.

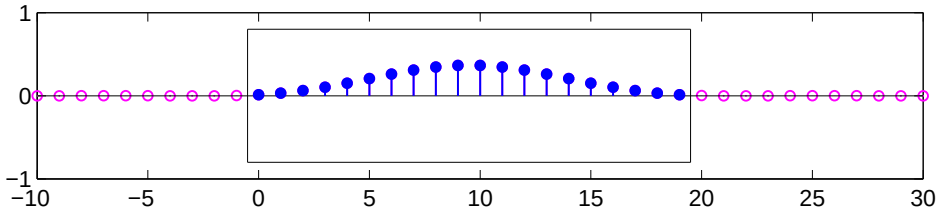

(a) $v_n^0(20, 0.2) \quad \lambda_0(20, 0.2) = 0.999952$

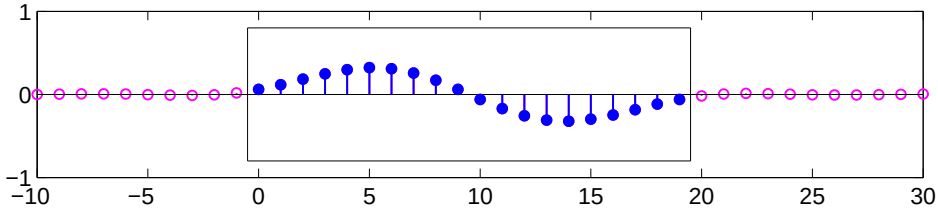

(b) $v_n^1(20, 0.2) \quad \lambda_1(20, 0.2) = 0.997802$

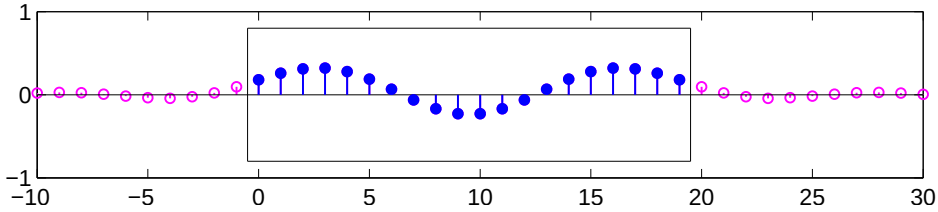

(c) $v_n^2(20, 0.2) \quad \lambda_2(20, 0.2) = 0.961277$

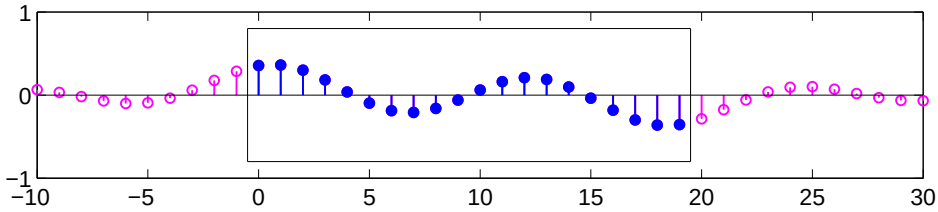

(d) $v_n^3(20, 0.2) \quad \lambda_3(20, 0.2) = 0.724589$

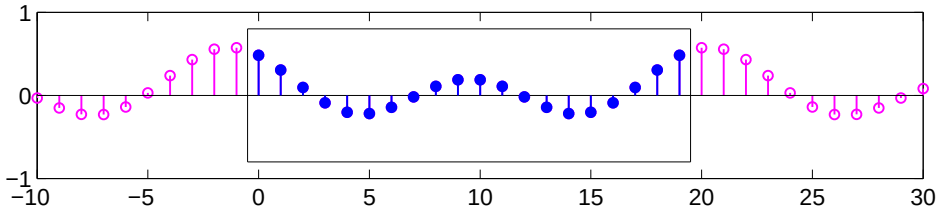

(e) $v_n^4(20, 0.2) \quad \lambda_4(20, 0.2) = 0.272321$

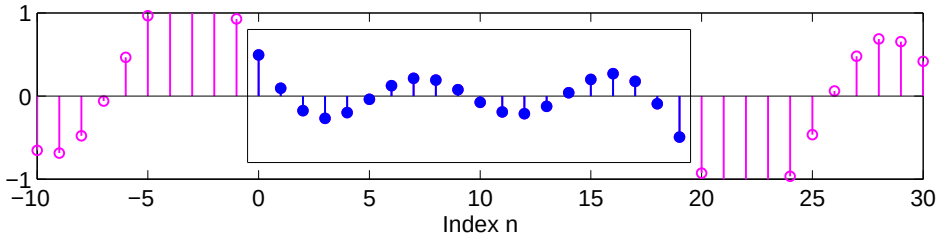

(f) $v_n^5(20, 0.2) \quad \lambda_5(20, 0.2) = 0.040849$

Figure 3.1: Slepian series for length $N = 20$ and $W = 0.2$. The first six basis functions are shown along with the bandlimited extension. The region of the defined series is shown with the inner box. Beyond the critical basis function around $m = 4$ the eigenvalues drop rapidly and the bandlimited extension increases in magnitude with less of the signal energy within the inner series.

Whilst the extensive works of Slepian [142, 167] set out some asymptotic approximations, the Slepian series have no simple algebraic expression. Their properties and behaviours can all be derived from the eigenequation (3.11) from which they are derived. Whilst this may make them appear as a fairly esoteric function, the same is true of many other transcendental functions. It is only that we are more familiar with functions such as the Bessel functions or even trigonometric functions that we consider them easier to use and apply.

The nature and behaviour of the eigenvalues $\lambda_m(N, W)$ has been studied in detail [167] and is key to the result of the $2WT$ result discussed in Section 2.2. From the analysis of Slepian, we note the approximation for the eigenvalues [167, eq (61)],

$$\lambda_m(N, W) \approx \frac{1}{1 + \exp\left[-b\left(2WN - m - 1/2\right)\right]}$$
$$b = \frac{\pi^2}{\log(8N) + \log(\sin 2\pi W) + \gamma} \tag{3.13}$$

where $\gamma = 0.5772156\ldots$ is the Euler-Mascheroni constant. This leads to the following assumption.

Assumption 3.5 Exponential upper bound for Slepian series eigenvalue.
The eigenvalue $\lambda_m(N, W)$ associated with the m^{th} basis function of the Slepian series of length N and associated bandwidth W is bounded from above by

$$\lambda_m(N, W) \leq e^{b(2WN-m-1/2)} \quad \text{where} \quad b = \frac{\pi^2}{\log(8N) + \log(\sin 2\pi W) + \gamma}. \tag{3.14}$$

The bound (3.14) is a true upper bound for the approximation (3.13) of the eigenvalue and is tight in the limit $m \to N - 1$ for large N. The assumption that this upper bound also holds for the true eigenvalue has been validated through an extensive computational investigation up to $N \approx 200$ for $0 < W < 1/2$. Across this range the bound was satisfied and there was no indication at the boundaries of the test range that the bound would not hold across a much larger domain.

A critical review of the current practice in signal processing reveals that far too often we apply the theories of complex exponential basis expansions through techniques such as the Fourier transform, without being aware of the effect of the inherent assumption of periodicity. This can cause fundamental limitations in the accuracy of signal approximation and negatively impact communications system performance [169]. This section should serve to highlight some of the theory and encourage the use of the Slepian series for representing a finite section of a non-periodic discrete sampled signal.

3.6 Dimensionality of Restricted Direction of Arrival Field

The preceding sections have demonstrated that a multipath field over a finite domain of interest with radius R can be represented by $2N+1$ terms α_n with $N \cong \pi e R/\lambda$ [42]. Furthermore, where the direction of arrival is restricted to an angular section A, this sequence is representative of a bandlimited sequence with bandwidth $A/2\pi$. Thus we can use the Slepian series basis of length $2N+1$ and associated bandwidth $W = A/2\pi$. Following convention, the Slepian series are indexed $n = 0, \ldots, N-1$ whilst our modal coefficients are indexed $n = -N, \ldots, N$. Thus we use the index shifted Slepian series $v^m_{n+N}(2N+1, A/2\pi)$.

Consider an approximation of the α_n, $n = -N, \ldots, N$ coefficients using the first M basis function from the Slepian series,

$$\widehat{\alpha}_n = \sum_{m=0}^{M-1} c_m v^m_{n+N}(2N+1, A/2\pi)\,. \tag{3.15}$$

The sum is over the M terms, $M \leq 2N+1$. We will use the shorter notation v^m_{n+N} from this point dropping the length and bandwidth specification of the Slepian series. The Slepian series is a complete real orthonormal basis so the coefficients c_m can be determined by projection,

$$c_m = \sum_{n=-N}^{N} \alpha_n v^m_{n+N}. \tag{3.16}$$

In the case of $M = 2N+1$ the representation is complete and $\widehat{\alpha}_n = \alpha_n$.

Definition 3.6 Slepian Approximation for Spatial Field.
The M^{th} order Slepian approximation to the N^{th} order modal field is given by

$$\widehat{u}_N(\boldsymbol{x}) = \sum_{n=-N}^{N} \widehat{\alpha}_n \beta_n(\boldsymbol{x}) = \sum_{n=-N}^{N} \sum_{m=0}^{M-1} c_m v^m_{n+N} \beta_n(\boldsymbol{x}) \tag{3.17}$$

where

$$c_m = \sum_{n=-N}^{N} \alpha_n v^m_{n+N} \qquad \text{and} \qquad \widehat{\alpha}_n = \sum_{m=0}^{M-1} c_m v^m_{n+N}(2N+1, A/2\pi)\,. \tag{3.18}$$

Lemma 3.7 Approximation of Restricted DOA Field.
Given a field with restricted direction of arrival,

$$u(\boldsymbol{x}) = \int_{-A}^{A} g(\theta) e^{jk\boldsymbol{x}.\widehat{\boldsymbol{\theta}}} d\theta \qquad g \in L^2(\mathbb{S}^1), \tag{3.19}$$

the field $u(\boldsymbol{x})$ on the domain $\mathbb{B}_R^2 = \{\boldsymbol{x} \in \mathbb{R}^2 : \|\boldsymbol{x}\| \leq R\}$ can be approximated by a field with $M \leq 2N+1$ parameters c_m,

$$\widehat{u}_N(\boldsymbol{x}) = \sum_{n=-N}^{N} \sum_{m=0}^{M-1} c_m v_{n+N}^m \beta_n(\boldsymbol{x}) \tag{3.20}$$

where $N = \lceil ekR/2 \rceil$ with the error $\|u - \widehat{u}_N\|_R$ bounded and decreasing exponentially for

$$\frac{M}{2N+1} \geq \frac{A}{\pi}. \tag{3.21}$$

A brief explanation of this Lemma is warranted. The lower bound for the required number of terms M grows linearly with the ratio of the support of the angular spectrum compared to that of a full receiver $2A/2\pi = A/\pi$. The maximum number of terms is the same for the full receiver being $2N+1$.

Proof of Lemma 3.7. Given the orthogonality of β_n on the domain of interest $\|\boldsymbol{x}\| < R$, it can be seen that

$$\|u - \widehat{u}_N\|_R^2 = \|u - u_N\|_R^2 + \|u_N - \widehat{u}_N\|_R^2 \tag{3.22}$$

and using the triangle inequality we can obtain

$$\|u - \widehat{u}_N\|_R \leq \|u - u_N\|_R + \|u_N - \widehat{u}_N\|_R . \tag{3.23}$$

The first term of the error bound $\|u - u_N\|_R$ can be made small by the appropriate selection of $N > \pi eR/\lambda$ [42], beyond which this term will decrease exponentially. This results in a sequence of $2N+1$ terms α_n, $n = -N, \ldots, N$ to represent the spatially limited approximation of the field $u_N(\boldsymbol{x})$.

The second term of the error bound (3.23), $\|u_N - \widehat{u}_N\|_R$ is the residual field error from the Slepian expansion of the $2N+1$ term bandlimited sequence. The Slepian series are also orthogonal for $n = -\infty, \ldots, \infty$ with the energy in this infinite extension given by λ_m^{-1}

where λ_m is the eigenvalue associated with the m^{th} Slepian sequence. The energy in the infinite sequence obtained by extrapolating the $2N+1$ terms using the complete Slepian sequence must have less energy than the original α_n sequence. This provides the inequality

$$\sum_{n=-\infty}^{\infty} |\alpha_n|^2 \geq \sum_{m=0}^{2N} \frac{|c_m|^2}{\lambda_m} \geq \frac{1}{\lambda_M} \sum_{m=M}^{2N} |c_m|^2 \tag{3.24}$$

since λ_m is strictly decreasing. Given that $\|\beta_n\|_R$ is approximately bounded by $2R/k$, consider the second term of (3.22) and use the result (3.24) to obtain

$$\begin{aligned} \|u_N - \widehat{u}_N\|_R^2 &= \sum_{n=-N}^{N} (\alpha_n - \widehat{\alpha}_n)^2 \|\beta_n\|_R^2 \leq \frac{2R}{k} \sum_{m=M}^{2N} |c_m|^2 \\ &\leq \frac{2R}{k} \lambda_M \sum_{n=-\infty}^{\infty} |\alpha_n|^2. \end{aligned} \tag{3.25}$$

Using Assumption 3.5, and making the substitutions $N \triangleq 2N+1$ and $W \triangleq A/2\pi$ gives the bound

$$\lambda_m \leq \exp\left[b \left(\frac{A(2N+1)}{\pi} - m - 1/2 \right) \right] \tag{3.26}$$

where

$$b = \frac{\pi^2}{\log(16N+8) + \log(\sin A) + \gamma}. \tag{3.27}$$

Thus $\lambda_m \leq 1$ and decreases exponentially for

$$m \geq \frac{A}{\pi}(2N+1) - \frac{1}{2}. \tag{3.28}$$

The Herglotz condition, $g \in L^2(\mathbb{S}^1)$, implies that the total energy in the infinite bandlimited sequence $\sum |\alpha_n|^2$ is finite. This combined with (3.25) and (3.22) completes the proof. □

Theorem 3.8 Dimensionality of a Multipath Field with Restricted Direction of Arrival. *A field generated by far-field sources with direction of arrival restricted to* $[-A, A]$, $A \leq \pi$, *with domain of interest constrained to* $\mathbb{B}_R^2 = \{\boldsymbol{x} \in \mathbb{R}^2 : \|\boldsymbol{x}\| \leq R\}$, *has an essential dimension of*

$$D = 2N' + 1 \quad \text{where} \quad N' = \left\lceil \frac{ekR}{2} \frac{A}{\pi} \right\rceil \tag{3.29}$$

with the definition of effective dimension as stated in Definition 3.2.

Proof of Theorem 3.8. Following from Lemmas 3.3,3.4 and 3.7, we have a constructive representation for the field where the error is well behaved for $M > A(2N+1)/\pi - 1/2$. Since $a/\pi \leq 1$ we can simplify this expression in line with the previous works to state the dimensionality as $2N' + 1$ where $N' = \lceil ekR/2 \; A/\pi \rceil$ with $\lceil \cdot \rceil$ the integer ceiling function. This completes the proof. □

This result builds on the previous dimensionality results for an isotropic field. As discussed in Section 2.3 this bound is not asymptotically tight for large regions and overestimates the true dimensionality. We can use the same reasoning of the Slepian series approximation to a truncated field of order $N = \lceil kR \rceil$. This provides the result for an approximation of the dimensionality of the multipath field with restricted direction of arrival

$$D = 2 \left\lceil \frac{kRA}{\pi} \right\rceil + 1. \tag{3.30}$$

3.7 Numerical Analysis of Multipath Dimensionality

The previous section set out a proof for the central dimensionality result of this chapter. In this section we compare the bound obtained with numerical calculations based on the actual restricted direction of arrival field basis expansion. In order to determine the dimensionality of the space of restricted direction of arrival fields over a finite domain, we need to determine the optimal basis for representation of such fields. The solution to this problem can be posed as an eigenequation which can be solved numerically. This approach will be discussed in greater detail in Chapter 4 Section 4.5 of this thesis.

The wave functions with restricted direction of arrival that are most concentrated in the domain $\mathbb{B}_R^2$ satisfy the eigenequation

$$\lambda_n g_n(\theta) = \frac{1}{4\pi^2} \int_{-A}^{A} g_n(\phi) \int_{\mathbb{B}_R^2} e^{kj\boldsymbol{x}.(\widehat{\boldsymbol{\phi}}-\widehat{\boldsymbol{\theta}})} d\boldsymbol{x} d\phi = \frac{kR}{2\pi} \int_{-A}^{A} g_n(\phi) \frac{J_1(zR)}{z} d\phi \tag{3.31}$$

with $z = 2\sin((\phi - \theta)/2)$. The theory behind this eigenequation is presented in Section 4.3 and the specific case of a circular region is analysed in Section 4.4.

A Q point quadrature rule on the interval $[-A, A]$ is used such that

$$\int_{-A}^{A} g(\theta) d\theta \approx \sum_{i=1}^{Q} w_i g(\theta_i). \tag{3.32}$$

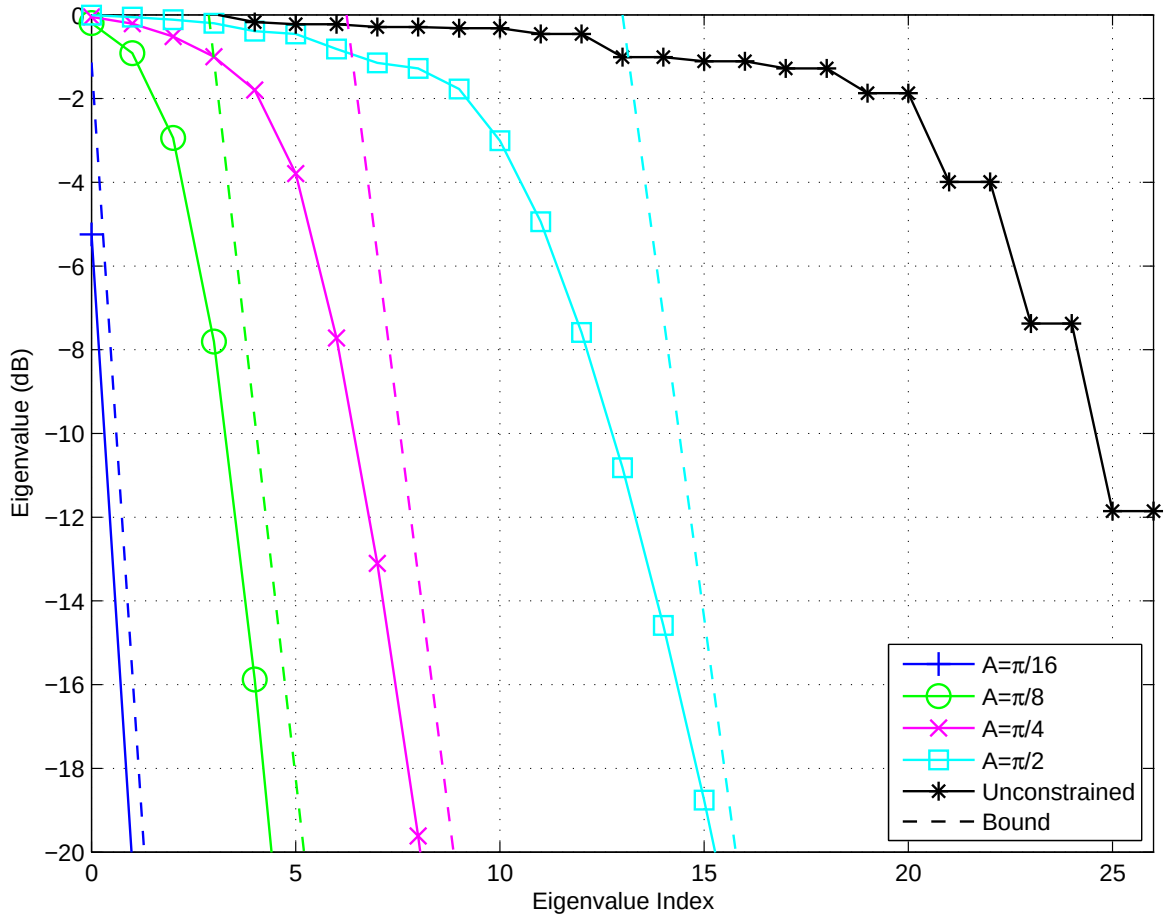

Figure 3.2: Plot of the eigenvalues and bounds for a region $R = 2\lambda$ with successive restriction on the directions of arrival. The eigenvalues reflect the number of significant degrees of freedom of the field. The dashed line for each case is the bound (3.26). The bound for the eigenvalues represent a fairly tight bound on the actual eigenvalues at around -20dB. This corroborates the linear relationship of dimensionality to the angular range of the field.

We can approximate (3.31) with the linear system of equations. This provides a numerical approximation of the first Q eigenvalues of the eigenequation (3.31) as the eigenvalues of a $Q \times Q$ matrix. This numerical method for solving such equations is detailed in Section 4.5.

Figure 3.2 compares the numerically determined eigenvalues for the constrained angle of arrival problem to the bound presented (3.26). This figure shows the upper bound and linear dependence on the effective dimensionality with the direction of arrival restriction. For the figure, at $R = 2/\lambda$ a truncation point $N = \lceil kR \rceil = 13$ was selected. The use of $N = \lceil keR/2 \rceil = 18$ presents a generous bound in all cases.

3.8 Summary and Contributions

Together with the preceding chapter, this chapter has provided an analysis of the dimensionality of a two-dimensional multipath field. The dimensionality is dependent on the size of the region of observation and the angular diversity of the incident field.

Given a two-dimensional multipath field over a region with radius R and the arrival from sources restricted to the range $|\theta| < A$ the dimensionality of the field is given by

$$D = 2\left\lceil \frac{kRA}{\pi} \right\rceil + 1 = 2\left\lceil \frac{2RA}{\lambda} \right\rceil + 1. \tag{3.33}$$

For large regions $R \gg \lambda$, this dimensionality is consistent with a modelling error across the region of -20dB. A representation of a random multipath field with this number of terms would be expected to capture 99% of the energy of the random field. For smaller regions and low dimensionality a more conservative estimate with a formal error bound would be $2\lceil eRA/\lambda \rceil + 1$.

The following specific contributions were made in this chapter:

1. Provided a formal proof of the linear bound between restricting the direction of arrival for a multipath field and the associated field dimensionality. This result will be the subject of further analysis in Chapter 4.

2. Constructed an approximation for the optimal basis function of a restricted direction of arrival multipath field. A field over $\|x\| \leq R$ with direction of arrival constrained to $[-A, A]$ can be represented by

$$\widehat{u}_N(\boldsymbol{x}) = \sum_{0}^{M-1} c_m \widehat{\beta}_m(\boldsymbol{x}) \qquad M \leq 2N+1, \quad N = \left\lceil \frac{ekR}{2} \right\rceil \tag{3.34}$$

$$\widehat{\beta}_m(\boldsymbol{x}) = \sum_{n=-N}^{N} v_{n+N}^m J_n(k\,\|\boldsymbol{x}\|) e^{jn\theta_{\boldsymbol{x}}} \qquad m < M \tag{3.35}$$

   where v_{n+N}^m is the $(n+N)^{\text{th}}$ term of the m^{th} order Slepian series of length $2N+1$ with bandwidth $A/2\pi$ [167]. The functions $\widehat{\beta}_m(\boldsymbol{x})$ approximate the optimal basis functions and can be used as an efficient representation for a multipath field with restricted angular diversity.

3. Detailed the Slepian series and provided an example application where it can be used to represent a finite sequence of samples drawn from an infinite aperiodic bandlimited process.

In conclusion, both the size of the domain of interest and the extent of angular diversity linearly impact the dimensionality of a multipath spatial field. Removing the integer ceiling function from the bound we can see in the limit that $D = 2\ kR\ A/\pi$ when $kRA/\pi \gg 1$. This is analogous to the bandlimited finite length signal dimensionality result $2WT$ detailed in Section 2.2. It is apparent from the investigation that there are some similarities between the two bodies of research. However, the spatial domain and the circular and spherical spatial regions introduce additional complexity and nuances to the problem. Generally, the two areas share several key observations:

- The dimensionality is asymptotic to a simple expression as it becomes large.
- Care must be taken when the expression predicts a small dimensionality since the transition from significant to insignificant terms in any expansion is not abrupt.
- Obtaining specific approximations and formal bounds for the truncation error and dimensionality is a difficult and tedious task.

As has been the case historically for the bandlimited signals, a better understanding of the dimensionality and the nature of the basis functions will aid in the development of performance bounds and suitable algorithms. This is an essential part of the development and use of continuous spatial models for signal processing, especially in the area of spatial MIMO communications.

The nature of the angular diversity considered in this chapter was a uniform distribution of sources over a single angular sector. In practice, we often deal with more general source distributions, or characterisations of random processes that describe the nature of the source distribution. Also, the domain of interest may be something other than a simple circular region. In the following chapter we will consider the process of determining the optimal basis representation for a spatial field over a general domain of interest and a more general description of the angular source distribution.

Chapter 4

Angular Domain Representation of a Random Multipath Field

4.1 Introduction

Recent interest in the use of multiple antenna communications systems (MIMO) stemmed from key publications [6, 13] that suggested the potential for a linear growth in capacity with the number of antennas utilised. It was soon realised that correlation between the antenna elements due to the nature of wave propagation and the scattering environment would have a negative effect on capacity [21, 30].

In a random multipath field there is a direct relationship between the spectrum of received power across the incident angular range and the spatial correlation of the field [172–175]. Determining the spatial correlation would require extensive measurement of the field throughout a spatial region. Alternately, an estimate of the angular power distribution may come from knowledge of the characteristics and distribution of scatterers in the multipath propagation environment. For this reason it is useful to have a framework to represent and analyse a multipath random field in the angular domain. Such a framework will facilitate the understanding and modelling of the spatial aspects of the wireless channel. The set of directions the multipath is coming from is something that can be directly measured and has direct physical interpretation.

The use of the angular domain also provides a simplification of the problem of modelling multipath fields. A two-dimensional narrow-band field can be represented by either the field amplitude and phase across the two dimensions, or alternately by a far-field distribution over a single dimension of angle of arrival. The angular domain implicitly captures the constraint

of the wave equation by only representing fields that can be generated by propagating waves. Similarly in three dimensions, a three-dimensional spatial wave-field is constrained to satisfy the wave equation, but the angular domain description is only two dimensional (function of elevation and azimuth).

Various MIMO models based on the angular domain representation have been proposed. The work of Pollock et. al. [47] utilised a truncation of the modal representation of the field at the transmitter and receiver. The virtual channel model proposed by Sayeed [66] uses a discrete set of resolvable angular ranges to model the channel.

This chapter is concerned with the most efficient representation of a random multipath field in the angular domain. The detailed analysis of the spatial field at a single end of the channel provides a framework which can then be extended to consider the complete MIMO channel. Recent results have demonstrated that a multipath field has a finite essential dimensionality [41, 78, 80]. Thus, given an arbitrary power spectrum, it should be possible to represent this random process with a finite number of deterministic function components combined with random weights (random variables). This chapter addresses the question of determining the optimal deterministic components (functions in the angular domain) and analysing the critical attributes of the system that will influence the solution. This work has been submitted for publication and is currently under review [176].

The remainder of the chapter is structured as follows. Section 4.2 introduces the angular domain for representing a random multipath field and sets out the problem of determining the optimal finite dimensional angular representation. Section 4.3 derives an eigenequation that determines the optimal basis for representing a multipath field in the angular domain. This is the main result of the chapter. Section 4.4 shows that the eigenequation has a simple solution for the circular isotropic two-dimensional field, but is not tractable for other configurations. Section 4.5 presents a suitable numerical method to obtain specific solutions. Section 4.6 provides a study of the gross effects and complexity of the basis functions as the power spectrum and region shape are altered. Section 4.7 considers the effect of the region and angular spectrum on the number of significant components. Section 4.8 provides a summary and closing remarks.

The contribution of this chapter is the formal development of a framework for representing a multipath random field in the angular domain. The formulation follows classic signal theory [159] with new material covering the application to the random multipath spatial field. The new framework and analysis considers more general region shapes beyond the simple uniform linear array, which has been covered in other works. The region of interest for the spatial field shapes the optimal representation for the spatial field. The numerical

method and examples presented provide some insight into the critical factors effecting the basis function for the angular domain representation.

4.2 Problem Formulation

4.2.1 Angular Domain Representation

To address the problem of modelling a random multipath field, we consider a scalar wave-field $u(\boldsymbol{x})$ for $\boldsymbol{x} \in \mathbb{R}^3$. As discussed in Section 1.4, the main interest is in spatial fields and the characteristics of wave propagation. We restrict our attention to the case of narrow-band fields. For a region free of sources, $u(\boldsymbol{x})$ will satisfy the wave equation, also known as the Helmholtz equation [91, 177],

$$\triangle u(\boldsymbol{x}) + k^2 u(\boldsymbol{x}) = 0, \tag{4.1}$$

where $\triangle$ is the Laplacian, and $k = 2\pi/\lambda$ is known as the wave number.

The wave equation constraint implies that the field in a region free of sources can be completely determined from the field around a surface enclosing that region. This property is referred to as Huygen's principle [91]. Regardless of the richness or complexity of the scattering environment, there will still be a level of correlation between two points in a random field [174]. It is thus apparent that representing a field by its complete continuous spatial field value $u(\boldsymbol{x})$ is not the most efficient representation. The spatial correlation can be better captured by using appropriate basis functions that characterise the expected variation of a wave field across space.

A standard model of a multipath field is to represent it as a superposition of plane waves

$$u(\boldsymbol{x}) = \sum_p a_p e^{jk\boldsymbol{x}.\widehat{\boldsymbol{\theta}}_p} \tag{4.2}$$

where the plane wave of index p has complex amplitude $a_p \in \mathbb{C}$ and propagates in the direction of the unit vector $\widehat{\boldsymbol{\theta}}_p$. The term $\boldsymbol{x}.\widehat{\boldsymbol{\theta}}_p$ denotes the inner product between the two vectors in $\mathbb{R}^3$.

This representation can be generalised to a continuous distribution of sources

$$u(\boldsymbol{x}) = \int_{\mathbb{S}^2} g(\widehat{\boldsymbol{\theta}}) e^{jk\boldsymbol{x}.\widehat{\boldsymbol{\theta}}} ds(\widehat{\boldsymbol{\theta}}) \tag{4.3}$$

where $\mathbb{S}^2$ denotes the unit sphere, $s(\widehat{\boldsymbol{\theta}})$ the surface element of $\mathbb{S}^2$ with unit normal vector $\widehat{\boldsymbol{\theta}}$. The function $g(\widehat{\boldsymbol{\theta}})$ can be considered as the angular amplitude distribution of far-field sources that represents the field.

When the function $g(\widehat{\boldsymbol{\theta}})$ is restricted to be a member of the space of square integrable functions, $L_2(\mathbb{S}^2)$, this represents bounded incident energy. This implies the field will be reasonably behaved in that $\lim_{R\to\infty} \frac{1}{R} \|u\|_R < \infty$. In this case the representation is known as a Herglotz wave function and $g(\widehat{\boldsymbol{\theta}})$ is called the Herglotz kernel [91, 165].

4.2.2 Random Multipath Field

The framework introduced in the previous section provides an angular domain representation of a spatial field. We model the random multipath propagation environment as a process generating random fields. Each realisation of the random process will have an associated angular domain representation $g(\widehat{\boldsymbol{\theta}})$. We proceed by considering the statistics of these realisations.

A commonly accepted model is that of the Rayleigh fading non line of sight multipath field. In this case the random nature of the field is completely captured in its second order statistics [26, 30, 63, 66, 67]. This is typical of an environment where the multipath scenario is created by a number of independent paths which are fading due to movement and the constructive and destructive effects of doppler interference.

Another useful assumption is that of uncorrelated scatterers [178]. We assume an infinite number of far-field scatterers with independent fading amplitudes. Taking the expectations over the realisations of the random field, the following properties of the angular representation $g(\widehat{\boldsymbol{\theta}})$ are defined,

$$E\left\{g(\widehat{\boldsymbol{\theta}})\right\} = 0 \qquad \text{Zero mean} \tag{4.4}$$

$$E\left\{g(\widehat{\boldsymbol{\theta}})\overline{g(\widehat{\boldsymbol{\phi}})}\right\} = 0 \qquad \widehat{\boldsymbol{\theta}} \neq \widehat{\boldsymbol{\phi}} \qquad \text{Uncorrelated in Angle} \tag{4.5}$$

$$\int_{\mathbb{S}^2} E\left\{g(\widehat{\boldsymbol{\theta}})\overline{g(\widehat{\boldsymbol{\phi}})}\right\} ds(\widehat{\boldsymbol{\phi}}) = P(\widehat{\boldsymbol{\theta}}) \qquad \text{Angular Power Spectrum} \tag{4.6}$$

with $\overline{g(\widehat{\boldsymbol{\phi}})}$ representing the complex conjugate of the function. The function $P(\widehat{\boldsymbol{\theta}})$ is known as the angular power spectrum and represents the relative power coming from any direction. Definitions (4.5) and (4.6) can be stated succinctly as

$$E\left\{g(\widehat{\boldsymbol{\theta}})\overline{g(\widehat{\boldsymbol{\phi}})}\right\} = P(\widehat{\boldsymbol{\theta}})\delta(\widehat{\boldsymbol{\theta}} - \widehat{\boldsymbol{\phi}}) \tag{4.7}$$

where $\delta(\widehat{\boldsymbol{\theta}}-\widehat{\boldsymbol{\phi}})$ is the Dirac delta function. While it is often formulated as $P(\widehat{\boldsymbol{\theta}}) = E\left\{g(\widehat{\boldsymbol{\theta}})\overline{g(\widehat{\boldsymbol{\theta}})}\right\}$, this is incomplete and hence not strictly true. To represent a wide sense stationary process, the angular representation $g(\widehat{\boldsymbol{\theta}})$ must become uncorrelated, even for an infinitesimal angular shift. If $g(\widehat{\boldsymbol{\theta}})$ was to also have finite power, then note that at the origin

$$E\left\{u(\boldsymbol{x})\overline{u(\boldsymbol{x})}\right\} = \int_{\mathbb{S}^2}\int_{\mathbb{S}^2} E\left\{g(\widehat{\boldsymbol{\theta}})\overline{g(\widehat{\boldsymbol{\phi}})}\right\} ds(\widehat{\boldsymbol{\theta}})ds(\widehat{\boldsymbol{\phi}}) = 0 \tag{4.8}$$

with the integral vanishing since $E\left\{g(\widehat{\boldsymbol{\theta}})\overline{g(\widehat{\boldsymbol{\theta}})}\right\}$ is finite and will only be non zero on a set of measure zero. Thus assuming $P(\widehat{\boldsymbol{\theta}}) = E\left\{g(\widehat{\boldsymbol{\theta}})\overline{g(\widehat{\boldsymbol{\theta}})}\right\}$ also requires the multiplication or division by ∞ where appropriate. This is not consistent with the development of a formal framework.

The associated spatial field will also be zero mean, with second order statistics

$$E\left\{|u(\boldsymbol{x})|\right\} = 0 \tag{4.9}$$

$$\begin{aligned} E\left\{|u(\boldsymbol{x})|^2\right\} &= E\left\{u(\boldsymbol{x})\overline{u(\boldsymbol{x})}\right\} = \int_{\mathbb{S}^2}\int_{\mathbb{S}^2} E\left\{g(\widehat{\boldsymbol{\theta}})\overline{g(\widehat{\boldsymbol{\phi}})}\right\} e^{jk\boldsymbol{x}.\widehat{\boldsymbol{\theta}}}e^{-jk\boldsymbol{x}.\widehat{\boldsymbol{\phi}}}ds(\widehat{\boldsymbol{\theta}})ds(\widehat{\boldsymbol{\phi}}) \\ &= \int_{\mathbb{S}^2} P(\widehat{\boldsymbol{\theta}})ds(\widehat{\boldsymbol{\theta}}). \end{aligned} \tag{4.10}$$

With suitable normalisation, define

$$\int_{\mathbb{S}^2} P(\widehat{\boldsymbol{\theta}})ds(\widehat{\boldsymbol{\theta}}) = 1, \tag{4.11}$$

representing a field with unit variance throughout all space. The spatial correlation function,

$$\rho(\boldsymbol{x},\boldsymbol{x}') = E\left\{u(\boldsymbol{x})\overline{u(\boldsymbol{x}')}\right\} = \int_{\mathbb{S}^2} P(\widehat{\boldsymbol{\theta}})e^{jk(\boldsymbol{x}-\boldsymbol{x}').\widehat{\boldsymbol{\theta}}}ds(\widehat{\boldsymbol{\theta}}) = \rho(\boldsymbol{x}'-\boldsymbol{x}), \tag{4.12}$$

represents the correlation between any two points in the field. The function is only dependent on the vector linking the two points $\boldsymbol{x}$ and $\boldsymbol{x}'$. The statistics of the field are stationary over all space. For this reason, the model is often referred to as the wide sense stationary uncorrelated scatterer model (WSSUS). In practice, the statistics of the field will not be stationary over all space, however this is a reasonable assumption when the antenna region is small compared with the geometry of the scattering objects.

For an isotropic field in three dimensions, $P(\widehat{\boldsymbol{\theta}}) = 1/4\pi$. The spatial correlation is

$$\rho(\boldsymbol{x},\boldsymbol{x}') = \frac{1}{4\pi}\int_{\mathbb{S}^2} e^{jk(\boldsymbol{x}-\boldsymbol{x}').\widehat{\boldsymbol{\theta}}}ds(\widehat{\boldsymbol{\theta}})$$

$$= \frac{1}{4\pi} \int_{\mathbb{S}^2} \sum_{n=0}^{\infty} \sum_{m=-n}^{n} j^n j_n(k \|\boldsymbol{x} - \boldsymbol{x}'\|) Y_m^n \left(\frac{\boldsymbol{x} - \boldsymbol{x}'}{\|\boldsymbol{x} - \boldsymbol{x}'\|} \right) \overline{Y_m^n(\widehat{\boldsymbol{\theta}})} ds(\widehat{\boldsymbol{\theta}})$$

$$= j_0(k \|\boldsymbol{x} - \boldsymbol{x}'\|) = \mathrm{sinc}\,(k \|\boldsymbol{x} - \boldsymbol{x}'\|) \tag{4.13}$$

using the spherical harmonic expansion of a plane wave [91]. The functions $Y_m^n(\cdot)$ are the spherical harmonic functions with unit vector argument with $\int_{\mathbb{S}^2} Y_m^n(\widehat{\boldsymbol{\theta}}) ds(\widehat{\boldsymbol{\theta}}) = 4\pi\delta_m\delta_n$ and $Y_m^n(\cdot) = 1$. The zero order spherical Bessel function is equal to the sinc function $j_0(z) = \mathrm{sinc}(z) = \sin(z)/z$. Equation (4.13) is a classic result known in electromagnetic [4] and acoustic [179] engineering.

The first zero of $\mathrm{sinc}\,(k \|\boldsymbol{x} - \boldsymbol{x}'\|)$ is at $\lambda/2$, though points beyond this are still correlated. This example demonstrates how the angular domain representation implicitly captures the wave equation constraint and provides a compact means of characterising the scattering environment. The angular domain provides an intuitive representation of the channel and is of more practical interest than the spatial correlation function.

From (4.7) it is noted that the angular representation, $g(\widehat{\boldsymbol{\theta}})$, will have infinite variance for any direction where $P(\widehat{\boldsymbol{\theta}}) \neq 0$. Since the field is stationary over all space, it must have infinite power. Hence a realisation, $g(\widehat{\boldsymbol{\theta}})$ of our random process satisfying (4.7) will not be a member of $L_2(\mathbb{S}^2)$. However, when projected onto a square integrable function, $f \in L_2(\mathbb{S}^2)$, the result will have finite power,

$$\begin{aligned} E\left\{ |\langle g, f \rangle|^2 \right\} &= E\left\{ \int_{\mathbb{S}^2} g(\widehat{\boldsymbol{\theta}}) \overline{f(\widehat{\boldsymbol{\theta}})} ds(\widehat{\boldsymbol{\theta}}) \int_{\mathbb{S}^2} f(\widehat{\boldsymbol{\phi}}) \overline{g(\widehat{\boldsymbol{\phi}})} ds(\widehat{\boldsymbol{\phi}}) \right\} \\ &= \int_{\mathbb{S}^2} \int_{\mathbb{S}^2} E\left\{ g(\widehat{\boldsymbol{\theta}}) \overline{g(\widehat{\boldsymbol{\phi}})} \right\} \overline{f(\widehat{\boldsymbol{\theta}})} f(\widehat{\boldsymbol{\phi}}) ds(\widehat{\boldsymbol{\theta}}) ds(\widehat{\boldsymbol{\phi}}) \\ &= \int_{\mathbb{S}^2} P(\widehat{\boldsymbol{\theta}}) f(\widehat{\boldsymbol{\theta}}) \overline{f(\widehat{\boldsymbol{\theta}})} ds(\widehat{\boldsymbol{\theta}}) < \infty. \end{aligned} \tag{4.14}$$

Thus in the style of Gallager [11], rather than deal directly with the random process, this work will consider its projection in an appropriate Hilbert space.

4.2.3 Finite Dimensional Representation

The preceding sections have shown the random process characterising a multipath field can be represented in the angular domain. Previous works have introduced the notion of the essential finite dimensionality of a multipath field. An arbitrary multipath field, when considered over a finite region, can be well approximated by a finite dimensional representation [41, 42, 84]. This section will consider the problem of finding the optimal finite dimensional representation in the angular domain.

Our representation for a particular realisation will take the form

$$g_N(\widehat{\boldsymbol{\theta}}) = \sum_{n=0}^{N-1} \alpha_n g_n(\widehat{\boldsymbol{\theta}}), \tag{4.15}$$

where the coefficients α_n capture the random nature of the field and $g_n(\widehat{\boldsymbol{\theta}})$ are a set of deterministic basis functions. For an optimal representation, the coefficients α_n should be uncorrelated and the basis functions selected to minimise the expected norm of some objective or error function [159, 180, 181].

Such a representation captures the characteristics of a random multipath field in a practically useful manner. The random nature is captured through the coefficients being random variables, whilst the wave nature of the multipath is captured through the deterministic basis functions. Use of the optimal set of basis functions will allow a given accuracy to be achieved with the minimal set of random variables.

Given the angular domain framework, the following questions are posed and addressed:

- *What is the optimal set of basis functions for the angular representation?*
- *What aspects of the multipath environment are required to determine them?*

4.3 Optimal Basis for Spatially Constrained Field

This section will derive the optimal basis representation for a spatially constrained field. The angular framework developed in the previous section is used to derive some properties of the desired basis functions. A maximisation problem is formulated to determine the optimal basis set. This leads to an integral equation for which the eigenfunctions provide the desired basis. We adopt the assumptions of the zero mean Rayleigh fading uncorrelated scatter model for the remainder of this chapter. In practice, we are interested in representing and generating realisations of the random field. We draw on the theory of representing a random process through an orthogonal series expansion [159, 180, 181].

From the definition of the angular power spectrum (4.7), the correlation function for the random process generating $g(\widehat{\boldsymbol{\theta}})$ will be non-stationary, unbounded and discontinuous. As a result of this, we cannot directly use the classical Karhunen-Loéve expansion to determine an appropriate orthogonal expansion of the form (4.15) [182]. This section develops an appropriate space, basis, and ordering for the angular representation of a random multipath field with a specific angular power spectrum.

4.3.1 Angular Representation of a Spatially Constrained Field

Definition 4.1 Space of far-field distributions.
Given a particular angular power spectrum, $P(\widehat{\boldsymbol{\theta}})$, let $\mathcal{F}$ be the space of square integrable functions defined on

$$\Omega = \{\widehat{\boldsymbol{\theta}} \in \mathbb{S}^2 : P(\widehat{\boldsymbol{\theta}}) \neq 0\} \tag{4.16}$$

with associated inner product

$$\langle f, g \rangle_{\mathcal{F}} = \int_{\Omega} \frac{1}{P(\widehat{\boldsymbol{\theta}})} f(\widehat{\boldsymbol{\theta}}) \overline{g(\widehat{\boldsymbol{\theta}})} ds(\widehat{\boldsymbol{\theta}}) \tag{4.17}$$

and induced norm

$$\|g\|_{\mathcal{F}}^2 = \langle g, g \rangle_{\mathcal{F}} = \int_{\Omega} \frac{1}{P(\widehat{\boldsymbol{\theta}})} |g(\widehat{\boldsymbol{\theta}})|^2 ds(\widehat{\boldsymbol{\theta}}). \tag{4.18}$$

To ensure a proper formulation, $P(\widehat{\boldsymbol{\theta}})$ must be non-zero and continuous on some open interval in $\mathbb{S}^2$ such that Ω is not a set of measure zero.

We can consider that $\mathcal{F}$ is a linear subspace of $L_2(\mathbb{S}^2)$ with an implicit projection obtained since $\Omega \subseteq \mathbb{S}^2$. Thus $\mathcal{F}$ is a closed and separable Hilbert space [183]. The reason for weighting the inner product with the reciprocal of the power spectrum, $\left(P(\widehat{\boldsymbol{\theta}})\right)^{-1}$, will become apparent in Theorem 4.2. It is the weighting which connects orthogonality on the space $\mathcal{F}$ to independence in the expansion of the random field. The integral is restricted to the region Ω for which $\left(P(\widehat{\boldsymbol{\theta}})\right)^{-1}$ is defined. There is a question of convergence of the integral as $P(\widehat{\boldsymbol{\theta}}) \to 0$. For a member of the space $f \in \mathcal{F}$, the norm $\|f\|_{\mathcal{F}}$ must be defined and hence where $P(\widehat{\boldsymbol{\theta}})$ is small, the angular domain representation $f(\widehat{\boldsymbol{\theta}})$ must also be small. In this way, rather than causing any convergence issues, the distribution of $P(\widehat{\boldsymbol{\theta}})$ serves to weight the angular representations $f \in \mathcal{F}$ towards the regions where $P(\widehat{\boldsymbol{\theta}})$ is of a significant magnitude.

We now consider a white noise random process in this space. Whilst such a process will have infinite energy and does not strictly lie in the space $\mathcal{F}$, we can consider the projection of this process onto the basis functions of the space. A classically known theorem is that white noise projects isotropically to all dimensions of a separable Hilbert space [11].

Theorem 4.2 White Random Process in $\mathcal{F}$ has Angular Power Spectra $P(\widehat{\boldsymbol{\theta}})$.
A white random process where each coefficient to an orthonormal basis in $\mathcal{F}$ has unit variance and is independent has an associated angular spectra distribution $P(\widehat{\boldsymbol{\theta}})$.

$$g(\widehat{\boldsymbol{\theta}}) \triangleq \sum_{n=0}^{\infty} \alpha_n g_n(\widehat{\boldsymbol{\theta}}) \qquad \text{where} \qquad \begin{array}{l} \langle g_m, g_n \rangle_{\mathcal{F}} = \delta_{mn} \\ E\left\{\alpha_m \overline{\alpha_n}\right\} = \delta_{mn} \end{array} \qquad \text{and} \tag{4.19}$$

implies

$$E\left\{g(\widehat{\boldsymbol{\theta}})\overline{g(\widehat{\boldsymbol{\phi}})}\right\} = P(\widehat{\boldsymbol{\theta}})\delta(\widehat{\boldsymbol{\theta}} - \widehat{\boldsymbol{\phi}}). \tag{4.20}$$

Proof of Theorem 4.2. Consider a sampling function $f_\varepsilon(\widehat{\boldsymbol{\theta}}, \widehat{\boldsymbol{\phi}})$ defined as

$$f_\varepsilon(\widehat{\boldsymbol{\theta}}, \widehat{\boldsymbol{\phi}}) = \begin{cases} \frac{1}{\pi\varepsilon^2} & \left\|\widehat{\boldsymbol{\theta}} - \widehat{\boldsymbol{\phi}}\right\| < \varepsilon \\ 0 & \text{elsewhere} \end{cases}. \tag{4.21}$$

It can be seen that

$$\lim_{\varepsilon \to 0} \int_{\mathbb{S}^2} f_\varepsilon(\widehat{\boldsymbol{\theta}}, \widehat{\boldsymbol{\phi}}) ds(\widehat{\boldsymbol{\theta}}) = 1 \qquad \text{and} \tag{4.22}$$

$$\lim_{\varepsilon \to 0} \int_{\mathbb{S}^2} g(\widehat{\boldsymbol{\theta}}) f_\varepsilon(\widehat{\boldsymbol{\theta}}, \widehat{\boldsymbol{\phi}}) ds(\widehat{\boldsymbol{\theta}}) = g(\widehat{\boldsymbol{\phi}}). \tag{4.23}$$

Assuming $g(\widehat{\boldsymbol{\theta}})$ is continuous, (4.23) arises from the mean value theorem. This provides an approximation of the angular delta function $\delta(\widehat{\boldsymbol{\theta}} - \widehat{\boldsymbol{\phi}})$ which remains square integrable provided $\varepsilon > 0$. Thus we can project $f_\varepsilon(\widehat{\boldsymbol{\theta}}, \widehat{\boldsymbol{\phi}})$ into $\mathcal{F}$ using the orthonormal basis $g_n(\widehat{\boldsymbol{\theta}})$

$$f_\varepsilon(\widehat{\boldsymbol{\theta}}', \widehat{\boldsymbol{\phi}}) = \sum_{n=0}^{\infty} \left\langle f_\varepsilon(\widehat{\boldsymbol{\theta}}, \widehat{\boldsymbol{\phi}}), g_n(\widehat{\boldsymbol{\theta}}) \right\rangle g_n(\widehat{\boldsymbol{\theta}}'). \tag{4.24}$$

This is required to formally prove the theorem since strictly the distribution $\delta(\widehat{\boldsymbol{\theta}} - \widehat{\boldsymbol{\phi}})$ cannot be projected into $\mathcal{F}$ for $\widehat{\boldsymbol{\phi}} \in \Omega$ and cannot be used in the inner product.

Now given the representation of the angular distribution process (4.19)

$$\begin{aligned} E\left\{g(\widehat{\boldsymbol{\theta}})\overline{g(\widehat{\boldsymbol{\phi}})}\right\} &= E\left\{\sum_{n=0}^{\infty} \alpha_n g_n(\widehat{\boldsymbol{\theta}}) \sum_{m=0}^{\infty} \overline{\alpha_m} \overline{g_m(\widehat{\boldsymbol{\phi}})}\right\} \\ &= \sum_{n=0}^{\infty}\sum_{m=0}^{\infty} E\left\{\alpha_n \overline{\alpha_m}\right\} g_n(\widehat{\boldsymbol{\theta}}) \overline{g_m(\widehat{\boldsymbol{\phi}})} \\ &= \sum_{n=0}^{\infty} g_n(\widehat{\boldsymbol{\theta}}) \overline{g_n(\widehat{\boldsymbol{\phi}})}. \end{aligned} \tag{4.25}$$

Now consider the product $P(\widehat{\boldsymbol{\phi}})f_\varepsilon(\widehat{\boldsymbol{\theta}},\widehat{\boldsymbol{\phi}})$ for $\widehat{\boldsymbol{\theta}} \in \Omega$ using the expansion (4.24) and assuming $P(\widehat{\boldsymbol{\theta}})$ to be continuous

$$P(\widehat{\boldsymbol{\phi}})f_\varepsilon(\widehat{\boldsymbol{\theta}},\widehat{\boldsymbol{\phi}}) = P(\widehat{\boldsymbol{\phi}})\sum_{n=0}^{\infty}\int_\Omega \frac{1}{P(\widehat{\boldsymbol{\theta}}')}f_\varepsilon(\widehat{\boldsymbol{\theta}}',\widehat{\boldsymbol{\phi}})\overline{\boldsymbol{g}_n(\widehat{\boldsymbol{\theta}}')}ds(\widehat{\boldsymbol{\theta}}')g_n(\widehat{\boldsymbol{\theta}}) \tag{4.26}$$

$$= P(\widehat{\boldsymbol{\phi}})\sum_{n=0}^{\infty}\frac{1}{P(\widehat{\boldsymbol{\phi}})}g_n(\widehat{\boldsymbol{\theta}})\overline{g_n(\widehat{\boldsymbol{\phi}})} \quad \varepsilon \to 0 \tag{4.27}$$

$$= \sum_{n=0}^{\infty} g_n(\widehat{\boldsymbol{\theta}})\overline{g_n(\widehat{\boldsymbol{\phi}})} \quad \text{since } P(\widehat{\boldsymbol{\phi}}) \neq 0 \quad \forall \quad \widehat{\boldsymbol{\phi}} \in \Omega. \tag{4.28}$$

Equating (4.25) and (4.28) and noting that $P(\widehat{\boldsymbol{\theta}}) = 0$ and $g_n(\widehat{\boldsymbol{\theta}}) = 0$ for all $\widehat{\boldsymbol{\theta}} \notin \Omega$ and taking the limit as $\varepsilon \to 0$ we obtain

$$E\left\{g(\widehat{\boldsymbol{\theta}})\overline{g(\widehat{\boldsymbol{\phi}})}\right\} = P(\widehat{\boldsymbol{\phi}})\delta(\widehat{\boldsymbol{\theta}} - \widehat{\boldsymbol{\phi}}) = P(\widehat{\boldsymbol{\theta}})\delta(\widehat{\boldsymbol{\theta}} - \widehat{\boldsymbol{\phi}}) \tag{4.29}$$

which completes the proof. □

For a general random process, an optimal representation of the form (4.15) will have uncorrelated coefficients or, if the process is Gaussian (which we shall assume for simplicity), independent coefficients [159]. Thus we see that Theorem 4.2 creates the link between efficient representation of the random process for the angular distribution $P(\widehat{\boldsymbol{\theta}})$ and the orthogonality of the basis functions in $\mathcal{F}$.

Since the random process generating $g(\widehat{\boldsymbol{\theta}})$ is white, any realisation $g(\widehat{\boldsymbol{\theta}})$ will not be a member of the space $\mathcal{F}$. Consider

$$E\left\{\int_\Omega g(\widehat{\boldsymbol{\theta}})\overline{g(\widehat{\boldsymbol{\theta}})}ds(\widehat{\boldsymbol{\theta}})\right\} = E\left\{\int_\Omega \sum_{m=0}^{\infty}\alpha_m g_m(\widehat{\boldsymbol{\theta}})\sum_{n=0}^{\infty}\overline{\alpha_n g_n(\widehat{\boldsymbol{\theta}})}ds(\widehat{\boldsymbol{\theta}})\right\}$$

$$= \sum_{n=0}^{\infty} E\left\{\alpha_n\overline{\alpha_n}\right\}\|g_n\|_{\mathcal{F}}^2 = \sum_{n=0}^{\infty} 1 \to \infty. \tag{4.30}$$

Hence the norm of $g(\widehat{\boldsymbol{\theta}})$ in $\mathcal{F}$ is not defined. The realisation $g(\widehat{\boldsymbol{\theta}})$ is considered through its projection onto $\{g_n\} \in \mathcal{F}$. Theorem 4.2 suggests any orthonormal basis is suitable for the representation. This is a consequence of representing a stationary random field with infinite spatial extent. With no specified domain of interest, all basis sets are equally valid. The finite dimensional representation we are interested in will be optimal for representing fields in a specified bounded domain of interest.

There is a close analogy here with the representation of a random process generating an infinite sequence of discrete samples and having a known frequency power spectra. Whilst

the power spectrum may constrain the bandwidth, the sequence is free to exist over an infinite time range, thus there is no preferred set of basis functions unless we constrain the time range of interest.

Since $\|g\|_{\mathcal{F}}$ is not defined, it is meaningless to consider the error in the angular domain resulting from the finite dimensional representation, $\|g - g_N\|_{\mathcal{F}}$. Our goal is to approximate the spatial field over a finite region of space, so we must consider the error introduced by the finite dimension representation to the reconstructed spatial field in this domain of interest.

Definition 4.3 Space of Spatially Constrained Fields.
Consider a bounded domain of interest $\Lambda \subset \mathbb{R}^3$ with bounded extent such that $\boldsymbol{x}, \boldsymbol{y} \in \Lambda$ implies that $\|\boldsymbol{x} - \boldsymbol{y}\| < \infty$. Define $\mathcal{S}$ as the space of square integrable fields over the domain of interest, Λ, with associated inner product

$$\langle u, v \rangle_{\mathcal{S}} = \int_{\Lambda} u(\boldsymbol{x}) \overline{v(\boldsymbol{x})} d\boldsymbol{x} \tag{4.31}$$

and induced norm $\|u\|_{\mathcal{S}}^2 = \langle u, \overline{u} \rangle_{\mathcal{S}}$.

From the definition of the angular domain (4.3), we define an operator between $\mathcal{F}$ and $\mathcal{S}$.

Definition 4.4 Wave-Field Mapping Operator and its Adjoint.
Define $\mathbf{A}$ as an operator mapping an angular representation, $f \in \mathcal{F}$, to a wave-field, $v \in \mathcal{S}$,

$$\mathbf{A} : \mathcal{F} \to \mathcal{S} \quad \triangleq \quad v(\boldsymbol{x}) = \int_{\Omega} f(\widehat{\boldsymbol{\theta}}) e^{jk\boldsymbol{x}.\widehat{\boldsymbol{\theta}}} ds(\widehat{\boldsymbol{\theta}}) \quad \boldsymbol{x} \in \Lambda \tag{4.32}$$

with the associated adjoint operator $\mathbf{A}^*$ mapping a spatial field $v' \in \mathcal{S}$ to an angular representation $f' \in \mathcal{F}$,

$$\mathbf{A}^* : \mathcal{S} \to \mathcal{F} \quad \triangleq \quad f'(\widehat{\boldsymbol{\theta}}) = P(\widehat{\boldsymbol{\theta}}) \int_{\Lambda} v'(\boldsymbol{x}) e^{-jk\boldsymbol{x}.\widehat{\boldsymbol{\theta}}} d\boldsymbol{x} \quad \widehat{\boldsymbol{\theta}} \in \Omega. \tag{4.33}$$

The adjoint is defined such that $\langle v, \mathbf{A}f \rangle_{\mathcal{S}} = \langle \mathbf{A}^* v, f \rangle_{\mathcal{F}}$ for any $v \in \mathcal{S}$ and $f \in \mathcal{F}$,

$$\begin{aligned} \langle v, \mathbf{A}f \rangle_{\mathcal{S}} &= \int_{\Lambda} v(\boldsymbol{x}) \left\{ \int_{\Omega} \overline{f(\theta)} e^{-jk\boldsymbol{x}.\widehat{\boldsymbol{\theta}}} ds(\widehat{\boldsymbol{\theta}}) \right\} d\boldsymbol{x} \\ &= \int_{\Omega} \frac{1}{P(\widehat{\boldsymbol{\theta}})} \left\{ P(\widehat{\boldsymbol{\theta}}) \int_{\Lambda} v(\boldsymbol{x}) e^{-jk\boldsymbol{x}.\widehat{\boldsymbol{\theta}}} d\boldsymbol{x} \right\} \overline{f(\theta)} ds(\widehat{\boldsymbol{\theta}}) \\ &= \langle \mathbf{A}^* v, f \rangle_{\mathcal{F}} . \end{aligned} \tag{4.34}$$

As stated previously, the basis functions $g_n(\widehat{\boldsymbol{\theta}})$ should be selected such that the finite representation $g_N(\widehat{\boldsymbol{\theta}})$ from (4.15) is optimal, however since $g \notin \mathcal{F}$ the error function $\|g - g_N\|$ is meaningless. From the definition (4.32) we can extend the domain of $\mathbf{A}$ to all integrable functions $L_1(\mathbb{S}^2)$. Given $g \in L_1(\mathbb{S}^2)$, we consider the error of the finite angular representation to the spatial field on the domain of interest Λ,

$$\|\mathbf{A}g - \mathbf{A}g_N\|_\Lambda . \tag{4.35}$$

This provides a method to order the basis elements of $\mathcal{F}$ and determine an optimal representation of the field in the domain of interest. Each g_n will map to a field with norm $\|\mathbf{A}g_n\|_{\mathcal{S}}^2 = \langle \mathbf{A}g_n, \mathbf{A}g_n \rangle_{\mathcal{S}}$. This represents the contribution of each component to a realisation of the random field over the domain of interest. In comparison to the discrete sequence, this is analogous to constraining the time period over which we are interested in the sequence values. We then are interested in the basis functions that match the desired power spectrum and are confined mostly to the time period of interest.

This approach to constraining the domain of interest and ordering the basis function elements leads to the following theorem.

Theorem 4.5 Finite Dimension Angular Representation of Spatially Constrained Field. *Given a bounded domain of interest, Λ, an optimal N term finite dimensional representation in the angular domain , $\mathcal{F}$, for a random spatial field with WSSUS angular power spectrum $P(\widehat{\boldsymbol{\theta}})$ will be*

$$g_N^{(P,\Lambda)}(\widehat{\boldsymbol{\theta}}) = \sum_{n=0}^{N-1} \alpha_n g_n^{(P,\Lambda)}(\widehat{\boldsymbol{\theta}}) \tag{4.36}$$

where α_n are unit variance, independent random complex coefficients. The set $\{g_n^{(P,\Lambda)}\}$ are the orthonormal eigenfunctions in $\mathcal{F}$, ordered in decreasing eigenvalue $\lambda_n^{(P,\Lambda)}$, of

$$\begin{aligned} \lambda_n^{(P,\Lambda)} g_n^{(P,\Lambda)}(\widehat{\boldsymbol{\theta}}) &= \mathbf{A}^* \mathbf{A} g_n^{(P,\Lambda)}(\widehat{\boldsymbol{\phi}}) \\ &= P(\widehat{\boldsymbol{\theta}}) \int_\Lambda \int_\Omega g_n^{(P,\Lambda)}(\widehat{\boldsymbol{\phi}}) e^{jk\boldsymbol{x}.(\widehat{\boldsymbol{\phi}}-\widehat{\boldsymbol{\theta}})} ds(\widehat{\boldsymbol{\phi}}) d\boldsymbol{x} \end{aligned} \tag{4.37}$$

with the expected error in the field from truncation

$$E\left\{ \left\| \mathbf{A}g - \mathbf{A}g_N^{(P,\Lambda)} \right\|^2 \right\} = \sum_{n=N}^{\infty} \lambda_n^{(P,\Lambda)} \tag{4.38}$$

and this truncation error will be optimal over all possible choices of basis functions g_n.

Proof of Theorem 4.5. For convenience we suppress the explicit notation $\cdot^{(P,\Lambda)}$.

We consider the problem of finding a unit norm function $\boldsymbol{g}_n \in \mathcal{F}$, $\|g_n\|_{\mathcal{F}} = 1$ that when projected into $\mathcal{S}$, $\mathbf{A}g_n \in \mathcal{S}$, achieves the maximum norm $\|\mathbf{A}g_n\|_{\mathcal{S}}$. We can normalise by $\|g_n\|_{\mathcal{F}}$ and use the adjoint operator $\mathbf{A}^*$ to state the equivalent problems

$$\sup_{\|g_n\|_{\mathcal{F}}=1} \|\mathbf{A}g_n\|_{\mathcal{S}}^2 \quad \equiv \quad \sup_{g_n} \frac{\langle \mathbf{A}g_n, \mathbf{A}g_n \rangle_{\mathcal{S}}}{\langle g_n, g_n \rangle_{\mathcal{F}}} \quad \equiv \quad \sup_{g_n} \frac{\langle g_n, \mathbf{A}^*\mathbf{A}g_n \rangle_{\mathcal{F}}}{\langle g_n, g_n \rangle_{\mathcal{F}}}. \tag{4.39}$$

The solution for this problem is obtained when g_n are the eigenfunctions of the composite operator $\mathbf{A}^*\mathbf{A}$. Using the definitions of the projection operators, Definition 4.4, this leads directly to the eigenequation (4.37). An equation of this form is known as a Fredholm integral equation of the second kind and the integrand is often expressed as the product of a kernel with the function,

$$\lambda_n g_n(\widehat{\boldsymbol{\theta}}) = \int_{\Omega} K(\widehat{\boldsymbol{\theta}}, \widehat{\boldsymbol{\phi}}) g_n(\widehat{\boldsymbol{\phi}}) ds(\widehat{\boldsymbol{\phi}}) \qquad K(\widehat{\boldsymbol{\theta}}, \widehat{\boldsymbol{\phi}}) = P(\widehat{\boldsymbol{\theta}}) \int_{\Lambda} e^{jk\boldsymbol{x}.(\widehat{\boldsymbol{\phi}}-\widehat{\boldsymbol{\theta}})} d\boldsymbol{x}. \tag{4.40}$$

The trace of the kernel,

$$\int_{\Omega} K(\widehat{\boldsymbol{\theta}}, \widehat{\boldsymbol{\theta}}) = \int_{\Omega} P(\widehat{\boldsymbol{\theta}}) ds(\widehat{\boldsymbol{\theta}}) \int_{\Lambda} d\boldsymbol{x} = \int_{\Lambda} d\boldsymbol{x}, \tag{4.41}$$

will be bounded for a finite domain Λ as defined in Definition 4.3. This is equal to the sum of the eigenvalues [184] and there will be a countable set of solutions with non-zero eigenvalues which can be ordered $\lambda_0 \geq \lambda_1 \geq \ldots \lambda_n \geq 0$ [182].

Consider the following integral

$$\begin{aligned} \int_{\Omega}\int_{\Omega}\int_{\Lambda} g_m(\widehat{\boldsymbol{\theta}})\overline{g_n(\widehat{\boldsymbol{\phi}})} e^{jk\boldsymbol{x}.(\widehat{\boldsymbol{\theta}}-\widehat{\boldsymbol{\phi}})} d\boldsymbol{x} ds(\widehat{\boldsymbol{\theta}}) ds(\widehat{\boldsymbol{\phi}}) &= \lambda_m \int_{\Omega} \frac{1}{P(\widehat{\boldsymbol{\phi}})} g_m(\widehat{\boldsymbol{\phi}})\overline{g_n(\widehat{\boldsymbol{\phi}})} ds(\widehat{\boldsymbol{\phi}}) \\ &= \overline{\lambda}_n \int_{\Omega} \frac{1}{P(\widehat{\boldsymbol{\theta}})} g_m(\widehat{\boldsymbol{\theta}})\overline{g_n(\widehat{\boldsymbol{\theta}})} ds(\widehat{\boldsymbol{\theta}}) \end{aligned} \tag{4.42}$$

$$\Rightarrow \quad \left(\lambda_n - \overline{\lambda_m}\right) \int_{\Omega} \frac{1}{P(\widehat{\boldsymbol{\theta}})} g_m(\widehat{\boldsymbol{\theta}})\overline{g_n(\widehat{\boldsymbol{\theta}})} ds(\widehat{\boldsymbol{\theta}}) = \left(\lambda_m - \overline{\lambda_n}\right) \langle g_m, g_n \rangle_{\mathcal{F}} = 0. \tag{4.43}$$

From this it is noted that the eigenvalues, λ_n, will be real and that the eigenfunctions for distinct eigenvalues will be orthogonal in $\mathcal{F}$. With suitable normalisation, g_n is a complete orthonormal basis for $\mathcal{F}$.

From Theorem 4.2, it was shown that the coefficients, α_n, of the field with associated angular power spectrum $P(\widehat{\boldsymbol{\theta}})$ are drawn from a set of unit variance, independent random variables.

We define g_N from the first N terms of such a representation,

$$g_N(\widehat{\boldsymbol{\theta}}) = \sum_{n=0}^{N-1} \alpha_n g_n(\widehat{\boldsymbol{\theta}}) \qquad \psi_N(\boldsymbol{x}) = (\mathbf{A}g_N)(\boldsymbol{x}) = \sum_{n=0}^{N-1} \alpha_n \left(\mathbf{A}g_n\right)(\boldsymbol{x}). \tag{4.44}$$

The expected value of the error in the reconstructed field,

$$\varepsilon_N = E\left\{\|\mathbf{A}g - \mathbf{A}g_N\|_{\mathcal{S}}^2\right\} = E\left\{\left\|\sum_{n=N}^{\infty} \alpha_n \mathbf{A}g_n\right\|_{\mathcal{S}}^2\right\} \tag{4.45}$$

$$= \sum_{m=N}^{\infty}\sum_{n=N}^{\infty} E\left\{\alpha_m \overline{\alpha_n}\right\} \left\langle \mathbf{A}g_m, \mathbf{A}g_n\right\rangle_{\mathcal{S}} = \sum_{n=N}^{\infty} \lambda_n. \tag{4.46}$$

The eigenvalues λ_n are from a self adjoint operator and thus cannot be less than zero. Thus the sequence of errors ε_N as N is increased forms a non-increasing sequence. Since the eigenvalues are ordered in decreasing magnitude, the expectation of the error ε_N will be minimal across all possible choices for any orthogonal set of functions g_n. Thus the representation (4.36) is the optimal finite N-dimensional representation with respect to the error of the associated field across the domain of interest Λ. □

This theorem demonstrates that both the angular power spectrum *and the domain of interest* are required to determine the optimal set of angular basis functions for representing the random field.

For a random multipath field with angular spectra $P(\widehat{\boldsymbol{\theta}})$, an expansion of the form (4.15) is a weighted sum of the first N basis functions. This provides the most efficient N parameter representation for an instance of the random field. The truncation of a random field to this N dimensional representation will introduce an approximation error. The expected value of the mean square error in the field across the domain of interest Λ will be minimal when using this optimal set of basis functions.

4.3.2 Comments on Optimal Basis Representation

From the preceding results we see that the way in which the field is measured over space has a direct bearing on the optimal angular representation of the random field. The eigenequation sets out the relationship and interaction between the angular power spectrum and the spatial region. This affects the number of terms and characteristics of the angular functions that should be used to represent the random field.

- The random process representing the multipath field in the angular domain will have infinite variance in any single direction and is not a member of $L_2(\Omega)$.

- The random process can be represented by its projection onto a set of basis functions in the space $\mathcal{F}$. If the basis is orthonormal in $\mathcal{F}$ and the coefficients of the basis unit variance random independent variables, then the field will have an associated angular power spectrum $P(\widehat{\boldsymbol{\theta}})$.

- By considering the domain of interest for representing the field, we can obtain an ordered set of basis functions $g_n^{(P,\Lambda)}$ which are dependent on both the angular power spectrum and the domain of interest.

- By truncating the representation to the first N terms, we can obtain an N-dimensional subspace which will be optimal amongst all possible choices of N-dimensional basis with respect to the mean squared error on Λ.

- The optimal angular representation provides a means to generate realisations which appropriately model the random field by weighting the N basis functions with a set of independent identically distributed complex normal random variables.

A useful interpretation for this result is to consider the observation of a field over a finite domain as a filtering operation. The input to this filter has infinite dimensionality and in the angular domain resembles a "white" process with amplitude weighted with respect to angle. The components of this input which will suffer the least attenuation through the observation filter are the solutions of the eigenequation. This provides a basis and representation in the input space (angular domain) to efficiently model the observation of a multipath field over the region of space. We refer to this as an angular representation of a spatially constrained field.

All the terms of (4.36) in the angular domain space $\mathcal{F}$ are weighted equally. Adding more terms will continue to increase the power of the field representation. The series $\{g_N\}$ is not convergent since

$$E\left\{\|g_N - g_{N-1}\|_{\mathcal{F}}\right\} = E\left\{\alpha_N \overline{\alpha_N}\right\} = 1 \tag{4.47}$$

which is consistent with the infinite point variance of $P(\widehat{\boldsymbol{\theta}})$ from (4.7). However the series of associated fields $\{u_N\} = \{\mathbf{A}g_N\}$ is convergent in $\mathcal{S}$ since

$$E\left\{\|\mathbf{A}g_N - \mathbf{A}g_{N-1}\|_{\mathcal{S}}\right\} = \lambda_N E\left\{\alpha_N \overline{\alpha_N}\right\} \to 0 \quad \text{as} \quad N \to \infty. \tag{4.48}$$

This is a corollary of the diminishing representation error in the truncation as N is increased. The higher order basis functions g_n become progressively spatially "high passed", having less energy in the domain of interest Λ.

4.3.3 Relationship to Karhunen-Loéve Expansion

Since the correlation function in the angular domain, (4.7), was not bounded, it is not possible to develop a Karhunen-Loéve expansion directly in the angular domain. An alternate approach is to consider a representation of the random field in the spatial domain [81]. The spatial correlation function, $\rho(\boldsymbol{x}, \boldsymbol{x}')$ defined in (4.12), is stationary and continuous thus allowing the use of a Karhunen-Loéve expansion to represent the field as an orthonormal expansion over a finite domain Λ. The Karhunen-Loéve expansion optimal provides a unique optimal expansion (in the MMSE sense) of a random process restricted to a bounded domain [159],

$$u(\boldsymbol{x}) = \sum_{n=0}^{N-1} \sqrt{\lambda_n}\alpha_n u_n(\boldsymbol{x}) \tag{4.49}$$

where the basis set $\{u_n\}$ and eigenvalues λ_n are the eigenfunctions of the integral equation

$$\lambda_n u_n(\boldsymbol{x}') = \int_\Lambda \rho(\boldsymbol{x}', \boldsymbol{x}) u_n(\boldsymbol{x}) d\boldsymbol{x} \tag{4.50}$$

with the kernel of this Fredholm equation being the spatial correlation function.

Taking a finite set of the terms of (4.49) provides an optimal finite dimensional representation in the sense of the expected mean square error for representing any realisation of the random process. The use of the notation, λ_n and α_n, equivalent to Theorem (4.5), is deliberate and justified by the following theorem. The eigenequation derived from the spatial Karhunen-Loéve expansion is equivalent to that obtained from considering the optimal decomposition in the angular domain.

Theorem 4.6 Equivalence of Angular Representation and Karhunen-Loéve Expansion.
The spatial Karhunen-Loéve expansion provides an equivalent representation to that obtained in Theorem 4.5 in that the eigenequations

$$\lambda_n u_n(\boldsymbol{x}') = \int_\Lambda \rho(\boldsymbol{x}', \boldsymbol{x}) u_n(\boldsymbol{x}) d\boldsymbol{x} \tag{4.51}$$

and

$$\lambda_n^{(P,\Lambda)} g_n^{(P,\Lambda)}(\widehat{\boldsymbol{\theta}}) = P(\widehat{\boldsymbol{\theta}}) \int_\Lambda \int_\Omega g_n^{(P,\Lambda)}(\widehat{\boldsymbol{\phi}}) e^{jk\boldsymbol{x}.(\widehat{\boldsymbol{\phi}}-\widehat{\boldsymbol{\theta}})} ds(\widehat{\boldsymbol{\phi}}) d\boldsymbol{x}, \tag{4.52}$$

are equivalent with a one to one correspondence between the normalised associated eigenfunctions

$$\sqrt{\lambda_n} u_n(\boldsymbol{x}) = \int_\Omega g_n(\widehat{\boldsymbol{\theta}}) e^{jk\boldsymbol{x}.\widehat{\boldsymbol{\theta}}} ds(\widehat{\boldsymbol{\theta}}). \tag{4.53}$$

Considering the eigenequation for the angular domain, the domain of interest Λ is reflected in the kernel of the integral equation. For the spatial case, the domain of interest affects the domain of integration.

Proof of Theorem 4.6. Take the eigenequation (4.37) from Theorem 4.5 and apply the wavefield operator $\mathbf{A}$ from (4.32) to both sides,

$$\begin{aligned}
\text{LHS} &= \lambda_n \int_\Omega g_n(\widehat{\boldsymbol{\theta}}) e^{jk\boldsymbol{x}'.\widehat{\boldsymbol{\theta}}} ds(\widehat{\boldsymbol{\theta}}) = \lambda_n u_n(\boldsymbol{x}') \\
\text{RHS} &= P(\widehat{\boldsymbol{\theta}}) \int_\Omega g_n(\widehat{\boldsymbol{\phi}}) \int_\Lambda e^{jk\boldsymbol{x}.(\widehat{\boldsymbol{\phi}}-\widehat{\boldsymbol{\theta}})} d\boldsymbol{x} ds(\widehat{\boldsymbol{\phi}}) e^{jk\boldsymbol{x}'.\widehat{\boldsymbol{\theta}}} ds(\widehat{\boldsymbol{\theta}}) \\
&= \int_\Lambda \int_\Omega P(\widehat{\boldsymbol{\theta}}) e^{jk(\boldsymbol{x}'-\boldsymbol{x}).\widehat{\boldsymbol{\theta}}} ds(\widehat{\boldsymbol{\theta}}) \int_\Omega g_n(\widehat{\boldsymbol{\phi}}) e^{jk\boldsymbol{x}.\widehat{\boldsymbol{\phi}}} ds(\widehat{\boldsymbol{\phi}}) d\boldsymbol{x} \\
&= \int_\Lambda \rho(\boldsymbol{x}', \boldsymbol{x}) \int_\Omega g_n(\widehat{\boldsymbol{\phi}}) e^{jk\boldsymbol{x}.\widehat{\boldsymbol{\phi}}} ds(\widehat{\boldsymbol{\phi}}) d\boldsymbol{x} = \int_\Lambda \rho(\boldsymbol{x}', \boldsymbol{x}) u_n(\boldsymbol{x}) d\boldsymbol{x}.
\end{aligned} \tag{4.54}$$

Since $g_n(\widehat{\boldsymbol{\theta}})$ is arbitrary, $\int_\Omega g_n(\widehat{\boldsymbol{\theta}}) e^{jk\boldsymbol{x}'.\widehat{\boldsymbol{\theta}}}$ represents an arbitrary wave function giving an equivalent form to the Karhunen-Loéve eigenequation (4.50). The desired functions u_n are orthonormal on Λ, and since $\|\mathbf{A} g_n\|_{\mathcal{S}}^2 = \lambda_n$, we obtain the equivalence relationship (4.53). □

4.4 Angular Representation for Specific Configurations

4.4.1 Circular Region with Isotropic Field

As an example, we can consider the case of a two-dimensional field isotropic field with a circular region. In this case we can represent $\widehat{\boldsymbol{\theta}}$ and $\widehat{\boldsymbol{\phi}}$ as single parameter angles in the range $\Omega = [0, 2\pi]$ with $P(\theta) = 1/2\pi$. The associated domain of interest $\Lambda = \mathbb{B}_2^R = \{\boldsymbol{x} : \|\boldsymbol{x}\| \leq R\}$.

The integral equation (4.37) can be written for the two-dimensional case,

$$\lambda_n g_n(\theta) = \mathbf{A}^*\mathbf{A}g_n(\phi) = \int_\Omega g_n(\phi) \left\{ P(\theta) \int_\Lambda e^{jk\boldsymbol{x}.(\widehat{\boldsymbol{\phi}}-\widehat{\boldsymbol{\theta}})} d\boldsymbol{x} \right\} d\phi. \tag{4.55}$$

The kernel of this integral equation is evaluated for $\Lambda = \mathbb{B}_2^R$ and $P(\theta) = 1/2\pi$

$$\begin{aligned} K(\theta,\phi) = P(\theta) \int_{\mathbb{B}_R^2} e^{jk\boldsymbol{x}.(\widehat{\boldsymbol{\phi}}-\widehat{\boldsymbol{\theta}})} d\boldsymbol{x} &= P(\theta) \int_0^R \int_0^{2\pi} e^{jk\boldsymbol{x}.(\widehat{\boldsymbol{\phi}}-\widehat{\boldsymbol{\theta}})} r d\theta' dr \\ &= \frac{1}{2\pi} \int_0^R \int_0^{2\pi} e^{jkzr\cos(\theta')} r d\theta' dr = \int_0^R J_0(kzr) r dr \\ &= \frac{R}{kz} J_1(kzR) \end{aligned} \tag{4.56}$$

with $z = 2\sin((\phi-\theta)/2)$, $J_n(\cdot)$ is the n^{th} order Bessel function and using an integral of J_0 from [185]. Since the integration in the kernel is over a circular region, the kernel (4.56) is periodic in both θ and ϕ with period 2π. Furthermore, the kernel is invariant in a circular sense under translation in either argument, that is $K(\theta+\Delta,\phi) = K(\theta,\phi-\Delta)$. Hence, this eigenequation is equivalent to a circular convolution for which the eigenfunctions are known to be the harmonic complex exponentials. Thus the resultant normalised eigenfunctions are

$$g_n(\theta) = \frac{1}{2\pi} e^{jn\theta} \quad n = -\infty, \ldots, \infty. \tag{4.57}$$

Using Definition 4.4, the associated spatial field, using the Jacobi-Anger expansion [91],

$$\begin{aligned} u_n(\boldsymbol{x}) = (\mathbf{A}g_n)(\boldsymbol{x}) &= \int_0^{2\pi} g_n(\theta) e^{jk\boldsymbol{x}.\widehat{\boldsymbol{\theta}}} d\theta \\ &= \frac{1}{2\pi} \int_0^{2\pi} e^{jn\theta} \sum_{m=-\infty}^{\infty} j^m J_m(k\left\|\boldsymbol{x}\right\|) e^{jm(\theta_{\boldsymbol{x}}-\theta)} d\theta = j^n J_n(k\left\|\boldsymbol{x}\right\|) e^{jn\theta_{\boldsymbol{x}}}. \end{aligned} \tag{4.58}$$

with $\theta_{\boldsymbol{x}}$ the associated angle of the polar coordinates of the point $\boldsymbol{x}$. The associated eigenvalues from (4.55) are the square of the norm on the domain of interest of the transformed basis functions g_n,

$$\begin{aligned} \lambda_n &= \int_0^R \int_0^{2\pi} J_n^2(k\left\|\boldsymbol{x}\right\|) r d\theta dr = 2\pi \int_0^R J_n^2(kr) r dr \\ &= \pi R^2 \left(J_n^2(kR) - J_{n-1}(kR) J_{n+1}(kR) \right). \end{aligned} \tag{4.59}$$

The eigenvalues can be approximated $\lambda_n \approx 2R/k$ for $n < kR$ and $\lambda_n \approx 0$ for $n > kR$ with a sharp transition around $n = kR$. This property has been discussed in previous works [41, 42, 84] and also Chapter 2 with a similar set of basis functions derived for the field. The sum

of the eigenvalues and trace of the kernel [184] is simply the area $\sum_{n=1}^{\infty} \lambda_n = \pi R^2$.

A similar result can be obtained for the three-dimensional case with the angular basis functions being the spherical harmonics. In this case, the order of truncation is again $N = kR$, however with two angular dimensions the spherical harmonics are doubly indexed giving $(N+1)^2$ terms compared with $2N+1$ for the two-dimensional case.

4.4.2 Circular Region with Single Direction of Arrival

If the power spectrum is discrete from a single direction θ' then in the limit $P(\theta) = \delta(\theta - \theta')$. We can evaluate the eigenequation (4.37),

$$\begin{aligned} \lambda_n g_n(\theta) &= \delta(\theta - \theta') \int_{\Lambda} \int_{\Omega} g_n(\phi) e^{jk\boldsymbol{x}.(\widehat{\boldsymbol{\phi}} - \widehat{\boldsymbol{\theta}})} d\phi d\boldsymbol{x} \\ &= \delta(\theta - \theta') \int_{\Omega} g_n(\phi) \frac{2\pi R}{kz} J_1(kzR) d\phi \end{aligned} \tag{4.60}$$

with $z = 2\sin((\phi - \theta)/2)$ and $(\widehat{\boldsymbol{\phi}} - \widehat{\boldsymbol{\theta}})$ is the vector difference between the two-dimensional unit vectors corresponding to angles ϕ and θ. By inspection, if $\lambda_n \neq 0$ then $g_n(\theta) = 0$ for all $\theta \neq \theta'$. Thus (4.60) permits a single nontrivial solution

$$g_0(\theta) = \delta(\theta - \theta'), \qquad \lambda_0 = \frac{2\pi R}{kz} J_1(kzR) = \pi R^2 \tag{4.61}$$

since the integral is zero everywhere except $\phi = \theta'$ at which point $z = 0$ and the (4.60) gives the eigenvalue directly.

It is worth noting here that our space $\mathcal{F}$ is not formally defined for the case where $P(\theta) = \delta(\theta)$ or for any case where $P(\theta)$ is unbounded. In generalising the above, the eigenequation (4.37) reduces to a countable set of linear equations when $P(\theta)$ is only non-zero on a set Ω of measure zero. A more detailed proof would be required to establish this formally.

We present the framework here for the general case of $P(\theta)$ being bounded and normalised $\int_{\Omega} P(\theta) d\theta = 1$. The result of (4.61) can be established by considering a narrow angular power spectrum

$$P(\theta) = \begin{cases} 1/2\Delta & |\theta| < \Delta \\ 0 & \text{elsewhere} \end{cases} \tag{4.62}$$

and noting that

$$\frac{2\pi R}{kz} J_1(kzR) \approx \pi R^2, \qquad kzR \ll 1. \tag{4.63}$$

By inspection, we obtain an approximation of the first solution as $\Delta \to 0$,

$$g_0(\theta) \approx \begin{cases} 1/2\Delta & |\theta| < \Delta \\ 0 & \text{elsewhere} \end{cases} \qquad \lambda_0 \to \pi R^2. \tag{4.64}$$

The eigenvalue λ_0 approaches πR^2 from below. Since $\sum_{n=0}^{\infty} \lambda_n = \pi R^2$, and all eigenvalues are non-negative, the remainder of the eigenvalues vanish as $\Delta \to 0$.

This approach can be generalised to an arbitrary region. The singular nature of the power spectra $P(\theta)$ permits only a single solution of (4.60) being $g_0(\theta) = \delta(\theta - \theta')$ regardless of the region shape. This solution represents a plane wave across the region, $u_0(\boldsymbol{x}) = e^{jk\boldsymbol{x}.\widehat{\boldsymbol{\theta}}_{\boldsymbol{x}}}$. Since this has a constant unity magnitude across the region Λ, the eigenvalue λ_0 will be the area of the region Λ.

4.4.3 Circular Region with Restricted Direction of Arrival

The examples presented in the two previous sections demonstrate the extremes of an isotropic and unimodal angular power spectrum. The isotropic case will have a number of significant components of the order of $2kR$ whilst the single mode case will have a single term. Intuitively, the dimensionality will be related to the spread of the angular spectrum [82, 84, 157].

Consider the kernel for a restricted direction of arrival as set out in (4.56),

$$\lambda_n g_n(\theta) = \int_{-\Delta}^{\Delta} \frac{2\pi R}{2\Delta kz} J_1(kzR) g_n(\phi) d\phi \tag{4.65}$$

with $z = 2\sin((\phi - \theta)/2)$. This kernel applies a smoothing low pass to the function $g_n(\theta)$ and is structurally similar to a circular $\mathrm{sinc}(\cdot)$ function. The eigenequation is thus similar to that obtained when considering bandlimited functions [142].

Some further discussion of the dimensionality and basis functions for the restricted direction of arrival case can be found in Chapter 3.

4.4.4 Uniform Linear Array

Consider the domain or interest associated with the spatial region of a line $\Lambda = \{(x, y) : |x| < W, |y| < R\}$. For small W,

$$\boldsymbol{x}.(\widehat{\boldsymbol{\phi}} - \widehat{\boldsymbol{\theta}}) \approx y\,(\sin\phi - \sin\theta) \tag{4.66}$$

and the integral equation kernel from (4.55) becomes

$$\int_{\Lambda} e^{jk\boldsymbol{x}.(\widehat{\boldsymbol{\phi}}-\widehat{\boldsymbol{\theta}})} d\boldsymbol{x} \approx \int_{-W}^{W}\int_{-R}^{R} e^{jk(\sin\phi-\sin\theta)} dydx$$
$$= \frac{2\sin\left(kR(\sin\phi-\sin\theta)\right)}{k(\sin\phi-\sin\theta)} 2W. \tag{4.67}$$

This does not lead towards any convenient solutions for the eigenequation. For small angles around the broadside of the array, we can approximate $\sin\theta \approx \theta$. If we normalise by the effective area of the uniform linear array, $4RW$, we obtain the eigenequation

$$\lambda_n g_n(\theta) = P(\theta) \int_{\Omega} g_n(\phi)\mathrm{sinc}(kR(\theta-\phi))d\phi. \tag{4.68}$$

This is a kernel that has received much attention associated with bandlimited functions [85, 142, 159]. For small ranges around the broadside of the array we would expect the number of significant eigenvalues to increase linearly with the angular spread.

4.4.5 Other configurations

Whilst there is extensive literature on the problem of finding analytic solutions of a Fredholm integral equation, for this problem such solutions typically exist only for very simple or construed regions and power spectra. The ability to determine an analytic solution for a specific practical configuration will be limited. Existing techniques involve solving a related differential equation, or numerical approximations [186]. For different region shapes, alternate co-ordinate systems could be considered to match the region boundary [187]. Since the wave equation is separable for at least eleven coordinate systems [188] this presents some possibilities, for example the use of prolate spheroidal coordinates [160, 189].

4.5 Numerical Solution of the Eigenequation

The eigenequation (4.37) informs the solution for efficiently representing a random multipath field. Whilst this approach provides a high level of precision, it will often lead to complex series expansions for the solutions, see example [190]. Analytic solutions are known only for fairly simple configurations requiring careful geometric arrangements of the problem and thus having limited application. An alternative is to carry out numerical analysis to reveal the dominant macroscopic effects and the effects of varying the region shape or angular power spectrum.

There is extensive literature on approaches for solving such integral equations numerically [191–193]. The two approaches considered here are the Nyström method and approximation by a separable kernel. A more thorough analysis of these and other approaches can be found in other references [194, 195].

For the case of the two-dimensional field, the domain of the integral equation $\Omega \subset \mathbb{S}^1$ which is equivalent to the periodic domain $[0, 2\pi]$. The analysis is tailored to the specific integral equation

$$\lambda_n g_n(\theta) = \int_\Omega K(\theta, \phi) g_n(\phi) d\phi \qquad K(\theta, \phi) = P(\theta) \int_\Lambda e^{jk\boldsymbol{x}.(\widehat{\boldsymbol{\phi}} - \widehat{\boldsymbol{\theta}})} d\boldsymbol{x}. \tag{4.69}$$

It is shown that the integral equation can be solved numerically with a set $2\lceil kR \rceil + 1$ linear equations with R being the radial extent of the domain of interest Λ. This implies that only a certain amount of information from the angular spectrum, $P(\theta)$ is relevant.

Whilst some of the principles discussed can be extended to the angular domain associated with a three-dimensional field, the domain $\mathbb{S}^2$ creates additional complications. The field of numerical interpolation and integration on the sphere is a extensive topic unto itself [196–199]. We consider here only the integral equation associated with the two-dimensional field.

4.5.1 Nyström Method

The Nyström method is a simple approach to reduce the integral equation to a set of linear equations using a quadrature formula [191, 192]. It is applicable when the angular power spectrum is smooth and continuous, resulting in a well conditioned integrand. The integral can be approximated with a set of regular quadrature points $\theta_q = 2\pi(q-1)/Q$ and weights

$w_q = 2\pi/Q$,

$$\lambda_n g_n(\theta) = \int_\Omega K(\theta,\phi) g_n(\phi) d\phi = \frac{2\pi}{Q} \sum_{q=1}^{Q} K(\theta,\theta_q) g_n(\theta_q). \tag{4.70}$$

Evaluating this equation at the quadrature points gives the matrix eigenequation

$$\lambda_n \boldsymbol{g}_n = \boldsymbol{K}\boldsymbol{g}_n \quad \boldsymbol{g}_n = \begin{bmatrix} g_n(\theta_1) \\ \vdots \\ g_n(\theta_Q) \end{bmatrix} \quad \boldsymbol{K} = \frac{2\pi}{Q} \begin{bmatrix} K(\theta_1,\theta_1) & \cdots & K(\theta_1,\theta_Q) \\ \vdots & \ddots & \vdots \\ K(\theta_Q,\theta_1) & \cdots & K(\theta_Q,\theta_Q) \end{bmatrix}. \tag{4.71}$$

The solutions obtained for $\{g_n(\theta_q)\}$ can be interpolated with the reconstruction formula

$$g_n(\theta) = \frac{1}{\lambda_n} \sum_{q=1}^{Q} w_q K(\theta,\theta_q) g_n(\theta_q). \tag{4.72}$$

The main benefit of this approach is its simplicity. It has been shown to perform well across a wide class of problems [192] and is easily implemented [193].

To determine the number of quadrature points required, consider the spatial integral

$$\begin{aligned} \int_\Lambda e^{jk\boldsymbol{x}.(\widehat{\boldsymbol{\theta}}-\widehat{\boldsymbol{\phi}})} d\boldsymbol{x} &= \int_\Lambda \sum_{m=-\infty}^{\infty} J_m(k\left\|\boldsymbol{x}\right\|) e^{jm(\theta_{\boldsymbol{x}}-\theta)} \sum_{n=-\infty}^{\infty} J_n(k\left\|\boldsymbol{x}\right\|) e^{-jn(\theta_{\boldsymbol{x}}-\phi)} d\boldsymbol{x} \\ &= \sum_{m=-\infty}^{\infty} \sum_{n=-\infty}^{\infty} e^{-jm\theta} e^{jn\phi} \int_\Lambda J_m(k\left\|\boldsymbol{x}\right\|) J_n(k\left\|\boldsymbol{x}\right\|) e^{j\theta_{\boldsymbol{x}}(m-n)} d\boldsymbol{x}. \end{aligned} \tag{4.73}$$

For a region with maximum radius R, $J_n(k\left\|\boldsymbol{x}\right\|) \leq J_n(kR) \approx 0$ for $n > kR$. With only kR significant terms, the spatial component of the kernel is a smooth bandlimited function. When $P(\theta)$ is also a smooth bandlimited function, the number of quadrature points required will of the order $2kR + \Delta$, with additional points $\Delta \geq 1$ as required to increase the accuracy.

4.5.2 Modified Nyström Method

If $P(\theta)$ contains any singularities, it is noted that these will be reflected directly in the solutions $g_n(\theta)$. For such angular power spectrums it is no longer appropriate to directly sample

the kernel. Consider the related integral equation

$$\lambda_n \widetilde{g}_n(\theta) = \int_{\mathbb{S}^1} S(\theta,\phi) P(\phi) \widetilde{g}_n(\phi) d\phi \qquad \text{where} \quad S(\theta,\phi) = \int_{\Lambda} e^{jk\boldsymbol{x}.(\widehat{\boldsymbol{\phi}}-\widehat{\boldsymbol{\theta}})} d\boldsymbol{x} \tag{4.74}$$

which is equivalent to (4.69) with $g_n(\theta) = P(\theta)\widetilde{g}_n(\theta)$. In this case, $P(\phi)$ now captures the only discontinuity in the integral and can be considered a weighting function on the domain. This leads to a quadrature rule such that

$$\int_{\mathbb{S}^1} P(\theta) f(\theta) d\theta = \sum_{q=1}^{Q} \widetilde{w}_q f(\theta_q). \tag{4.75}$$

This quadrature rule should be satisfied for the maximal order of the integrand function $f(\theta)$. Letting $Q = 2M + 1$ the following system of equations is obtained to determine $\widetilde{w}_q$,

$$\int_{\mathbb{S}^1} P(\theta) e^{-jm\theta} d\theta = \sum_{q=1}^{Q} \widetilde{w}_q e^{-jm\theta_q}, \quad m = -M, \ldots, M. \tag{4.76}$$

For regular spaced $\theta_q = 2\pi(q-1)/Q$ the weights, $\widetilde{w}_q$, will be samples of the finite Fourier series expansion of $P(\theta)$,

$$\widetilde{w}_q = \widetilde{P}(\theta_q) = \sum_{m=-M}^{M} \gamma_m e^{jm\theta_q} \qquad \text{where} \quad \gamma_m = \frac{1}{2\pi} \int_0^{2\pi} P(\theta) e^{-jm\theta} d\theta. \tag{4.77}$$

This leads to an alternate set of equations to solve. It can be shown that this approach is equivalent to using the smoothed version of the angular power spectrum, $\widetilde{P}(\theta)$ directly in (4.71). The modified kernel samples

$$\widetilde{K}(\theta_p, \theta_q) = \widetilde{P}(\theta_p) S(\theta_p, \theta_q) = \widetilde{P}(\theta_p) \int_{\Lambda} e^{jk\boldsymbol{x}.(\theta_q - \theta_p)} d\boldsymbol{x}, \tag{4.78}$$

are used in (4.71), whilst the actual kernel $K(\theta, \theta_q)$ is used for interpolation in (4.72).

Improvements and variations of the Nyström method can be made through the selection of the quadrature rule. For a three-dimensional field, the domain $\mathbb{S}^2$ presents a greater complexity, however the area of integration on a sphere is well studied with many available quadrature rules [196, 198, 200, 201]. The smoothing of the three-dimensional angular power spectrum $P(\widehat{\boldsymbol{\theta}})$ can be obtained by a truncation of the spherical harmonic expansion of P on $\mathbb{S}^2$.

4.5.3 Separable Kernel using Harmonic Exponentials

Equation (4.73) demonstrates a linear decomposition of the eigenequation using a set of complex harmonic exponential functions. From this it is apparent that there exists a separable approximation of the kernel with a finite number of terms. The range of the kernel and the solutions of the integral equation will span the same linear subspace [195].

Writing the solutions and the angular power spectrum as linear combinations of the harmonic exponentials

$$g_n(\theta) = P(\theta) \sum_{m=-\infty}^{\infty} \alpha_m e^{-jm\theta} \qquad P(\theta) = \sum_{m=-\infty}^{\infty} \gamma_m e^{jm\theta}. \tag{4.79}$$

The integral equation (4.69) becomes

$$\begin{aligned} \lambda_n P(\theta) \sum_{m=-\infty}^{\infty} \alpha_m e^{-jm\theta} &= P(\theta) \int_{\mathbb{S}^1} \sum_{p=-\infty}^{\infty} \sum_{q=-\infty}^{\infty} e^{-jp\theta} e^{jq\phi} J_{pq} P(\phi) \sum_{s=-\infty}^{\infty} \alpha_s e^{-js\phi} d\phi \\ \Rightarrow \lambda_n \sum_{m=-\infty}^{\infty} \alpha_m e^{-jm\theta} &= \sum_{p=-\infty}^{\infty} \sum_{q=-\infty}^{\infty} e^{-jp\theta} J_{pq} \int_{\mathbb{S}^1} e^{jq\phi} \sum_{r=-\infty}^{\infty} \sum_{s=-\infty}^{\infty} \gamma_{r-s} \alpha_s e^{-jr\phi} d\phi \\ \Rightarrow \lambda_n \alpha_m &= 2\pi \sum_{q=-\infty}^{\infty} J_{mq} \sum_{s=-\infty}^{\infty} \gamma_{q-s} \alpha_s \end{aligned} \tag{4.80}$$

where

$$J_{pq} = \int_{\Lambda} J_p(k \left\| \boldsymbol{x} \right\|) J_q(k \left\| \boldsymbol{x} \right\|) e^{j\theta_{\boldsymbol{x}}(p-q)} d\boldsymbol{x}. \tag{4.81}$$

From the nature of the Bessel functions, J_{pq} will be negligible for either index greater in magnitude than beyond $M = \lceil kR \rceil$. Truncating this set of equations at order M gives

$$\lambda_n \boldsymbol{a} = \boldsymbol{J}\boldsymbol{C}\boldsymbol{a} \quad \boldsymbol{J} = \begin{bmatrix} J_{-M,-M} & \cdots & J_{-M,M} \\ \vdots & \ddots & \vdots \\ J_{M,-M} & \cdots & J_{M,M} \end{bmatrix} \quad \boldsymbol{C} = \begin{bmatrix} \gamma_0 & \cdots & \gamma_{-2M} \\ \vdots & \ddots & \vdots \\ \gamma_{2M} & \cdots & \gamma_0 \end{bmatrix} \tag{4.82}$$

where $\boldsymbol{a} = [\alpha_{-M}, \ldots, \alpha_M]^T$, $\boldsymbol{C}$ is the Hermitian Toeplitz matrix as shown and $\boldsymbol{J}$ is the matrix of terms J_{pq}. By solving for the eigenvectors $\boldsymbol{a}$, we can substitute the $2M+1$ coefficients α_m back into (4.79) to form a truncated approximation of the actual solution.

For a radially symmetric region, $J_{pq} = 0$ for $p \neq q$ and $\boldsymbol{J}$ is diagonal. For circular region $J_{pp} = 2\pi \int_0^R J_p^2(kr) r dr$. The eigenvalues of (4.82) will be the same as those of $\boldsymbol{J}^{1/2}\boldsymbol{C}\boldsymbol{J}^{1/2}$ which is the correlation matrix for the coefficients of an expansion using the basis for a

circular region and isotropic field. Analysis of this matrix was proposed in [81] as an algorithm for the numerical calculation of the random field eigenvalues. The numerical approach presented here encompasses this algorithm as a special case.

4.5.4 Validation of Numerical Methods

The preceding sections detailed two numerical methods for solving the integral equation related to the angular domain representation of a multipath field. Present here are two examples to validate the proposed numerical methods. Both approaches suggest the use of a relatively small linear system of equations with $2\lceil kR \rceil + 1$ unknowns. Higher accuracy can be easily achieved by using slightly more points than this critical threshold.

The first example presented is that of a circular region with unit wavelength radius and angular power spectrum constrained to $\pm\pi/4 = \pm 45^\circ$. For this region $kR \approx 6.3$ suggesting the use of a truncation order of $M = 7$ and 15 quadrature points $\theta_q = 2\pi q/(2M+1)$ for $n = -M, \ldots, M$. There will be around 4 significant eigenvalues for this configuration.

The second example is a more complex configuration with an elliptical region with major axis 2λ and minor axis $\lambda/2$. The angular power spectrum used was bimodal with Laplacian distributions centred at 0° and 45°. With a radial extent of λ this configuration again suggests a truncation order of 7 with 15 sampling points.

A schematic for the geometry of the two examples is shown in Figure 4.1. Table 4.1 lists the first 6 eigenvalues for the configurations along with the approximations using the two proposed methods solved with 15 unknowns. Both approximations are reasonably accurate with the Fourier method providing the best match.

Figures 4.2 and 4.3 show the approximated angular power spectra and eigenfunctions. It is evident that the main characteristics of the eigenfunctions are captured by the numerical methods using only 15 sampling points or unknowns in the matrix equation. The Fourier separation method provides a more accurate solution for the eigenfunctions. Both methods provide very accurate solutions for the first 4 eigenfunctions with discrepancies only noticed in the higher order eigenfunctions.

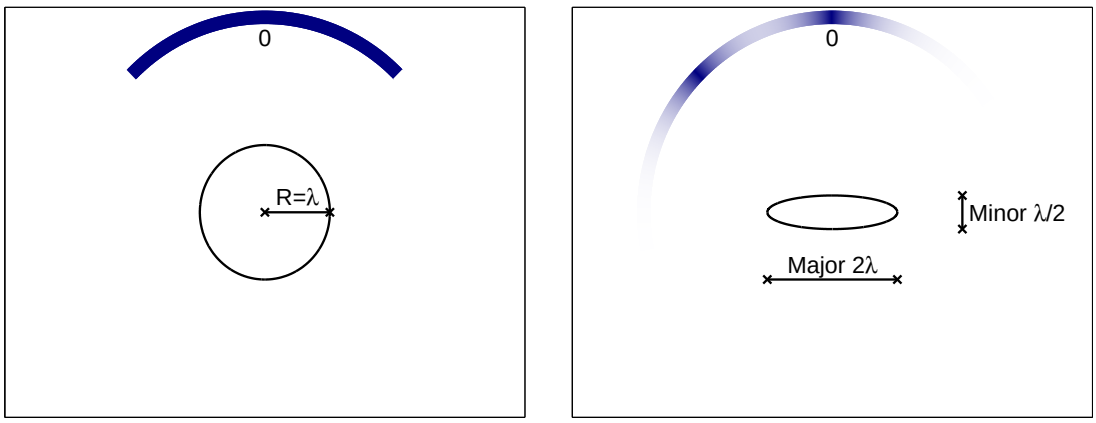

(a) Circular region $R = \lambda$ with uniform angular power spectrum

(b) Elliptical region major axis 2λ, minor axis $\lambda/2$ with bimodal Laplacian angular power spectrum

Figure 4.1: Schematic showing the geometry of the region shape and angular source distributions used in the validation examples.

(a) Circular region $R = \lambda$ with uniform angular power spectrum

Term Num	Exact Value	Method 1 Nyström	Method 2 Separable
1	1.2222	1.2225	1.2222
2	1.0418	1.0935	1.0417
3	0.6315	0.5313	0.6314
4	0.2007	0.2339	0.1994
5	0.0390	0.1123	0.0366
6	0.0056	0.0163	0.0043

(b) Elliptical region major axis 2λ, minor axis $\lambda/2$ with bimodal Laplacian angular power spectrum

Term Num	Exact Value	Method 1 Nyström	Method 2 Separable
1	0.5714	0.5721	0.5719
2	0.1759	0.1771	0.1766
3	0.0237	0.0222	0.0241
4	0.0098	0.0096	0.0098
5	0.0030	0.0058	0.0031
6	0.0010	0.0031	0.0011

Table 4.1: Comparison of the eigenvalues obtained from the two numerical methods for solving the spatial eigenequation. The eigenvalues are well approximated using a matrix equation with only $2\lceil kR \rceil + 1 \approx 15$ unknowns. The method using the Fourier separation of the kernel provides greater accuracy.

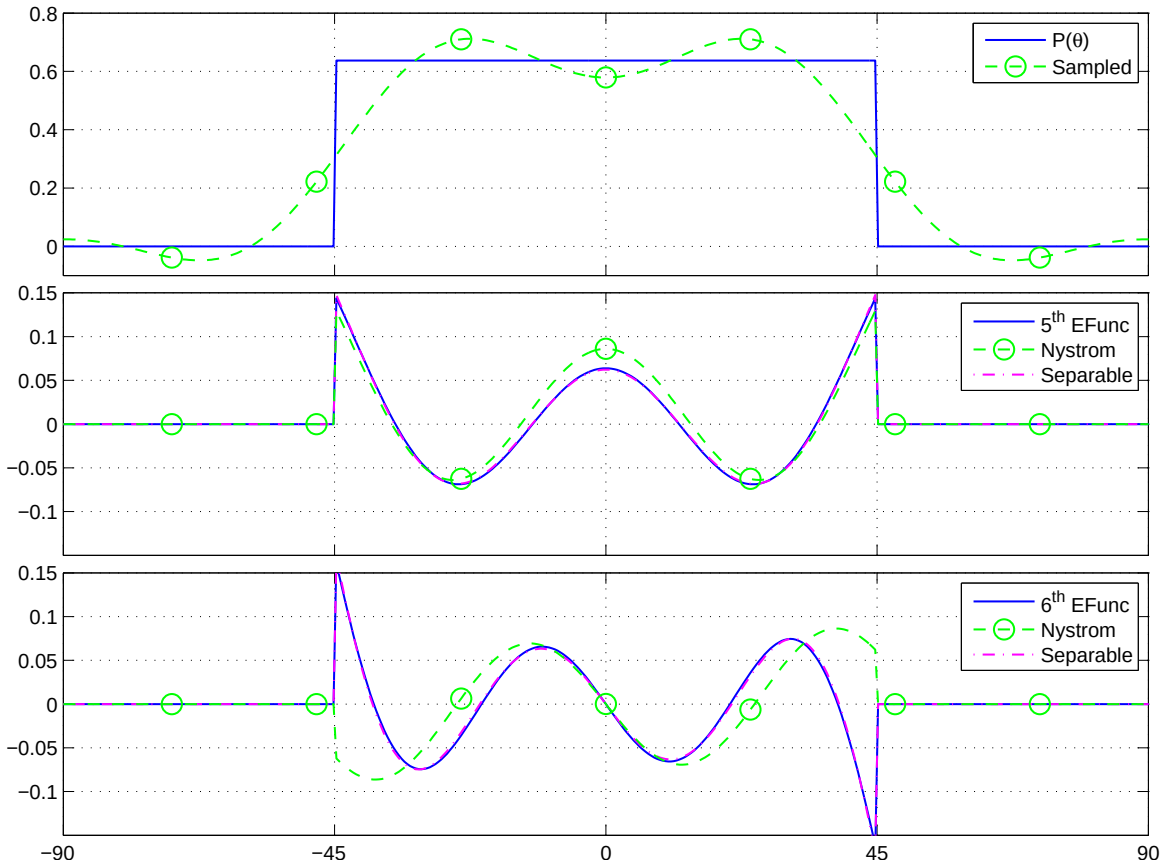

Figure 4.2: Comparison of eigenfunctions obtained from numerical methods with $R = \lambda$ and an angular power spectrum restricted to $|\theta| < 45°$. The first panel shows the actual and smoothed sampled angular power spectrum. The next two panels show eigenfunctions 5 and 6 and the approximations obtained. The Fourier separation approach provides the better approximation.

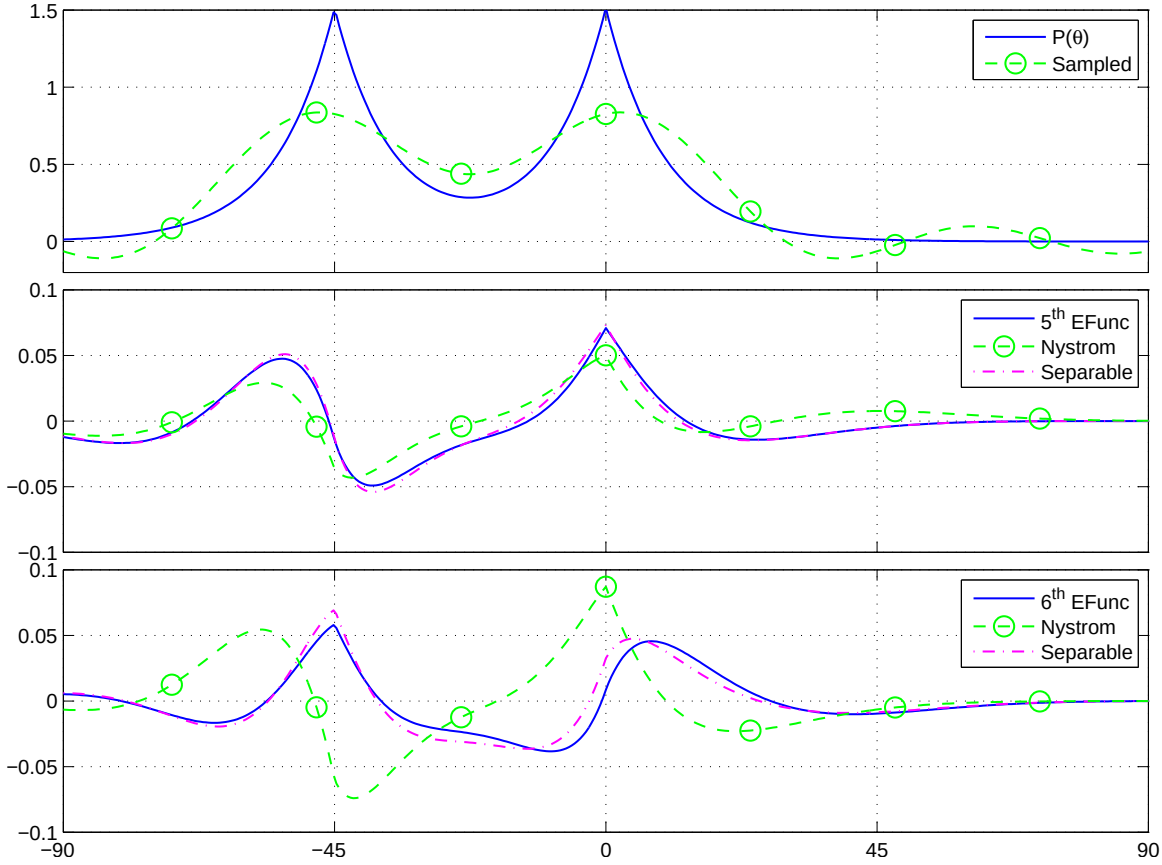

Figure 4.3: An elliptical region with major axis of 2λ and minor axis $\lambda/2$. The angular power spectrum is bimodal Laplacian distributed. Whilst the Nyström method is inaccurate for the 6^{th} eigenfunction, it is noted that this component represents -29dB of the random field energy.

4.5.5 Discussion of Numerical Method

The analysis and example demonstrates that accurate solutions to the integral equation can be obtained numerically. The order of the system of linear equations used to solve the Fredholm integral equation is related to the radius of the spatial region and thus the domain of interest. Solving for $2\lceil kR \rceil + 1$ unknowns using the Fourier separation method provides excellent results.

This work also demonstrates the insensitivity of the optimal basis functions $g_n(\widehat{\boldsymbol{\theta}})$ to components of the power spectrum $P(\widehat{\boldsymbol{\theta}})$ beyond a threshold resolution. In the two-dimensional case this was directly related to the Fourier series of the power spectrum. The Nyström method was dependent only on terms up to order $M = \lceil kR \rceil$ whilst the Fourier separation method was dependent on terms up to order $2M$. The Nystöm method requires a greater level of smoothing and thus less information from the angular spectrum. Taking the higher limit, we assert the following:

Observation 4.7 Significant aspects of angular power spectrum for modelling random multipath field.
Take an arbitrary angular power spectrum, $P(\theta)$, for a two-dimensional random multipath field. The terms of the Fourier expansion of $P(\theta)$ to order $2\lceil kR \rceil$ define an equivalent power spectrum, $\widetilde{P}(\theta)$ which captures all aspects of P relevant to the field observed over a region contained within a disc of radius R.

$$\widetilde{P}(\theta_q) = \sum_{n=-2M}^{2M} \gamma_n e^{jn\theta_q}\Big|_{M=\lceil kR \rceil} \qquad \text{where} \quad \gamma_n = \frac{1}{2\pi}\int_0^{2\pi} P(\theta)e^{-jn\theta}d\theta. \tag{4.83}$$

Derivation for Observation 4.7. Consider the two-dimensional spatial correlation function

$$\begin{aligned}\rho(\boldsymbol{x},\boldsymbol{x}') &= \int_{\mathbb{S}^1} P(\theta)e^{jk(\boldsymbol{x}-\boldsymbol{x}').\widehat{\boldsymbol{\theta}}}d\theta = \sum_{n=-\infty}^{\infty} j^n J_n(k\,\|\boldsymbol{x}-\boldsymbol{x}'\|)e^{-in\theta_{\boldsymbol{x}\boldsymbol{x}'}}\int_{\mathbb{S}^1} P(\theta)e^{-jn\theta}d\theta \\ &= \sum_{n=-\infty}^{\infty} j^n\gamma_n J_n(k\,\|\boldsymbol{x}-\boldsymbol{x}'\|)e^{-in\theta_{\boldsymbol{x}\boldsymbol{x}'}}.\end{aligned} \tag{4.84}$$

Given the bounded domain of interest, $\|\boldsymbol{x}-\boldsymbol{x}'\| < 2R$. Noting the high pass nature of the Bessel functions, $J_n(k\,\|\boldsymbol{x}-\boldsymbol{x}'\|) \approx 0$ for $n > k\,\|\boldsymbol{x}-\boldsymbol{x}'\| > 2kR$. Given γ_n are the Fourier coefficients of the power spectrum $P(\theta)$ it is evident that only the first $2kR$ terms are significant to the spatial correlation in the region. □

This result is consistent with previous works that have shown that for small angular distribu-

tions, it is the spread of angles excited and not the exact shape of the angular power spectrum that is significant to channel modelling, spatial correlation and capacity [47, 174, 202, 203].

4.6 Numerical Study of Angular Basis Functions

The eigenequation (4.37) informs the solution for efficiently representing a random multipath field. Unfortunately it is only easily solved for fairly simple configurations. However, as shown in the previous section, it is possible to obtain accurate solutions to the eigenequation using a relatively low order numerical approximation.

This numerical technique allows us to investigate the impact of various changes to the region shape and power spectrum. To facilitate the analysis, we consider a two-dimensional region and azimuth only source distribution.

4.6.1 Basis Functions with Non-Uniform Angular Power Spectrum

Reducing the support of the angular power spectrum causes a concentration of the received energy into the low order terms. The limiting case is that of a single eigenvalue as seen in Section 4.4.2. The basis functions are constrained to the range of non-zero $P(\theta)$. They resemble the prolate spheroidal wave functions [142] as the range of the angular spectrum is decreased. As the order is increased, the discontinuity at the edge of the angular spectrum becomes more pronounced. This is illustrated in Figure 4.4. The eigenvalues are normalised such that they sum to unity.

For comparison, the effect of a truncated Gaussian power spectrum with the same angular variance is shown in Figure 4.5. It is evident that the functions and eigenvalues become consistent with the uniform angular power spectrum for small angular variance. Since the integral kernel is smooth, the solution to the eigenequation is insensitive to details in the angular power spectrum finer than a certain resolution. The angular spread of the power spectrum becomes the dominant factor.

4.6.2 Basis Functions for Elliptical Region

The effect of the region shape on the eigenvalues and basis functions is also considered. A simple perturbation to a circular region is effected by changing the scale along one axis resulting in an elliptical region. This perturbation will cause a smaller number of eigenvalues

to become more dominant compared to the circular region. The limiting case is similar to a line array for which the number of significant eigenvalues is related to the array length. The eigenvalues and basis functions for an elliptical region are shown in Fig 4.6. It is evident that the eigenfunctions for this configuration are nontrivial functions.

4.7 Dimensionality of Optimal Representation

In Chapter 3 and Chapter 4 we considered the dimensionality for the representation of a multipath field in a circular region. The field was considered both with a uniform angular power spectrum and a restricted range of angles. For the isotropic case the basis functions are the complex exponentials. For the restricted angular range, the basis functions can be approximated by the prolate spheroidal wave functions. Further perturbations were shown to introduce greater complexity into the basis functions, suggesting that convenient solutions for such cases are unlikely.

Of interest in the general case is the essential dimensionality, or number of significant terms, that could be utilised if the correct basis was determined for a particular scenario. This provides a measure of the sub optimality of using the basis obtained from the isotropic case. This is a property of the eigenvalues from (4.37). In particular, we can consider the number of terms required for the expected residual error in a finite representation to fall below a set threshold.

Definition 4.8 Dimensionality of a Multipath Field.
For any set of eigenvalues from (4.37), given $\varepsilon > 0$ there exists some integer $D(\varepsilon)$ such that,

$$D(\varepsilon) = \arg\min_{n} \left\{ \frac{\sum_{m \geq n} \lambda_m}{\sum_m \lambda_m} < \varepsilon \right\}. \tag{4.85}$$

Of general interest is the value of $N = D(0.01)$ for which our N term finite representation (4.36) will capture 99% of the multipath energy. The modelling error in using such a representation would be equivalent to a 20dB signal to noise ratio. We use this threshold as the definition of the essential dimensionality to analyse the eigenvalues obtained from the integral equation.

Strictly, $D(\varepsilon)$ can only take on integer values. Of particular interest are the situations for which $D(\varepsilon)$ will be fairly small such as a communications system with a small number of antenna in a confined spatial region. The impact of changes to the region shape and field angular power distribution will be obscured by the coarse quantisation. To facilitate the

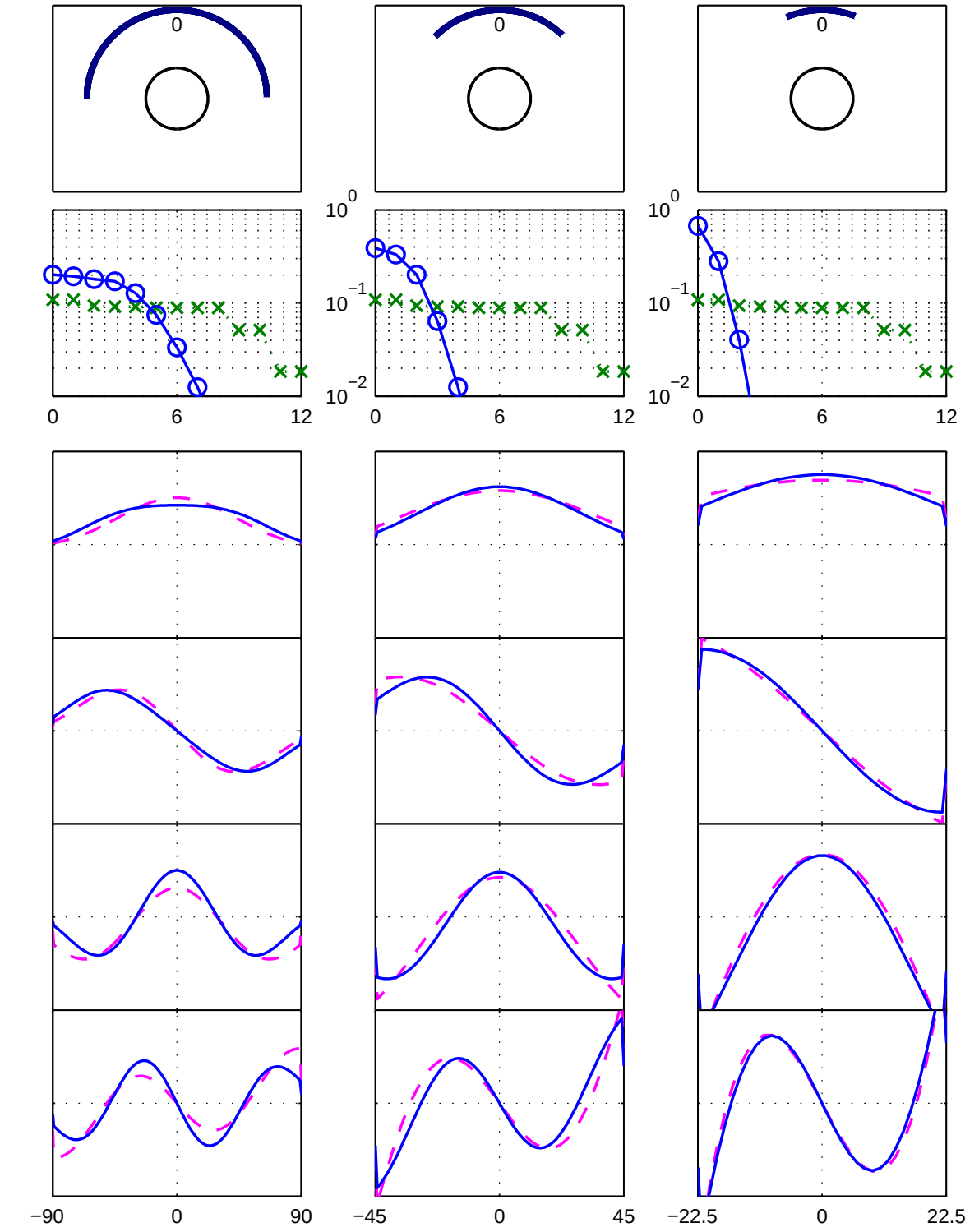

(a) Restricted to $\pm 90°$ (b) Restricted to $\pm 45°$ (c) Restricted to $\pm 22.5°$

Figure 4.4: Eigenvalues and first four angular basis functions for a circular region ($R = \lambda$) and uniform restricted angular spectrum. The top plot in each column provides a schematic of the region and source distribution. The second plot shows the restricted ($\circ$) and eigenvalues with those for the uniform spectrum ($\times$) also plotted for comparison. Restricting the angular range lowers the number of significant eigenvalues. The remaining four plots in each column show the basis functions, with the equivalent prolate spheroidal functions shown as a dashed line. The angular basis functions are zero beyond the domain shown in the figures.

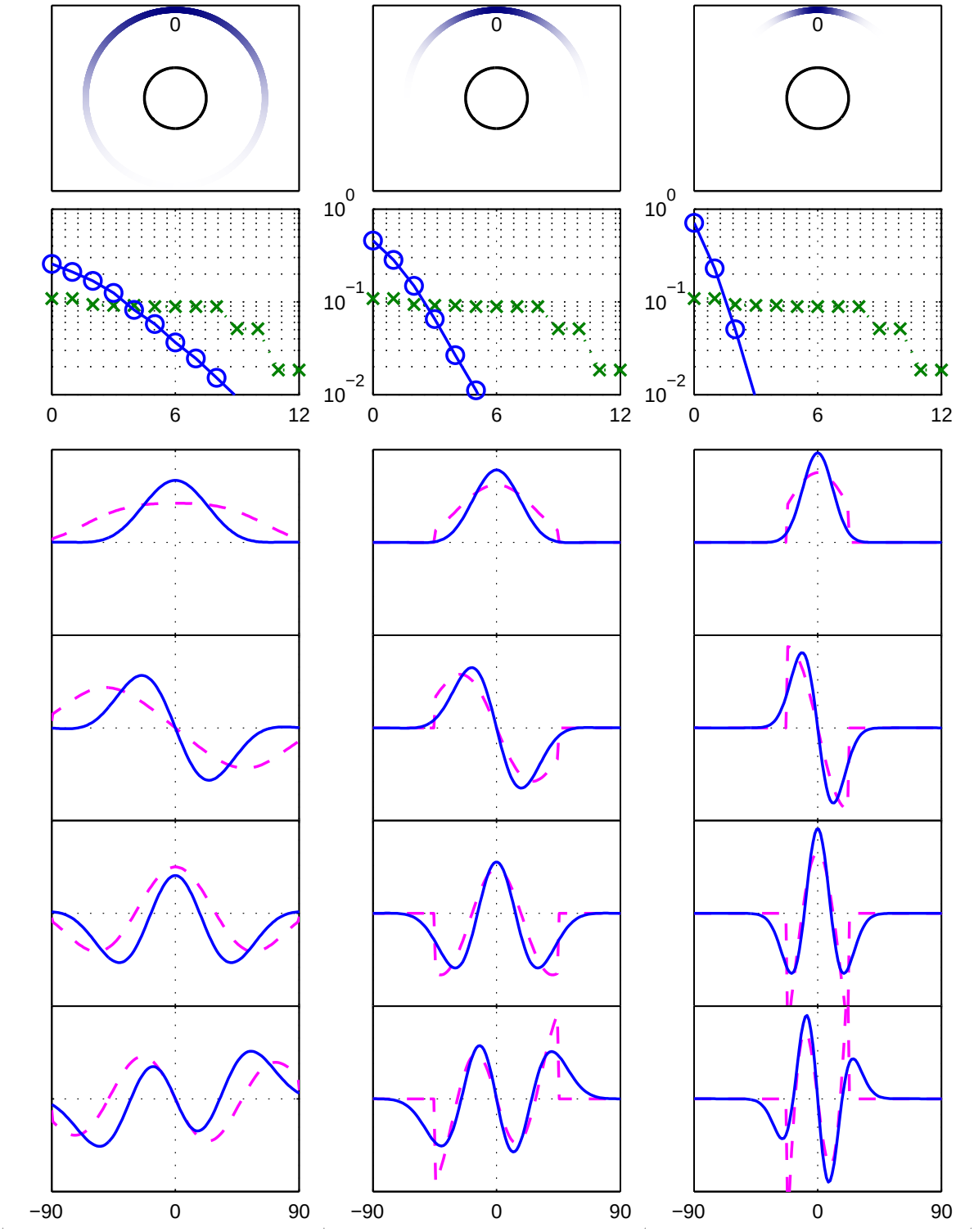

(a) Gaussian with $\sigma = 52°$ (b) Gaussian with $\sigma = 26°$ (c) Gaussian with $\sigma = 13°$

Figure 4.5: Eigenvalues and first four angular basis functions for a circular region ($R = \lambda$) and a truncated Gaussian angular source spectrum. The top plot in each column provides a schematic of the region and source distribution. The second plot shows the Gaussian spectrum ($\circ$) eigenvalues with the uniform spectrum ($\times$) eigenvalues also plotted for comparison. The remaining four plots in each columns show the basis functions for the Gaussian distribution. For comparison, the dashed line depicts the basis function for a uniform angular spread with the same angular variance.

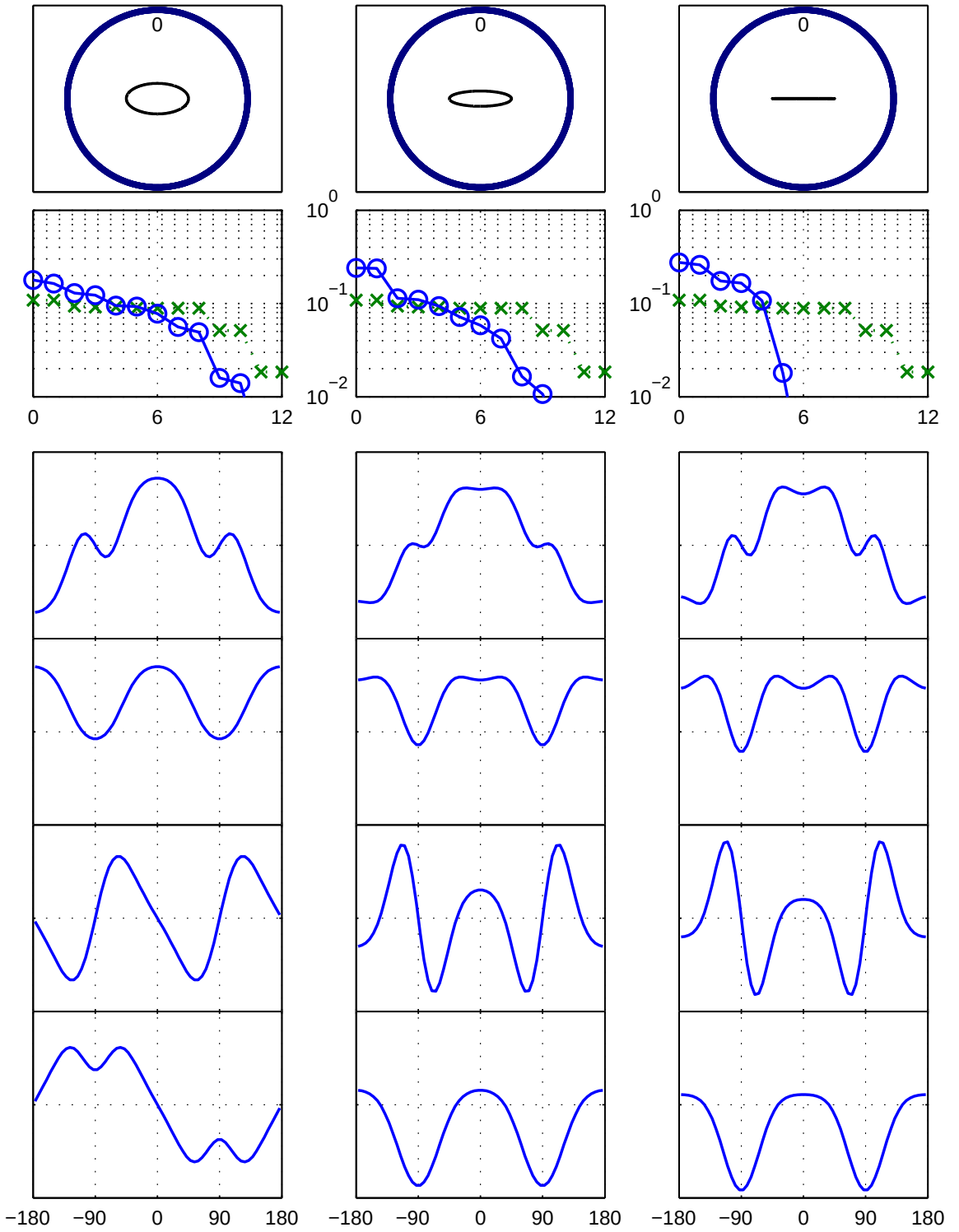

(a) Ellipse Axes 2λ and λ (b) Ellipse Axes 2λ and $\lambda/2$ (c) Uniform Linear Array

Figure 4.6: Eigenvalues and first four angular basis functions for an elliptical region with an unrestricted uniform angular source distribution. The top plot in each column shows a schematic of the region geometry and source distribution. The second plot shows the eigenvalues for the elliptical region ($\circ$) with the eigenvalues of a circular region ($\times$) shown for comparison. As the region becomes more elliptical, the eigenvalues converge towards the limiting case of a line array which is shown for comparison in the third column. For the elongated domain of interest and uniform linear array, the basis functions are nontrivial.

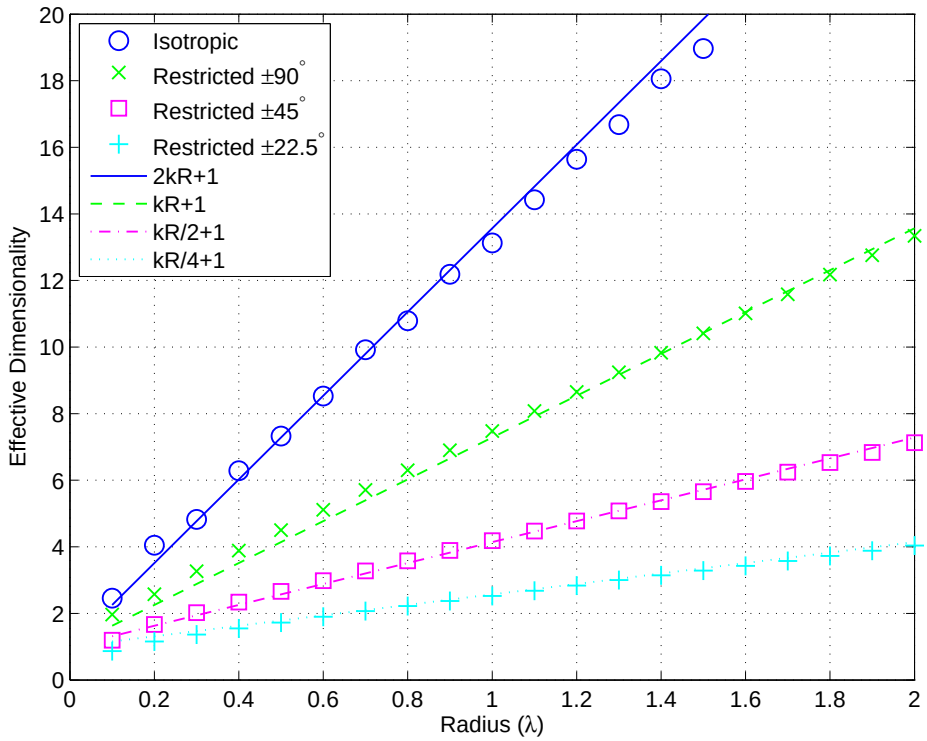

Figure 4.7: Essential dimension of a region with restricted uniform angular power spectrum. Scattered points are obtained from the numerical eigenvalues obtained from (4.37). Lines are plotted to show the empirical relationship $D = 2kRA/\pi + 1$ which shows an excellent correspondence. This figure demonstrates that dimensionality varies linearly with the radius and angular range.

analysis, we use an exponential interpolation to obtain a fractional dimensionality. The procedure is detailed in Appendix A. The fractional definition of essential dimension provides smooth curves which aid in analysing the impact of configuration changes in the following examples.

Figure 4.7 show the essential dimension as the radius is varied for four different angular power spectra. The power spectra are uniformly distributed across $|\theta| < A$ for $A = 180°$, $90°$, $45°$ and $22.5°$. The values for $D(0.01)$ obtained from the eigenvalues of (4.37) are shown to be approximated by,

$$D(0.01) \approx 2kR\frac{A}{\pi} + 1. \tag{4.86}$$

Whilst the scattered points are obtained from the eigenequation results, the lines are direct plots of the simple relationship (4.86) and have not been in any way fitted to the data. The general relationship is to be expected, as discussed in Chapter 2, Section 3. The match between the scatter points and the lines will depend on the selected threshold value. A lower

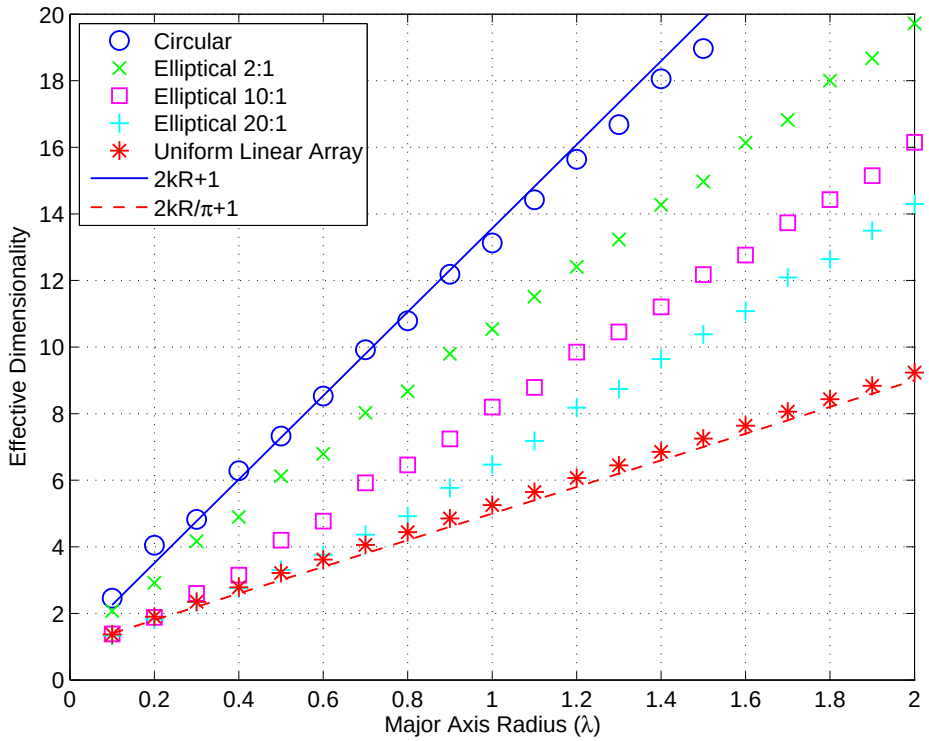

Figure 4.8: Essential dimension of an elliptical region with uniform angular power spectrum. Scattered points are obtained from the numerical eigenvalues obtained from (4.37). Lines show the empirical relationship for a circle ($D = 2kR + 1$) and uniform linear array ($D = 2kR/\pi + 1$). Between these limits the variation of dimensionality with radius is dependent on the shape of the region.

threshold value would shift all the scatter points towards a higher effective dimensionality. In this case, the threshold of 0.01 provides an excellent match for the simple dimensionality expression (4.86).

For the isotropic case, an upper bound on the dimensionality of a multipath field as $N = 2\lceil ekR/2 \rceil + 1$ has been rigorously proven [41, 42]. From the plots in Figure 4.7 it can be seen that the lower value from (4.86) is a better match for the dimensionality as defined in Definition 4.8.

The next area of investigation is to study the impact of changes to the region shape. An elliptical region is selected as a simple perturbation of the circular region. Keeping the length of the major axis the same, the region is contracted by decreasing the minor axis. Figure 4.8 shows the effect of the overall region size and ratio of major to minor axis on the dimensionality. The field is isotropic from all angles. The dimensionality is decreased as the region becomes more elliptical. The limiting case of the uniform linear array with

$$D(0.01) \approx 2kR\frac{1}{\pi} + 1. \tag{4.87}$$

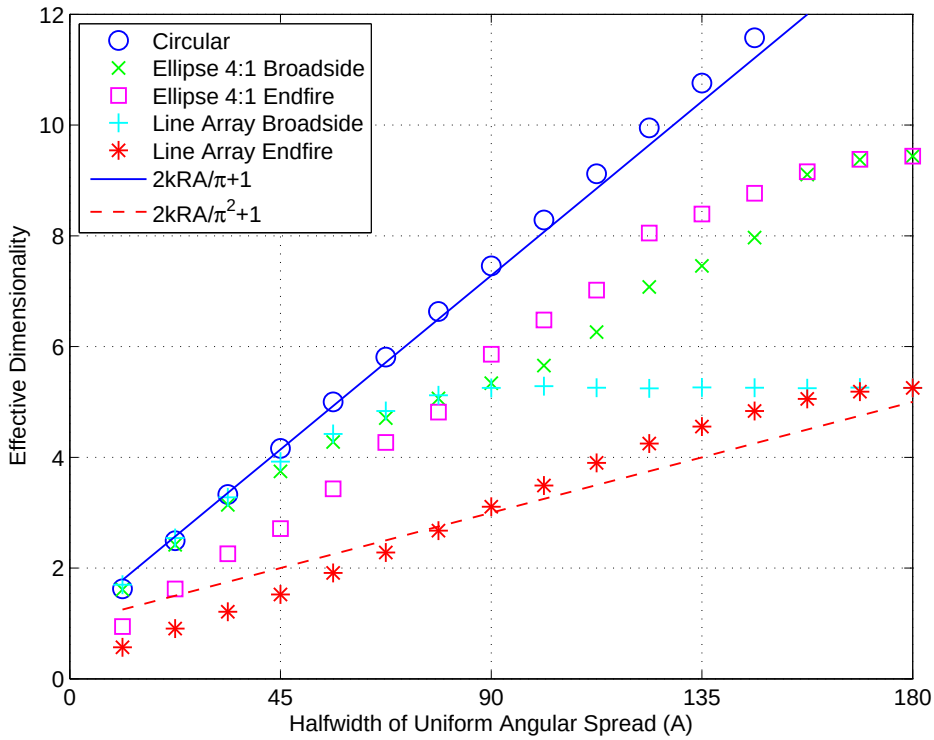

Figure 4.9: The effect of increasing angular spread on the dimensionality. The incident field is constrained to $|\theta| < A$ where A is the halfwidth of the uniform angular spread. The region lies within a radius of λ giving a major axis or linear array of length 2λ. For the asymmetric regions (elliptical and line array) the points are shown for the mean direction of arrival being aligned with the end or broad side of the array. The relative orientation has a significant impact on the dimensionality.

This is also a lower bound on the dimensionality. The scatter points approach this lower bound as the minor axis becomes insignificant compared with the wavelength ($\ll \lambda/20$). For such a region there is little diversity obtained from the width of the region since the field cannot change significantly over this distance.

Further analysis can introduce both a perturbation to the region shape and a restriction to the directions of arrival. For a circular region, the growth in dimensionality with the angular spread is linear. With an elliptical region, the growth in dimensionality is dependent on the relative orientation of the region shape and the mean direction of arrival. Figure 4.9 demonstrates the change in essential dimensionality with the angular spread. An increase in angular spread has more impact on the dimensionality when the mean direction of arrival is to the broad side of the region. The effect is minimised when the direction of arrival is collinear with the major axis of the region.

Finally consider the effect of a small angular range as it is moved around the array. The contribution to dimensionality will be maximal when aligned with the broad side of the region. The geometry for the region and angular power spectrum is shown in Figure 4.10.

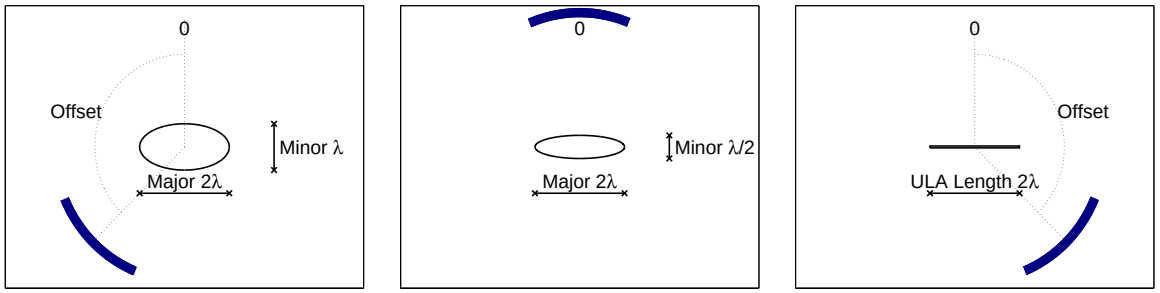

(a) Ellipse with 2:1 axis ratio shown for -135° offset of mean angle

(b) Ellipse with 4:1 axis ratio shown for 0° offset of mean angle

(c) Uniform linear array shown for 135° offset of mean angle

Figure 4.10: Schematic of the geometries for the regions and offset in the mean angle. The three figures show the three cases for which the data points are plotted in Figure 4.11. The angular range is $\pm 12.25^\circ$ around the varied offset angle. A different offset angle is shown in each of the three figures.

The effect of the shift in mean angle offset on the dimensionality of the field is shown in Figure 4.11. The angular range is 12.25° or $A = \pi/8$ radians.

Consider the kernel, (4.67), for a uniform linear array. Using trigonometric identities it follows that

$$\begin{aligned}\lambda_n g_n(\theta) &= P(\theta) \int_\Omega g_n(\phi) \text{sinc}\left(2kR\cos(\frac{\theta+\phi}{2})\sin(\frac{\theta-\phi}{2})\right) d\phi \\ &\approx P(\theta) \int_{\theta'-A}^{\theta'+A} g_n(\phi) \text{sinc}\left(kR\cos(\theta')(\theta-\phi)\right) d\phi \end{aligned} \tag{4.88}$$

with $\theta' = (\theta+\phi)/2$ and for small $\theta - \phi$. This is the much studied bandlimited kernel with asymptotic dimensionality of $2kR\cos(\theta')A/\pi$ [142]. For a small angular spread and elongated region, it is proposed that the dimensionality will vary as

$$D(0.01) = 2kR\frac{A|\cos(\theta)|}{\pi} + 1. \tag{4.89}$$

This line is plotted in Figure 4.11 and provides a good match for the limiting case of the uniform linear array.

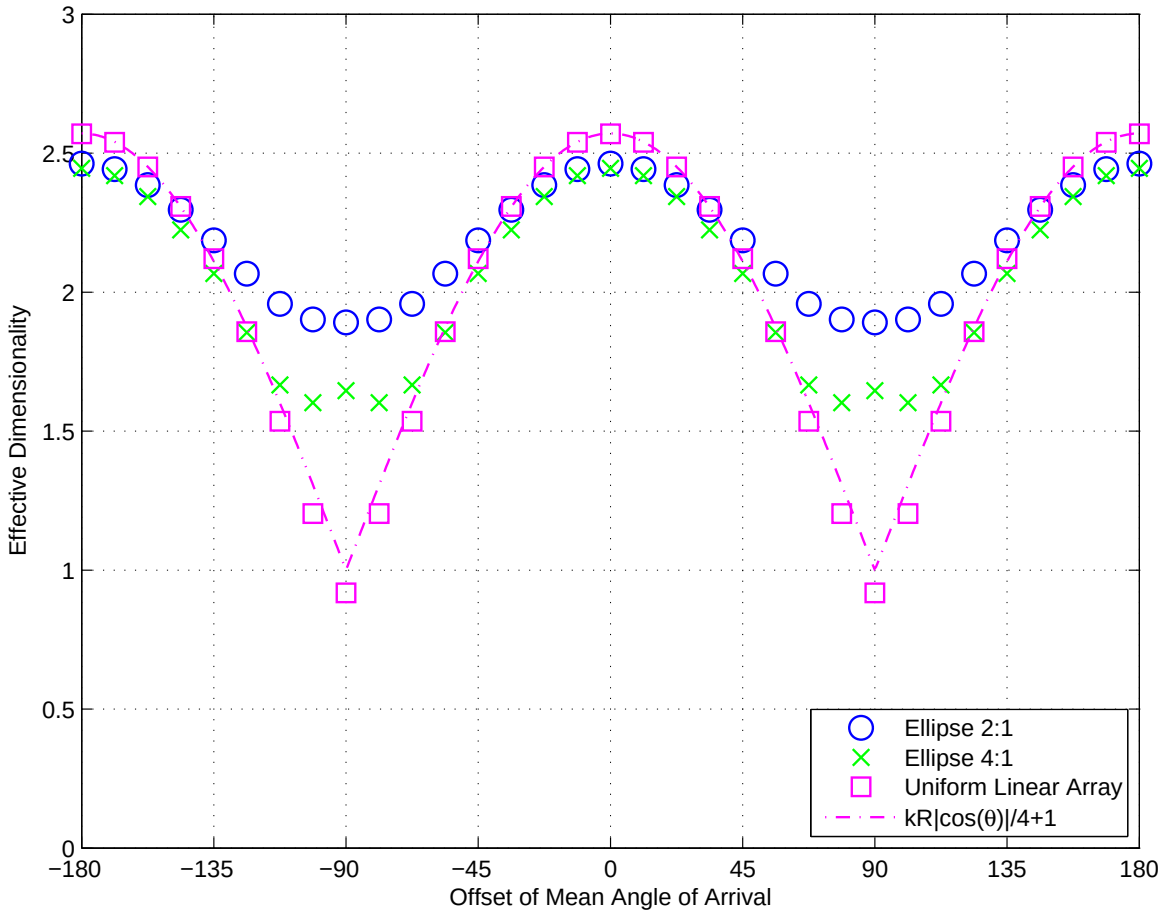

Figure 4.11: The effect of relative orientation between the array and the direction of arrival. The source distribution is restricted to a range of $\pm 12.25°$ and offset from the broadside of the elongated region by the abscissa angle. The dimensionality is maximised when the source distribution is aligned with the broad side of the array at $0°$ and $180°$. The variation is more severe as the region becomes increasingly elliptical. Also shown is the theoretical curve that would be expected for a small angular range incident on a uniform linear array.

4.8 Summary and Contributions

This chapter presented a theoretical framework for the representation of a random multipath field in the angular domain. The framework leads to an integral equation whose solutions are the optimal basis function for such a representation. In analysing this equation it is clear that the most efficient representation depends directly on the scattering environment, through the angular power spectrum $P(\theta)$, and also the way in which the field is measured or observed, through the defined domain of interest Λ. Whilst the integral equation only leads to analytical solutions in the simplest cases, it was shown that it can be accurately solved numerically, providing a means to obtain the optimal angular representation.

The following specific contributions were made in this chapter:

1. Developed a framework for the representation of a random multipath field in the angular domain. The angular domain representation implicitly captures the wave equation constraint. In addition, in comparison with a direct representation of the multipath field in space, the angular domain has one less dimension. The angular power spectra for a multipath field corresponds with the physical and engineering intuition of a spatial channel model.

2. Derived an integral eigenequation to determine the optimal set of deterministic angular basis functions for representing a random multipath field. The solution of this integral equation is dependent on both the angular power spectrum and the spatial domain of interest for the field. How the field is observed or measured has a direct bearing on the optimal representation in the angular domain.

3. Demonstrated that the integral equation in the angular framework has a direct correspondence to the Karhunen-Loéve expansion in the spatial domain. This result validated the consistency and optimality of the proposed framework.

4. Derived the closed form solutions to the eigenequation for the cases of an isotropic field and singular direction of arrival with a circular region. Investigated and concluded that the eigenequation is not easily soluble in closed form for general configurations.

5. Detailed two suitable numerical techniques to accurately approximate the solution of the integral equation using a discrete matrix equation. Demonstrated that the size of the matrix is determined by the extent of the domain of interest with a matrix dimension of $2\lceil kR \rceil + 1$ required for a two-dimensional region with maximum radius R and field wavenumber $k = 2\pi/\lambda$.

6. Demonstrated that the high resolution details in the power spectrum, $P(\widehat{\boldsymbol{\theta}})$, beyond a certain point are largely irrelevant in determining the optimal representation. For the two-dimensional case it was shown that only the low order Fourier coefficients of $P(\theta)$ are significant. The critical characteristics of the system for determining the optimal basis set are the physical extent of the region of interest and the low frequency content of the angular power spectrum.

7. Presented examples to characterise the way in which the shape and distribution of the region and the power spectrum interact and effect the number of significant solutions of the eigenequation. This directly relates to the optimal number of terms needed to represent the random field. These examples demonstrated the macroscopic aspects of the interaction between the angular power spectrum and the domain of interest.

8. Introduced the essential dimensionality as the number of terms required to capture 99% of the energy of the random multipath field. This represents a 20dB signal to truncation error ratio. Analysis of the eigenvalue results demonstrated that this threshold is consistent with previously stated expressions for dimensionality. In particular, a circular region with a uniform restricted angular power spectrum has dimensionality $D = 2kR\,A/\pi + 1$, where the range of incident angles is restricted to $\pm A$ about the mean angle.

Chapter 5

Spatial Limits to Direction of Arrival Estimation

5.1 Introduction and Motivation

The previous chapters have addressed the issue of dimensionality and effective representation of a spatial field. A field over a finite region can be well modelled to an arbitrary precision by a finite set of basis functions. In the presence of noise, an observed field cannot be arbitrarily complex. Although space is continuous, the nature of wave propagation restricts the possible variation of the spatial field across the observation volume. This result will have important practical implications when considering the ability to resolve or estimate parameters from the incident field.

The implications of the dimensionality result for the capacity of a multiple antenna system have recently been highlighted [122] with the notion of an intrinsic capacity of a region of [138, 146]. These works suggest capacity bounds and limiting performance for multiple antenna communication systems. In this chapter we extend this work to a different but related problem, that of estimating a source's direction of arrival.

The question that will be posed and addressed in this chapter is:-
Is there a spatial limit to the ability to resolve direction of arrival?

Direction of arrival (DOA) estimation is an area of research that has achieved much attention over the last few decades. The problem of DOA estimation is generally approached with algorithms, estimates and bounds tied to specific sensor array geometries. An alternative approach is to consider the fundamental limits imposed by the dimensionality or degrees of freedom of the spatial field being observed.

In Chapter 2 results were presented regarding the effective finite dimensionality of a wavefield over a bounded region of space. Chapter 4 demonstrated that the number and functional form of the basis functions representing these degrees of freedom was dependent on the angular power spectrum and the shape and size of the region of interest. The effective dimensionality and nature of the basis functions will constrain the number of independent sources that can be resolved and resolution with which their direction can be estimated. In this chapter we consider the impact of the region size on the performance of direction of arrival estimation. The work represents an extension of some work which was previously published [129] and has been submitted for publication [204].

Section 5.2 of this chapter provides a review and classification of some of the key literature in this area. In Section 5.3 we provide a numerical investigation based on a finite element uniform circular array that supports the intuition of fundamental limits to DOA performance. Section 5.4 presents a new continuous sensor model and develops an appropriate noise model that is consistent with the conventional sensor noise model in the limit of a large number of sensors. Using this framework, Section 5.5 presents the derivation of the Cramér-Rao bound for DOA estimation of one and two sources given a finite observation region. These bounds are verified through further numerical analysis in Section 5.6.

The main contribution of this chapter is the development of a continuous sensor noise model and its application to determine the fundamental limits of performance for direction of arrival estimation. The numerical analysis provides support and validation of the theoretical results presented. From these results it is apparent that the number of sources that can be resolved, given a finite observation region, are directly related to the essential dimensionality of the multipath field.

The dimensionality of the field will be related to the size and general shape of the region of interest. In this chapter we focus on the limits resulting from the region size. Further discussion of the impact of the region shape can be found in Chapter 4.

5.2 Review of Direction of Arrival Literature

Direction of arrival (DOA) estimation is an important problem in signal processing with direct applications in radar, imaging, and wireless communications. Conventional approaches to examining the performance limitations of DOA estimators have focussed on deriving resolution bounds based on sensor array geometry (size, shape and number of sensors).

A recent publication dedicated to the topic demonstrates the continued and active interest in the area [205]. The topic is directly related to the modelling and understanding of the spatial channel in MIMO systems. A preliminary treatise by Landmann et al. [206] provides an intuitive discussion of how the resolution and limits of direction of arrival estimation is related to MIMO channel sounding and modelling.

In this section we present a review of the key literature in the area, particularly that which provides a context for the research presented in this chapter.

5.2.1 Direction of Arrival Estimation

The problem of general direction of arrival estimation became of significant interest around the time of the Second World War. Whilst early practical systems employed physical means of direction finding, the theoretical analysis and potential for signal processing advances in the area was realised early on. Significant advances in the area coincided with the advance of electronics and signal processing over the last three decades [207].

The Bartlett beamformer [208] was proposed in the 1950s. This approach utilised a Fourier analysis of the antenna array signals to resolve the direction of arrival. Enhanced techniques of spectral analysis, such as the Capon beamformer [209] were then applied to increase resolution [210]. The development of signal subspace approaches to resolving multiple source directions of arrival created significant interest in the area. The MUSIC algorithm [211] and general subspace techniques [212] offered computationally effective approaches to the problem. Further advances such as Root-MUSIC [213] and ESPRIT algorithm [214] soon followed. Maximum likelihood [215–217] and spatio-temporal parametric models have also been developed [218].

The nature of the signal model, particularly for the uniform linear array, is the same as that for detecting complex sinusoids in noise [210]. As a result, advances, analysis and results in the two fields have proceeded largely in parallel. Maximum likelihood techniques are generally superior [216, 219] but computationally complex requiring multi-dimensional maximisation. The signal subspace approaches are popular since they are computationally less intensive

and facilitate practical implementation. The MUSIC algorithm requires a one-dimensional search whilst the ESPRIT algorithm is centred on a singular value decomposition [207]. With appropriate weighting it has been shown the subspace techniques have the same asymptotic properties as the maximum likelihood estimates [212] and even simple MUSIC is known to be asymptotically efficient [220].

The general approach to direction of arrival estimation is to integrate the sensor outputs over time to estimate the covariance. This approach suffers a degradation with non stationary (in direction of arrival) sources [221]. An alternate approach is to consider the temporal evolution of directions of arrival and make use of tracking algorithms to improve performance. Simple recursive tracking algorithms were proposed [222] leading to the development of a Kalman filter framework [223]. This allowed the estimation of direction and angular velocity [224] with state models for modelling target dynamics [225]. The problem of tracking and dynamic sources is not considered in this work.

5.2.2 Uncertainty in Direction of Arrival Estimates

In conjunction with the development of algorithms for estimating direction of arrival, many works are concerned with understanding the theoretical limits of performance. The achievable accuracy of an unbiased estimate of an unknown parameter is bounded by the Cramér-Rao bound (CRB) [226]. In [219, 227], the Cramér-Rao bound (CRB) is derived for an array with a known geometry and white noise. This result has since been extended to a variety of other, more complicated, noise models [228, 229]. In such results, the CRB is given in matrix form with a strong dependence on the geometry of the sensor array. A review of the area ([230] and refs therein) presents some simplified expressions, but largely for the uniform linear array. With more general geometries, it is difficult to investigate more fundamental limitations on DOA performance.

There have been attempts to simplify and interpret the CRB [231] and its derivation [232]. Results are presented for the case of multiple sources incident on a uniform linear array [233]. The CRB expressions can be simplified making some mild assumptions [234]. Asymptotic expressions of the CRB for one and two sources for a uniform linear array have been derived [235].

Whilst the CRB is a local measure of uncertainty [230], there is an additional problem of ambiguities in the array manifold [236]. Linear combinations of the array from several directions can be degenerate, creating problems in resolving direction of arrival.

5.2.3 Number of Sources that can be Resolved

Another related area of research is concerned with the number of discrete sources that can be resolved by an array. The problem relates to the uniqueness of the data generated by multiple sources [237]. It has been suggested that the number of sources that can be resolved is related to the co-array of sensor locations or the level of redundancy in the array [238–240]. Such approaches provide a theoretical analysis based on numerical uniqueness [241, 242] and do not reflect the uncertainty introduced by noise. A numerical study showed the accuracy of resolving direction of arrival degrades rapidly as the sources become closer than the beam-width of the array [243].

In MIMO systems the presence of correlated scattered sources created additional complications [244]. For multiple reflections of a single source, it is possible to use some of the structure of the signal to enhance the resolution [245].

There is a need for clearer practical limits to the number of sources that can be resolved by an array. An engineering intuition would suggest that the limit is dependent on some macroscopic property of the array such as the spatial extent and general shape rather than on the numerical nuances of the sensor geometry.

5.2.4 Impact of Sensor Array Geometry

The uncertainty for direction of arrival estimation is related to the geometry of the sensor array. Much of the work in this area has been concerned with uniform linear arrays and appropriate element spacings [246]. Greater resolution can be obtained with non-uniform linear arrays and maximum non-redundancy [238]. Such designs are usually concerned with minimising the number of sensors, optimising the effective aperture [247] and reducing array ambiguities [248]. Such arrays are under-sampled and will suffer from some ambiguities for multiple sources [236], and although this does not always preclude resolving the sources [249] it creates problems for signal subspace approaches.

A recent analysis provides a method of antenna array design by considering the impact of the array geometry on the CRB [250]. The work considers planar arrays with relatively simple geometries. Optimal and isotropic sensor geometries for direction of arrival estimation were considered in [251]. A comprehensive study for three-dimensional arrays was carried out [252] establishing a simple geometric relationship between sensor placement and the CRB. This relationship was shown to correspond to the sensor array moment of inertia [251, 253]. This approach provides more general expressions for the CRB for discrete sensor based measurements.

For this work we consider the use of unpolarised sensors, or the analysis of a scalar field. The use of vector sensors for field measurements offers advantages in the estimation of direction of arrival [254, 255].

5.2.5 Review and Discussion

The review of the literature shows an extensive amount of research in the area. The results presented are generally specific to array configurations and often constrained to linear arrays or simple geometries. The most relevant result to this research is the link between the Cramér-Rao bound and the sensor moments of inertia.

Often in practice, all that is certain is the physical extent over which the array can interact with the spatial field. Antennas do not simply sample the field at a point. Multi-mode sensors [102], mutual coupling [256] and other array uncertainties and interactions [257] must be considered in addition to the sensor geometry.

In this chapter we present an alternate framework for considering the limiting performance of a DOA estimator based on a continuous measurement over a given region. With this approach we consider how the performance of DOA is fundamentally limited by the spatial extent of the array without the need to consider the specific geometry of the sensor placement. Previous work [128, 258] considered the spatial limits of DOA through simulations. In this chapter we expand on this result and provide a more detailed theoretical investigation leading to general results for the performance of direction of arrival estimation.

5.3 Numerical Investigation of Limits to DOA Estimation

To confirm the intuition of a spatial limit to the resolution of direction of arrival we can perform some numerical simulations. A popular algorithm for estimating the direction of arrival of sources from data is the MUSIC algorithm [211]. The MUSIC algorithm offers computational advantages over a maximum likelihood approach, requiring only a one-dimensional search for multiple sources. For large signal to noise ratios it is statistically efficient with performance approaching that of the maximum likelihood estimator [227]. For these reasons we use it to provide a preliminary investigation of the spatial limiting performance to direction of arrival estimation.

5.3.1 MUSIC Algorithm

The music algorithm uses a signal subspace formulation to estimate the directions of arrival for multiple sources. Assume P sources with narrow-band signal samples $\boldsymbol{s}(n)$ for time samples $n = 1, \ldots, N$. We assume the following signal model for $Q > P$ sensors,

$$\boldsymbol{y}(n) = \mathbf{A}(\boldsymbol{\theta})\boldsymbol{s}(n) + \boldsymbol{w}(n) \quad \mathbf{A}(\boldsymbol{\theta}) = \left[\begin{array}{ccc} \boldsymbol{a}(\theta_1) & \ldots & \boldsymbol{a}(\theta_P) \end{array} \right] \tag{5.1}$$

where $\mathbf{A}(\boldsymbol{\theta})$ is the $Q \times P$ array response steering matrix with a column for each source direction. Assume the source signal $\boldsymbol{s}(n)$ is zero mean with variance $\mathbf{R}_{\boldsymbol{s}}$ and the noise vector $\boldsymbol{w}(n)$ is white in space and time with variance $\sigma^2_{\boldsymbol{w}}$. The covariance of the signal vector $\boldsymbol{y}$ is

$$\mathbf{R} = E\left\{\boldsymbol{y}\boldsymbol{y}^H\right\} = \mathbf{A}(\boldsymbol{\theta})\mathbf{R}_{\boldsymbol{s}}\mathbf{A}^H(\boldsymbol{\theta}) + \sigma^2_{\boldsymbol{w}}\mathbf{I}. \tag{5.2}$$

The first term of the covariance will have maximum rank of P. Thus the $Q - P$ smallest eigenvalues of $\mathbf{R}$ will match the noise variance $\sigma^2_{\boldsymbol{w}}$. Construct an estimate of the covariance matrix from the data

$$\widehat{\mathbf{R}} = \frac{1}{N}\sum_{n=1}^{N} \boldsymbol{y}(n)\boldsymbol{y}^H(n) \tag{5.3}$$

and consider the ordered eigenvalues of $\widehat{\mathbf{R}}$ as $\widehat{e}_q$, for $q = 1, \ldots, Q$. We estimate the noise subspace from the $Q-P$ smallest eigenvalues, and use the associated eigenvectors as a basis,

$$\widehat{\mathbf{E}}_n = \left[\begin{array}{ccc} \widehat{\boldsymbol{e}}_{P+1} & \widehat{\boldsymbol{e}}_{P+2} & \ldots \quad \widehat{\boldsymbol{e}}_Q \end{array} \right]. \tag{5.4}$$

This is then used to search over our direction parameter θ using the inverse of the projection of the array steering vector onto the noise subspace. The MUSIC spectrum is defined as

$$S_{\mathrm{MUSIC}}(\theta) = \frac{\boldsymbol{a}^H(\theta)\boldsymbol{a}(\theta)}{\boldsymbol{a}^H(\theta)\widehat{\mathbf{E}}_n\widehat{\mathbf{E}}_n^H\boldsymbol{a}(\theta)}. \tag{5.5}$$

The area of subspace based parameter estimation has received much attention in the last few decades. There are many techniques for enhancing the performance of the MUSIC algorithm for specific array geometries and noise conditions [207]. The MUSIC algorithm is known to be asymptotically efficient [220]. We present simulations using the basic MUSIC algorithm to gain a qualitative understanding of the limits of the array size on direction of arrival estimation. This will throw light on the factors that limit the performance of direction of arrival estimation and inform the theoretical investigation of fundamental limits.

5.3.2 MUSIC Spectra for Multiple Sources

Consider a 15 element uniform circular array with a number, P, of uncorrelated unity power sources distributed uniformly in direction. This source configuration provides the least bias and interaction between the estimated direction of arrival parameters. We are interested in the minimum size of the region required to correctly resolve the P sources. Figure 5.1 shows the MUSIC spectra for $P = 4, 8$ and 12 sources. This simulation clearly demonstrates that the minimum radius at which the sources are resolved increases with the number of sources. The radius for resolving the sources is approximately 0.3λ, 0.6λ and 0.9λ respectively.

The previous simulation was for a specific array geometry with 15 sensors. If the limiting factor for the resolution of direction of arrival is the spatial extent of the array, we would expect changing the number of sensors to have little effect. Figure 5.2 shows the MUSIC spectra for $P = 12$ incident sources with $Q = 15, 30$ and 45 sensors. Whilst the larger number of sensors creates a smoother MUSIC spectra, the transition point beyond which the sources are successfully resolved remains at approximately 0.9λ independent of the number of sensors.

As discussed in Chapter 2, an increase in the signal to noise ratio will have some effect on the significant number of dimensions of the observed field. Figure 5.3 shows a simulation of the 45 element uniform circular array with 12 sources as the effective signal to noise ratio is increased. A significant increase in the signal power only has a small secondary effect on the critical radius for resolving the sources.

From these simulations, it is apparent that the spatial extent of a sensor array creates an intrinsic limit to the number of sources that can be resolved. We will now investigate this further analytically.

5.4 Continuous Sensor Framework

The previous section provided an investigation of the ability of a uniform circular array to resolve source direction. The focus of this chapter is to investigate the fundamental limits of direction of arrival estimation without reference to a particular sensor array configuration. The concept of the continuous spatial field was introduced in Chapter 2 and it was shown that fields constrained by the wave equation have a finite dimensionality. In this section we develop a signal model for the spatial field utilising the continuous spatial modes.

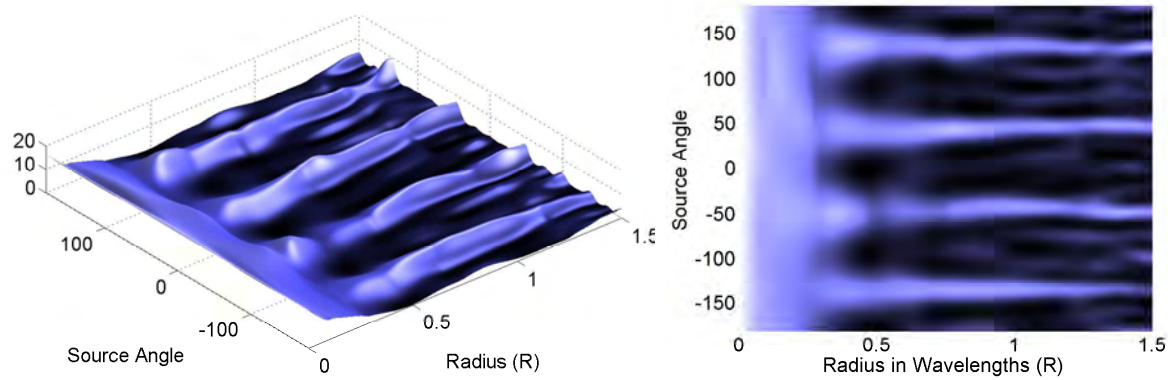

(a) $P = 4$ Sources

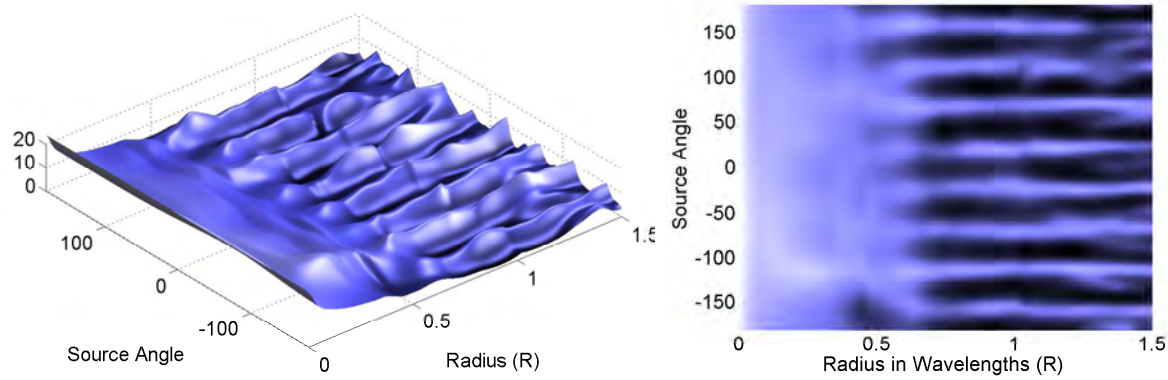

(b) $P = 8$ Sources

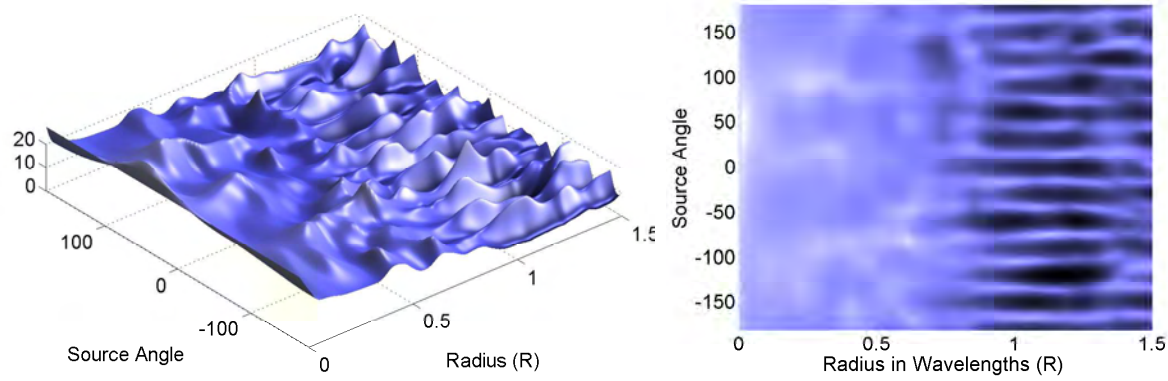

(c) $P = 12$ Sources

Figure 5.1: Simulation of the estimation of multiple source direction of arrival using the MUSIC algorithm with an 15 element UCA. As the number of sources is increased, the minimum radius at which all of the sources are resolved also increases. The ability to resolve is related to the effective dimensionality of the field in the sensor region. The vertical axis in the 3D plot represents the MUSIC spectrum value in dB.

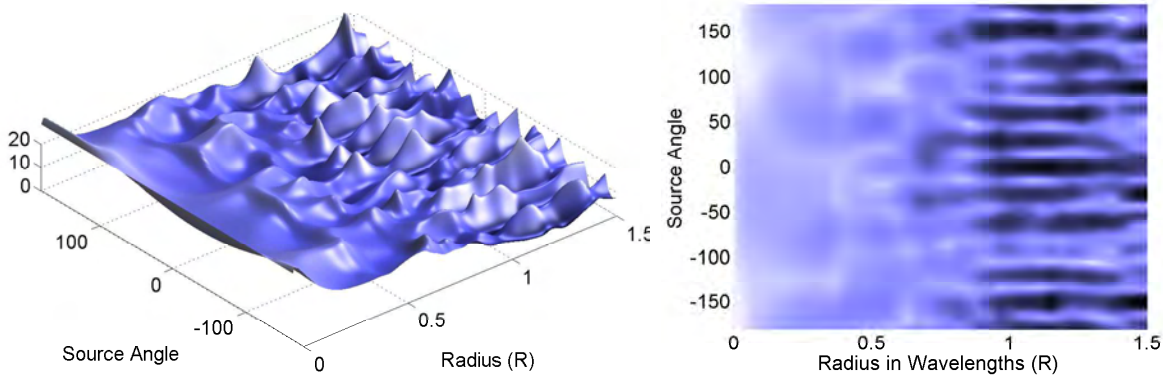

(a) $Q = 15$ Element UCA

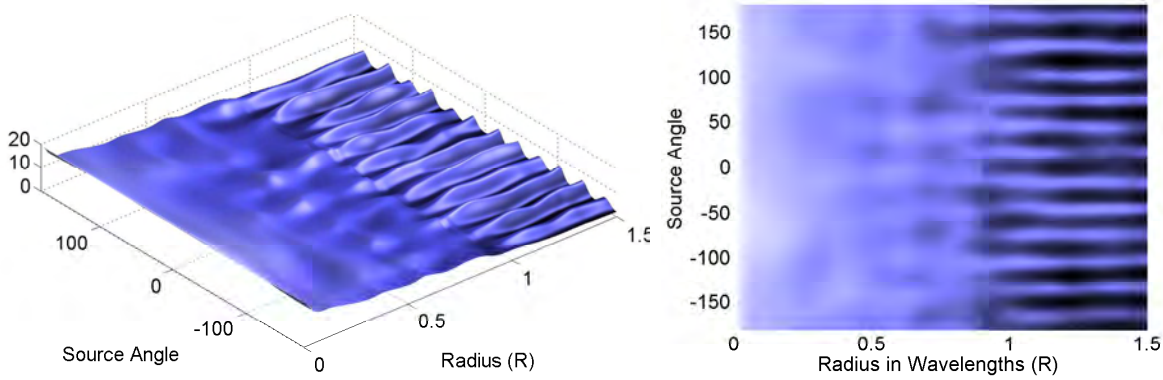

(b) $Q = 30$ Element UCA

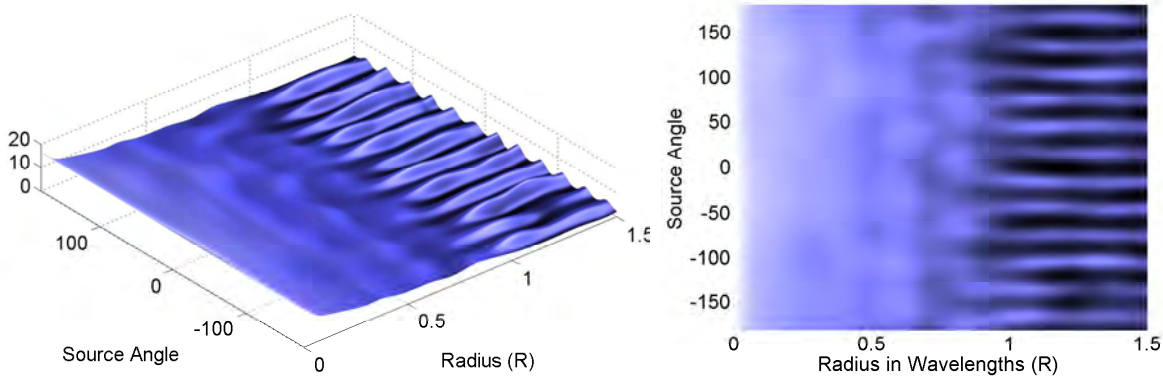

(c) $Q = 45$ Element UCA

Figure 5.2: With $P = 12$ sources, the number of elements in the uniform circular array is increased. The radius at which all of the sources can be resolved is fairly invariant as the number of sensors is increased. Intuitively, the number of sources that can be resolved is intrinsically related to the extent of the sensor array and not the sensor geometry. The vertical axis in the 3D plot represents the MUSIC spectrum value in dB.

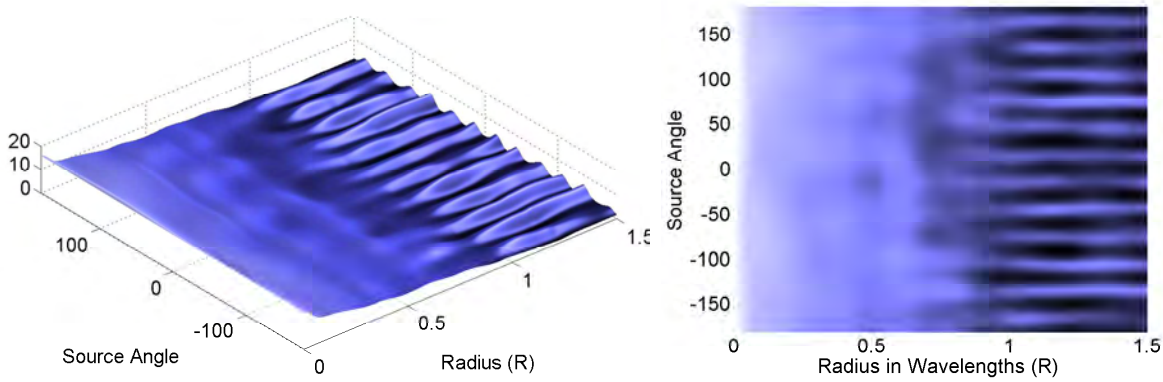

(a) Signal to Noise Ratio 20dB

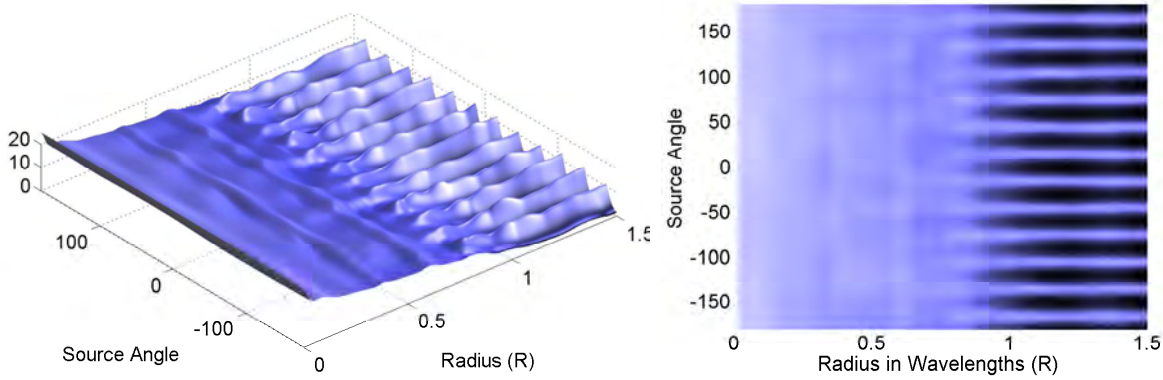

(b) Signal to Noise Ratio 30dB

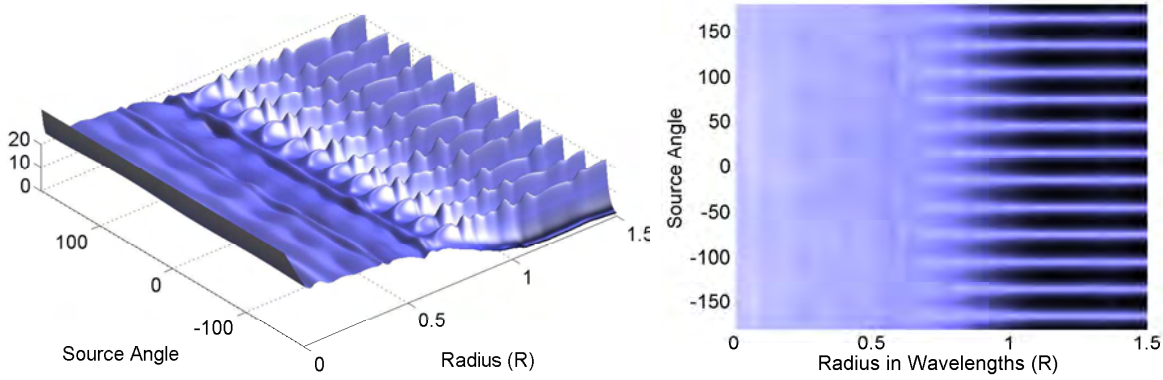

(c) Signal to Noise Ratio 40dB

Figure 5.3: With $P = 12$ sources and a $Q = 45$ sensor uniform circular array, the effective signal to noise ratio is varied. While the resolving radius is decreased with increasing signal to noise ratio, a 100 fold increase in the signal power only reduces the radius from 0.9λ to approximately 0.7λ. The resolution threshold is largely independent of the signal to noise ratio. The vertical axis in the 3D plot represents the MUSIC spectrum value in dB.

5.4.1 Continuous Field Model

Let $u(\boldsymbol{x}, n)$ represent the field over the sensor array region Λ at time sample n. The field will be continuous and satisfy the wave equation, allowing representation through a countable basis. The series expansion for the field on Λ will be convergent in the mean, thus

$$u(\boldsymbol{x}, n) = \sum_{m=-\infty}^{\infty} \alpha_m(n)\beta_m(\boldsymbol{x}), \tag{5.6}$$

in the sense that

$$\lim_{M\to\infty} \left\| u(\boldsymbol{x}, n) - \sum_{m=1}^{M} \alpha_m(n)\beta_m(\boldsymbol{x}) \right\|_{\Lambda} = 0 \tag{5.7}$$

with the basis functions β_m orthogonal over Λ. This equation characterises the synthesis of the field from a set of coefficients $\alpha_m(n)$. Chapter 4 dealt with the determination of such a basis. The basis will span the space of possible solutions to the wave equation, and in this sense is complete.

Given the field over the region Λ, we can perform an analysis to determine the continuous mode coefficients. This is the normalised inner product

$$\alpha_m(n) = \|\beta_m\|_{\Lambda}^{-2} \langle u(\boldsymbol{x}, n), \beta_m(\boldsymbol{x}) \rangle_{\Lambda} = \|\beta_m\|_{\Lambda}^{-2} \int_{\Lambda} u(\boldsymbol{x}, n)\overline{\beta_m(\boldsymbol{x})} d\boldsymbol{x}, \tag{5.8}$$

where $\|\beta_m\|_{\Omega}^2 = \int_{\Omega} |\beta_m(\boldsymbol{x})|^2 d\boldsymbol{r}$ is the usual norm. This framework captures the idea of a continuous sensor across the measurement volume to recover the mode coefficients. These coefficients contain all the information about the field and consequently can be used in the direction of arrival estimation framework. As we have seen in Chapter 2, only a finite number of modal coefficients will be required to accurately represent the field over a finite region Λ.

5.4.2 Noise Model

In practice, any system will be limited by noise. Our ability to recover and use the modal coefficients from the analysis (5.8) will be constrained by noise. To analyse these limits, we need to develop a suitable noise model in the continuous domain. To provide a context for any results, we desire a noise model that is in some way consistent with the conventional sensor noise model.

Consider a set of Q sensors located at positions $\boldsymbol{x}_q$, $q = 1, \ldots, Q$. The sensor outputs, y_q can be viewed as discrete time spatial samples of the underlying field,

$$y_q(n) = u(\boldsymbol{x}_q, n) + w_q(n) \quad n = 1, \ldots, N. \tag{5.9}$$

The conventional model assumes spatially and temporarily white Gaussian noise[1] with variance $E\left\{w_m(n)\overline{w_{m'}(n')}\right\} = \delta_{mm'}\delta_{nn'}\sigma^2$.

Consider a large number of sensors placed evenly throughout the measurement region Λ. Since the field is continuous and bounded we can write

$$\lim_{Q\to\infty} \frac{|\Lambda|}{Q} \sum_{q=1}^{Q} u(\boldsymbol{x}_q, n)\overline{\beta_m(\boldsymbol{x}_q)} = \int_\Lambda u(\boldsymbol{x}, n)\overline{\beta_m(\boldsymbol{x})} d\boldsymbol{r} \qquad \boldsymbol{x}_q \in \Lambda. \tag{5.10}$$

where $|\Lambda| = \int_\Lambda d\boldsymbol{x}$ represents the volume of the region. Using this in the analysis equation (5.8) gives an estimate of the modal coefficient

$$\begin{aligned} \widehat{\alpha}_m(n) &= \|\beta_m\|_\Lambda^{-2} \frac{|\Lambda|}{Q} \sum_{q=1}^{Q} y_q(n)\overline{\beta_m(\boldsymbol{x}_q)} \\ &= \alpha_m + \|\beta_m\|_\Lambda^{-2} \frac{|\Lambda|}{Q} \sum_{q=1}^{Q} w_q(n)\overline{\beta_m(\boldsymbol{x}_q)}. \end{aligned} \tag{5.11}$$

The second term is a linear combination of the sensor noise and has variance

$$\begin{aligned} \sigma_m^2 &= \frac{|\Lambda|^2}{\|\beta_m\|_\Lambda^4 Q^2} E\left\{ \sum_{q=1}^{Q} w_q(n)\overline{\beta_m(\boldsymbol{x}_q)} \sum_{q'=1}^{Q} \overline{w_{q'}(n)}\beta_m(\boldsymbol{x}_{q'}) \right\} \\ &= \frac{|\Lambda|^2}{\|\beta_m\|_\Lambda^4 Q^2} \sigma^2 \sum_{q=1}^{Q} \beta_m(\boldsymbol{x}_q)\overline{\beta_m(\boldsymbol{x}_{q'})} = \frac{|\Lambda|^2}{\|\beta_m\|_\Lambda^2 Q^2} \sigma^2. \end{aligned} \tag{5.12}$$

The noise in estimating the modal coefficient is scaled by the volume of the measurement region, divided by the number of sensors and the squared norm of the basis function on the region. This at first may seem counterintuitive, since the noise decreases with a larger number of sensors. This is a result of the model assuming independent noise on each sensor. As more sensors are added, each detects the field with an independent noise term which can be averaged out. More measurements increases the effective signal to noise ratio in estimating the modal coefficients, thus the modal noise decreases.

[1] Where the noise is not white, it can be whitened with an appropriate linear transformation based on the noise covariance structure.

5.4.3 Continuous Sensor Model

Consider a signal transformation to whiten the noise on the modes,

$$z_m(n) = \sqrt{C_m}\alpha_m(n) + \widehat{w}_m(n) \qquad \text{where} \qquad C_m = \|\beta_m\|_\Lambda^2 \, Q/|\Lambda|. \tag{5.13}$$

The scaling factor C_m is a function of the region, number of sensors and basis. The noise, $\widehat{w}_m(n)$, has unit variance and is independent in time and for each mode.

The continuous sensor signals $z_m(n)$, provide a countable set of outputs. If the basis functions, β_m, are normalised over some region enclosing Λ, all but a finite set of $\|\beta_m\|_\Lambda^2$ will be negligible [80]. The scaling of the modal coefficient estimates captures the inherent dimensionality of the spatial field.

This model is consistent with the standard sensor model for large Q. For small Q, the samples $\beta_m(\boldsymbol{r}_q)$ will not be orthogonal. This will mean that the model of (5.13) will not be valid. The noise term in the modes $\widehat{w}_m(n)$ will not be unit variance with the overall noise power across the observed modes increasing. If the space is under sampled with less Q samples than the number of observed modes, the noise terms $\widehat{w}_m(n)$ will also become correlated. In this sense, the continuous signal model developed provides a bound of the performance of a system with a finite number of sensors. It assumes the minimum achievable noise power and noise correlation in the estimation of the modal signals. In practice, finite sensor and sampling issues will further limit system performance [83].

5.4.4 Signal Model

For the direction of arrival problem, we consider a set of P sources with directions $\boldsymbol{\theta} = [\theta_1, \ldots, \theta_P]$ with associated narrow-band signals $\boldsymbol{s}(n) = [s_1(n), \ldots, s_P(n)]^T$. The narrow-band assumption ensures the signalling bandwidth is sufficiently small that the delayed signal across Ω is constant [259, p. 34][2]. This approximation permits the signal model

$$\boldsymbol{z}(n) = \mathbf{A}(\boldsymbol{\theta})\boldsymbol{s}(n) + \boldsymbol{w}(n) \quad \mathbf{A}(\boldsymbol{\theta}) = [\boldsymbol{a}(\theta_1) \ldots \boldsymbol{a}(\theta_Q)] \tag{5.14}$$

where $\mathbf{A}(\boldsymbol{\theta})$ is the response matrix with an infinite column for each of the source directions θ_p. This gives us a similar framework to that used in discrete sensor DOA problems, however the signal space is the scaled coefficients of the field synthesis equation (5.6). This signal

[2]This can be achieved through narrow-band signalling, or appropriate signal sub-banding. For example, the 802.11 standard uses OFDM with 64 subcarriers occupying a 20MHz band. This creates a 312.5 kHz bandwidth for signalling on each subcarrier. Thus narrow-band assumption is valid for $R \ll 960\mathrm{m}$.

space represents the complete information that could be obtained from the measurement region Λ subject to the constraint of the noise model. We use this to determine the limiting performance of direction of arrival estimation.

5.5 Bounds on the Performance of DOA Estimation

5.5.1 Continuous Circular Array

We apply the framework developed in the previous section to a circular region. As set out in Chapter 4, Section 4.4.1, a suitable basis which is orthogonal for any radially symmetric region is

$$u(\boldsymbol{x}) = \sum_{m=-\infty}^{\infty} \alpha_m \beta_m \quad \text{with} \quad \beta_m = j^m J_m(k \left\| \boldsymbol{x} \right\|) e^{jm\theta_{\boldsymbol{x}}}, \tag{5.15}$$

where $J_m(\cdot)$ is the Bessel function of order m, $k = 2\pi/\lambda$ is the wave number and $\theta_{\boldsymbol{x}}$ is the angle in polar coordinates of $\boldsymbol{x}$. The coefficients α_m in this expansion for a plane wave with incident direction θ are $\alpha_m = e^{-jm\theta}$ [91].

The case of a uniform circular array corresponds to the sensors placed at the edge of the region with radius R. The scaling factor (5.13) for this case is

$$C_m = \frac{Q}{2\pi R} \int_0^{2\pi} \left| \beta_m(\boldsymbol{x}) \right|^2 R d\theta = Q J_m^2(kR). \tag{5.16}$$

The columns of the array steering matrix $\mathbf{A}$ for this basis will be

$$\boldsymbol{a}(\theta) = \left[\ldots, \sqrt{C_{-m}} e^{jm\theta}, \ldots, \sqrt{C_m} e^{-jm\theta}, \ldots \right]^T. \tag{5.17}$$

5.5.2 The Cramér-Rao Lower Bound

The achievable accuracy of an unbiased estimate of an unknown parameter is bounded by the Cramér-Rao bound (CRB) [226]. We are interested in the variance of an estimate of the directions of arrival $\boldsymbol{\theta}$. Since the signals, $\boldsymbol{s}(n)$, are also unknown, they must be accounted for in the estimation. Two estimation frameworks are typically presented [128]. The deterministic or conditional signal model formulation estimates the actual signals [227], whilst the stochastic or unconditional formulation provides an estimate of the signal covariance [232, 260]. The deterministic CRB is lower than the stochastic [260] and is often used as a good estimator of performance for large number of sensors [261]. To approach the deterministic CRB an estimator must determine the actual signals from each direction. This becomes infeasible with a low signal to noise ratio [259, 262].

Generally, the noise power is also an unknown parameter that has to be estimated. The form of the CRB remains unchanged if the noise level σ^2 is a known or estimated parameter [263].

Since we are interested in the limiting case of many sensors and reasonable signal to noise ratio, the deterministic CRB will be used in this work as an overall lower bound.

$$\text{CRB} = \frac{\sigma^2}{2N}\left\{\text{Re}\left[\left(\mathbf{D}^H\mathbf{D} - \mathbf{D}^H\mathbf{A}\left(\mathbf{A}^H\mathbf{A}\right)^{-1}\mathbf{A}^H\mathbf{D}\right)\odot \mathbf{R}_{\boldsymbol{s}}{}^T\right]\right\}^{-1}, \tag{5.18}$$

where

$$\mathbf{D} \triangleq \left[\frac{\partial}{\partial\theta_1}\boldsymbol{a}(\theta_1), \ldots, \frac{\partial}{\partial\theta_P}\boldsymbol{a}(\theta_P)\right]. \tag{5.19}$$

The matrix $\mathbf{R}_{\boldsymbol{s}}$ is the sample covariance matrix for the signals $\boldsymbol{s}$ and $\odot$ represents the elementwise Schur-Hadamard product of the matrices. The matrix $\mathbf{A} \equiv \mathbf{A}(\boldsymbol{\theta})$ is dependent on the source directions. Whilst the matrices are infinite, it is to be noted that $C_m \approx 0$ for $m > kR$. Previous work [41] models this effect as a truncation. In this framework the dimensionality is introduced through the scaling $\sqrt{C_m}$ in (5.13) which lowers the effective signal to noise ratio in the higher order terms. As will be shown, we can obtain analytical results without truncating the equations.

5.5.3 Cramér-Rao Bound for Circular Array with Single Source

The case for a single source ($P = 1$) provides the ultimate lower bound for any direction estimation. The continuous representation allows considerable simplifications using addition and recurrence relations for integer order Bessel functions [162]. From (5.18) the three main terms to be computed are $\mathbf{A}^H\mathbf{A}$, $\mathbf{D}^H\mathbf{D}$ and $\mathbf{D}^H\mathbf{A}$.

$$\mathbf{A}^H\mathbf{A} = \sum_{m=-\infty}^{\infty} C_m = Q \sum_{m=-\infty}^{\infty} J_m^2(kR) = Q \tag{5.20}$$

$$\mathbf{D}^H\mathbf{D} = \sum_{m=-\infty}^{\infty} m^2 C_m = Q \sum_{m=-\infty}^{\infty} m^2 J_m^2(kR) = \frac{Qk^2R^2}{2} \tag{5.21}$$

$$\mathbf{D}^H\mathbf{A} = \sum_{m=-\infty}^{\infty} -mC_m = 0. \tag{5.22}$$

More detailed workings are provided in Appendix B, Section B.3. Assuming a source of unit power $\mathbf{R}_{\boldsymbol{s}} = 1$, the following closed form expression for the CRB is obtained,

$$\text{CRB}_{P=1} = \frac{\sigma^2}{2N}\frac{2}{Qk^2R^2} = \frac{\sigma^2}{QN}\frac{1}{k^2R^2}. \tag{5.23}$$

The first factor represents the impact of noise. Since the noise is independent the noise power is scaled by the product of the number of sensors and number of observations (QN). We can consider this term the reciprocal of the effective array signal to noise ratio QN/σ^2.

The second factor represents the effect of the spatial extent of the array. A common measure of resolving ability is the Rayleigh resolution limit, equal to $\lambda/2R$ [230]. It is reasonable to expect the variance to scale with the square of this term corresponding to the $1/R^2$ factor. The result obtained here is also consistent with the CRB relationship with the sensor moment of inertia [251, 253].

5.5.4 Cramér-Rao Bound for Circular Array with Two Sources

To consider the ability to resolve independent sources, we analyse the case of two uncorrelated sources separated by some angle $\Delta\theta$. The source correlation will be the identity matrix, $\mathbf{R}_{\boldsymbol{s}} = \mathbf{I}$, thus from (5.18) we see that only the diagonal entries of the bound calculation are required. Complete workings are provided in Appendix B, Section B.4 and summarised here:

$$\mathbf{A}^H\mathbf{A} = Q\begin{bmatrix} 1 & \overline{\mu} \\ \mu & 1 \end{bmatrix} \tag{5.24}$$

$$\mathbf{D}^H\mathbf{D} = \begin{bmatrix} \frac{Qk^2R^2}{2} & \cdots \\ \cdots & \frac{Qk^2R^2}{2} \end{bmatrix} \tag{5.25}$$

$$\mathbf{D}^H\mathbf{A} = Q\begin{bmatrix} 0 & \overline{\nu} \\ \nu & 0 \end{bmatrix} \tag{5.26}$$

Since we assume uncorrelated sources, $\mathbf{R}_{\boldsymbol{s}} = \mathbf{I}$, the off diagonal terms of $\mathbf{D}^H\mathbf{D}$ do not effect the bound as a result of the elementwise product in (5.18).

$$\begin{aligned}\mu &= \sum_{m=-\infty}^{\infty} e^{jm\Delta\theta}J_m^2(kR) = J_0\left(2kR\sin\frac{\Delta\theta}{2}\right) \\ &= J_0(kR\Delta\theta) + O\left((\Delta\theta)^4\right)\end{aligned} \tag{5.27}$$

$$\begin{aligned}\nu &= \sum_{m=-\infty}^{\infty} -me^{jm\Delta\theta}J_m^2(kR) = -jkR\cos(\Delta\theta)\,J_1\left(2kR\sin\frac{\Delta\theta}{2}\right) \\ &= -jkRJ_1(kR\Delta\theta) + O\left((\Delta\theta)^3\right).\end{aligned} \tag{5.28}$$

The approximations are valid for small $\Delta\theta$. Substituting these results into 5.18, the diagonal term for the Cramér-Rao bound for two uncorrelated sources is

$$\begin{aligned}\text{CRB}_{P=2} &= \frac{\sigma^2}{2QN}\left(\frac{k^2R^2}{2} + \frac{\nu^2}{1-\mu^2}\right)^{-1} \\ &\approx \frac{\sigma^2}{QN}\frac{1}{k^2R^2}\left(1 - \frac{2J_1^2(kR\Delta\theta)}{1-J_0^2(kR\Delta\theta)}\right)^{-1}.\end{aligned} \tag{5.29}$$

The form is similar to (5.23) with the addition of a second term. Using the summation identity $J_0^2(z) + 2\sum_{n=1}^{\infty} J_n^2(z) = 1$ [160, 9.1.76 p.363] it is evident that the bracketed expression is bounded by 0 and 1. As expected, the variance can only increase due to the presence of the second source. The result is asymptotically equal to the single source case for large $kR\Delta\theta$. With a large aperture, or sufficiently spaced sources, the variance of estimating direction of arrival is not influenced by the presence of a second source.

5.5.5 Discussion of Two Source Result

The result presented for the Cramér-Rao for two sources allows an investigation of the ability to resolve source directions of arrival. By considering the point at which the variance is equal to the source separation we can determine the limiting resolution [264].

$$\begin{aligned}\mathrm{CRB}_{P=2} &\approx \frac{\sigma^2}{QN}\frac{1}{k^2R^2}\left(1-\frac{2J_1^2(kR\Delta\theta)}{1-J_0^2(kR\Delta\theta)}\right)^{-1} = (\Delta\theta)^2 \\ \frac{QN}{\sigma^2} &= \mathrm{SNR} = \frac{1}{(kR\Delta\theta)^2}\left(1-\frac{2J_1^2(kR\Delta\theta)}{1-J_0^2(kR\Delta\theta)}\right)^{-1}.\end{aligned} \tag{5.30}$$

The right hand side of this is a function only of the product $kR\Delta\theta$. This reveals some insights about the limits to resolving the direction of arrival.

For a fixed signal to noise ratio, the minimum source separation that can be resolved is inversely proportional to the radius. This result is a more general case of previous results that relate resolution to the length or number of elements of a uniform linear array [230].

The relationship also reveals how the ability to resolve sources will change with the signal to noise ratio. Consider the case of small values for $kR\Delta\theta$,

$$\begin{aligned}\mathrm{SNR} &= \frac{1}{(kR\Delta\theta)^2}\left(\frac{1-J_0^2(kR\Delta\theta)-2J_1^2(kR\Delta\theta)}{1-J_0^2(kR\Delta\theta)}\right)^{-1} \\ &= \frac{1}{(kR\Delta\theta)^2}\left(\frac{\sum_{n=2}^{\infty}J_n^2(kR\Delta\theta)}{\sum_{n=1}^{\infty}J_n^2(kR\Delta\theta)}\right)^{-1} \approx \frac{1}{(kR\Delta\theta)^2}\left(\frac{J_2^2(kR\Delta\theta)}{J_1^2(kR\Delta\theta)}\right)^{-1} \\ &\approx \frac{1}{(kR\Delta\theta)^2}\left(\frac{(kR\Delta\theta)^4/64}{(kR\Delta\theta)^2/4}\right)-1 = \frac{16}{(kR\Delta\theta)^4} \qquad kR\Delta\theta \ll 1\end{aligned} \tag{5.31}$$

using small argument approximations of the Bessel function [160].

The relationship and approximation is shown in Figure 5.4. The resolution angle for two sources is shown to decrease with the fourth root of the signal to noise ratio. Specifically,

$$\Delta\theta \approx \frac{2}{kR}\mathrm{SNR}^{\frac{1}{4}}. \tag{5.32}$$

This result is consistent, up to a proportionality constant, with that reported previously for the case of the uniform linear array [233, 264]. The result here is for a general shaped region that lies in the interior of the circular domain. The derivation presented here offers a closed form expression for the Cramér-Rao bound without requiring a series expansion. This is useful for exposing the structure of the problem and determining the relationship between signal to noise ratio and resolution.

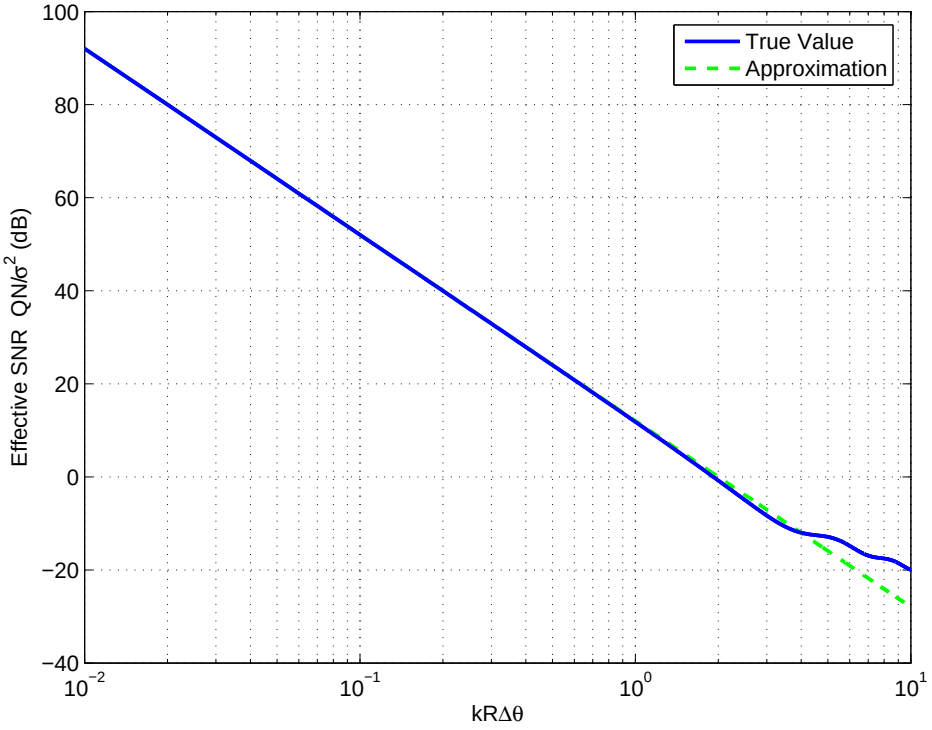

(a) Function on logarithmic scale

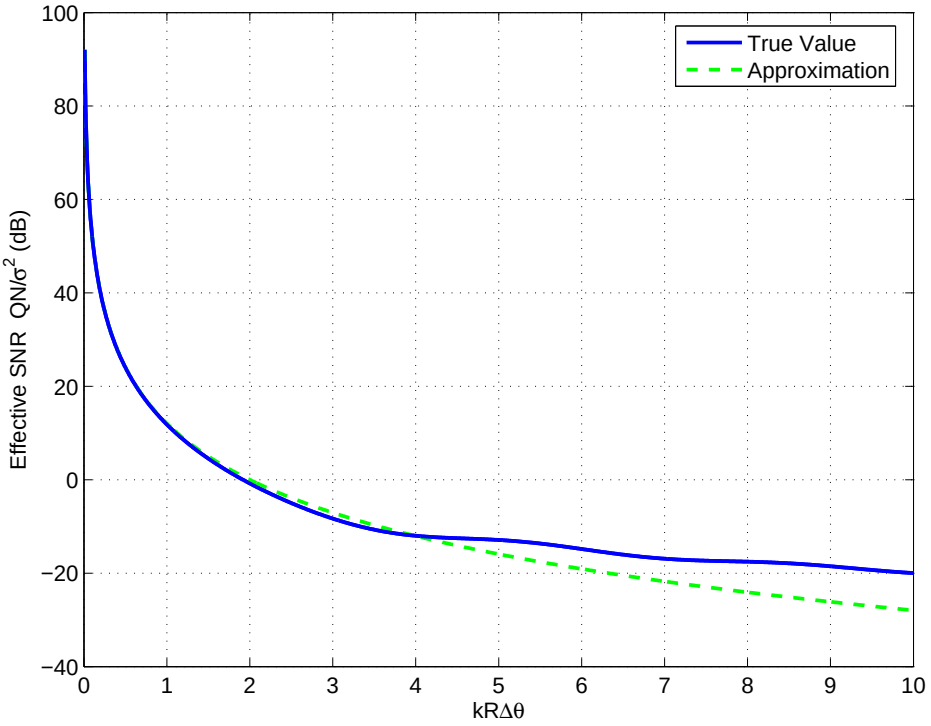

(b) Function and small argument approximation

Figure 5.4: Relationship between the signal to noise ratio and the minimum resolvable direction of arrival angle. The full expression is given by (5.30). It is well approximated by SNR$= 16(kR\Delta\theta)^{-4}$ for small arguments and large effective SNR.

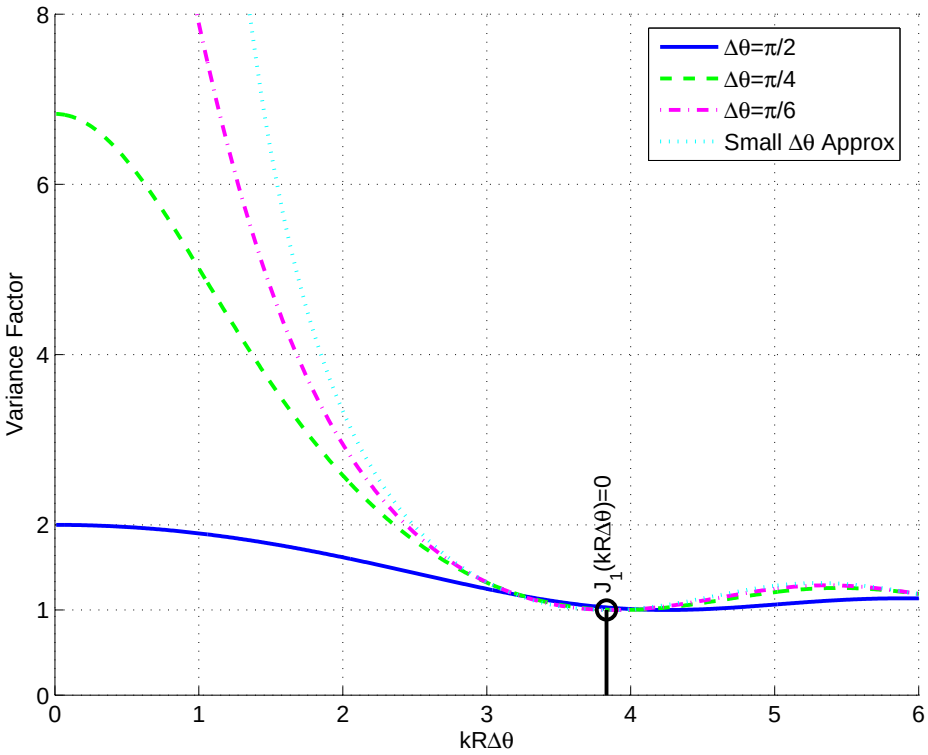

Figure 5.5: Factor for the increased variance of estimating source direction of arrival with a second source present. The factor decreases to unity near $J_1(kR\Delta\theta) = 0$ at $kR\Delta\theta \approx 3.8$.

From (5.29) it is evident that when $J_1(kR\Delta\theta) = 0$ the variance of the estimate for each source direction is not affected by the second source. Consider the increased variance factor,

$$\frac{\text{CRB}_{P=2}}{\text{CRB}_{P=1}} = \left(1 - \frac{2\cos^2(\Delta\theta)\, J_1^2\left(2kR\sin\frac{\Delta\theta}{2}\right)}{1 - J_0^2\left(2kR\sin\frac{\Delta\theta}{2}\right)}\right)^{-1} \approx \left(1 - \frac{2J_1^2(kR\Delta\theta)}{1 - J_0^2(kR\Delta\theta)}\right)^{-1}, \quad (5.33)$$

it becomes unity at this point and remains close to unity thereafter as shown in Figure 5.5. For the case of a set of P uncorrelated sources spread around the observer, $\Delta\theta = 2\pi/P$. For performance to match that of the sources in isolation $kR\Delta\theta > 3.8 > \pi$ which corresponds to an upper bound of $P < 2kR$ sources. This is consistent with the dimensionality results from Chapter 2 Section 2.3, and will be demonstrated through further simulations in this chapter.

5.6 Numerical Analysis

5.6.1 Analysis of Continuous Array Spatial Cramér-Rao Bound

In this section we examine the effect of varying region size, and number of sources on the spatial CRB. In calculating the bound from (5.18), the infinite matrices had to be truncated. The numerical analysis presented uses a truncation size $N \gg kR$ introducing a negligible error.

We restrict our attention to the case of reasonably high signal to noise ratios where the performance of an estimator will approach the CRB [265]. All results are presented for an effective array signal to noise ratio of 20dB ($QN/\sigma^2 = 100$). This would generally be expected to be above the threshold regime.

Firstly we consider the spatial CRB for a number of equal power, equally spaced and uncorrelated sources ($\mathbf{R}_{\boldsymbol{s}} = \mathbf{I}$). By virtue of symmetry, this configuration has the lowest equal variance for the position of each source [128] and we need only consider one term of the CRB matrix. Figure 5.6 shows the effect of increasing the number of sources. The square root of the CRB, which represents the standard deviation of the estimate, is plotted in units of degrees.

The single source case has the form (5.23). With multiple sources, the performance in estimation approaches the single source case beyond a threshold radius. Below this critical threshold the performance diverges rapidly. This is consistent with the notion of the dimensionality of a spatial region [41, 84] – we would expect poor performance when the number of sources exceeds the approximate dimensionality of the spatial field. The points at which the effective dimensionality and number of sources are equal ($2kR + 1 = P$) are shown on the figure. At this point the multi-source CRB is within a factor of two of the single source case. The notion of dimensionality provides an alternative to "sensor-based" identifiability constraints set out in [266] and [237].

It has been suggested that the number of sources that can be resolved is related to the co-array formed from all the unique inter element spacings of the sensor array [239, 240]. Such approaches provide a theoretical analysis based on numerical uniqueness [241, 242] and do not reflect the uncertainty introduced by noise. The result we present here encapsulates the limitations placed in practice due to the spatial extent and inherent noise of the array. Exceeding these limits becomes exceedingly difficult due to the exponential decrease in the power of the modal expansion terms beyond the critical dimensionality (see Chapter 2 for discussion).

5.6.2 Comparison with Discrete Sensor Cramér-Rao Bound

We provide for comparison results from a discrete sensor uniform circular array (UCA). The signal space for a Q sensor UCA can be expressed as in (5.14), with the steering array

$$\boldsymbol{a}(\theta) = \left[e^{-jkR\tau_1(\theta)}, \ldots, e^{-jkR\tau_Q(\theta)}\right]^T \tag{5.34}$$

where $\tau_q(\theta) = \cos\left(\theta - 2\pi(q-1)/Q\right)$ for $q = 1, \ldots, Q$.

The CRB is obtained from (5.18). For the single source case, $\mathbf{A}^H\mathbf{A} = Q$, and for $Q \geq 3$,

$$\mathbf{D}^H\mathbf{D} = k^2R^2\sum_{q=1}^{Q}\sin^2\left(\frac{2\pi(q-1)}{Q}\right) = \frac{Qk^2R^2}{2} \tag{5.35}$$

$$\mathbf{D}^H\mathbf{A} = \sum_{q=-1}^{Q} jkR\sin\left(\frac{2\pi(q-1)}{Q}\right) = 0 \tag{5.36}$$

giving the same result as that obtained for the continuous CRB (5.23). The expression for two or more sources is not easily simplified.

Figure 5.7 compares the continuous CRB to that obtained for a 15 sensor UCA. Below a threshold radius, the performance of the UCA matches the limiting case for the continuous sensor model. The threshold remains fairly constant as the number of sources is changed. This threshold is related to the essential dimensionality. At a radius of $R = 1.1\lambda$, the dimensionality is $2kR + 1 \approx 15$. The performance of a 15 sensor array degrades beyond this point since insufficient sensors are present to uniquely capture the degrees of freedom of the spatial field. The continuous CRB provides a lower bound for the UCA performance. The single source CRB provides an overall bound.

It should be noted that the CRB is a measure of the localised uncertainty in an estimate and does not consider aliasing artifacts and array [230]. As the number of sensors falls below the degrees of freedom of the array, it becomes increasingly likely that the array will suffer from ambiguities. The condition for ambiguities in linear arrays has been studied [267, 268], however the case for circular arrays is more complex [269]. Generally it is accepted that the sensors should be placed no more than $\lambda/2$ apart. This corresponds to $Q \geq 2\pi R2/\lambda = 2kR$ [151]. The results presented here are consistent with this.

The numerical analysis presented demonstrates that the sensor array CRB is lower bounded by the spatial CRB. This is quite a powerful result. It shows that the performance of an array based DOA estimator will be bounded by the maximal spatial extent of the array, independent of the number of sensors. In the limit of a large number of sensors in the region, the performance converges to the spatial CRB.

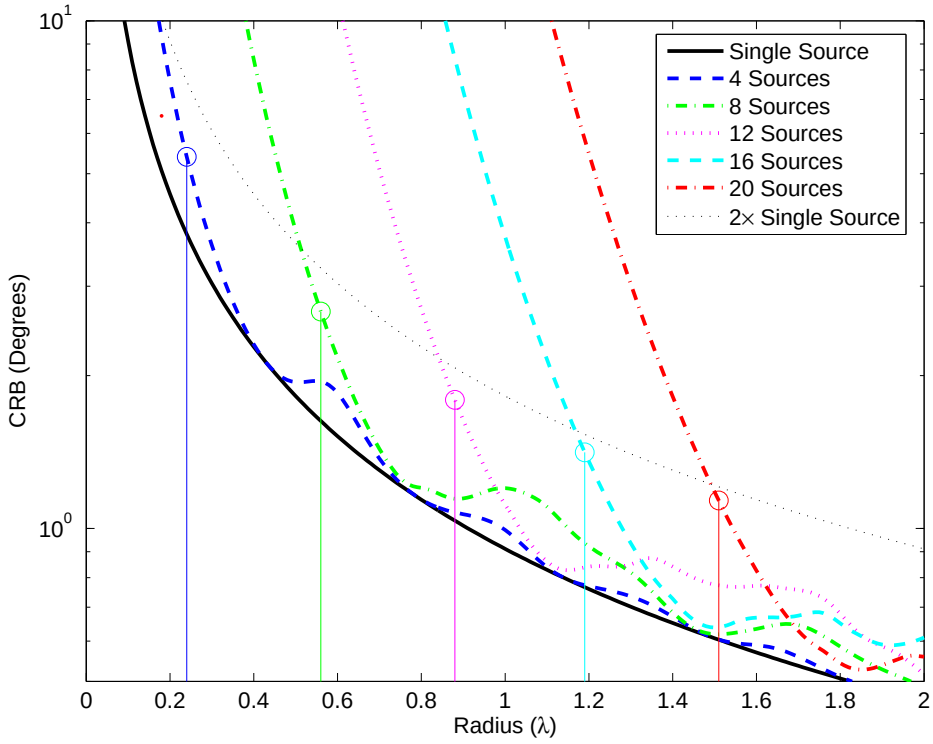

Figure 5.6: Impact of region size on Cramér-Rao bound ($\sqrt{CRB}$ degrees) for direction estimation given a number of equal power distributed sources. Variance of the DOA estimation with P sources approaches that for a single source when $2kR + 1 > P$. These points are shown on the plot.

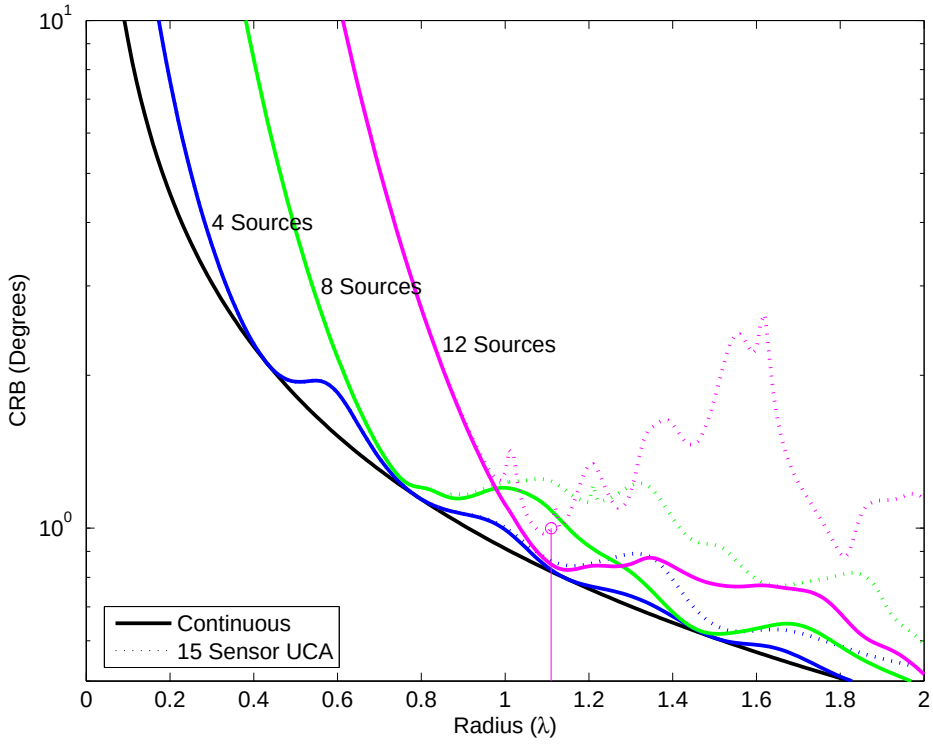

Figure 5.7: Comparison of the continuous Cramér-Rao bound with that of a 15 element uniform circular array. The UCA achieves the limiting performance up to a threshold radius at $2kR + 1 = 15$ ($R \approx 1.1$ shown).

5.7 Comparison of Circle and Disc Array

The previous numerical analysis was carried out for the case of a circular array at the edge of the region. A similar analysis can be performed for the case of a set of sensors spread homogenously throughout the entire circular region. We refer to this configuration as a disc array.

The complete workings for this case are presented in Appendix B, sections B.5 and B.6. The expressions obtained are somewhat more complex with

$$C_m = Q\left(J_m^2(kR) - J_{m-1}(kR)J_{m+1}(kR)\right) \tag{5.37}$$

$$\text{CRB}_{P=1} = \frac{\sigma^2}{QN}\frac{2}{k^2R^2} \tag{5.38}$$

$$\text{CRB}_{P=2} \approx \frac{\sigma^2}{QN}\frac{2}{k^2R^2}\left(1 - \frac{\left(J_1\left(kR\Delta\theta\right) + J_3\left(kR\Delta\theta\right)\right)^2}{1 - \left(J_0\left(kR\Delta\theta\right) + J_2\left(kR\Delta\theta\right)\right)^2}\right)^{-1}. \tag{5.39}$$

Firstly consider the noise scaling coefficient C_m. In the limit for large kR [160, 9.2.1 p. 364]

$$J_m(kR) \approx \sqrt{\frac{2}{\pi kR}}\cos\left(kR - \frac{2\pi m + 1}{4}\right) \tag{5.40}$$

from which we can see that $C_m \approx 2/\pi kR$, unlike the circular array for which the signal in some modes will vanish where $J_m(kR) \approx 0$. The continuous sensor over the disc does not have the problem of degenerate modes, however the CRB variance is increased by a factor of two. Since the total signal energy is the same in both cases, $\sum C_m = Q$, the circular array will have a larger range of C_m terms of significant value. This is shown in Figure 5.8.

Fig. 5.9 shows a plot comparing the CRB for the circular array and the disc array. The results are plotted for an effective array signal to noise ration of 20dB ($QN/\sigma^2 = 100$). The array spread across the disc will perform worse than a uniform circular array with equal radius. This seems at first counterintuitive – additional information about the field through the interior should improve performance. The paradox is resolved by recalling the signal model used – the sensors each add additional noise and they must be evenly distributed through the entire volume.

The largest signal phase change with respect to direction occurs at the perpendicular extremities of the region. For this reason, if the noise is generated by the sensor, it is optimal to place all sensors as far apart as possible and therefore at the edge of the circular region. This result is consistent with that presented for a discrete set of sensors [251]. The circular array

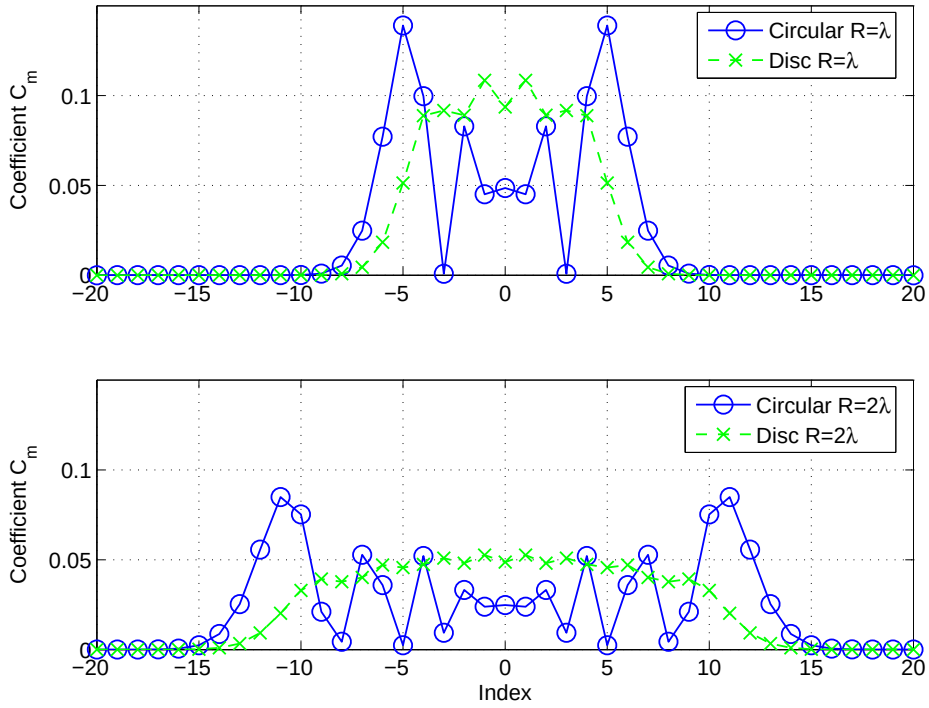

Figure 5.8: Comparison of the signal mode scaling coefficients for a circular and disc array. The circular mode scaling becomes degenerate at or near zeroes of the Bessel function whilst the disc is relatively constant.

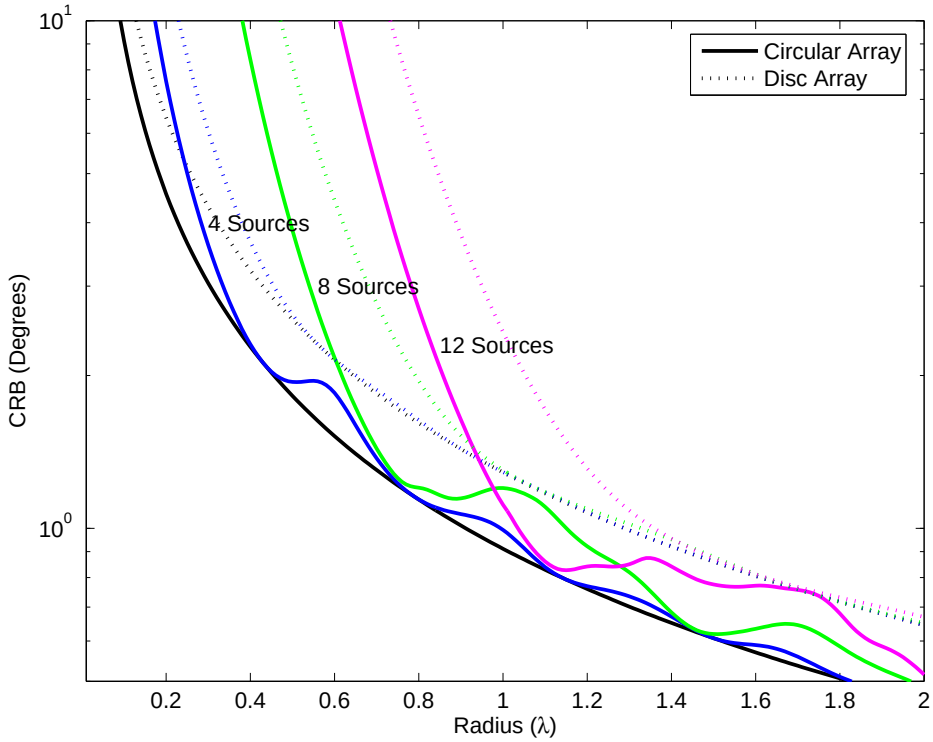

Figure 5.9: Comparison of the Cramér-Rao bound for a circular and disc array. For a fixed array signal to noise ratio, the disc array results in an increased variance for DOA estimation and a larger critical radius. When sensor noise is constant, it is optimal to place all sensors at the edge of the region.

provides more signal in the higher order modes which allow better resolution of the direction of arrival.

The expression (5.39) for the two source Cramér-Rao bound includes some additional terms compared with the circular array two source CRB (5.29). However, in the limit of closely spaced sources, this expression has the same relationship between resolvable angle and signal to noise ratio. The variance for the disc array is a factor of two larger than the circular array, however the variance scaling as the two sources move closer together is quite similar. This is shown in Figure 5.10. It is evident that the two expressions have the same asymptotic form for small angular separations.

5.8 Summary and Contributions

A review of the existing literature demonstrates that the theoretical performance of direction of arrival estimation is generally linked to specific sensor array geometries or problem scenarios. The continuous framework presented provides a technique for analysing the impact of the spatial extent of an array on direction of arrival performance without concern for the specific array geometry. The framework can be used to derive a simple form for the Cramér-Rao bound for the cases of a single source and two uncorrelated sources. These expressions show how the extent of the array creates a fundamental limit on the ability to resolve and estimate the direction of arrival of sources.

The size of the region also has a direct impact on the number of sources that can be resolved. From numerical analysis, it is apparent that P sources can be resolved once a critical radius is reached such that $2kR + 1 > P$. The CRB for a discrete uniform circular array is lower and converges to the continuous case rapidly once the number of sensors $Q > 2kR + 1$. Thus we present a simple bound for the performance of a uniform circular array with N measurements taken from Q sensors for P sources,

$$\sigma_\theta \geq \frac{\sigma}{\sqrt{QN}} \frac{1}{kR} \qquad P < 2kR + 1 < Q \tag{5.41}$$

This result stems from the consideration of the effective dimensionality of the measurement region. A sufficient number of sensors are required to match the degrees of freedom which the spatial field can exhibit. When the number of sources exceeds the degrees of freedom of the spatial field, estimation of direction of arrival becomes increasingly difficult.

The following specific contributions were made in this chapter:

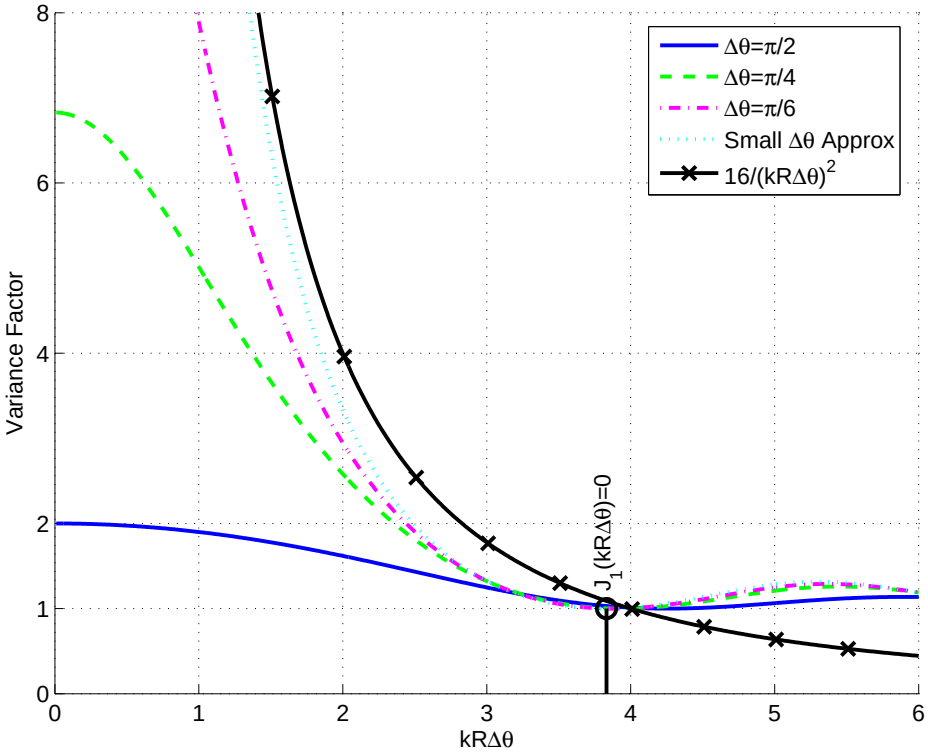

(a) Circular array

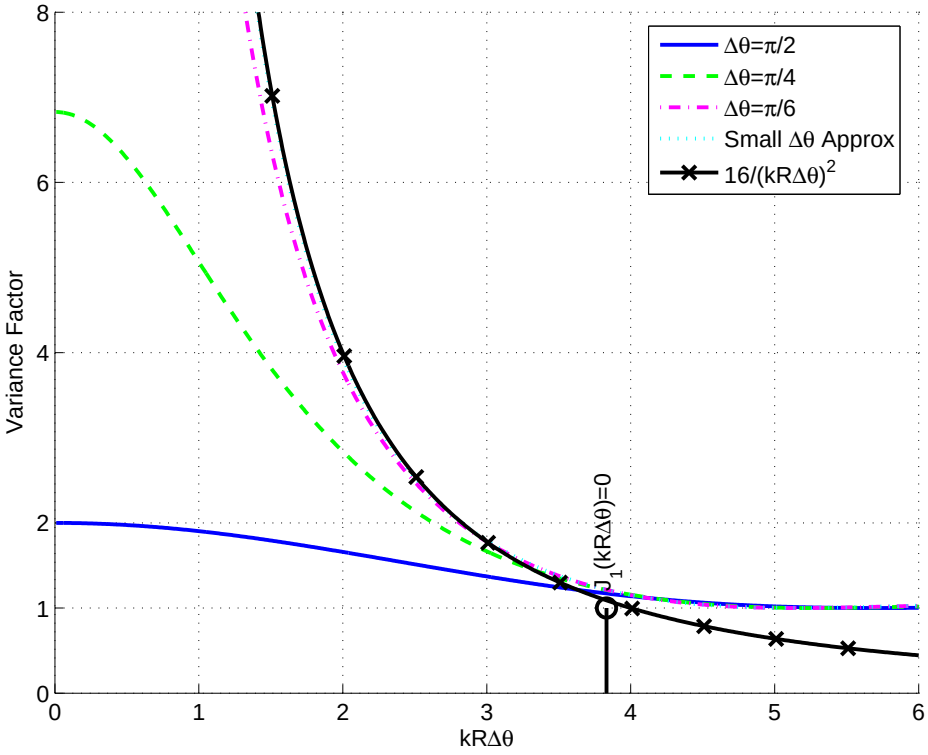

(b) Disc array

Figure 5.10: Comparison of the variance factor with two sources for the circular and disc arrays. The variance factor is quite similar and has the same asymptotic form as $kR\Delta\theta$ becomes small. Equivalent performance to a single source is achieved at the same point near $J_1(kR\Delta\theta) = 0$.

- Developed a continuous field framework for analysing the direction of arrival problem. This allows for a generalised measurement volume to be considered in the performance analysis.
- Developed a noise model that is consistent with the conventional model of sensor noise in the limit of a large number of sensors. This noise model allows us to consider the limiting performance of direction of arrival estimation in the continuous framework.
- Derived a simple expression for the Cramér-Rao lower bound for the case of a single source.
- Derived the Cramér-Rao lower bound for the case of two uncorrelated sources separated in angle.
- Analysed the CRB for two sources and derived a relationship for the limiting resolution of the array as a function of array size and signal to noise ratio. This result was presented and shown to be consistent with similar results for the case of a uniform linear array.
- Demonstrated, through numerical analysis, the relationship between the essential dimensionality of the spatial field in the measurement region and the number of sensors required and number of discrete sources that can be resolved.
- Analysed the bounds developed and presented a comparison to results for a conventional sensor array. The results presented in this chapter are shown to be consistent with previous results in the literature. The general spatial framework developed provides a more general approach and therefore more general results which are not specific to a particular array geometry.

The direction of arrival problem is generally posed with the assumption of the sources being discrete and in the far-field. Whilst this structure facilitates the signal processing, it may not be valid in practice. From the analysis in this chapter, it is also evident that there are fundamental limits to the number of sources that can be accurately resolved. One approach to characterising the spatial wireless channel has been to use antenna arrays to resolve discrete paths or propagation, employing direction of arrival techniques. In the following chapter an alternative approach will be presented that is more suited to the natural dimensionality and information limits of the spatial field when observed over a finite volume.

Chapter 6

Stochastic MIMO Model Utilising Dimensionality and Modes

6.1 Introduction

6.1.1 Background and Motivation

The previous chapters have investigated the dimensionality and representation of a spatial multipath field. Chapter 2 reviewed the approximation of a spatial field using a finite set of spatial modes. Chapter 4 investigated the properties of these modes. Chapter 5 demonstrated that the dimensionality creates a limit for the ability to resolve the direction of arrival of a source.

Wireless communications systems achieve the transmission of information through the excitation and detection of electromagnetic fields. Whilst these fields exist continuously over space and time, they are constrained in complexity by virtue of the wave equation described in Chapter 1. A means of characterising the complexity or diversity of possible spatial fields over a finite volume is to consider the dimensionality or degrees of freedom. This was the subject of Chapter 2. Where there is only a single degree of freedom, it will only be possible to achieve one channel or independent path of communication between the sender and receiver. Additional degrees of freedom or dimensionality allow additional independent paths which can be used to achieve a higher power or spectral efficiency in a communications system.

The degrees of freedom of a spatial field is directly related to the size and shape of the region of interest. This has a bearing on the accuracy and amount of information that can

be obtained from the spatial field. In this chapter we are concerned with effect of the region size on an appropriate channel model. The additional impact of the region shape could be incorporated using some of the results from Chapter 4. This chapter presents a framework for modelling the spatial channel incorporating the effective spatial dimensionality.

The development and use of spatial channel models is an important area of research for multiple antenna (MIMO) communication systems. In practice, the capacity that can be achieved will be limited by the extent to which the spatial environment supports parallel independent data paths. Models for the spatial propagation channel are therefore important for the design, development and testing of system designs. A good channel model will be simple and provide a channel simulation that is consistent with measured data. The channel model must capture the important characteristics of the physical channel.

There are two categories of stochastic channel models. Geometric or double directional models [70] describe the statistics of physical multipath component parameters (directions of arrival and departure, delay and amplitude). Analytic models approximate the complete statistics of the antenna transfer parameters [63] and provide a simple means for generating random channel matrices representative of a measured environment.

The geometric channel models require a large number of parameters to describe the general characteristics and distributions of the paths. Parameters include the number of discrete paths, the distributions of path direction, the angular spread of each path and correlations between paths. As we have shown, it is only possible to resolve the directions of a fixed number of paths given the receive region size, therefore this type of geometric model tends to have redundancy in the parameters.

Analytic models provide a simple alternative. However, both the spatial aspects of the channel and the characteristics of the antenna arrays are captured in the model. In this way, any simulation is restricted to the specific arrays used for the measurement.

In this chapter we address the following question:-
Is there an alternative approach to creating a model of the spatial channel without reference to specific directional paths ?

This work is an extended version of a paper that was presented at the Vehicular Technology Conference, May 2006 [125].

6.1.2 Review of MIMO Channel Models

Consider a MIMO system with N_T transmit elements and N_R receive elements. The transmitted signals $\boldsymbol{s}$ and received signals $\boldsymbol{y}$ are related by

$$\boldsymbol{y} = \mathbf{H}\boldsymbol{s} + \boldsymbol{w} \tag{6.1}$$

where $\mathbf{H}$ is the $N_R \times N_T$ matrix of complex channel coefficients and $\boldsymbol{w}$ is the noise vector at the receiver.

The statistical models considered [30, 66, 67, 270] assume the channel to be well modelled by second order statistics. This is generally true of non line of sight MIMO channels such as those expected in indoor environments. In this case the elements of $\mathbf{H}$ are zero mean [26, 63]. The correlation matrix for the channel coefficients, $\mathbf{R_H}$ is obtained,

$$\mathbf{R_H} = E\left\{\overrightarrow{\mathbf{H}}\overrightarrow{\mathbf{H}}^H\right\}, \tag{6.2}$$

where $\cdot^H$ is the Hermitian operation, and $\overrightarrow{\cdot}$ is the vector operation which stacks the columns of a matrix. Expectations $E\{\cdot\}$ are taken over all channel matrix realisations. The matrix $\mathbf{R_H}$ is an $N_T N_R \times N_T N_R$ complex positive definite Hermitian matrix with $(N_T N_R)^2$ degrees of freedom. It is possible to approximate $\mathbf{R_H}$ with fewer parameters. Specific examples are the Kronecker model with $N_T^2 + N_R^2$ parameters [30], the virtual channel model with $N_T N_R$ parameters [66] and the recent Weichselberger model with $N_T^2 + N_R^2 + N_T N_R - N_T - N_R$ parameters [270].

A review of these models [63] demonstrated that the Weichselberger model provided the best match to measured data. It also has the largest parameter space. Whilst the virtual channel separates the propagation channel from the array geometry, it was shown to overestimate channel diversity and capacity.

In this chapter, we present a MIMO channel model with the following properties:

- A simple analytic framework for generating channels.
- Ability to match measured channel data.
- The minimum number of internal parameters.
- Separability of antenna array and spatial channel.

The proposed model quantifies the relationship between the size of the array and number of internal modelling parameters. Further, modelling accuracy can be adjusted with a single

parameter. It applies to two-dimensional environments, with straight forward extension to three dimensions.

Section 6.2 presents a new model framework to satisfy question posed above. This is followed by a discussion in Section 6.3 highlighting the advantages of the proposed model. Section 6.4 demonstrates the properties of the proposed model through simulation and application to real MIMO data sets.

Whilst many MIMO channel models assume separability of the receiver and transmitter correlations, this approach has come under scrutiny [68, 69]. Recent work by Lamahewa et al. provides a parametric extension to the Kronecker style model to introduce joint correlations between the angle of departure from the transmitter and the angle of arrival [271–273]. The main contribution of this chapter is the development of a stochastic model that captures the joint distribution of the receiver and transmitter correlations from experimental data.

6.2 New Framework using Continuous Spatial Model

Chapter 2 reviewed the framework demonstrating that the signal subspace or wave-field observed by a receiver with finite volume has limited dimensionality or degrees of freedom. The spatial region containing the antennas controls the spatial degrees of freedom, not the number of antennas [44]. This has been shown from the perspective of the wave equation constraint [41, 80] and an antenna signal subspace perspective [84].

We can express an arbitrary received or transmitted wave-field in terms of a set of basis functions suited to the problem. These can be interpreted as the most concentrated solutions to the wave equation [80], for example through a truncation of the Jacobi-Anger expansion of a plane wave [91] to $2M+1$ terms, which is accurate over a finite volume,

$$e^{jk\boldsymbol{x}.\widehat{\boldsymbol{\phi}}} \cong \sum_{m=-M}^{M} \left[J_m(k\,\|\boldsymbol{x}\|)e^{-jm\theta_{\boldsymbol{x}}}\right] e^{jm\phi}, \tag{6.3}$$

where $\widehat{\boldsymbol{\phi}}$ is a unit vector with direction ϕ. Drawing from previous work [44], with transmitter antennas located at $\boldsymbol{x}_n$ and receiver antennas at $\boldsymbol{y}_n$, the modal decomposition of a channel matrix is

$$\mathbf{H} = \mathbf{J}_R \mathbf{H}_S {\mathbf{J}_T}^H, \tag{6.4}$$

where the $N_T \times M_T$ and $N_R \times M_R$ configuration matricies $\mathbf{J}_T$ and $\mathbf{J}_R$, respectively, are defined as

$$\begin{aligned}[\mathbf{J}_T]_{nm} &= j^m J_m(k\|\boldsymbol{x}_n\|)e^{jm\theta_{\boldsymbol{x}_n}} \\ [\mathbf{J}_R]_{nm} &= j^m J_m(k\|\boldsymbol{y}_n\|)e^{jm\theta_{\boldsymbol{y}_n}},\end{aligned} \tag{6.5}$$

where $[\cdot]_{nm}$ is the matrix element in row m and column n, and the antenna positions $\boldsymbol{x}_n$ and $\boldsymbol{y}_n$ have been expressed in the polar coordinates $(\|\boldsymbol{x}_n\|, \theta_{\boldsymbol{x}_n})$ and $(\|\boldsymbol{y}_n\|, \theta_{\boldsymbol{y}_n})$, $J_m(\cdot)$ is the m^{th} order Bessel function and $k = 2\pi/\lambda$ is the wave number.

The configuration matrices depend only on the geometry and size of the transmitter and receiver antenna arrays. Configuration matrices may additionally include the effects of antenna directionality and mutual coupling, either through modelling or calibration of array elements.

The coupling matrix $\mathbf{H}_S$ with dimension $(2M_R+1)\times(2M_T+1)$ captures the spatial coupling between regions independent of the artifacts of antenna geometry. Dimensions M_R and M_T are proportional to the aperture size of each antenna array. As was discussed in Chapter 2, the truncation order $M \gtrsim \lceil kR \rceil$ where R is antenna aperture radius.

For a rich scattering environment, the elements of $\mathbf{H}_S$ will be independent, whereas the elements of $\mathbf{H}$ will be correlated due to antenna proximity. The modal decomposition provides a natural framework for representing the diversity of the spatial channel. We note that similar observations have been used in [66].

Consider the correlation matrix for $\mathbf{H}_S$,

$$\mathbf{R}_{\mathbf{H}_S} = E\left\{\overrightarrow{\mathbf{H}_S}\overrightarrow{\mathbf{H}_S}^H\right\}. \tag{6.6}$$

A common assumption for the non line of sight channel in statistical models is that the channel is well modelled by its second order statistics. $\mathbf{R}_{\mathbf{H}_S}$ provides a full parametrisation of the MIMO channel in this case with $(2M_T+1)^2(2M_R+1)^2$ degrees of freedom. For dense antenna arrays, $2M_T+1 < N_T$ and $2M_R+1 < N_R$ thus providing a smaller parameter space than $\mathbf{R}_{\mathbf{H}}$ as evaluated in (6.2).

The elements of $\mathbf{H}_S$ are a set of correlated random variables. We seek a model to generate instances of $\mathbf{H}_S$ and thus $\mathbf{H}$ from independent random variables. Consider the application of unitary matrices, $\mathbf{A}$ and $\mathbf{B}$, to $\mathbf{H}_S$,

$$\mathbf{H}'_S = \mathbf{A}^H\mathbf{H}_S\mathbf{B}. \tag{6.7}$$

This transformation preserves the energy in $\mathbf{H}_S$ and can be selected to de-correlate the elements of $\mathbf{H}'_S$. The correlation matrix for the rotated matrix $\mathbf{H}'_S$ can be expressed

$$\begin{aligned}\mathbf{R}_{\mathbf{H}'_S} &= E\left\{\overrightarrow{\mathbf{A}^H\mathbf{H}_S\mathbf{B}}\overrightarrow{\mathbf{A}^H\mathbf{H}_S\mathbf{B}}^H\right\} \\ &= (\mathbf{B}^T \otimes \mathbf{A}^H)\mathbf{R}_{\mathbf{H}_S}(\mathbf{B}^T \otimes \mathbf{A}^H)^H \end{aligned} \tag{6.8}$$

using definition (6.7), the matrix Kronecker product $\otimes$, and identity $\overrightarrow{\mathbf{ABC}} = (\mathbf{C}^T \otimes \mathbf{A})\overrightarrow{\mathbf{C}}$ [274]. The elements of $\mathbf{H}'_S$ will be independent with $\mathbf{R}_{\mathbf{H}'_S}$ diagonal if and only if the eigenvectors of $\mathbf{R}_{\mathbf{H}_S}$ are Kronecker separable. This assumption is restrictive but has been shown to match real world data for $\mathbf{R}_{\mathbf{H}}$ [270]. Since the modal decomposition is linear, this result also applies to $\mathbf{R}_{\mathbf{H}_S}$.

If the correlation matrix $\mathbf{R}_{\mathbf{H}'_S}$ is diagonal then the receive side correlation $E\{\mathbf{H}_S{\mathbf{H}_S}^H\}$ will also be diagonal,

$$\begin{aligned} E\left\{\mathbf{H}'_S{\mathbf{H}'_S}^H\right\} = \mathbf{\Lambda} &= E\left\{\mathbf{A}^H\mathbf{H}_S\mathbf{B}\mathbf{B}^H{\mathbf{H}_S}^H\mathbf{B}\right\} = E\left\{\mathbf{A}^H\mathbf{H}_S{\mathbf{H}_S}^H\mathbf{A}\right\} \\ \mathbf{A}\,\mathbf{\Lambda}\,\mathbf{A}^H &= E\left\{\mathbf{H}_S{\mathbf{H}_S}^H\right\}, \end{aligned} \tag{6.9}$$

with $\mathbf{\Lambda}$ a diagonal matrix. Thus $\mathbf{A}$ is the eigenvector matrix of the receiver side modal correlation matrix. A similar result holds for $\mathbf{B}$. This is equivalent to the result presented by Weichselberger for the antenna channel [270].

The elements of $\mathbf{H}'_S$ will be independent but not identically distributed. This is modelled by the element-wise product of a weighting matrix $\mathbf{W}$ with an independent and identically distributed random matrix $\mathbf{G}$. Given a set of N data matrices $\mathbf{H}_n$ we can estimate the appropriate parameters and obtain the complete model as set out in Table 6.1.

The framework applies a Weichselberger style statistical model to the resultant modal channel matrix. The proposed model preserves the simplicity of analytic models and, if the measurement and target arrays are co-incident, $\mathbf{J}'_T = \mathbf{J}_T$ and $\mathbf{J}'_R = \mathbf{J}_R$, the model will match the performance of the Weichselberger approach. For dense arrays, it offers a more efficient parametrisation and the ability to decouple the spatial and array geometry aspects of the channel.

6.3 Discussion of the New Model Framework

The number of parameters to represent the model ($\mathbf{A}$, $\mathbf{B}$ and $\mathbf{W}$) are directly related to the modal truncation order. For densely packed arrays, there are significantly less than the $(N_R \times$

New Model Framework:
A MIMO channel model can be generated from a statistical model based on a modal representation of the field across the transmitter arrays. Given the maximum radius of the transmitter array R_T, the modal order required for the transmitter is $M_T \gtrsim \lceil kR_T \rceil$. Similarly, for a receiver with maximum radial extent R_R, the modal order required is $M_R \gtrsim \lceil kR_R \rceil$.

The channel is generated for a simulated target array geometry with N'_T transmit elements and $N'_T \times 2M_T + 1$ configuration matrix $\mathbf{J}'_T$ given by (6.5). The simulated receiver array geometry will have N'_R receive elements with $N'_R \times 2M_T + 1$ configuration matrix $\mathbf{J}'_R$.

The channel model is generated from the equation:

$$\mathbf{H}_{\text{model}} = \mathbf{J}'_R \, \mathbf{A} \, (\mathbf{W} \odot \mathbf{G}) \, \mathbf{B}^H \, {\mathbf{J}'_T}^H, \tag{6.10}$$

with $\odot$ the Schur product, and the matrices $\mathbf{A}$ and $\mathbf{B}$ the eigenvector matrices of the receiver and transmitter correlations,

$$\mathbf{A} \, \mathbf{\Lambda}_R \, \mathbf{A}^H = \frac{1}{N} \sum_{n=1}^{N} \mathbf{H}_{Sn} {\mathbf{H}_{Sn}}^H, \tag{6.11}$$

$$\mathbf{B} \, \mathbf{\Lambda}_T \, \mathbf{B}^H = \frac{1}{N} \sum_{n=1}^{N} {\mathbf{H}_{Sn}}^H \mathbf{H}_{Sn}, \tag{6.12}$$

$\mathbf{W}$ is a weighting matrix,

$$[\mathbf{W}_{ij}^2] = \frac{1}{N} \sum |\mathbf{A}^H \mathbf{H}_{Sn} \mathbf{B}|^2 \tag{6.13}$$

and $\mathbf{G}$ is a $2M_R + 1 \times 2M_T + 1$ matrix of unit variance, independent normally distributed variables.

The modal space matrices $\mathbf{H}_{Sn}$ and thus channel statistics are generated from N measurements $\mathbf{H}_1, \mathbf{H}_2, \ldots, \mathbf{H}_N$ of the channel matrix using:

$$\mathbf{H}_{Sn} = \mathbf{J}_R^{-1} \mathbf{H}_n {\mathbf{J}_T}^{-H}, \tag{6.14}$$

where J_T is the $2M_T + 1 \times N_T$ configuration matrix for the measurement array with $N_T > 2M_T + 1$ transmit elements, and R_T is the $2M_R + 1 \times N_R$ configuration matrix for the measurement array with $N_R > 2M_R + 1$ receiver elements.

Table 6.1: Algorithmic representation of the proposed statistical channel model utilising spatial modes. The equations show the generation of the MIMO model for the desired target array configuration, and the analysis of the measured MIMO data to extract the statistical parameters.

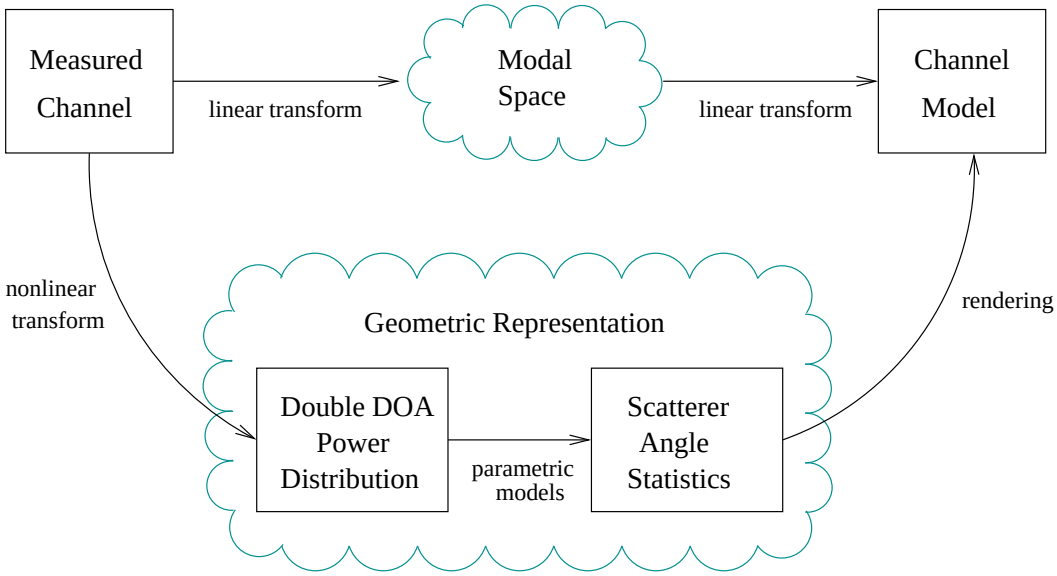

Figure 6.1: Schematic of data path for models comparing the conventional approach with the proposed framework.

$N_T)^2$ parameters of the correlation matrix $\mathbf{R_H}$. The correlation matrix of the mixing matrix $\mathbf{R_H}$ combines the characteristics of the spatial channel with those of the array geometries. The full statistical model contain redundant parameters which will manifest as transmission paths with negligible connection strengths.

The modal framework eliminates redundant parameters by eliminating antenna excitation or receive modes that do not couple well with real spatial fields. This yields the correlation matrix of the modal mixing matrix $\mathbf{R}_{\mathbf{H}_S}$. The modal decomposition is ideally suited to the physical nature of the problem and provides an efficient parametrisation of the channel [44]. The model makes the further assumption that the eigenvectors of $\mathbf{R}_{\mathbf{H}_S}$ can be represented as a Kronecker product following the approach of Weichselberger [270].

The proposed framework provides the ability to investigate the characteristics of the MIMO spatial channel for alternate array configurations. By changing the truncation order, the number of parameters can be adjusted to meet the desired level of model accuracy. The modal projection (6.14) provides a linear transformation to separate the antenna geometry from the spatial propagation model. It is computationally efficient and provides a simple path to creating a channel model from measured data as depicted in Figure 6.1.

In contrast, the array geometry can be abstracted with a geometric approach. This approach involves fitting a parameterised set of multipath components to the observed data using techniques such as SAGE [275, 276]. Such an approach is intuitive, but is computationally expensive and subsequent models of scatterer angle statistics can be complex. Characterisation of scatterer cluster shapes, distributions and correlations create a nonlinear and non-unique

parameterisations of the channel statistics. Generally in such models, as the channel is decomposed into a set of independent spatial paths, it is assumed that the variation of the gain along these paths will be independent and uncorrelated [28]. The new proposed model does not assume that spatial paths are independent, rather the assumption of independence is based on a more flexible eigenvector representation of the channel. Thus it would be expected that the new approach would be better able to capture a channel where discrete spatial paths show some level of correlation.

It is a requirement that the measurement arrays have sufficient elements to ensure the configuration matrices $\mathbf{J}_R$,$\mathbf{J}_T$ in (6.5) are well conditioned. This requirement is satisfied by typical channel sounding experiments [275–277] with element spacing at or below $\lambda/2$.

The model also has application when one array is under-sampled. If investigating the spatial channel at a mobile receiver given a fixed sparse base station array, the modal decomposition can be applied to one side. Essentially we replace (6.14) with $\mathbf{H}_{Sn} = \mathbf{J}_R'^{-1}\mathbf{H}_n$ and (6.10) with

$$\mathbf{H}_{\text{model}} = \mathbf{J}'_R \, \mathbf{A} \, (\mathbf{W} \odot \mathbf{G}) \, \mathbf{B}^H. \tag{6.15}$$

The modal framework provides a general method to transpose channel data for an alternate sensor configuration by providing a suitable basis with which to interpolate,

$$\mathbf{H}' = \mathbf{J}'_R \, \mathbf{J}_R^{-1} \, \mathbf{H} \, {\mathbf{J}_T^{-1}}^H \, {\mathbf{J}'_T}^H. \tag{6.16}$$

Provided the target (simulated) array is within the confines of the original volume sampled, there are no restrictions to the geometry that can be modelled with the framework. The modal decomposition provides an efficient basis to model the underlying physical wave-field over the entire antenna array volume.

The modal basis can also be used to extrapolate, however, the error due to uncertainty in field prediction increases rapidly beyond the extent of the original array [126].

6.4 Simulation and Validation of New Model

6.4.1 Approach for Model Comparison

In order to validate the proposed model, a set of simulations has been carried out. To compare the performance of the model with existing models, it is necessary to have some metric or

characteristic of model accuracy. We follow a similar approach to that proposed by Ozcelik, Czink and Bonek [63]. Three different aspects of the model are analysed.

For comparison of models, we use a Monte-Carlo simulation approach. First we consider the mean mutual information from a set of data obtained from the model to the set of original data

$$I = E\left\{\log_2 \det\left(\mathbf{I}_{N_R} + \frac{\rho}{N_T}\mathbf{H}\mathbf{H}^H\right)\right\}, \tag{6.17}$$

where $\mathbf{I}_{N_R}$ denotes the $N_R \times N_R$ identity matrix, ρ is the average signal to noise ratio and the expectation is over the snapshots of channel data. This provides a measure of the achievable capacity of the spatial channel, and is an important property to be preserved by the model.

The channel mean mutual information provides no indication of the correct structure of the channel with regards to the number of significant spatial communication modes. To compare this aspect of the channel model we use a measure of diversity,

$$D = \left(\frac{\mathrm{trace}\{\mathbf{R_H}\}}{\|\mathbf{R_H}\|_F}\right)^2 = \frac{\left(\sum_{m=1}^{N_R \times N_T} \lambda_m\right)^2}{\sum_{m=1}^{N_R \times N_T} \lambda_m^2}. \tag{6.18}$$

The diversity provides a measure of the spread of the eigenvalues of the channel. A higher diversity corresponds to a channel that has many signal paths of similar strength. A lower diversity corresponds to a channel with only a few strong signal paths. Higher diversity generally corresponds to a higher rate of capacity increase with respect to the signal to noise ratio.

To consider the ability of the model to capture the finer detail of the channel structure, we can analyse the effective double directional angular power spectrum. This is the joint distribution of the angles of departure and angles of arrival for the transmitter and receiver. A good channel model should be able to capture the finer detail in the double directional spectrum.

To consider the effects of the model on the spatial structure of the channel, we can use beamforming analysis to view the double directional spectrum of the original channel and compare this with the spectrum obtained from the various channel models. If the full correlation matrix is available, the Capon beam former provides an estimate of the signal power coming from each direction to the extent that it can be resolved by the array [63, 207, 209]. By evaluating the Capon beam former over the range of transmitter departure angles θ_T and receiver incident angles θ_R we can obtain the double directional spectrum. The Capon beam

former is evaluated as

$$S_{\text{CAPON}} = \frac{1}{\widetilde{\boldsymbol{a}}^H \mathbf{R}_{\mathbf{H}}^{-1} \boldsymbol{a}} \qquad \widetilde{\boldsymbol{a}} = \boldsymbol{a}_T(\theta_T) \otimes \boldsymbol{a}_R(\theta_R). \tag{6.19}$$

The steering vector $\boldsymbol{a}_T(\theta_T)$ represents the set of antenna gains at the transmitter that corresponds to a beam in direction θ_T. Similarly the vector $\boldsymbol{a}_R(\theta_R)$ is the receive array steering matrix at the angle of arrival θ_R.

For simulations, the data was normalised at each position for an effective 20dB signal to noise ratio. This matches with [270], and also is a range of operation experienced in many wireless systems [50].

6.4.2 Description and Validation of Experimental Data

To assess the performance of the proposed model, we use a set of experimental data obtained from indoor MIMO channel measurements. This data was recorded at Brigham Young University [278] using a wide band MIMO channel sounder with eight element $\lambda/2$ spaced circular arrays. A sample of the matrices across time and frequency were collated for each location. From the full data, 48 sets each having 640 channel matrices was extracted to represent the channel at different locations.

A requirement of the model framework set out in Section 6.2 is that the data is characterised by its second order statistics. We first validate this for the experimental data which will be used to test the model. This also serves to provide a baseline for the performance of the model – we would not expect any model based on the second order statistics to outperform the use of the complete correlation matrix $\mathbf{R}_{\mathbf{H}}$.

Figures 6.2 and 6.3 provide an analysis of the three measures of model performance for a complete second order model using the full $\mathbf{R}_{\mathbf{H}}$ correlation matrix. It can be seen that the data is well modelled by the second order statistics. This will serve as a baseline for the evaluation of the performance of the new model.

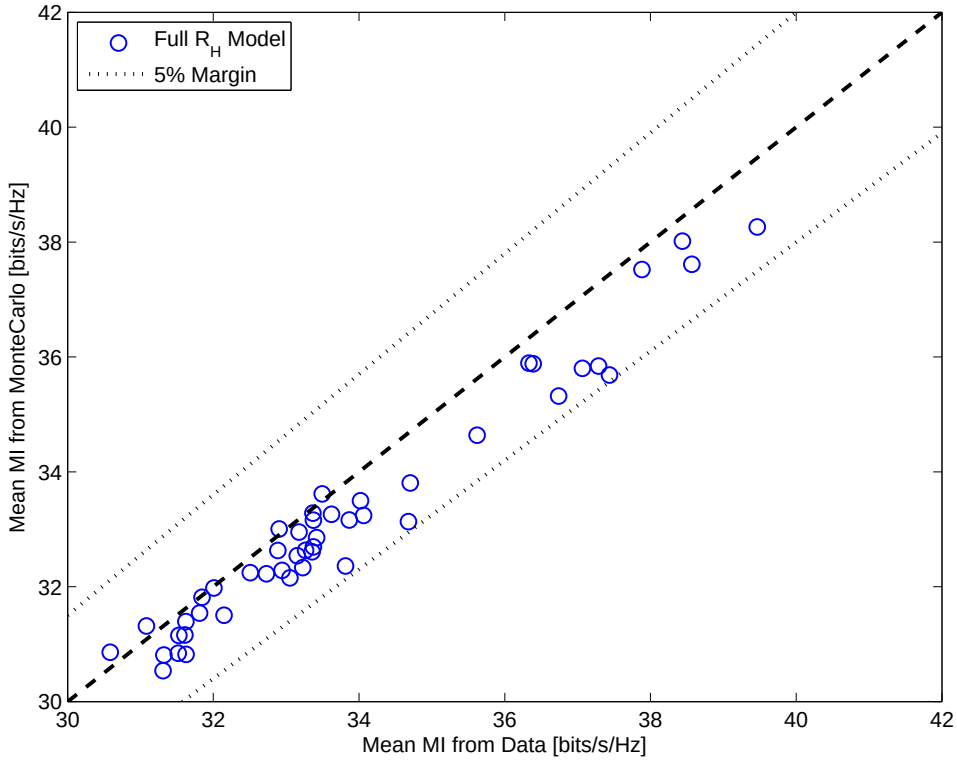

(a) Mean Mutual Information

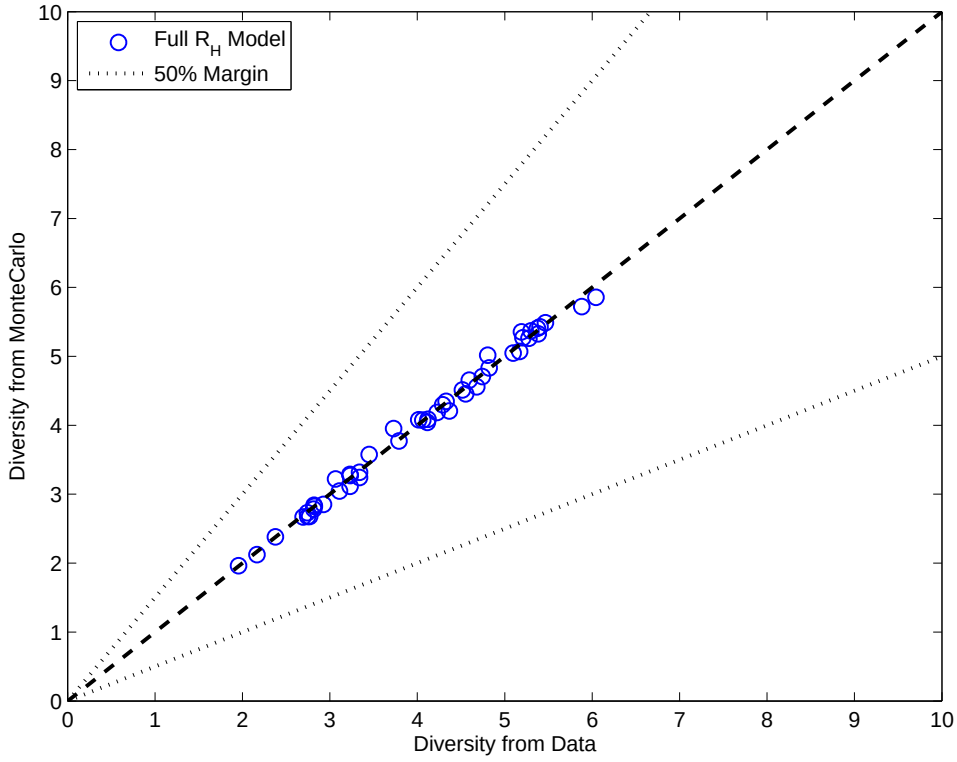

(b) Diversity

Figure 6.2: Comparison of measured and modelled mean mutual information and diversity. Validation that experimental data is well modelled by second order statistics. This comparison serves as a baseline for best performance of any second order based model.

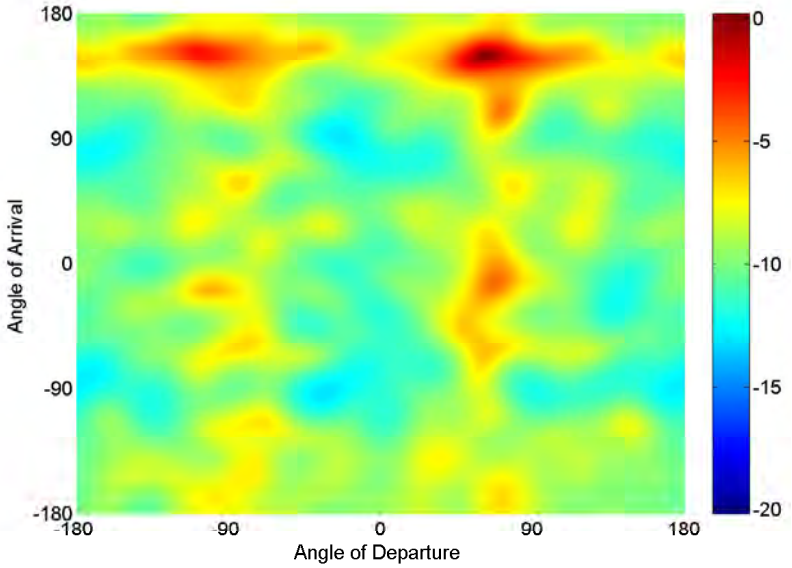

(a) Original Data Spectrum

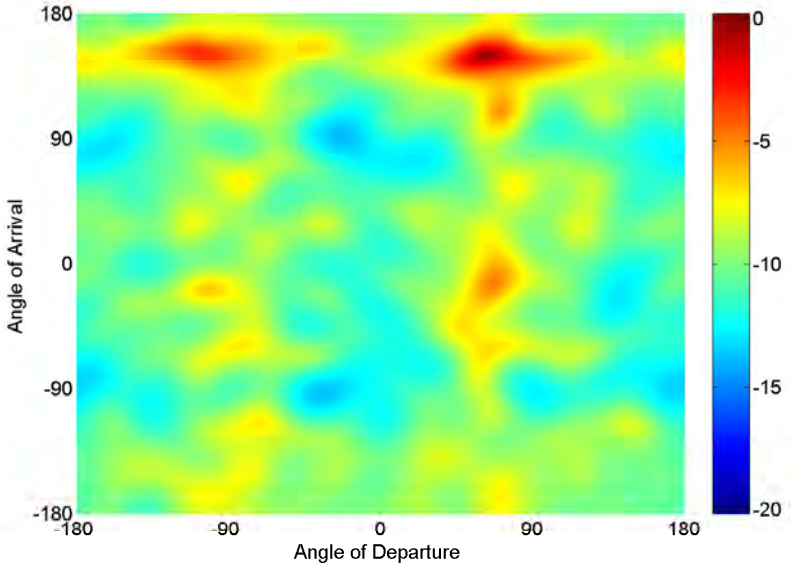

(b) Model Data Spectrum

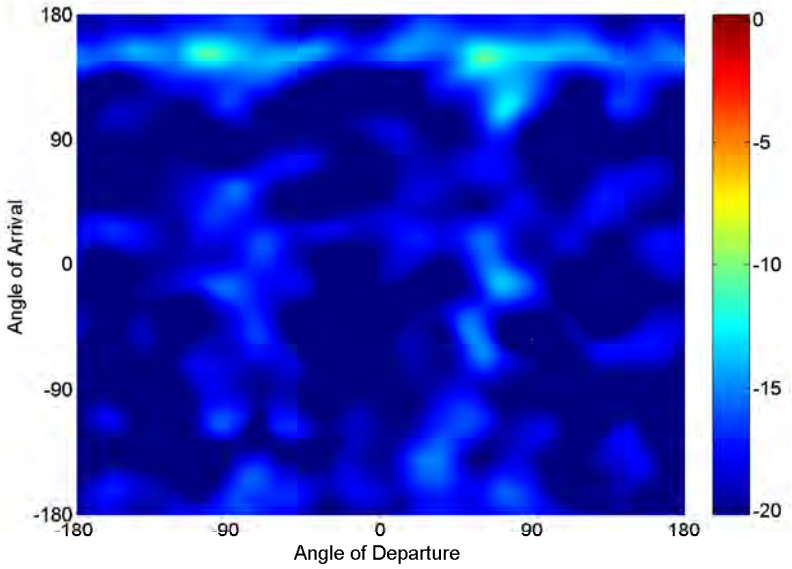

(c) Error in Spectra

Figure 6.3: Comparison of angular spectra for the original and second order statistically modelled data. The spectra are normalised to unity maximum with the colour scale in dB.

6.4.3 Comparison of Performance of New Model

Using the approach set out in Section 6.4.1 we can compare the performance of the new model framework to that of some other channel models. For reference we will use the Weichselberger model [270] and the older Kronecker Model [30]. For the simulations, 8 terms of the modal expansion were used requiring 176 coefficients to represent the model. The Weichselberger model also required 176 coefficients, whilst the Kronecker model employed 128 coefficients.

The comparison is shown in Figures 6.4 and 6.5. Proximity of the Mutual Information and Diversity points to the 45° line indicates the accuracy of the model. Given the similarity of the models, it is not surprising that the modal framework model has a similar level of performance to the Weichselberger model. The double directional angular power spectra for the two models are different, but display a similar level of detail in comparison to the original spectrum. The Kronecker model has fewer parameters, and as has been observed in previous works shows an underestimate of capacity and an overestimate of diversity [63]. All of the models tend to overestimate the diversity.

From this simulation and validation, it is shown that the new model framework provides a good model for the data with only 481 parameters compared with the 4096 parameters that would be required for the full correlation matrix. The modal framework performance is comparable with the Weichselberger model which would use 736 parameters. However, the framework offers the additional advantage of being able to consider the performance of the identified spatial channel with different array geometries. This is considered further in Section 6.4.5.

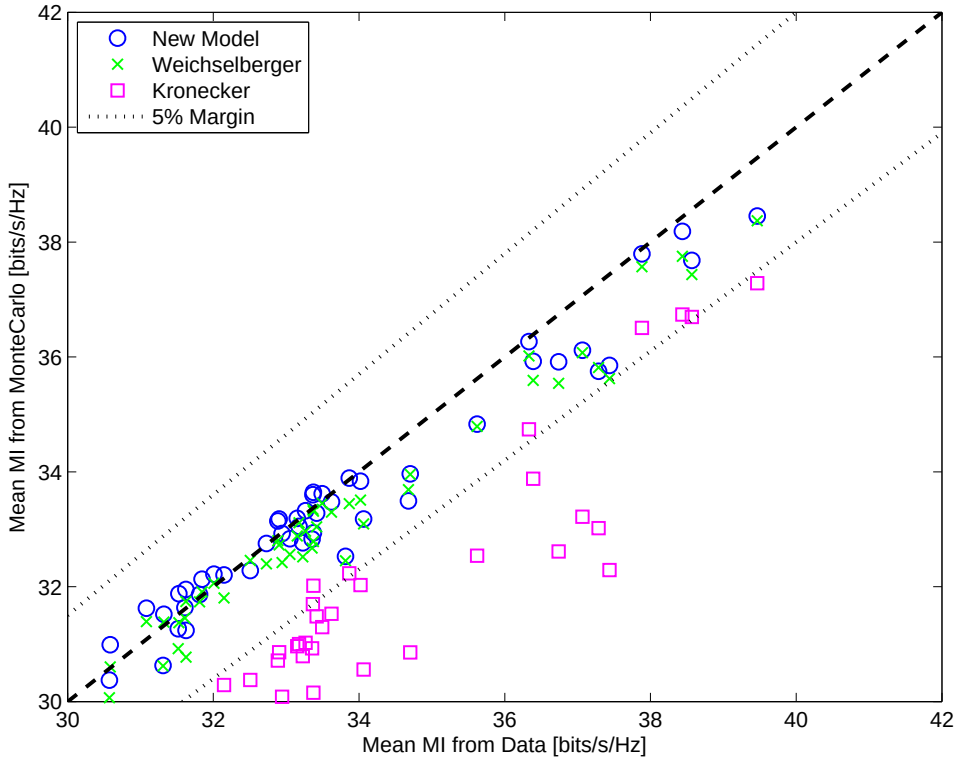

(a) Mutual Information

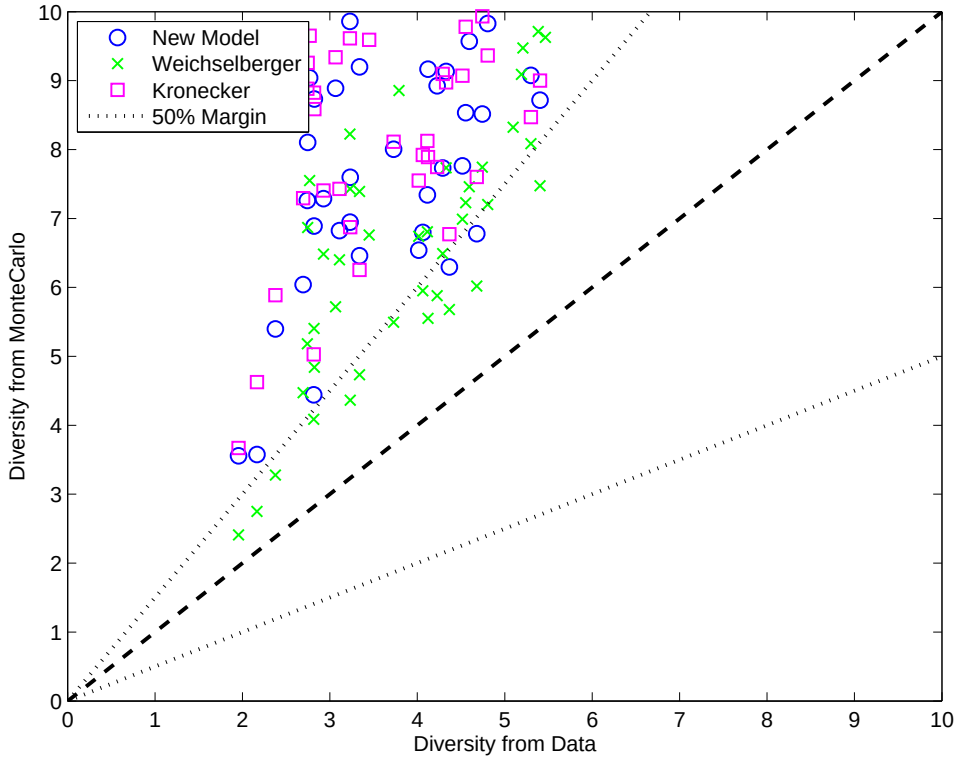

(b) Diversity

Figure 6.4: Comparison of the new spatial model framework with conventional statistical MIMO channel models. The Mean Mutual Information and Diversity are compared for the original and modelled data. The proposed approach has a comparable performance to the Weichselberger model whilst providing the significant advantage of modelling the channel independent of the array geometry.

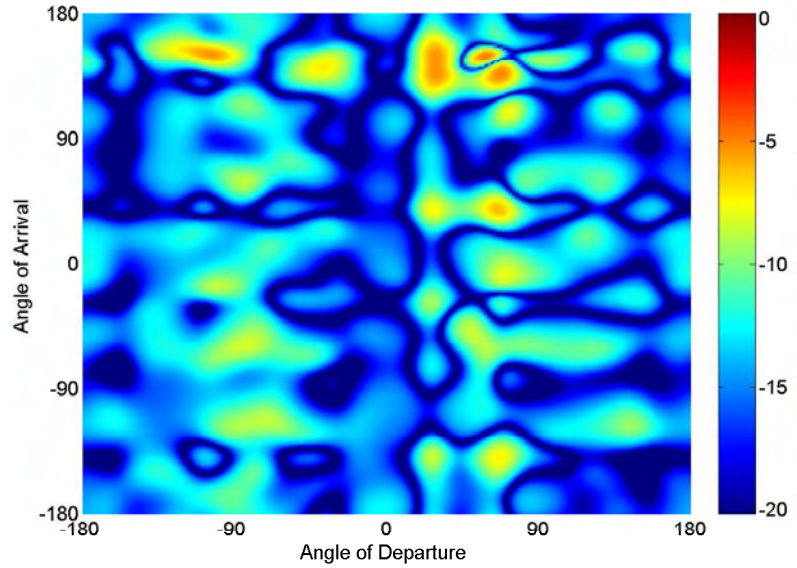

(a) Error in spectrum for proposed new model

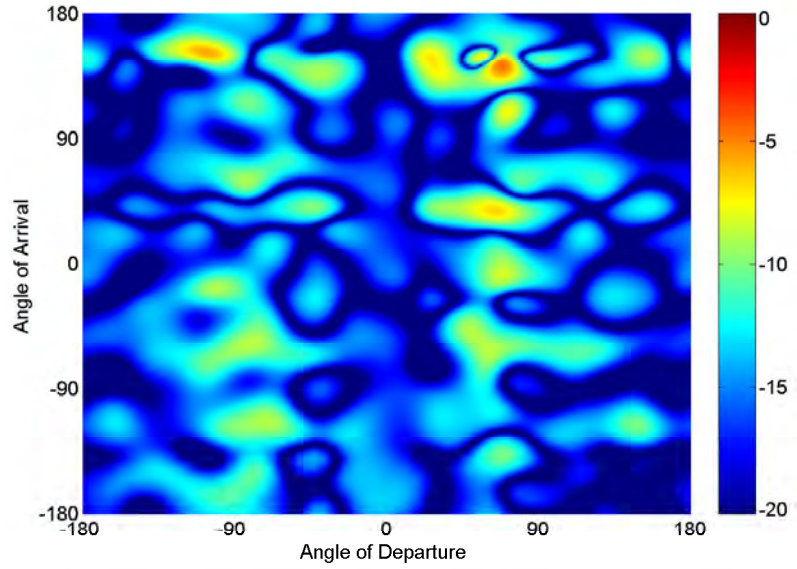

(b) Error in spectrum for Weichselberger model

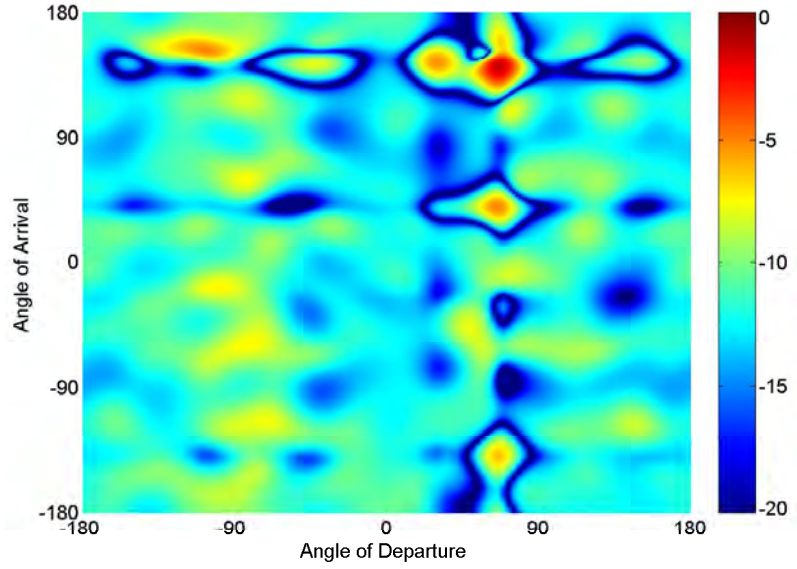

(c) Error in spectrum for Kronecker model

Figure 6.5: Comparison of the error in the angular spectra for proposed spatial model with two conventional channel models. The spectra are normalised with the colour scale in dB.

6.4.4 Performance of New Model with Dense Antenna Arrays

A significant advantage of the new model framework is offered for dense antenna arrays. In this case, the effective degrees of freedom is constrained by the spatial extent of the array and not by the number of antennas. To analyse the performance of the new model in such situations we make use of some synthetic data.

To generate synthetic data, an implementation of the channel model developed by the Third Generation Partnership Project (3GPP) Spatial Channel model ad-hoc working group was used [77]. Several scenarios were available for this model ranging from a suburban environment through to a pico-cell environment. The experimental data used in the previous section was best matched by the pico-cell environment.

Figure 6.6 compares a sample of the experimental data to that generated by the 3GPP Spatial Channel Model pico cell environment. Both plots represent the evolution of the channel over 2 seconds as the mobile station is moved through a distance of 63.5cm. The data is plotted for 8 received antennas from a single transmit antenna. It is noted that there is a similar level of fades, fade duration and antenna correlation in the two data sets.

To simulate a dense antenna array, a 16 element uniform circular array was simulated with the antenna elements placed one quarter wavelength apart. A comparison of the experimental and synthesised antenna arrays is shown in Figure 6.9. Use of the modal framework allows for a significant reduction in the number of parameters over other models.

The 16 element array radius was 0.65λ suggesting a truncation order of between 4 and 6 (See Chapter 2 for discussion). A comparison of the performance of the new model at various truncation orders is shown in Figures 6.7 and 6.8. The performance of the new model is comparable to that of the Weichselberger model at the higher suggested truncation order. The required accuracy can be traded against the number of parameters required by adjusting the truncation order. For the truncation at order $M = 4$ the modal model has half the parameters of the Kronecker model, yet still provides a better match of the mean mutual information. The joint angular spectra show the gradual degradation in the representation accuracy of the spatial channel model as the truncation order is decreased.

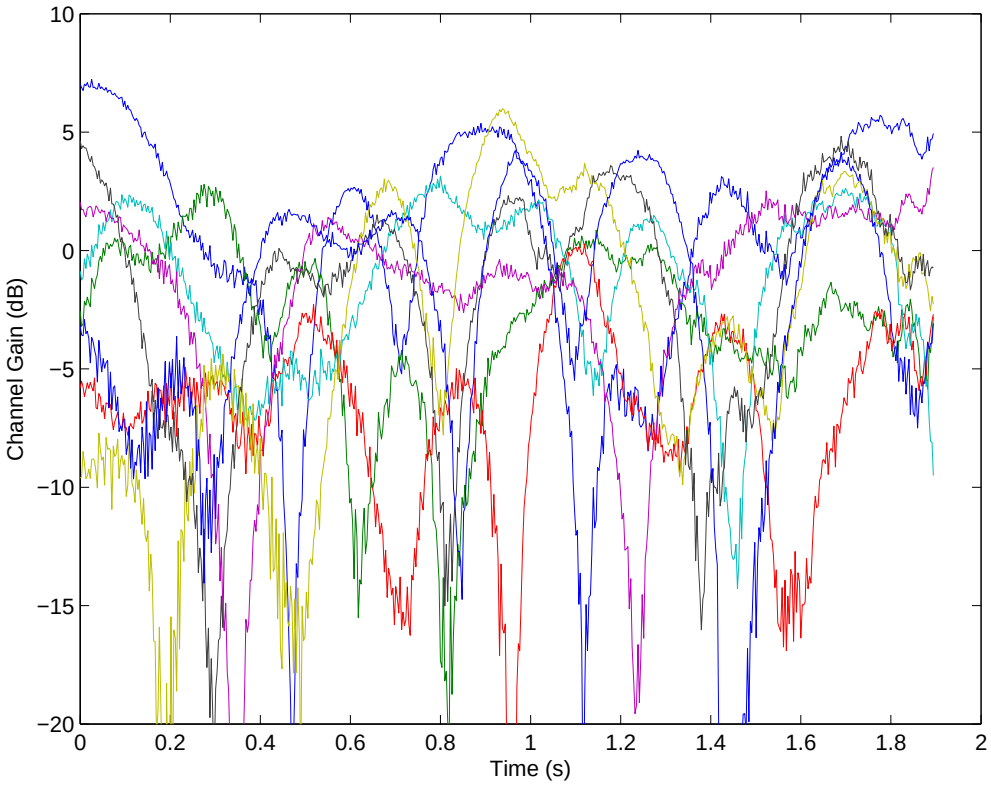

(a) Experimental Data

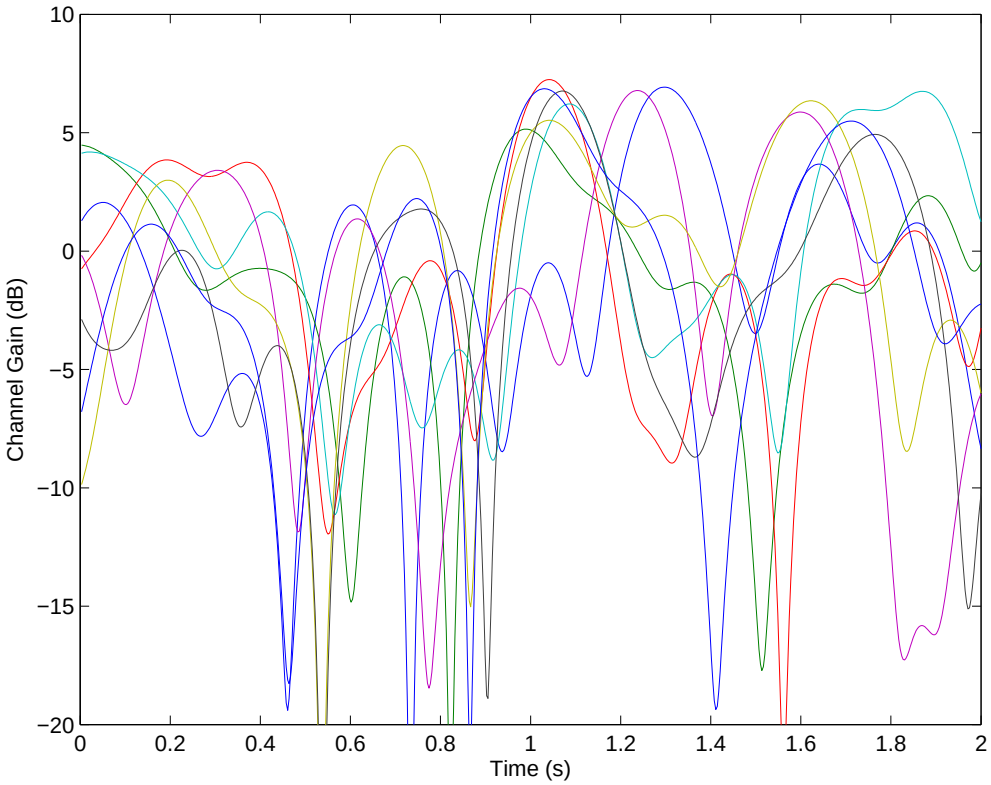

(b) Synthetic Data

Figure 6.6: Comparison of the experimental and synthetic data from 3GPP Spatial Channel model for a pico-cell environment. Since the simulation is only representative, the data cannot be directly compared. The experimental and synthetic data exhibit similar levels of fading and correlation.

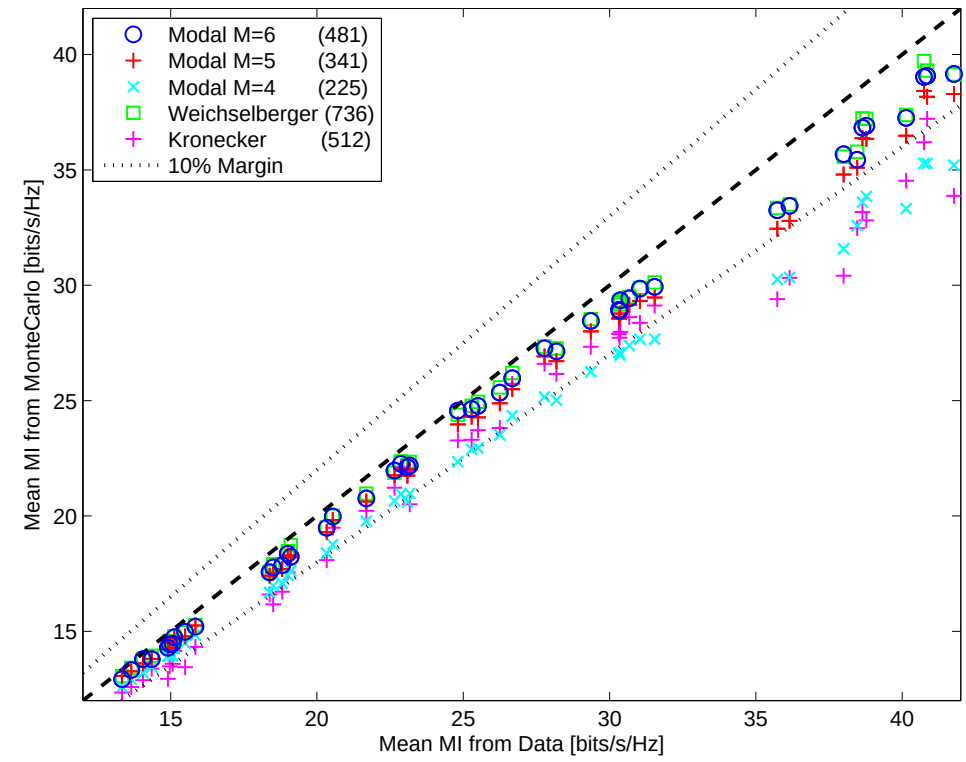

(a) Mutual Information

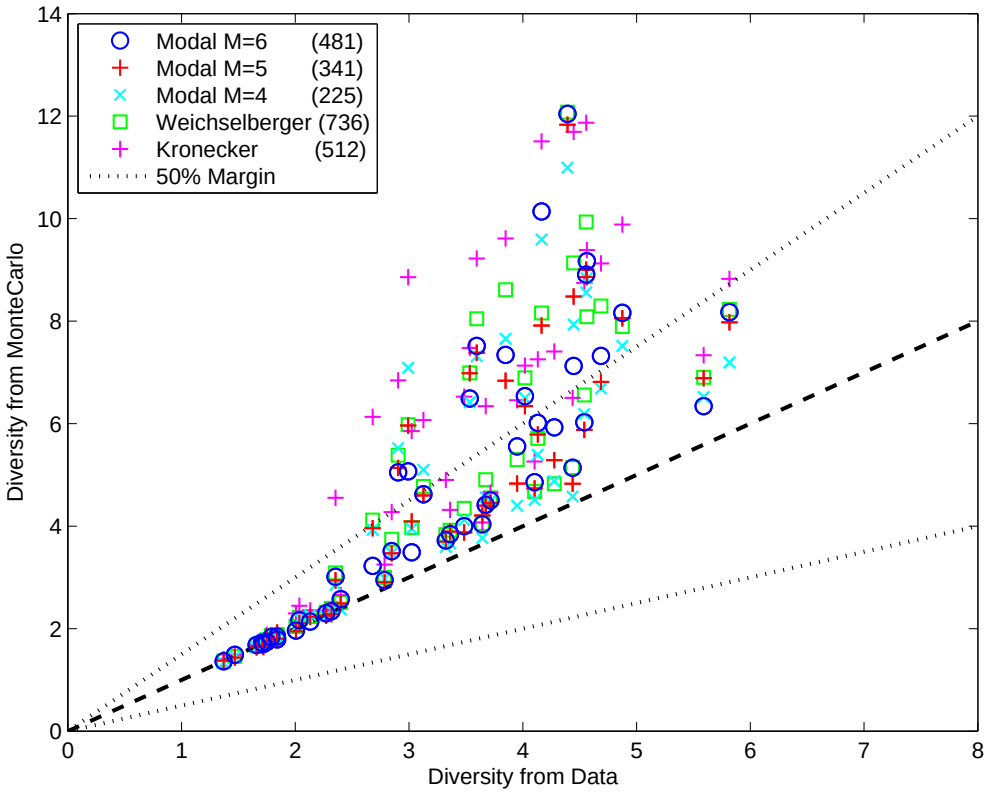

(b) Diversity

Figure 6.7: Performance of the new model with synthetic data for a dense antenna array. The model allows a significant reduction in the number of parameters based on the essential dimensionality of the measurement region.

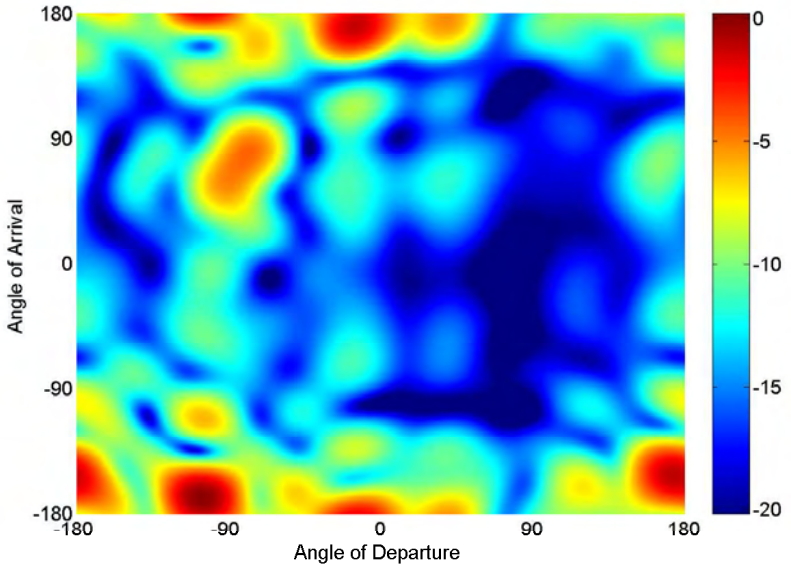

(a) Original data spectrum

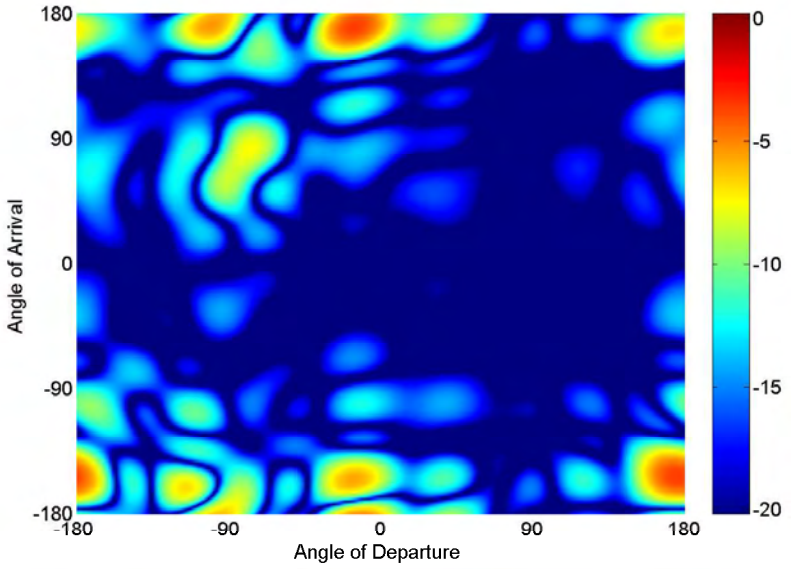

(b) Error in spectrum for New Model with $M = 6$

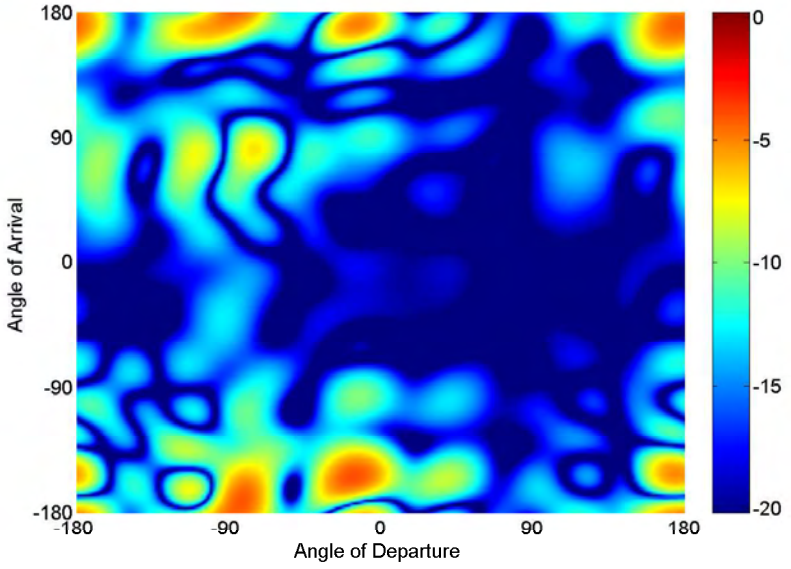

(c) Error in spectrum for New Model with $M = 4$

Figure 6.8: Comparison of the error in the angular spectra for different model order. The error in the model is increased as the truncation order is decreased.

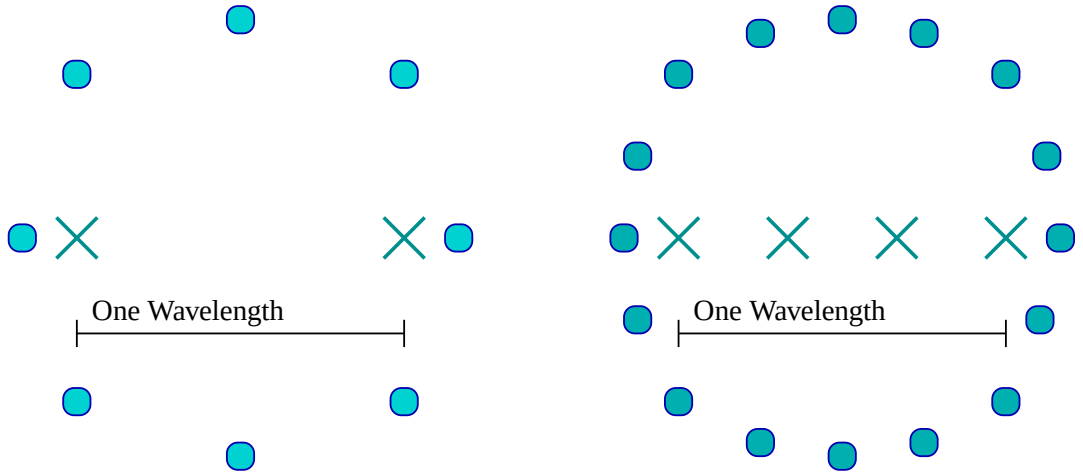

(a) Measured Data Array (b) Synthetic Data Array

Figure 6.9: Array geometries used for investigation of the use of model for prediction of MIMO channel. Positions show actual (○) and predicted (×) sensor locations.

6.4.5 Use of New Model to Model Alternate Array Configuration

The framework presented in Table 6.1 used the explicit notation of $\mathbf{J}_T, \mathbf{J}_R$ and $\mathbf{J}'_T, \mathbf{J}'_R$ to represent the measurement sensor array configuration matrices and modelled array configuration matrices. This gives the framework the ability to simulate the use of alternate array configurations, using the same set of spatial modal statistics captured from the measured array. To investigate this, we analyse two configurations:-

1. Using the experimental data [278], simulate the performance of a 2 element array, spaced approximately one wavelength, at the mobile station with the full 8 element uniform circular array at the base station.

2. Using the simulated data, simulate the performance of a one wavelength, 4 element uniform linear array at both the base station and mobile station.

To provide a comparison for the alternate array configuration with the experimental data, two pair of antenna from the array with the same spacing and orientation were used. With the synthetic data, it was possible to simulate the alternate array configuration using the same spatial channel configuration. The location of the initial and alternate sensor locations are shown in Figure 6.9.

The ability of the model to predict the characteristics of the spatial channel for the alternate array configurations is shown in Figure 6.10. It can be seen that the model is able to predict the mean mutual information with an accuracy better than 10%. The error is slightly larger

for the experimental data, which is to be expected since the true performance at the simulated sensor locations is only estimated from an similarly oriented set of actual sensors.

6.4.6 Use of New Model to Optimise Antenna Configuration

As a final example we demonstrate the use of the new model to use real world data in the analysis of an antenna configuration optimisation problem. The experimental data is used to create a model that captures the spatial aspects of the channel. This model can then be used to investigate the effect of antenna separation at the mobile station on the mean mutual information.

Fig. 6.11 shows the mean mutual information from a model simulation, as a function of the receiver element separation. There is a noticeable variation in the shape of the curves due to differing spatial channel characteristics captured by the model for each instance (position) represented in the data. Since the stochastic model is computationally efficient, more complicated array geometries could also be investigated.

For this data set, it is apparent that the optimal antenna separation would be around 0.3λ. Beyond this separation there is little gain in the mean mutual information, and in some cases a considerable drop. Whilst it would be arduous to perform this experiment in practice, the proposed model framework provides a means to capture the spatial channel and perform the configuration optimisation using the model.

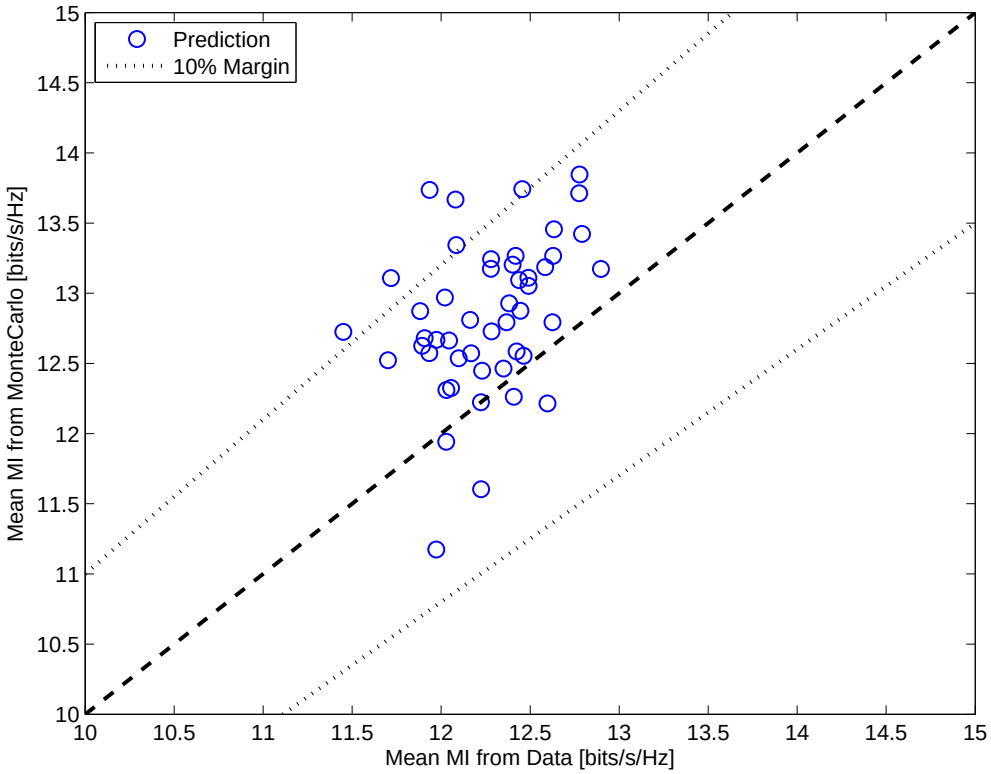

(a) Experimental Data to Predict 8×2

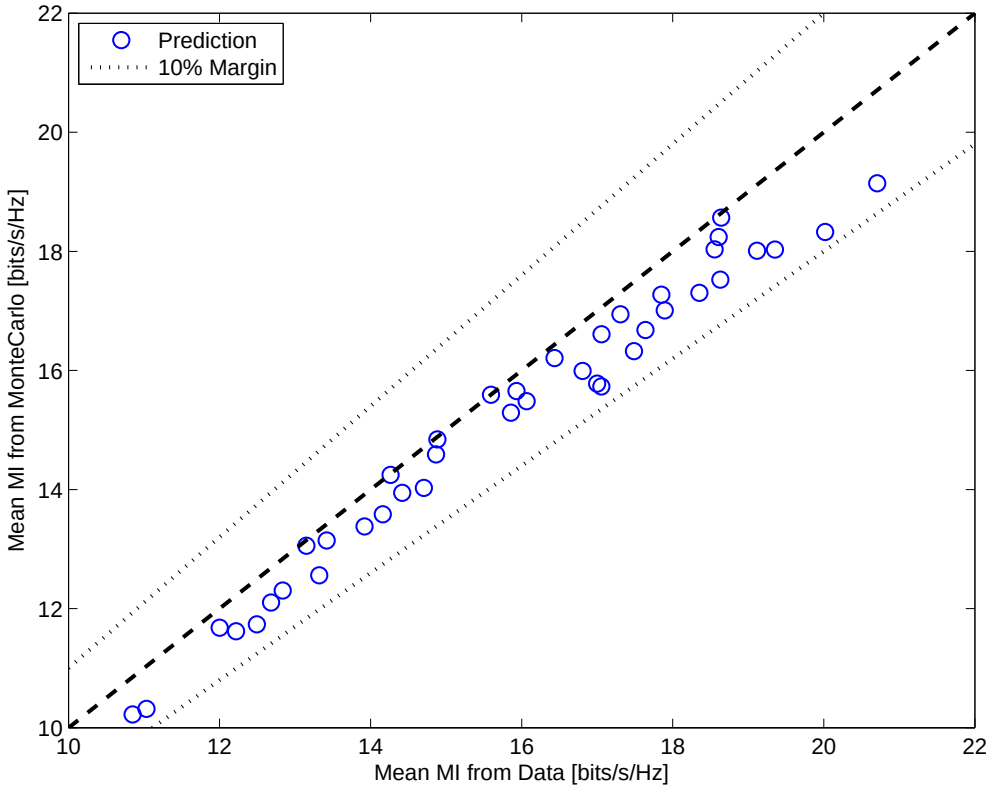

(b) Synthetic Data to Predict 4×4

Figure 6.10: Prediction of performance of an alternate array configuration. Data from the uniform circular array is used to create a model and simulate the performance of a uniform linear array within the measurement region. The array geometries are shown in Figure 6.9.

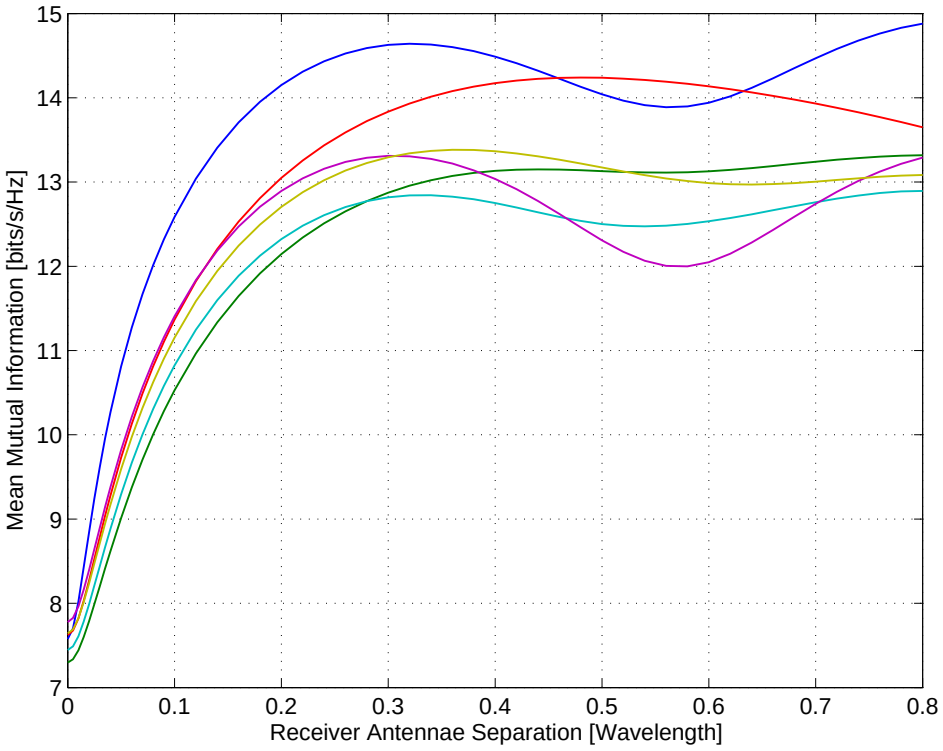

Figure 6.11: Use of the model for configuration optimisation. Prediction of performance versus antenna separation for 8x2 system. Individual traces represent the effect of the spatial channel characteristics, captured by the model, on the optimal antenna separation.

6.5 Summary and Contributions

The new model proposed creates a framework where the spatial MIMO channel is represented by coupling between spatial modes of the field at the receiver and transmitter. The mechanism for moving between the antenna and modal signal domains is provided by the antenna configuration matrix. This abstraction allows the characteristics of the antenna geometry to be removed from the model.

A stochastic framework was used to model the internal parameters in the modal space. This then also allows generation of MIMO channel data for any antenna configuration within a finite volume. The model represents an efficient parametrisation of the spatial characteristics of a MIMO channel.

The following specific contributions were made in this chapter:

- Proposed an alternative to multipath parameter estimation for capturing the characteristics of a physical propagation environment. The proposed framework avoids making any assumption on the number and nature of independent paths that create the spatial channel.
- Validated the proposed model through simulation using real experimental data and data generated from the comprehensive 3GPP Spatial Channel Model. The proposed model was shown to perform at least as well as other comparable models, but offers the significant advantage of abstracting the antenna array geometry.
- Demonstrated the advantage of a reduced parameter space when using the modal approach to model a channel in which the number of antennas exceeds the spatial dimensionality of the measurement regions.
- Analysed several example scenarios to demonstrate how the model can be used to simulate the performance of alternate antenna array configurations.

The proposed model and analysis of this chapter suggests that the modal framework is a viable alternative to double directional discrete path channel models. Since the modal framework efficiently represents the spatial field, the problems of over-parametrisation inherent in any discrete scatterer path model are avoided. The modal framework captures the spatial characteristics that can be accurately measured in the antenna regions, and the statistical framework adopted from the Weichselberger model provides a significant reduction in the parameter space for the model.

Chapter 7

Resolution of Spatial Location from within a Constrained Region

7.1 Introduction

The previous chapters have had a common theme of investigating the use of continuous spatial models for signal representation and analysing the limits of signal processing. The areas covered have included the questions of finite dimensional approximations and optimal representation, along with the application areas of direction of arrival estimation and MIMO channel modelling. This chapter is a continuation of this theme addressing another problem application area. The work serves to demonstrate how using a continuous spatial model for a sensor based problem can lead to a greater understanding of the problem of resolving the spatial location of a wireless source when the observation region is a constrained region of space.

The problem considered is that of localisation. We consider the ability of a single receiver to determine the location of a source. Localisation is intrinsically related to the receiver's ability to distinguish sources from different regions in space. Given that a receiver can detect the field over a bounded region of space, we are interested in studying the ability of the receiver to use measurements or observations within this constraint to estimate a source position.

This is a divergence from the more commonly studied location problem where location is achieved by a set of co-operating receivers distributed in space. Objects are located within the convex hull of the receivers using information regarding the time of arrival or power of the signals at the receivers. In this work, we consider a different problem – that of the ability of a single receiver to determine the location of transmitting objects outside of the receiver volume. In a sense, this is an extension of the direction of arrival problem.

The field of direction of arrival or beam-forming is well established and there are many results covering the performance of sensor arrays for resolving angle. Chapter 5 presented some theoretical work on the ability of a sensor array confined in space to determine direction of arrival. We consider in this chapter a theoretical approach to analysing the ability of a sensor array to resolve both the angle and distance of a source.

The approach taken is to first consider a simple problem in this area. We consider the case where only the intensity of the source can be detected over a finite volume. Section 7.2 sets out the problem formulation to address the questions posed. Some numerical analysis and investigations are detailed in Section 7.3 to gain an understanding of the problem. Section 7.4 develops some continuous sensor models to determine bounds for the number of distinct localisation regions. Section 7.5 considers the problem where the complete field information, intensity and phase, is used for localisation. A discussion of the results and comparison to some other results in the literature is provided in Section 7.6.

The main contribution of this work is to introduce an alternative approach to considering the problem of source localisation. The number of distinct source regions for a receiver is fundamental to the world view and efficient representation of source location that should be adopted by that receiver. It is related to the measure of information that can be obtained from the observed field regarding the source location. The introduction of continuous spatial field models to this problem will help to overcome distractions due to specific sensor arrangements and geometries. The problem considered is to bound the number of distinct locations that can be assigned to a source.

7.2 Problem Formulation

A set of Q sensors are located at positions $\boldsymbol{r}_q \in \mathbb{R}^2$ for $q = 1, \ldots, Q$ within a radius R such that $\|\boldsymbol{x}_q\| \leq R$. The sensors produce the measurement vector $\boldsymbol{y} = [y_1, \ldots, y_Q]^T$, where $y_q \in \mathbb{R}$, $y_q > 0$ is a measure of the signal strength or intensity of the source field at the location $\boldsymbol{x}_q$.

For an arbitrary uncooperative source, there may be no information regarding the power level transmitted. Assume that the intensity of the signal received is normalised such that it is unity at the origin. In this sense the problem relates to the ability to detect the location of a source given that a reasonable signal level is present at the receiver. In practice, the ability to detect source movement would decrease with the signal strength and consequently the source distance.

Given a source at position $\boldsymbol{x}$, the normalised intensity received by each sensor will be

$$y_q = \frac{\|\boldsymbol{x}\|}{\|\boldsymbol{x} - \boldsymbol{x}_q\|} \tag{7.1}$$

where $\|\cdot\|$ represents the length of the vector argument. This matches our normalisation and encapsulates the radial decay of intensity that would be expected in three-dimensional space. Designate this multidimensional function as a vector

$$\boldsymbol{y} = f(\boldsymbol{x}) = \begin{bmatrix} y_1 & \ldots & y_Q \end{bmatrix}^T. \tag{7.2}$$

Due to noise, or some other constraint, the receiver is only able to distinguish sets of signals that differ by a certain threshold. That is the measurements $\boldsymbol{y}$ and $\boldsymbol{y}'$ are considered indistinguishable if

$$\|\boldsymbol{y} - \boldsymbol{y}'\|_R^2 = \frac{1}{Q} \sum_{q=1}^{Q} \left| y_q - y_q' \right|^2 < \varepsilon^2. \tag{7.3}$$

The scaling by $1/Q$ is incorporated into this norm to normalise for the number of sensors present. The norm $\|\cdot\|_R$ represents the root mean squared difference for the sensor array.

Given this arrangement, we are interested in studying the ability to determine the location of the source from such measurements. Specifically the questions to be addressed are:-

- Is there some limit to the number of distinct locations that can be resolved or identified outside the observation region ?

- What can we say about the shape of the source regions that can be discerned ?
- How does this depend on the number and arrangement of the sensors ?

7.3 Numerical Investigation of Distinct Localities

7.3.1 Proposed Tiling Algorithm

A first observation is that the number of distinct localities will be infinite if the source is allowed arbitrarily close to the sensor array. This is noted from (7.1) that $\|f(\boldsymbol{x})\|_R \to \infty$ as $\boldsymbol{x} \to \boldsymbol{x}_q$. With this unbound normalised measurement there will be an infinite number of distinct zones around each sensor.

Consider the problem of the source and sensors lying in the same two-dimensional plane. The sensors are located within a disc of radius R. Define $\mathcal{S}$ as a region excluding the sensor array being points of norm S or greater,

$$\mathcal{S} = \left\{ \boldsymbol{x} \in \mathbb{R}^2 : \|\boldsymbol{x}\| \geq S > R \right\}. \tag{7.4}$$

We perform a tiling of the space $\mathcal{S}$ by constructing a set of points $\mathbb{P}$ such that any point in $\mathcal{S}$ is not more than a certain measurement threshold, ε, from a member of $\mathbb{P}$. Formally,

$$\forall \boldsymbol{x} \in \mathcal{S} \quad \exists \quad \boldsymbol{p} \in \mathbb{P} \quad \text{such that} \quad \|f(\boldsymbol{x}) - f(\boldsymbol{p})\|_R \leq \varepsilon. \tag{7.5}$$

Since we are interested in determining the number of distinct regions, we are looking for the smallest set $\mathbb{P}$ that satisfies this property. We can determine a reasonably small, though not optimal, set $\mathbb{P}$ by commencing with the empty set, $\mathbb{P} = \{\emptyset\}$ and progressively adding points from $\mathcal{S}$. As points are added to the tiling, we keep track of the region which is within ε of any point in $\mathbb{P}$,

$$\mathcal{P} = \bigcup_{\boldsymbol{x} \in \mathbb{P}} \left\{ \boldsymbol{x}' : \|f(\boldsymbol{x}') - f(\boldsymbol{x})\|_R < \varepsilon \right\}. \tag{7.6}$$

This is shown for a single point in Figure 7.1. We can then add another point from the set obtained when $\mathcal{P}$ is subtracted from $\mathcal{S}$ which is written as $\mathcal{S} \setminus \mathcal{P}$. This process can be continued until $\mathcal{S} \setminus \mathcal{P} = \{\emptyset\}$. At this point we conjecture that this can be achieved with a finite number of points in $\mathbb{P}$. This conjecture is proven in Section 7.4.1.

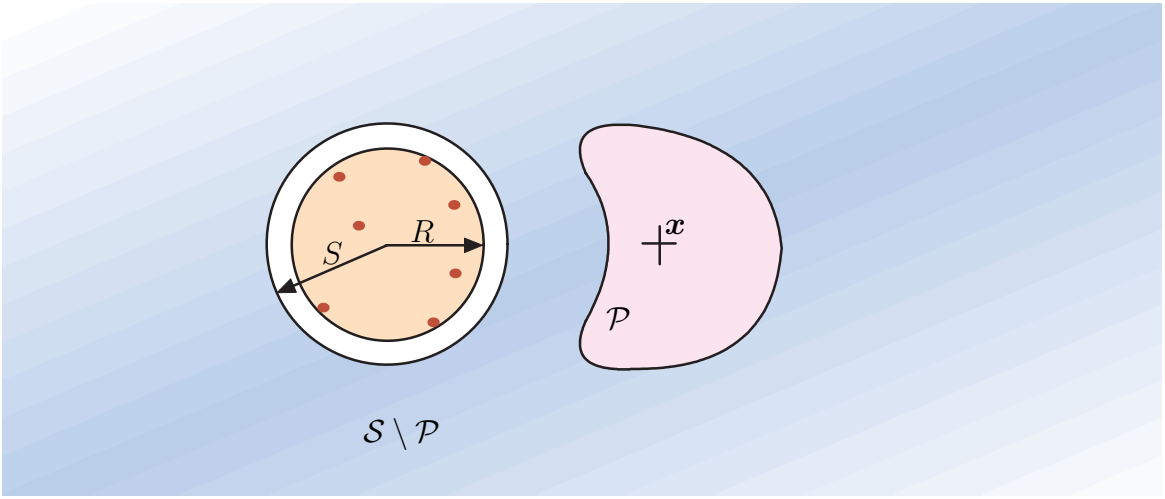

Figure 7.1: Schematic showing the set definitions for the tiling algorithm used in the numerical investigations. The sensors are confined to the central region with radius R. A single point $\mathbb{P} = \{\boldsymbol{x}\}$ is selected in the region $\mathcal{S}$ where $\|\boldsymbol{x}\| > S$. Around this point, the set $\mathcal{P} = \{\boldsymbol{x}' : \|f(\boldsymbol{x}') - f(\boldsymbol{x})\|_R < \varepsilon\}$ is removed or tiled from the set $\mathcal{S}$.

Whilst the process for selecting the next point in $\mathcal{S} \setminus \mathcal{P}$ to add to $\mathbb{P}$ can be arbitrary, a systematic approach can be obtained by selecting the point with minimum radius,

$$\mathbb{P} = \mathbb{P} \cup \arg \min_{\boldsymbol{x} \in \mathcal{S} \setminus \mathcal{P}} \|\boldsymbol{x}\| \,. \tag{7.7}$$

In this way, the algorithm starts by selecting points on the inner radius S, and proceeding outwards. This procedure creates a set of points that is a suboptimal ε covering of the set $\mathcal{S}$, however we can be sure that (7.5) will be satisfied.

This process is shown over a small region of $\mathcal{S}$ in Figure 7.2(a) with the addition to the set $\mathcal{P}$ shown for each of the four points in $\mathbb{P}$ for this tiling. The second part, Figure 7.2(b), shows the boundaries of the regions for a sensor measurement of half that used in the tiling algorithm. These regions do not overlap and in some cases just touch. This is a consequence of the fact that the norm used for determining a unique location, (7.3), is a valid norm and satisfies the triangle inequality.

Thus it can be seen that while the set $\mathbb{P}$ is a suboptimal covering of $\mathcal{S}$ at level ε, it is an insufficient set of points to cover $\mathcal{S}$ at level $\varepsilon/2$. If we calculate the number of points required for a tiling at level ε, this will represent the number of regions for some optimal tiling at a smaller level between $\varepsilon/2$ and ε.

Formally, define N_ε as the minimum integer for which there exists a set with N_ε elements that is a covering of $\mathcal{S}$ at level ε. The number of elements in the tiling $\mathbb{P}$ will be an upper bound

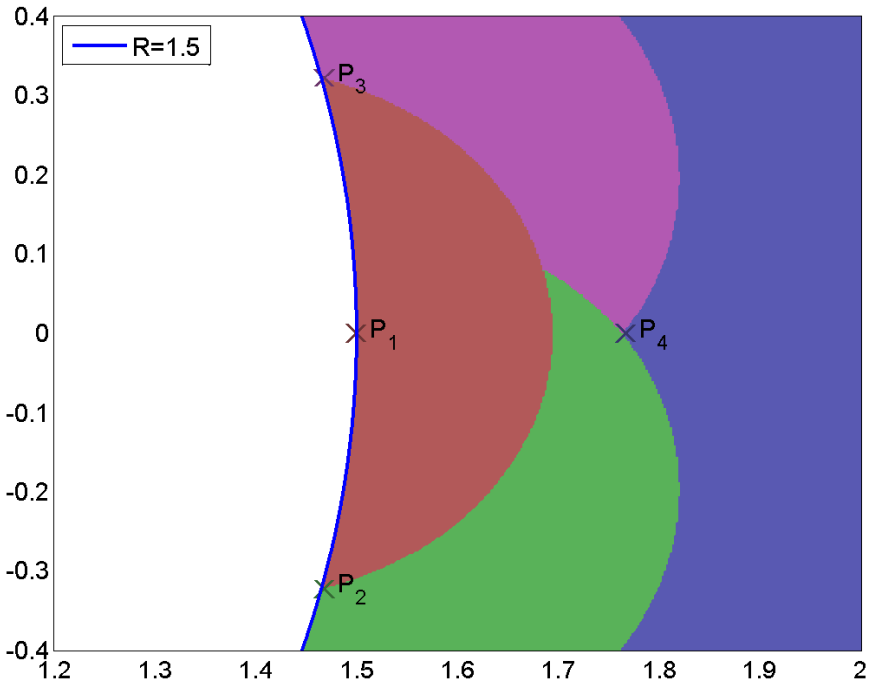

(a) Additional coverage of $\mathcal{S}$ for each P.

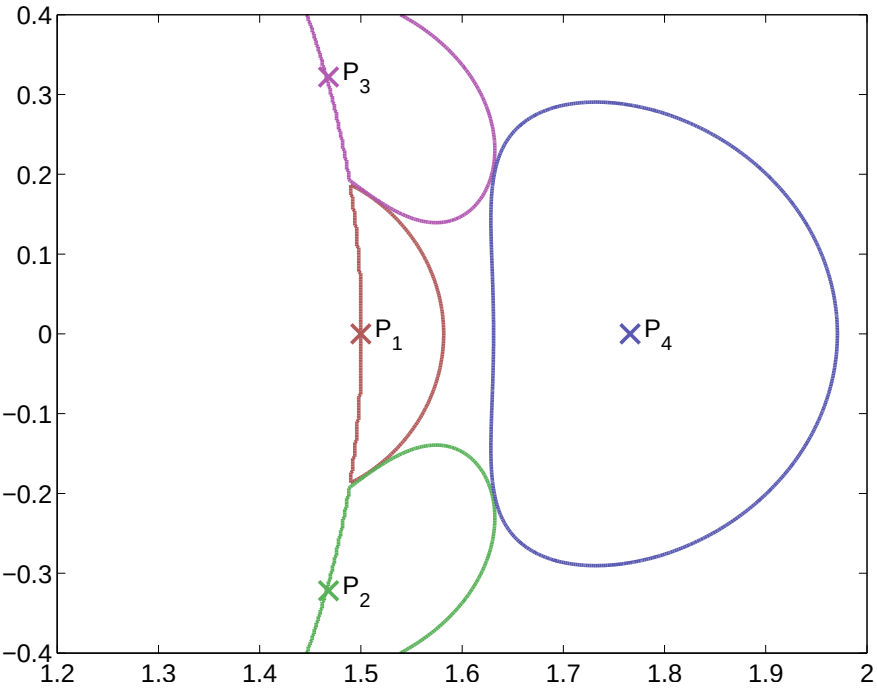

(b) Regions for half of the sensor error.

Figure 7.2: Demonstration of the tiling algorithm used to partition the space into resolvable locations. The simulation uses 8 sensors with unity radius and a minimum radius for $\mathcal{S}$ of 1.5. The threshold for the distinguishable locations was $\varepsilon = 0.2$. The first figure shows the tiling regions with $\|\boldsymbol{y} - \boldsymbol{y}'\|_R = \|f(\boldsymbol{x}) - f(\boldsymbol{x}')\|_R \leq \varepsilon$ for each of the four points added to the tiling. The second region shows the boundary of the region for $\|\boldsymbol{y} - \boldsymbol{y}'\|_R \leq \varepsilon/2$.

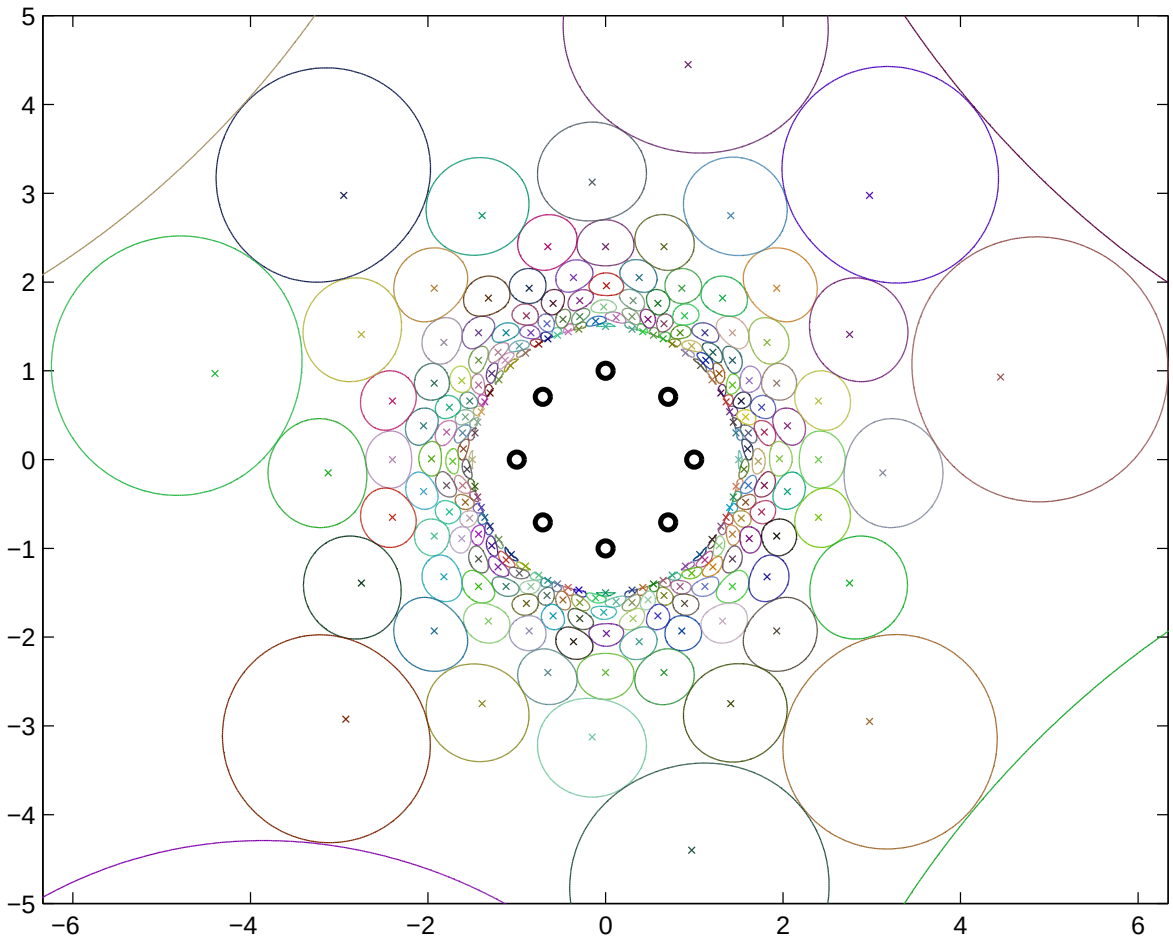

Figure 7.3: An example of the distinguishable location regions for an 8 element uniform circular array or radius $R = 1$. Points are plotted for radii greater than $S = 1.5$. The signal is normalised to be unity at the origin. The points correspond to a minimum spacing of $\varepsilon = 0.1$ with the contour shown representing $\varepsilon/2$. There are 216 distinct localisation regions.

for N_ε and a lower bound for $N_{\varepsilon/2}$. The tiling algorithm is not likely to be the algorithm used to partition the space for a practical application, however it serves to provide an upper bound.

7.3.2 Numerical Examples of Location Tiling

The numerical analysis is carried out using a fine grid of points to represent the set membership of $\mathcal{P}$. Whilst this is not an accurate numerical method, it is suitable for investigating the flavour of the problem. Tracking the exact boundary of $\mathcal{P}$ would be an arduous task. A suitable level of detail is obtained by making the grid size small enough to reveal the smallest regions near the region boundary with radius S.

Figure 7.3 shows a plot of such a point set obtained for an 8 element uniform circular array

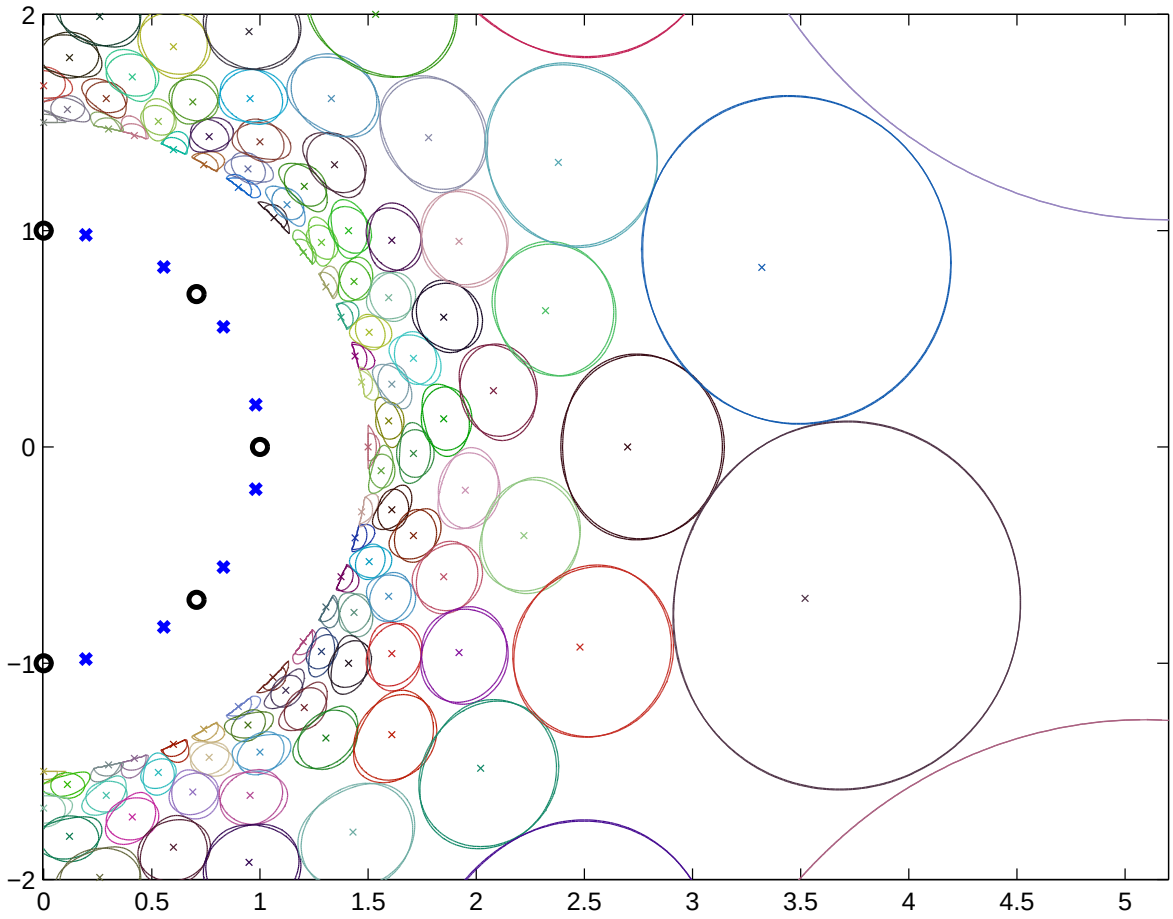

Figure 7.4: Comparison of the discernable region shapes for an 8 and 16 element UCA. The regions are fairly insensitive to the number of sensors, becoming almost identical for $R > 2$. The regions close to the array are slightly smaller. A complete tiling for the 16 element configuration would have 228 distinct regions.

with radius of $R = 1$ with minimum radius $S = 1.5$ for a value of $\varepsilon = 0.1$. The boundaries show on the plot represent the region around each point for which the level of distinguishable $\|\boldsymbol{y} - \boldsymbol{y}'\|_R = \varepsilon/2$. These regions do not overlap since the distance between any two points in the tiling is at least ε, $\|\boldsymbol{y} - \boldsymbol{y}'\|_R \geq \varepsilon$, and the norm as defined in (7.3) is sub-additive.

The regions become densely packed near the sensor array and grow in size further away from the array. Beyond the limits shown in the figure, all points become indistinguishable with one region covering the entire range of $\mathcal{S}$ beyond the regions shown. Thus the regions shown represent a complete tiling of the space $\mathcal{S}$.

With the same configuration as the previous example, the sensor geometry is changed to a 16 element uniform circular array. The shape of the localisation regions for the two different array geometries are compared in Figure 7.4. The characteristics of the regions are not overly sensitive to the number of sensors. While there is some variation in the region size and shape

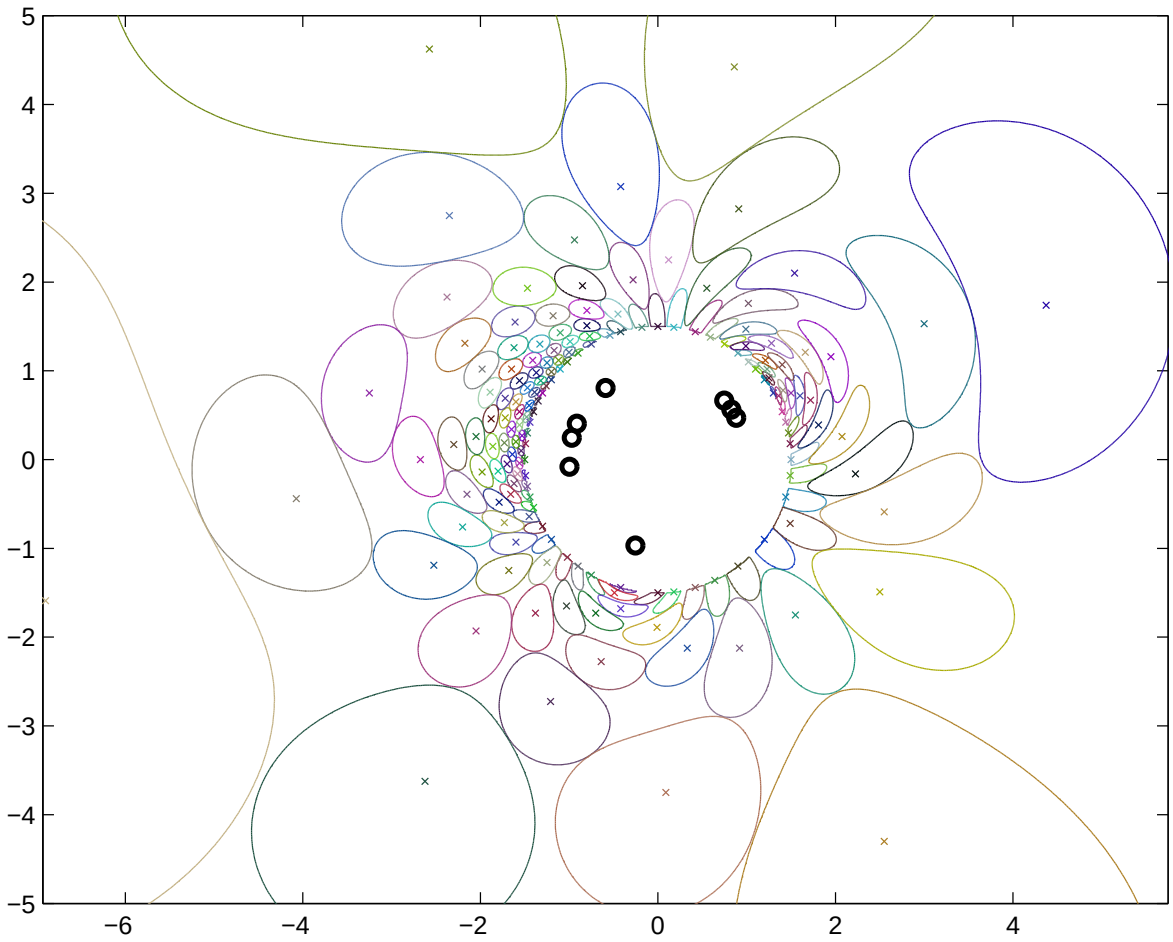

Figure 7.5: An example of the discernable location regions for an 8 element array with random sensor location on the circle with radius $R = 1$. The tiling covers points with radius greater than $S = 1.5$. The density of the indistinguishable regions varies with the sensor arrangement, and the total number is reduced to 161.

closer to the sensor array, any difference becomes negligible once the radius exceeds twice that of the sensor array.

Since the larger number of sensors offers an improved resolution close to the sensor array, the total number of distinguishable regions is increased. For the 16 element UCA the tiling has 228 points compared with 216 points for the 8 element UCA.

If a more random distribution of sensor locations is considered, the distortion in the region shapes becomes more apparent as shown in Figure 7.5. Region sizes are smaller closer to the clustered sensors and become larger for the orientations where the sensors are further apart. While the region shapes have changed, the total number of distinguishable regions has not changed significantly. For the example presented, the tiling consists of 161 points compared with 216 for the 8 element uniform circular array.

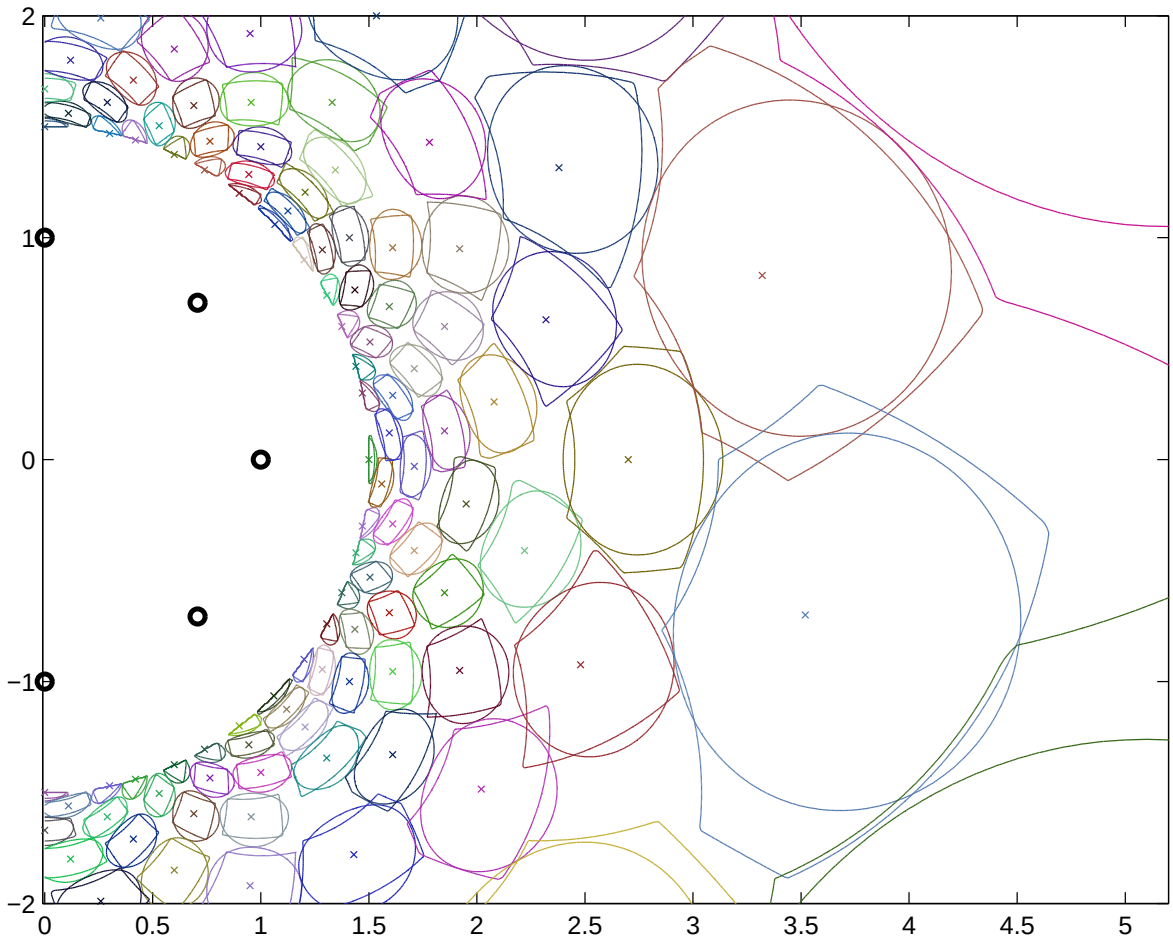

Figure 7.6: Comparison of the discernable location regions for two different detection norms. The threshold was selected so the regions are approximately the same size. The maximum sensor difference norm regions show abrupt corners and grow faster with increasing radius than the RMS norm.

The uniform circular array has desirable properties of symmetry and maximal minimum inter-element spacings. It is reasonable to expect that the tiling for the uniform circular array would provide an upper bound for the number of points in a tiling of an arbitrary array geometry confined to the same radius.

The previous examples used a measure of unique location detection, (7.3), being the root mean squared (RMS) of the difference in the intensity at the sensors. If the sensor measurements were in some way quantised, the indistinguishable region would be that for which the largest change in any sensor value was less than some threshold. This gives the norm

$$\|\boldsymbol{y} - \boldsymbol{y}'\|_{R'} = \max_q |y_q - y'_q| < \varepsilon'. \tag{7.8}$$

Figure 7.6 compares the region shapes of this norm to the previous norm (7.3). The general characteristics of the regions are similar, after appropriate scaling. For the example pre-

sented, a value of $\varepsilon' = 2\varepsilon$ create regions of a similar size. The new norm creates regions smaller than the RMS norm close to the sensor array where the proximity to one sensor will dominate. Further away, the new regions are larger since the contribution from multiple sensors is not considered in the norm. The region shapes for the single sensor show abrupt corners where there is a change in the sensor dominating the norm.

Although the problem has been formulated with discrete sensors, the examples show that beyond some limit the number of sensors is not significant to the ability to resolve the source location. A field across the measurement region is described by (7.1). This constrains the variation of the field across space in a similar way to the wave equation constraint previously studied in this thesis. The following sections will investigate this further by adopting a continuous spatial model of the signal space to address the questions posed in Section 7.2.

7.4 Intrinsic Limits of Resolving Spatial Location

The previous numerical examples demonstrated that distinguishable region size increased with the source distance. As the source is moved away, the intensity measured by each sensor, (7.1), will approach unity. This suggests a "horizon" beyond which it is not possible to resolve the location of a source with any certainty under (7.3).

7.4.1 Localisation Horizon

Consider the general case of Q sensors within a region of radius R, and the measurement condition (7.3). A sufficient condition for all sources located at a distance H or greater to be indistinguishable at level ε will be

$$\|1 - \boldsymbol{y}\|_R^2 = \frac{1}{Q}\sum_{q=1}^{Q}(1-y_q)^2 \leq \left(1 - \frac{H}{H-R}\right)^2 = \left(\frac{R}{H-R}\right)^2 \leq \varepsilon^2$$
$$H \geq R\left(1 + \frac{1}{\varepsilon}\right) \tag{7.9}$$

where the measurement vector $\boldsymbol{y}$ has elements $\boldsymbol{y} = f(\boldsymbol{x}) = [\, y_1 \ \ldots \ y_Q \,]^T$.

The previous examples where $R = 1$ and $\varepsilon = 0.1$ will have a horizon with radius less than 11. This is a strict upper bound for the horizon based on a worst case geometry. If the sensors

are spread evenly with radius R then

$$\begin{aligned}\|1-\boldsymbol{y}\|_R &\approx \frac{1}{2\pi}\int_0^{2\pi}\left(1-\frac{H}{H-R\cos\theta}\right)^2 d\theta = \frac{1}{2\pi}\int_0^{2\pi}\left(\frac{R\cos\theta}{H-R\cos\theta}\right)^2 d\theta \\ &\leq \frac{1}{2\pi}\int_0^{2\pi}\left(\frac{R\cos\theta}{H-R}\right)^2 d\theta = \frac{1}{2}\left(\frac{R}{H-R}\right)^2 \leq \varepsilon^2 \end{aligned} \tag{7.10}$$

which can be simplified to yield the result

$$H \geq R\left(1+\frac{1}{\sqrt{2}\varepsilon}\right). \tag{7.11}$$

This provides a superior approximation to (7.9) when the sensors are evenly spaced on the edge of the region. Figure 7.7 demonstrates the bound and approximation for a uniform and skewed distribution of sensors. For the uniform array, the actual horizon is approximately 7 units whilst the approximation is 8 and the bound is 11 units. For the skewed distribution the actual horizon is seen to approach the bound in some directions.

7.4.2 Number of Distinct Localities

The numerical examples from Section 7.3 demonstrated that a finite number of points tiled the space $\mathcal{S}$ external to the sensor array. Since the regions are of finite size and need only fill the space from radius, S, to the horizon, $H < \infty$, it should be possible to bound the number of distinct localities. This provides useful information, for example the amount of storage or bits required to specify the source location as determined by the receiver.

A first approximation for this bound can be obtained from the space of measured signals. From (7.1) the sensor values are bounded, with the extremum occurring for a source with radius S,

$$\frac{S}{S+R} \leq y_q \leq \frac{S}{S-R} \quad \forall \quad y_q \quad q=1,\ldots,Q. \tag{7.12}$$

Thus we can consider the Q-dimensional vector $\boldsymbol{y} = f(\boldsymbol{x}) = [\, y_1 \ \ldots \ y_Q \,]^T$ as lying in the Q-dimensional hypercube,

$$\boldsymbol{y} \in \left[\frac{S}{S+R}, \frac{S}{S-R}\right]^Q. \tag{7.13}$$

A grid of hypercubes covering this space with stride $a = 2\varepsilon/\sqrt{Q}$ will ensure every measurement lies within ε of a cube centre. The number of regions, N, is bounded by the number of

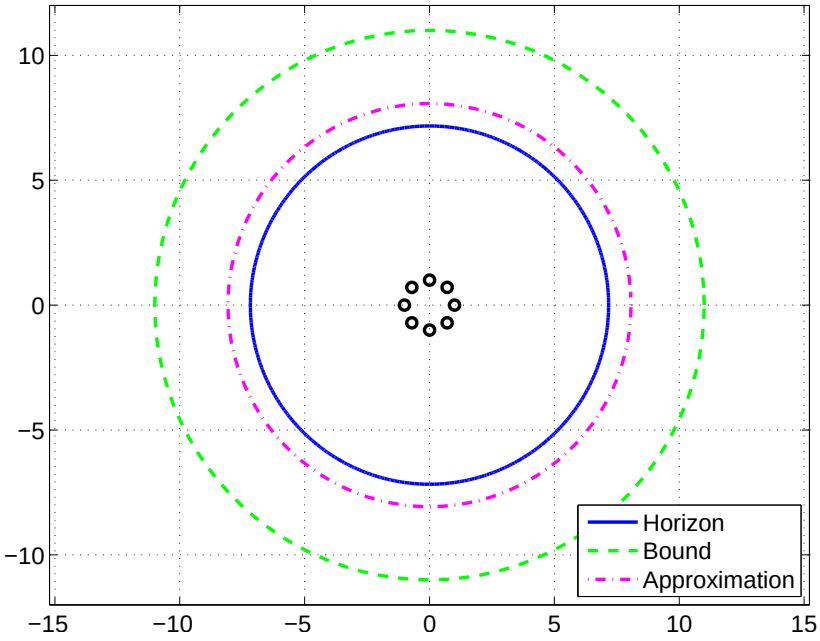

(a) Horizon, bounds and approximation for UCA.

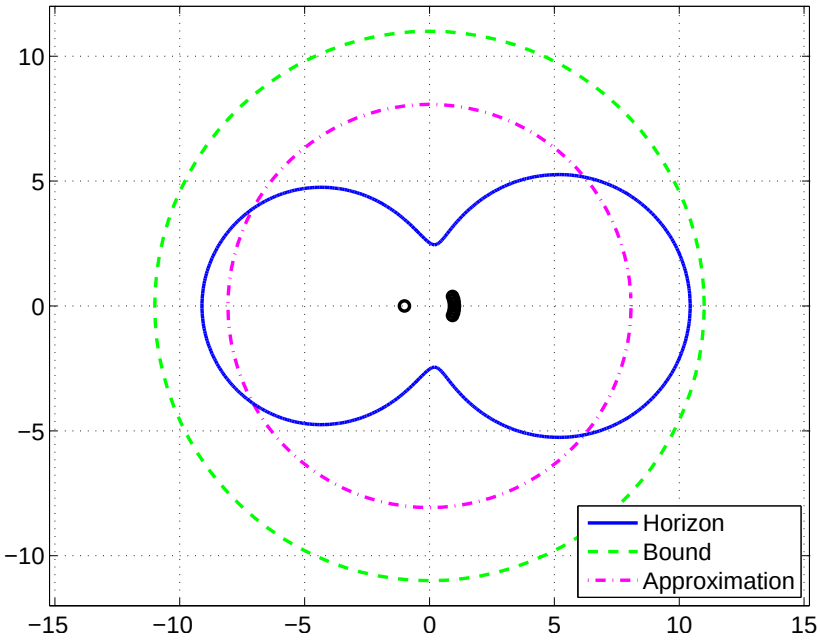

(b) Horizon for skewed array.

Figure 7.7: Comparison of the actual horizon with the bound and approximation for array with $R = 1$, $Q = 8$ and $\varepsilon = 0.1$. The bound (7.9) holds for all sensor geometries. The approximation (7.11) assumes a regular sensor geometry and approximates the uniform circular array (UCA) horizon.

Q-dimensional cubes to tile the space,

$$N \leq \left(\left(\frac{S}{S-R} - \frac{S}{S+R} \right) \frac{1}{a} \right)^Q = \left(\frac{SR}{S^2-R^2} \frac{\sqrt{Q}}{2\varepsilon} \right)^Q . \tag{7.14}$$

Whilst this shows a finite bound, it is extremely conservative. For the example $R = 1$, $S = 1.5$, $Q = 8$ and $\varepsilon = 0.1$, the bound is $N < 7 \times 10^9$. From the numerical investigation (Figure 7.4), we know that $N < 228$. The bound (7.14) grows with the number of sensors, however Figure 7.4 showed the regions are fairly independent of the number of sensors beyond some point. The bound is not particularly useful.

Since the bound is based on the sensor values being independent, it does not take into account the constraint of the continuous field across the region. The field cannot vary arbitrarily and must satisfy the (7.1). Only a small subset of the space in (7.13) can represent valid source locations. The problem is to find the number of points for an ε covering of this subset.

As an alternate approach, noting that the region sizes grow with increasing radius, at S the smallest region can be found from assuming a worst case of all sensors closest to the source,

$$\|\boldsymbol{y} - \boldsymbol{y}'\|^2 = \frac{1}{Q} \sum_{q=1}^{Q} (y_q - y'_q)^2 \leq \left(\frac{S}{R-S} - \frac{S+dS}{R-S-dS} \right)^2 \leq \varepsilon^2 \tag{7.15}$$

for two locations with radius S and $S + dS$. This leads to the bound

$$\|\boldsymbol{x} - \boldsymbol{x}'\| = dS \leq \frac{\varepsilon(S-R)^2}{R - \varepsilon(S-R)}. \tag{7.16}$$

For the example with $R = 1$, $S = 1.5$, and $\varepsilon = 0.1$ this corresponds to a radius of approximately 0.03 consistent with the plots in Figure 7.4. The number of regions of this size covering the region from S to H will be

$$\begin{aligned} N &= \frac{\pi(H^2 - S^2)}{\pi dS^2} = \frac{R^2(1+\frac{1}{\varepsilon})^2 - S^2}{\frac{\varepsilon^2(S-R)^4}{(R-\varepsilon(S-R))^2}} < \frac{R^2 \frac{1}{\varepsilon^2}(R - \varepsilon(S-R))^2}{\varepsilon^2(S-R)^4} \\ &< \frac{R^4}{\varepsilon^4(S-R)^4}. \end{aligned} \tag{7.17}$$

This provides a bound on the number of distinct regions that is independent of the number or orientation of the sensors. For the previous example, the bound is $N < 1.6 \times 10^5$. Whilst this is a lower bound than (7.14) it is still very conservative since the growth in the region size with radius is not taken into consideration.

7.4.3 Application of Continuous Spatial Model

Following the approach used previously for continuous spatial models, we can derive a natural set of basis functions to represent the field in the measurement region. Whilst the examples presented have considered two-dimensional space, we develop the continuous framework for the three-dimensional localisation problem. For a source at position $\boldsymbol{x}$ and the sensor located at $\boldsymbol{x}_q$, the fundamental solution of the Helmholtz equation can be expanded ([91] Theorem 2.10)

$$\frac{e^{ik\|\boldsymbol{x}-\boldsymbol{x}_q\|}}{\|\boldsymbol{x}-\boldsymbol{x}_q\|} = ik4\pi \sum_{n=0}^{\infty}\sum_{m=-n}^{n} h_n^{(1)}(k\,\|\boldsymbol{x}\|)Y_n^m(\widehat{\boldsymbol{x}})j_n(k\,\|\boldsymbol{x}_q\|)\overline{Y_n^m(\widehat{\boldsymbol{x}}_q)} \tag{7.18}$$

where $Y_n^m(\cdot)$ are the spherical harmonics defined on a unit vector argument, $j_n(\cdot)$ is the n^{th} order spherical Bessel function of the first kind, and $h_n(\cdot)$ is the n^{th} order spherical Hankel function of the first kind. The wave number $k = 2\pi/\lambda$ is related to the rate of change of the wave phase across space.

For the problem being considered, the sensors are only sensitive to the intensity of the field. This can be achieved by considering the limit of the fundamental solution as $k \to 0$. We can then consider small argument approximations for the spherical Bessel and Hankel functions,

$$j_n(z) = \frac{z^n}{1\cdot 3\cdots(2n+1)}\left(1+O(z^2)\right) \quad z\to 0 \tag{7.19}$$

$$h_n^{(1)}(z) = \frac{1\cdot 3\cdots(2n-1)}{iz^{n+1}}\left(1+O(x^2)\right) \quad z\to 0. \tag{7.20}$$

Substituting these into (7.18) and adding the normalisation (7.1) we obtain

$$y_q = \frac{\|\boldsymbol{x}\|}{\|\boldsymbol{x}-\boldsymbol{x}_q\|} = \sum_{n=0}^{\infty}\sum_{m=-n}^{n}\frac{4\pi}{(2n+1)\,\|\boldsymbol{x}\|^n}Y_n^m(\widehat{\boldsymbol{x}})\,\|\boldsymbol{x}_q\|^n\,\overline{Y_n^m(\widehat{\boldsymbol{x}}_q)}. \tag{7.21}$$

We are interested in the case where the source is some minimum distance from the receiver, $\|\boldsymbol{x}\| > S > R$. The signal observed by the receiver is constrained to $\|\boldsymbol{x}_q\| \le R$. Using this we can write

$$y_q = \sum_{n=0}^{\infty}\frac{4\pi R^n}{(2n+1)\,\|\boldsymbol{x}\|^n}\sum_{M=-n}^{n}Y_n^m(\widehat{\boldsymbol{x}})\beta_n^m(\widehat{\boldsymbol{x}}_q) \qquad \beta_n^m(\widehat{\boldsymbol{x}}_q) = \frac{\|\boldsymbol{x}_q\|^n}{R^n}\overline{Y_n^m(\widehat{\boldsymbol{x}}_q)}. \tag{7.22}$$

Since the sensor region is constrained, the basis functions β_n^m will be bounded. The coefficients decrease exponentially at a rate related to the ratio of the receiver and source radius $(R/\,\|\boldsymbol{x}\|)^n$. An expansion of the form (7.22) will be essentially finite dimensional.

From the problem definition in Section 7.2, we know the problem has only two degrees of freedom. The field generated by a source is uniquely specified by the source position, which for the two-dimensional problem studied has two degrees of freedom. The problem lies in finding a representation of the field which reflects this dimensionality and also allows us to easily determine the number of distinguishable fields.

Consider the summation identity for the spherical harmonics, ([91] Theorem 2.8)

$$\sum_{m=-n}^{n} Y_n^m(\widehat{\boldsymbol{x}})\overline{Y_n^m(\widehat{\boldsymbol{x}}_q)} = \frac{2n+1}{4\pi} P_n(\cos\theta) \tag{7.23}$$

where P_n is the Legendre function and θ is the angle between the directions of $\boldsymbol{x}$ and $\boldsymbol{x}_q$. Using this in equation (7.21) we obtain,

$$y_q = \frac{\|\boldsymbol{x}\|}{\|\boldsymbol{x}-\boldsymbol{x}_q\|} = \sum_{n=0}^{\infty} P_n(\cos\theta)\frac{\|\boldsymbol{x}_q\|^n}{\|\boldsymbol{x}\|^n}. \tag{7.24}$$

Since $|P_n(\cos\theta)| \leq 1$ [279], the terms contributing to y_q will decrease exponentially at least as fast as $(R/S)^n$. This expansion is not a basis function expansion since the argument of $P_n(\cos\theta)$ is dependent on both the source and receiver position.

7.4.4 Reflection in the Circle

Consider another approach to the problem where the sensor values are normalised

$$\|y\|_R = \frac{1}{Q}\sum_{q=1}^{Q} y_q^2 = 1 \tag{7.25}$$

and the distance between two measurements is calculated as the root mean squared sensor value 7.3). This normalisation is equivalent to having a unit average signal intensity across the array independent of the source distance.

If the sensor is confined to the circle $\|\boldsymbol{x}_q\| = R$, then for each position outside of the sensor array, there is an equivalent position inside. This can be observed by considering the geometry of the problem as shown in Figure 7.8. It is evident that these two points will lie on the same line extending from the origin of the circular array. From the radial source function (7.1) and normalisation (7.25) it can be seen that the measurements for points $\boldsymbol{x}$ and $\boldsymbol{x}'$ will be equivalent when

$$\|\boldsymbol{y}-\boldsymbol{y}'\|_R = \left\| \frac{f(\boldsymbol{x})}{\|f(\boldsymbol{x})\|_R} - \frac{f(\boldsymbol{x}')}{\|f(\boldsymbol{x}')\|_R} \right\|_R = 0. \tag{7.26}$$

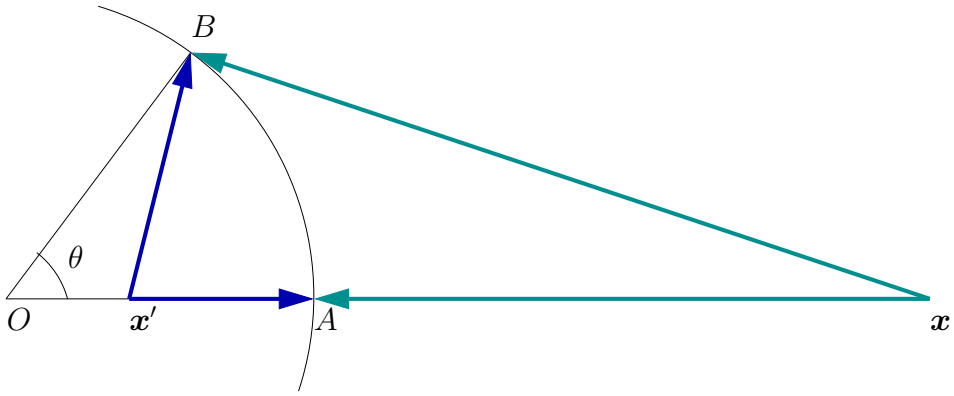

Figure 7.8: Geometry for the reflection of the location regions inside the uniform circular array.

Since each measurement y_q scales with the reciprocal of the distance between the source and sensor, this implies that the distances between the locations $\boldsymbol{x}$ and $\boldsymbol{x}'$ and any two points on the circle must be in the same ratio. We select two points, one being the intersection of the line extending from the origin through $\boldsymbol{x}$ and $\boldsymbol{x}'$, and the other at an arbitrary angle θ. Using the law of cosines for the associated triangles,

$$\begin{aligned} \frac{\|A-\boldsymbol{x}'\|}{\|B-\boldsymbol{x}'\|} &= \frac{\|A-\boldsymbol{x}\|}{\|B-\boldsymbol{x}\|} \\ \frac{R-x'}{\sqrt{R^2+x'^2-2Rx'\cos\theta}} &= \frac{x-R}{\sqrt{R^2+x^2-2Rx\cos\theta}}. \end{aligned} \tag{7.27}$$

This gives the quadratic equation to solve for the radius x' of the point $\boldsymbol{x}'$ as

$$x'^2 x\cos\theta + x'\left(x^2\cos\theta - R^2\cos\theta + R^2\right) - R^2 x\cos\theta - xR^2 = 0 \tag{7.28}$$

for which it can be shown that $x' = R^2/x$.

Thus each point in the region $\mathcal{S}$ is mapped into the finite region bounded by the circular array with radius R. This is convenient since the unbounded region $\mathcal{S}$ maps to a simple bounded region.

Figure 7.9 shows the regions of distinct localisation for the case of a uniform circular array with $R = 1$, $Q = 8$, $S = 1.5$ and $\varepsilon = 0.05$. For each distinct region in the space $\mathcal{S}$ there is a corresponding region within the array. Furthermore, the corresponding regions within the circular array are all approximately the same size. This provides a bounded region with two degrees of freedom across which the distance between regions of indistinguishability is relatively constant.

To determine the smallest region size, consider a region inside the circle at the reflection of

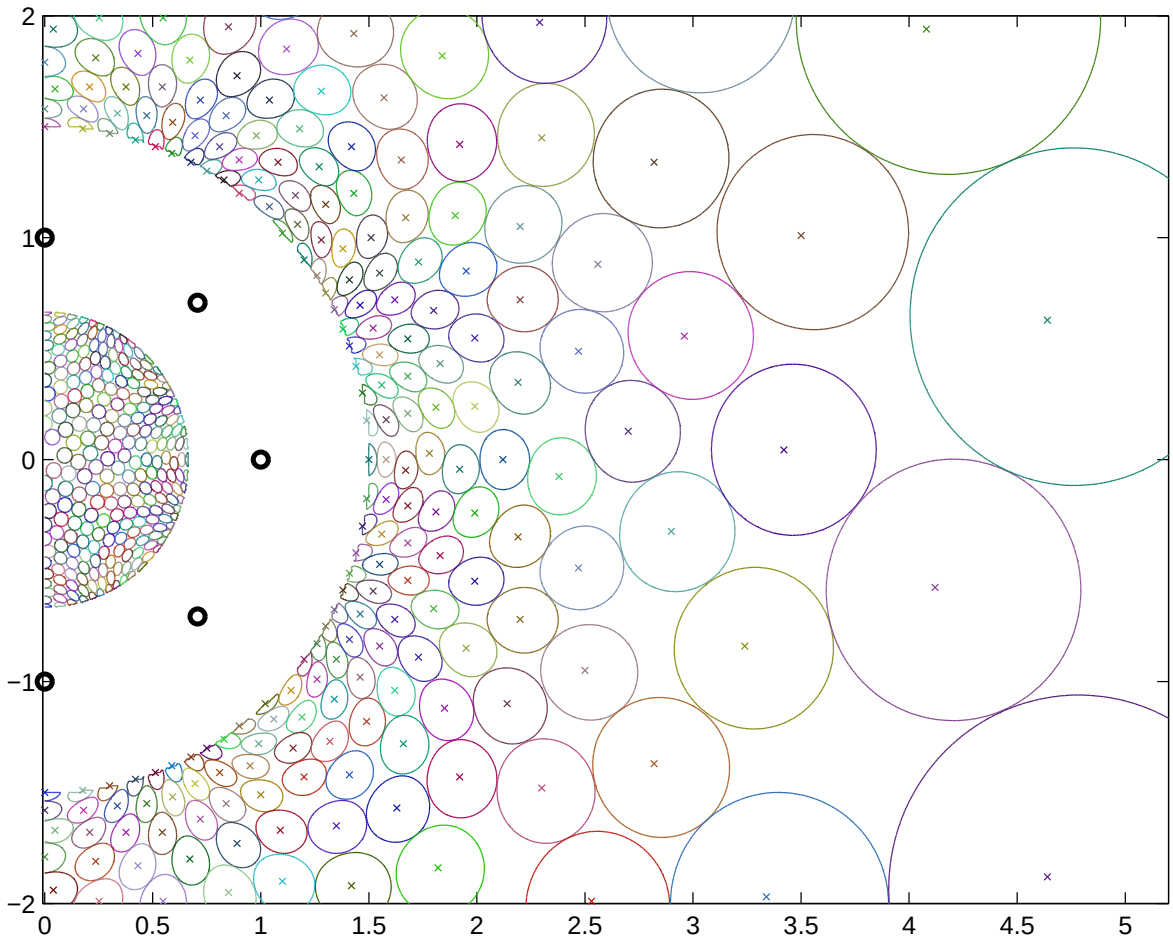

Figure 7.9: Reflection of the space of distinct localities for the uniform circular array. For each point outside the array, there is a corresponding point, resulting in the same measurement vector, located inside the array.

radius S. For two points at radius x and x', the detected signal difference will be

$$\|\boldsymbol{y} - \boldsymbol{y}'\|_R^2 \approx \frac{\sum_{q=1}^{Q} \left(\frac{1}{\sqrt{x^2+R^2-2Rx\cos\theta_q}} - \frac{1}{\sqrt{x'^2+R^2-2Rx'\cos\theta_q}} \right)^2}{\sum_{q=1}^{Q} \frac{1}{x^2+R^2-2Rx\cos\theta_q}} \tag{7.29}$$

where the approximation arises from the normalisation (7.25) being applied equally to both observations. This is valid for small perturbations $x \approx x'$. By numerical inspection, for the case of $R = 1$, $S = 1.5$ and $\varepsilon = 0.05$, the minimum region size is approximately 0.015. This is consistent with Figure 7.9.

The reflected regions inside the circle will fill the region from the origin to a radius of $1/S$. This is a finite area for which we can place a bound on the number of reflected regions with the smallest region size. This is independent of the number of sensors. For the example given this bound is $N < 2000$.

The simulations for the uniform circular array with signal intensity normalisation in Figure 7.9 consisted of 453 points in the tiling. This bound obtained by considering the reflected regions is within an order of magnitude of this result.

Whilst this approach leads to the best matching bound, it is specific to the case of a uniform circular array with the intensity normalisation. As can be seen from the figures, the size and number of distinct regions is comparable, thus this bound gives some indication of the number of localities for the original problem.

7.5 Localisation with Phase Coherent Receiver

The problem considered initially was the ability to localise a source given a receiver was only able to detect the field amplitude or intensity. This corresponds to the practical situation of processing a set of received signals without coherent phase detection across the array region. It was anticipated that this would be a simpler problem than considering the complete field information. However, the work to determine an appropriate continuous basis function expansion for the field observed in the sensor region was not successful.

Consider a configuration where the receiver has access to the field amplitude and phase across the sensor region. The phase information will improve the ability to resolve the direction of arrival and distance through the direction and curvature of the wavefront passing through the sensor region.

Assuming the amplitude and phase of the source is normalised at the origin, the signal model will be

$$y_q = \frac{\|\boldsymbol{x}\|\, e^{j2\pi\|\boldsymbol{x}-\boldsymbol{x}_q\|}}{\|\boldsymbol{x}-\boldsymbol{x}_q\|\, e^{j2\pi\|\boldsymbol{x}\|}}. \tag{7.30}$$

Figure 7.10 shows the distinguishable region tiling for the case of a circular array with $R = 1$, $Q = 8$, $S = 1.5$ and $\varepsilon = 0.2$. This can be compared to Figure 7.3 which considered the same configuration without phase information. In Figure 7.10 the space is more segmented in angle and the radial extent is comparable even though the detection threshold has been doubled.

For a distant source, the normalised field amplitude across the sensor region will be unity. For a continuous uniform circular array, the signal difference introduced by two distinct

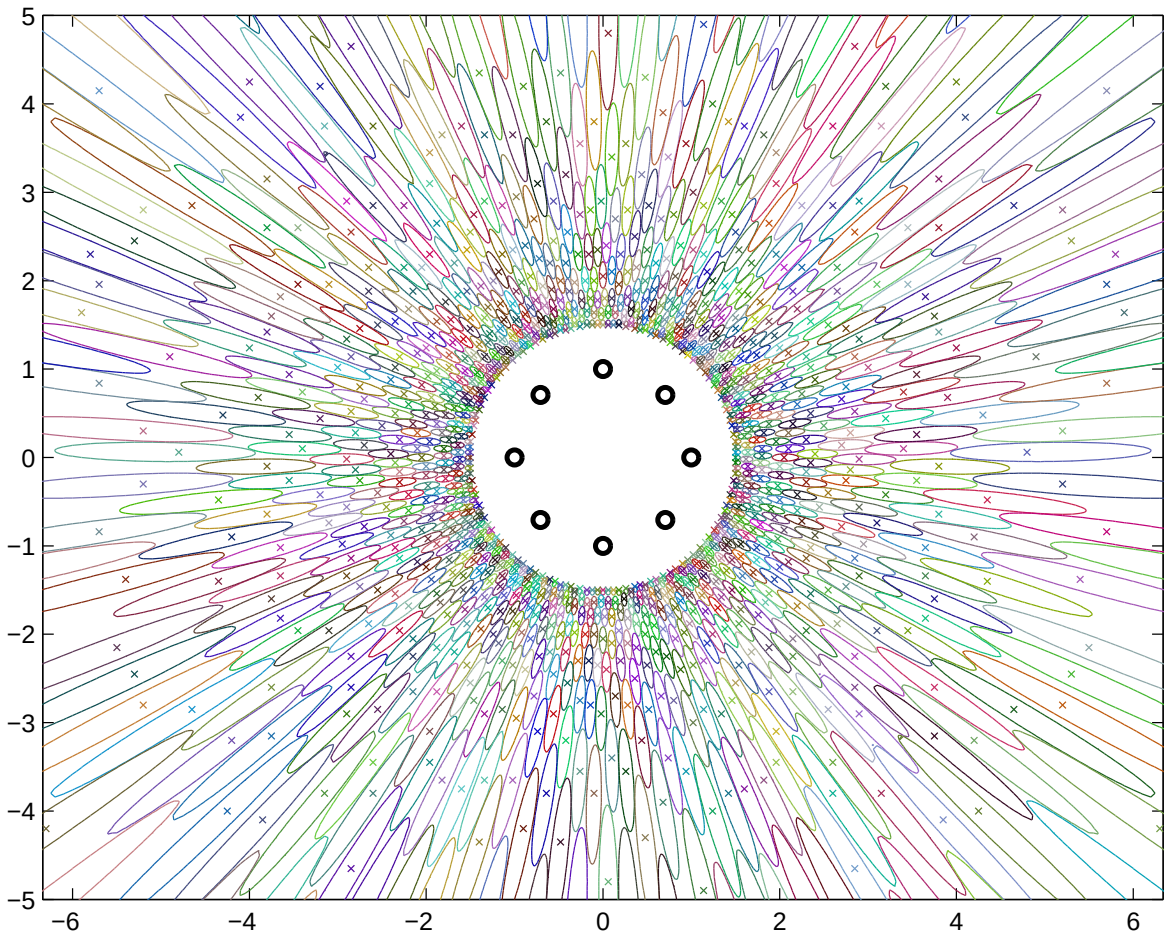

Figure 7.10: Distinguishable location regions using amplitude and phase information for a UCA $R = 1$, $Q = 8$, $S = 1.5$ and $\varepsilon = 0.2$. Compared to Figure 7.3 the ability to resolve angle and distance is significantly improved.

directions of arrival separated by an angle ϕ will be

$$\frac{1}{2\pi}\int_0^{2\pi} \left| e^{jkR\cos\theta} - e^{jkR\cos(\theta-\phi)} \right|^2 d\theta < \varepsilon^2. \tag{7.31}$$

For the value of $\varepsilon = 0.2$ in Figure 7.10, the value of ϕ that achieves the bound (7.31) is approximately $2.5°$. This corresponds to 144 distinct angular regions. This is consistent with the results presented from the numerical tiling in the figure.

The natural basis expansion for the three-dimensional narrow-band field was presented previously (7.18). With the sources at a distance $S > R$ this expansion can be truncated to a finite dimensional representation with $(N+1)^2$ terms where $N \approx kR$. This result has been presented in other works [80] and is a generalisation of the two-dimensional case discussed

in Chapter 2[1]. The sensor signals can be written

$$y_q = \frac{\|\boldsymbol{x}\|}{\|\boldsymbol{x} - \boldsymbol{x}_q\|} = \sum_{n=0}^{\infty} \sum_{m=-n}^{n} \alpha_n^m \beta_n^m(\boldsymbol{x}_q) \qquad \beta_n^m = j_n(k\,\|\boldsymbol{x}_q\|)\overline{Y_n^m(\widehat{\boldsymbol{x}}_q)}. \tag{7.32}$$

For this example there will be $(N+1)^2 = 49$ degrees of freedom. However, the valid coefficients for a normalised point source will be constrained to

$$\alpha_n^m = \frac{ik4\pi h_n^{(1)}(k\,\|\boldsymbol{x}\|)Y_n^m(\widehat{\boldsymbol{x}})}{h_0^{(1)}(k\,\|\boldsymbol{x}\|)}. \tag{7.33}$$

By definition this is a two-dimensional manifold. The unique determination of locations will be related to a weighted distance between the vectors of α_n^m coefficients. Thus the problem of determining the number of unique localisation regions would be related to determining the area of this manifold in an appropriately scaled space.

In general, the ability to resolve the distance of a source given measurements over a finite region is rather limited. As could be seen in Figure 7.10, the angular resolution provides a more numerous division of the space than the range resolution.

[1]The problem formulation was for a two-dimensional observation region with the sources lying in the same plane. However, the fundamental solution for three dimensions was used, (7.1), with the field intensity varying with the reciprocal of the radius. The wave equation in two dimensions permits a fundamental solution where the field intensity varies with the square root of the source radius. Whilst this is not a problem when considering general multipath fields and far-field source distributions as in the previous chapters, it is significant in the determination of the distinct localisation regions in the vicinity of the sensor array.

7.6 Discussion and Further Ideas

The distance from source to sensor can be approximated by

$$\begin{aligned}\|\boldsymbol{x}-\boldsymbol{x}_q\| &= \sqrt{\|\boldsymbol{x}\|^2+\|\boldsymbol{x}_q\|-2\|\boldsymbol{x}\|\|\boldsymbol{x}_q\|\cos\theta} \\ &\approx \|\boldsymbol{x}\|-\|\boldsymbol{x}_q\|\cos\theta+\frac{\|\boldsymbol{x}_q\|^2}{2\|\boldsymbol{x}\|}\sin^2\theta \end{aligned} \tag{7.34}$$

where $\theta=\theta_{\boldsymbol{x}}-\theta_{\boldsymbol{x}_q}$ is the angle between the source and sensor directions. For a uniform linear array, this equation is quadratic in the sensor element number and is sometimes referred to as the Fresnel approximation. For sources in the Fresnel region where (7.34) is a reasonable assumption, this can be used to simplify the signal model. A further simplification can be made to neglect the signal intensity. If the received signal is normalised, the signal model becomes

$$y_q = e^{\|\boldsymbol{x}_q\|\cos\theta+\|\boldsymbol{x}_q\|^2\sin^2\theta/2\|\boldsymbol{x}\|}. \tag{7.35}$$

This approach has been used to create an algorithm for passive localisation of near field sources [280].

It is a common assumption that sources beyond a certain distance appear as far-field sources with a planar wave front across the sensor array [281, 282]. This is a similar concept to the localisation horizon introduced in Section 7.4.1. For a uniform linear array of length $2R$ and a maximum phase variance of $\pi/8$ radians over the array, the far-field distance is $8R^2/\lambda$. This distance will increase with increasing frequency of the narrow-band signal. This contrasts the intensity only horizon (7.9) which was frequency independent. This implies that as the wavelength decreases, the signal phase dominates the size and shape of the localisation regions. This is consistent with the assumption of $k\to 0$ for the field intensity expansion (7.21). For the example presented in Figure 7.10 the effective far-field distance would be around 8 which is consistent with the numerical analysis.

The size of a sensor array for which the phase information will dominate localisation can be determined by considering (7.9)

$$\frac{8R^2}{\lambda} > R\left(1+\frac{1}{\varepsilon}\right) \quad\Rightarrow\quad R > \frac{\lambda}{8}\left(1+\frac{1}{\varepsilon}\right). \tag{7.36}$$

For the case considered in the examples, this corresponds to a radius of around 1.4λ. Thus in the example there is still some contribution from the intensity information. Figure 7.11 compares the distinguishable regions for the case of phase only and phase and intensity

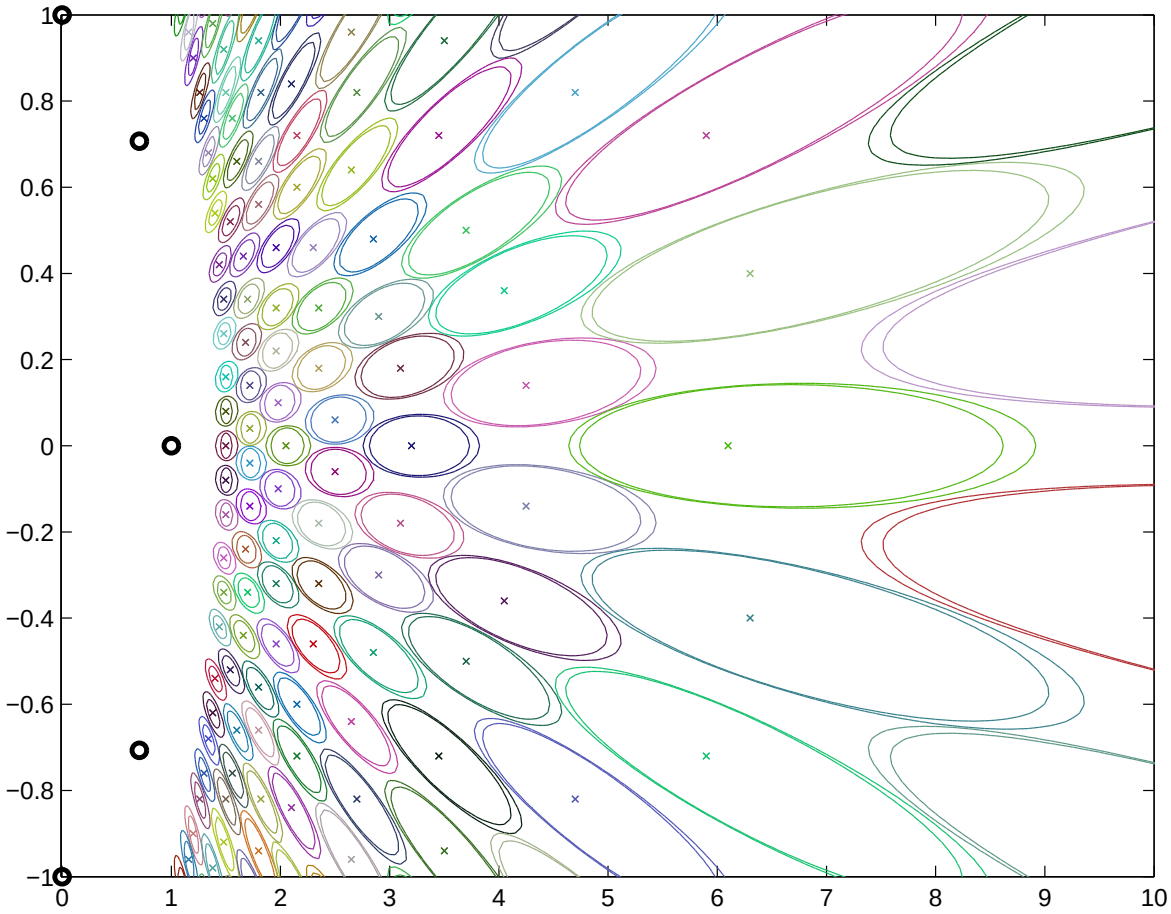

Figure 7.11: Comparison of localisation with phase only and complete field information. Analysis for a UCA $R = 1$, $Q = 8$, $S = 1.5$ and $\varepsilon = 0.2$. The regions with intensity information are slightly smaller. The regions beyond a radius of 8 are open ended.

measurements. The regions with both phase and intensity are slightly smaller. It can also be seen that the regions at a radius beyond 8 are extended to cover all radii beyond this.

The Cramér-Rao bound for passive range estimation is [283]

$$\frac{\sigma}{\|\boldsymbol{x}\|} \geq \left(\frac{\sqrt{10}}{2\pi}\right)\left(\frac{\lambda}{4R^2}\right) SNR^{-1/2} \tag{7.37}$$

which suggests that the regions of uncertainty will grow linearly with the radius of the source. This is consistent with the partitioning of the reciprocal space introduced in Section 7.4.4.

The problem of distinct localisation regions is particular to the way in which a receiver will view the electromagnetic environment in which it resides. Given a finite measurement resolution, it is apparent that there will be a fixed and finite number of distinct locations to which a source could be associated. Beyond some distance, it becomes impossible to determine the source range accurately.

7.7 Summary and Contributions

This work has detailed an attempt to analyse the number of distinct regions for a source that can be identified by a sensor array constrained to a finite volume. In essence, this problem is one of mapping the world, as viewed by the sensor array, to a set of discrete observable regions. The problem was addressed in the context of analysing only the intensity information obtained from the field, with the incident field considered to have unit power at the sensor origin.

The following specific contributions were made in this chapter:

- Demonstrated, through numerical analysis, that there will be a finite number of distinct location regions extending from outside the sensor array to an arbitrarily large distance.
- Presented an analysis of the sensor signal space and constructed a formal proof of the existence of a horizon radius beyond which all source locations will appear indistinguishable. This horizon is dependent on the radius of the sensor array and the detection threshold.
- Developed an analytic bound for the number of distinct locations that can be resolved. Since the field will be correlated over the sensor array, using an argument related to the number of distinct measurements without reference to the signal model produces a conservative bound for the number of distinct regions.
- Derived a tighter bound for the specific case of a uniform circular array based on a geometrical reflection argument and the regular tiling of a finite space. This bound is within an order of magnitude of the results obtained from the numerical investigations.
- Demonstrated that the addition of phase information provides a significant advantage in the ability to resolve both the direction of arrival and distance of a source.

Generally angular resolution is superior to range resolution. If intensity information is only available, beyond some radius, all sources will appear to be located in the same region of uncertainty. Where intensity and phase information is available, at a similar distance, range measurement becomes uncertain whilst the direction of arrival resolution remains effective.

The solutions and investigation of the problems posed was facilitated by considering a continuous model of the spatial field rather than by considering the signal vectors from a specific sensor array configuration.

Chapter 8

Conclusions and Further Research

8.1 Overview of Contributions

The contribution of this thesis is to provide the development and application of continuous spatial models to specific signal processing problems for multiple antenna systems. Conventional MIMO signal processing would model the system as a network with a discrete set of inputs and outputs. However, in practice, the antenna must reside in a physical space. The antennas interact with and detect a continuous electromagnetic field across the volume of the arrays. A level of correlation is to be expected due to the inherent nature of electromagnetic wave propagation.

A continuous model for the spatial field provides a way to incorporate the constraints of the wave equation into the signal processing framework of a communication system. This leads to improvements in the understanding and performance of the signal processing required. For example, the degrees of freedom of a spatial field does not grow with the volume of antenna region, but rather with the surface area of the boundary. In two dimensions this is a linear growth with the region radius, while in three dimensions the growth is quadratic. This is one order lower than the potential growth of the volume, and thus the number of antennas that could be placed in the region. Chapter 2 provided a greater understanding of the effective dimensionality of a spatial field, which is related to the point of diminishing returns for system performance as the number of antennas is increased. Chapter 3 presented some specific results related to the representation and dimensionality of a multipath field with restricted angles of arrival.

Given the continuous spatial model and its effective dimensionality, it is useful to understand the optimal basis for representing fields across that region. In Chapter 4, an angular domain

representation was introduced as an efficient way of characterising a random multipath field. Analysis of this representation provided a means to determine the optimal representation. Although this is informative, the basis functions obtained are nontrivial, transcendental, and useful only for the specific problem configuration. In practice, it is likely that the use of the general basis for a circular or spherical region would serve as an adequate approximation of the optimal basis.

The idea of a continuous spatial model is also useful in determining fundamental limits to system performance. A receiver will usually operate within some spatial constraint. Given this, there is a limit to the ability of a receiver to resolve the direction of arrival of a source. This problem was studied in Chapter 5. Additionally, a receiver can determine the direction and distance of a source. This problem was studied in Chapter 7. Considering the continuous spatial field, rather than discrete sensor measurements, this leads to some performance bounds for such position estimations.

Continuous spatial models incorporating the wave equation constraint provide a parsimonious representation of the wireless communications channel. Chapter 6 provided an application of the modal framework to the MIMO wireless channel. This was used to simulate measured channel data and the performance of the new model compared favourably with existing models whilst using a lower order parameterisation.

The research work contained in the thesis is a contribution towards developing ways to incorporate the physical constraints of space and wave propagation into models for multiple antenna systems. Some of the areas investigated in the course of this thesis were not bountiful. It is apparent that a simple approach to considering the discrete port system with arbitrary statistics can be quite robust, and the complexity added by considering the continuous spatial models is not justified in practice. The assumption of simple antenna sampling and radiation is also challenged by the complexities of practical antenna. However, the study of the continuous spatial field is useful for determining some overall limits and bounds on performance.

As systems use higher numbers and smaller antennas, the ideas of continuous sampling and interaction with the spatial field becomes more important. This thesis is a contribution towards the treatment of space as a structured medium that does not offer unlimited diversity as more signal paths are introduced. Compact MIMO systems must consider the spatial constraints imposed on the receiver and transmitter to determine and achieve optimal performance levels.

8.2 Open Problems and Further Research

In this section some ideas for further work and developments are presented. These are the open problems and conjectures that have been identified during the course of developing this thesis.

8.2.1 Relaxation of Narrow-band Assumption

In the representation of the multipath field, this work adopted the narrow-band source assumption, and therefore the results relate to a narrow-band field. The time evolution of the field $u(\boldsymbol{x})$ will be $u(\boldsymbol{x})e^{j\omega t}$ for the narrow-band frequency $\omega = 2\pi f$. This narrow-band assumption conveniently removes both time and frequency from our analysis allowing the investigation of the spatial aspect of the signal dimensionality.

To consider the dimensionality of a signals over space, time and frequency, we can assume independence of the results and scale the results of this work by $2WT$, as was suggested by [84]. However, the correct approach is to consider the complete wave equation

$$\triangle u(\boldsymbol{x}, t) - \frac{1}{c^2}\frac{\partial^2}{\partial t^2}u(\boldsymbol{x}, t) = 0 \tag{8.1}$$

which links time, space and implicitly frequency. A formal development of the dimensionality of a signal observed over a finite duration across a bounded domain and concentrated in some finite bandwidth remains an open problem.

It is conjectured that for the case of $2WT \gg 1$ and $2kR \gg 1$ the product of the spatial and bandlimited dimensionality is appropriate and asymptotically tight as $4kRWT \to \infty$. Further study of this problem would have application to achieving maximum spectral efficiency in a spatial wireless communications system.

8.2.2 Impact of Using Suboptimal Spatial Basis Functions

Starting with the problem definition of detecting or exciting a multipath field, we typically know the antenna geometry or shape of the region over which we can interact with the field. In some cases there will be additional a priori information regarding the scattering environment and thus the expected angular power spectra. The framework developed in Chapter 4 set out the procedure to determine the optimal basis functions to allow truncation of the infinite dimensional multipath field to a finite dimensional representation. However, in

a practical signal processing context, we may choose to adopt and utilise the standard basis set for a circular or spherical region and uniform power spectra.

A subject that would warrant further investigation is the impact of adopting the standard basis set over the optimal representation. Given the complexity and transcendental nature of the functions for an arbitrary region, it is worth considering the cost of adopting the simpler expression consisting of the Bessel functions and harmonic exponentials. If the internal signal processing is based on the generic basis functions, to achieve the same error in truncation, a larger number of terms will be required. This will cause an increase in storage, computational load and processing error[1]. However, the ability to utilise efficient algorithms based on the structure of the generic basis set may offset this cost. For example, it is possible to use a similar approach to the fast Fourier transforms for matching and convolution on the sphere [199].

To put this idea in context we return to the example of bandlimited functions presented in Section 2.2 and the Slepian series introduced in Section 3.5. For any bandlimited non periodic function, the optimal basis functions are related to the prolate spheroidal wave functions. This has been developed for both the continuous [142, 159] and discrete case [167]. However, in practice these are rarely used. The general approach is to consider a segment of the signal, window it to avoid edge artifacts and use the harmonic exponentials of the standard Fourier transform. Whilst this approach is not optimal, in most engineering applications it is sufficient and facilitated by a larger set of resources and wider familiarity amongst practitioners. The cost in most cases is a small drop in performance, easily compensated for by a slight increase in sampling rate or signal to noise ratio. In some applications this is not the case and system performance can be fundamentally limited by this oversight [169].

The Fourier basis becomes asymptotically efficient as the dimensionality of the signal space increases. Thus it is conjectured that the use of a priori information to shape the basis functions becomes more important in the case of a low dimensionality. In small mobile devices, at 2.5 Ghz the dimensionality of the covered field is of the order of 4 to 16. It follows that understanding and use of the optimal basis functions will be advantageous in such systems.

Part of this thesis has considered the existence, construction, characterisation and use of the optimal basis set for the spatial multipath field. An open problem is to determine the trade off between the benefits gained from using a priori information and the optimal basis against the added system complexity.

[1] For example, in any digital implementation, a fixed word length for representing values will lead to rounding errors. A larger number of parameters and dimensions will increase the required number of computations for any given result and thus increase the processing noise level.

8.2.3 Parametric Spatial Basis Functions and Approximations

Following on from the previous section, a valuable goal for additional research would be to determine some parametric families of functions that can be used to approximate the optimal basis set. In Chapter 3 an approximation for the basis functions for a uniform angular distribution over a restricted sector was developed. Similar results should be possible for other configurations of practical importance. In this way, if the use of the optimal basis function is advantageous, a constructive approximation can be employed rather than resorting to a numerical solution of the associated eigenequation.

It is also possible that there exists some simple closed form analytic solutions for the angular domain representation of the multipath field for specific angular spectra, $P(\widehat{\boldsymbol{\theta}})$, or region shapes, Λ. In developing this thesis, some time was spent in this endeavour, unfortunately with no compelling results. As a motivation, it should be noted that the trigonometric functions $\sin(\cdot)$ and $\cos(\cdot)$ also naturally arise from the solution of a similar eigenequation. Furthermore, the Bessel functions have an impressive pedigree and extensive development [163].

With the prevalence of powerful computers, it is easy to move from analytic investigations in favour of numerical studies. However, for the intrepid mathematical explorer, there is a rich history in Fredholm equations and Laplace equations and an enormous set of results which could be applied to this problem.

8.2.4 Bessel Function Bound and Dimensionality

The work of Section 2.5 conjectured the bound for the Bessel function

$$J_n(z) < \frac{1}{2} n^{-1/3} \left(\frac{z}{n}\right)^{n^{2/3}} \qquad n \geq 1. \tag{8.2}$$

Bessel functions have applications in a wide range of applied mathematics, and thus such bounds are an area of current and ongoing interest [284]. As such it would be valuable to further investigate and seek a proof of this or another tighter bound.

There is still room for an improved bound on the dimensionality result which would be suitable for small regions and still asymptotically tight as $R \to \infty$. The difficulties in developing such a bound were discussed in Section 2.5.3. This is an area for further development.

8.2.5 Impact of Antenna Geometry

Much of the work of this thesis has developed the concept of continuous spatial models and their application to wireless communications systems. By considering the dimensionality and representation of the underlying field it is possible to derive fundamental limits and bounds on the diversity of a multipath field over a bounded region. The placement of antenna and their interaction with the multipath field represents a process of spatial sampling. It is not possible for arbitrary performance gains[2] through this process [121]. However, there is the possibility of a significant loss of dimensionality through poor placement, coupling and interaction of the antenna.

There has been some reference to this issue in the existing literature with regard to antenna coupling [104, 115] and electromagnetic propagation issues within the array [39]. An interesting open problem is the impact of the specific antenna placement and loss of information through the implicit spatial sampling.

Ultimately we are interested in the underlying spatial field, and hence the problem is related to the approximation and estimation of the continuous function given a set of discrete samples [285]. The optimisation of multi-dimensional sampling points to achieve efficient function approximation, interpolation and integration is an area that has achieved much attention for the sphere [196] and also for more general regions [286]. Even in the case of a truly finite dimensional multipath field, given N basis functions on the sphere, it is not generally possible to create a set of N sampling points that will uniformly capture the information that exists in such a continuous field. In the case of the sphere, the quality of the field approximation is critically dependent on the choice of sampling points [287]. It is a significant result in this field that when moving from two dimensions to three dimensions, efficient sampling[3] on the sphere is no longer possible for more than 16 sensors [288].

The problem of finding a regular or optimal point set on the sphere for sampling and interpolation is surprisingly rich in theory. Whilst it is trivial to find a regular set of points spanning the circle, $\mathbb{S}^1 = [0, 2\pi]$, for the sphere S^2 and beyond $S^n, n > 2$ this is a problem presently only soluble through computational methods [196, 289]. The results that emerge from such work are rather remarkable with subtle structure and intricate patterns. This is surprising

[2] It should be noted that the general consistency between the spatial and antenna noise models is still an open problem. As such, the effective gain and noise floor of the antennas in an array will have an impact on the system performance. However, this is related to a shift in the sensitivity or relevant truncation error and not the underlying essential dimensionality.

[3] The definition of efficient sampling is related to extremal point sets and will not be introduced at this point. Briefly, if all sensors were to contribute an independent white noise, efficient sampling would permit all of the basis functions to be estimated with equal noise variance using the same number of sensors as there are basis functions.

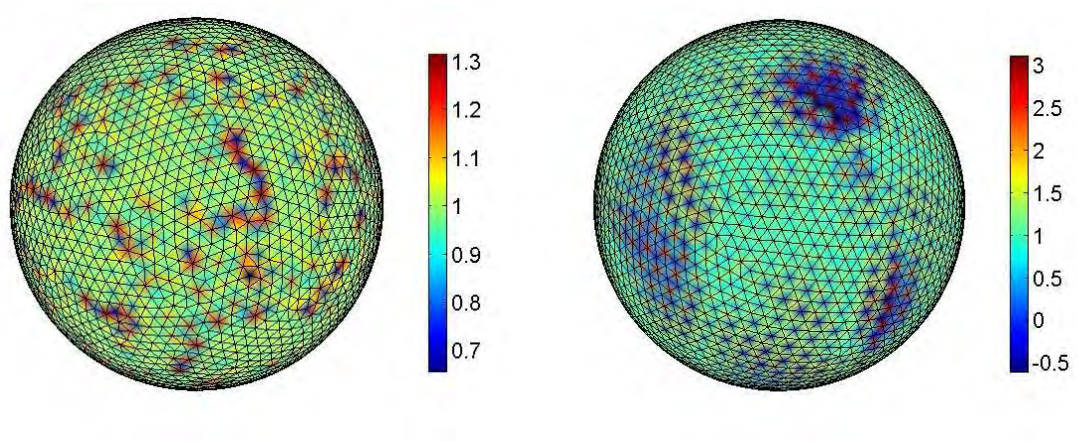

(a) Maximal determinant point set (b) Minimum energy point set

Figure 8.1: Distribution of maximal point sets on the sphere of order $N = 50$. Each set consists of 2601 points distributed on the surface of the sphere along with an associated weighting coefficient for integration cubature. The first set is optimised to maximise the determinant of the sampling matrix and thus minimise the conditioning number for signal reconstruction. The second set is optimised to minimise the energy of a system of repulsive charges on the sphere. Both sets display a significant range in the weighting coefficients with interesting and surprising structures.
Images reproduced from online resource [289] created by Robert Womersley.

given the goal and intuition would suggest large scale uniformity. To illustrate the point, two figures are adopted from [289] and shown in Figure 8.1. It is apparent that structures exists with a wide range of scale and complexity.

An area for further research would be to study the impact and significance of the specific antenna geometry, both theoretically and practically, on signal processing performance. The sampling locations may be important, however it is conjectured that an overall system performance may not be overly sensitive to the arrangement. Furthermore, an antenna will tend to return a signal representing an average of the field over the physical volume of the antenna[4]. In practice, the physical size of each antenna element may place constraints and even uniquely determine the possible arrangement of an array.

Similar problems have been addressed for the case of acoustic microphone arrays. In this area, the arrangement of the microphones does have an impact on the sensitivity and noise gain of the array [290]. Each input signal in a communications system incurs an implementation cost. Thus an important goal is to understand and avoid the arrangements that create degenerate or redundant antenna outputs, or equivalently unnecessarily lower system performance.

[4]Practical reasons prohibit the antenna from being vanishingly small. Much of the structure and details in Figure 8.1 arise from the construct of infinitesimal sampling. Spatial averaging at each sample point may eliminate such nuance and detail and reduce the significance of the exact geometry.

Chapter 4 set out the framework to determine the optimal basis functions for specific region shapes and angular spectra. The optimal antenna sampling configuration will be dependent on the optimal basis functions. For three dimensional fields, determining the optimal sampling configuration becomes a nontrivial problem. Thus there is significant scope for continued research and investigation in this area.

8.2.6 Development of Consistent Noise Models

The work of Chapter 5 demonstrated that the continuous spatial model could be used to derive an intrinsic bound on system performance independent of the antenna geometry used. However, as was discussed in Section 5.4.3, this approach depends on having a signal or noise model that is consistent between the expected sensor noise and the noise defined in a spatial sense.

Understanding the correspondence between spatial and sensor noise is a difficult issue, complicated by the potential for the theoretical discrete sensor placement on an uncountably infinite domain[5]. One approach to this problem is to consider sampling and representation of the field over finite volumetric blocks [146]. This implicitly imposes a finite upper bound on the model dimensionality, but can be useful when this limit is sufficiently higher than the expected field and system dimensionality. Interestingly, such approaches tend to adopt a finite division of space on the order of $\lambda/10$ which corresponds to a radius such that $2kR \approx 1$.

Intuitively a noise model should be matched to the physical processes that generate the noise. Practically, the value of a noise model depends on its simplicity and ability to predict observations. It is evident that the independent sensor noise model fails by predicting the ability for infinite precision if sensors are packed in a small volume. A fixed correlation matrix for the noise tends to imply a fixed sensor arrangement or system configuration. The development of a position dependent noise correlation function matches the noise being modelled on the spatial basis functions. However, this leads to a system signal to noise ratio that is dependent on the number of sensors and observation volume, as shown in (5.13).

In practice, noise sources include interfering electromagnetic fields, thermal electromagnetic radiative noise, antenna thermal noise, antenna noise coupling, antenna connection noise, amplification noise and processing noise. This can be fairly comprehensively modelled by two components – field or antenna noise and sensor or amplifier noise. The influence of these components will behave differently as more antennas are added to a system. The effect of antenna noise and noise coupling was investigated in [291]. The impedance matching,

[5] If we allow the spatial coordinates to be a real valued parameter, a white noise field must then have infinite power to become uncorrelated over an infinitesimal distance.

efficiency and coupling of antennas will also impact the nature of a suitable noise model [115].

8.2.7 Associated Spatial Dimensionality of a Single Antenna

In considering the consistence of noise models, an important question to be addressed is if it is possible to infer a limit to spatial wireless capacity over a region given a single antenna signal to noise ratio measurement. It is conjectured that such a correspondence is not possible without some additional parameter for the antenna. This parameter will reflect the volumetric footprint or theoretical region of interaction of the antenna with the continuous spatial field. This may or may not be related to the actual physical dimension of the antenna. Such a parameter will allow us to infer that the noise observed by that antenna represents the sum of the corruption of a set of spatial functions, whose number matches the dimensionality related to the volumetric footprint. Furthermore, the degree of coupling and correlation between antenna should be related to this volumetric footprint.

There is a direct analogy of this idea and conjecture to the discrete observation of a continuous time signal, as occurs when an oscilloscope or probe is attached to an electronic circuit. Whilst the the underlying noise process may be white, a set of samples of the voltage across the circuit show a finite variance. The spectral noise power (units of $\mathrm{W.Hz}^{-1}$) is the average of the observed signal power ($P = E\left\{V^2/R_{\mathrm{load}}\right\}$) across the assumed sensor bandwidth. In assuming the noise to be white, we must simultaneously accept that our ability to observe it is bandlimited[6].

For the spatial case, we could assume that there is an underlying white spatial noise that corrupts the continuous signal space. It follows that we must then average the observed antenna signal to noise ratio across the "spatial bandwidth" which is related to the volumetric footprint and associated dimensionality of the antenna.

Two samples in time will become correlated as the separating interval approaches the reciprocal of the sensor bandwidth. Similarly, the output of two antennas in space should become correlated as the separation approaches a distance related to the effective spatial dimensionality of the antenna. Rather than being a point sample, antennas interact with the field over a region of space. From the results in this thesis, we can assert that such a region has an associated essential dimensionality. This value will be critical to developing a consistent and practically useful noise model to match discrete sensor and spatial noise models.

[6] Alternatively we can assume a perfect sensor with a bandlimited noise process. Either way there is some limit, and we cannot ever completely observe in practice a white noise process – to do so would be to face the infinite. One need only review the plight of Cantor to understand the folly of attempting this.

Further work in this area would be required to formally develop this conjecture. However, from the preceding discussion, it should be apparent that without a spatial bandwidth for the antenna, it is meaningless to relate a single antenna signal to noise to an intrinsic spatial information limit.

8.3 Closing Remarks

Much of the literature related to MIMO systems deals with discrete signals and their statistical properties. This thesis has been an explorative investigation to develop a framework for signal processing which inherently incorporates space and the nature of wave propagation. Rather than adding statistical and correlation models to match observation, this work has sought to develop appropriate models and signal representations from fundamental principles.

The issue of the dimensionality of a signal space is not easily resolved, particularly in the case of a small dimensionality. In a sense, part of the problem is the desire to assert and bound a sudden threshold or transition where in practice it does not exist. The dimensionality results certainly indicate a point of diminishing returns. For a bandlimited function, the width of the transition from significant to insignificant basis functions varies with the logarithm of $2WT$ [142]. A similar result is conjectured for the dimensionality of a bounded region of a multipath field. Hence, the transition region will be significant for small regions.

Collectively the work in this thesis presents a broad range of results, from explorative development and conjectures through to some formal frameworks, theorems and proofs. As with the case of the dimensionality of the bandlimited function, the research in this area has opened up a rich array of mathematical detail and the potential for continued investigation over a much longer period. However, some of the results can seem obvious in that they are are consistent with implemented pragmatic engineering approaches. In reflection, the nature of conventional wireless communications is rather forgiving with the typical scattering environment offering a rich field diversity, the nominal wavelength of operation fairly small relative to the array size, and current practical limits on the economical number of signal processing channels. System performance is far more likely to be impacted by the choice of low noise radio frequency amplifiers than by the antenna arrangement.

It is evident that sensors and signal processing are becoming more affordable and ubiquitous. This is true both in the domain of wireless communications and also related domains such as acoustical signal processing. A developed understanding of the nature of wave-fields and the implications to signal processing is increasingly important to understand the fundamental possibilities and limitations for effective system design and implementation.

Appendix A

Interpolation of Dimensionality

By definition, the dimensionality of a space of functions can only take on integer values. However, the figures and numerical analysis of Chapter 4 were aimed at investigating the impact of the problem geometry on the effective dimensionality. Towards this goal, the number of function terms required to achieve a fixed truncation error was considered. With this number restricted to integer values, the trends in the figures were not easily apparent. To overcome this, the following approach was developed to infer a fractional dimensionality. This was based on the assumption of an exponential decrease in the truncation error around the truncation point as was shown in Chapter 2 and Chapter 3.

The truncation error is related to the trailing sum of the eigenvalues of the eigenequation developed in Section 4.3. The equation, (4.37), is repeated here

$$\lambda_n g_n(\widehat{\boldsymbol{\theta}}) = \mathbf{A}^*\mathbf{A} g_n(\widehat{\boldsymbol{\phi}}) = P(\widehat{\boldsymbol{\theta}}) \int_\Lambda \int_\Omega g_n(\widehat{\boldsymbol{\phi}}) e^{jk\boldsymbol{x}.(\widehat{\boldsymbol{\phi}}-\widehat{\boldsymbol{\theta}})} ds(\widehat{\boldsymbol{\phi}}) d\boldsymbol{x}. \tag{A.1}$$

Since the kernel of this integral equation is compact, and by virtue of the factors discussed in Chapter 2, the set of eigenvalues $\lambda_0, \ldots, \lambda_n$ can be ordered in descending value and will have an accumulation point at zero [184]. We restate Definition 4.8 for dimensionality,

Definition A.1 Dimensionality of Multipath Field.
For any set of eigenvalues from (4.37), given $\varepsilon > 0$ there exists some integer $D(\varepsilon)$ such that

$$D(\varepsilon) = \arg\min_n \left\{ \frac{\sum_{m \geq n} \lambda_m}{\sum_m \lambda_m} < \varepsilon \right\}. \tag{A.2}$$

The general measure of dimensionality adopted for the numerical analysis work in Chapter 4

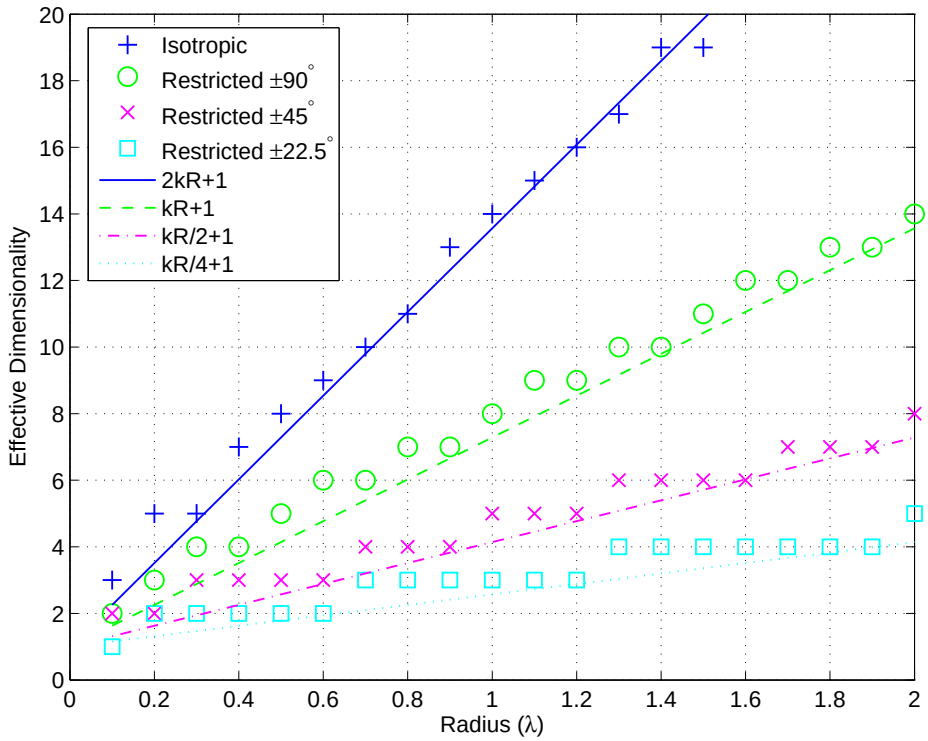

Figure A.1: Repeat of Figure 4.7 with the integer ceiling quantisation for the dimensionality. The trend is obscured by the coarse quantisation, especially at low dimensionality. The matching empirical lines approximate a lower bound for the dimensionality.

was $D(0.01)$. This is the point at which the cumulative sum of the eigenvalues exceeds 99% of the total sum of all eigenvalues.

The numerical analysis in Chapter 4 aims to illuminate how the essential dimension of a region varies with changes to incident wave-field and the region size, shape and orientation. For the examples given, the essential dimension has reasonably small values (< 20). At this scale, the coarse integer quantised values for D obtained from (A.2) obscure the underlying trend of dimensionality. For example, we can consider Figure 4.7 without fractional interpolation of the dimensionality. This is shown in Figure A.1.

Given the eigenvalues obtained from (A.1) we can obtain an indication of the fractional dimension by considering a continuous interpolation of the eigenvalues and considering the point at which the selected dimensionality threshold is crossed. Consider the function

$$f(n) = \frac{\sum_{m \geq n} \lambda_m}{\sum_m \lambda_m}. \tag{A.3}$$

The eigenvalues are numbered from index 0, thus $f(0) = 1$. Given the desired threshold ε, at some point $f(N) > \varepsilon$ and $f(N+1) \leq \varepsilon$. Provided ε is suitably small, around this point,

the function $f(n)$ will be exponentially decreasing. Consider the interpolated function

$$\widetilde{f}(z) = Ae^{-bz}. \tag{A.4}$$

Solving at the two data points $f(N)$ and $f(N+1)$ gives

$$b = \log\left(f(N)\right) - \log\left(f(N+1)\right) \tag{A.5}$$

$$A = f(N)e^{bN}. \tag{A.6}$$

Solving for $\widetilde{f}(z) = \varepsilon$, we obtain

$$z = N + \frac{\log\left(f(N)\right) - \log(\varepsilon)}{\log\left(f(N)\right) - \log\left(f(N+1)\right)}. \tag{A.7}$$

This can then be used to determine the fractional dimensionality from the set of eigenvalues.

To illustrate this method, we present two examples from the eigenvalue sets of Figure A.1. At the radius of λ the integer dimensionality for the $\pm 90^\circ$ and $\pm 45^\circ$ angular spread is 8 and 5 respectively. Figure A.2 shows the residual energy associated in the terms past the truncation point, $f(n)$ as calculated in (A.3). The exponential curve shown is fitted to the two points around the threshold value of 0.01. This is used to calculate the fractional dimensionality of 4.18 and 7.5 respectively. The plots in Figure A.1 also clearly show that the decrease in residual error is exponential beyond the critical threshold.

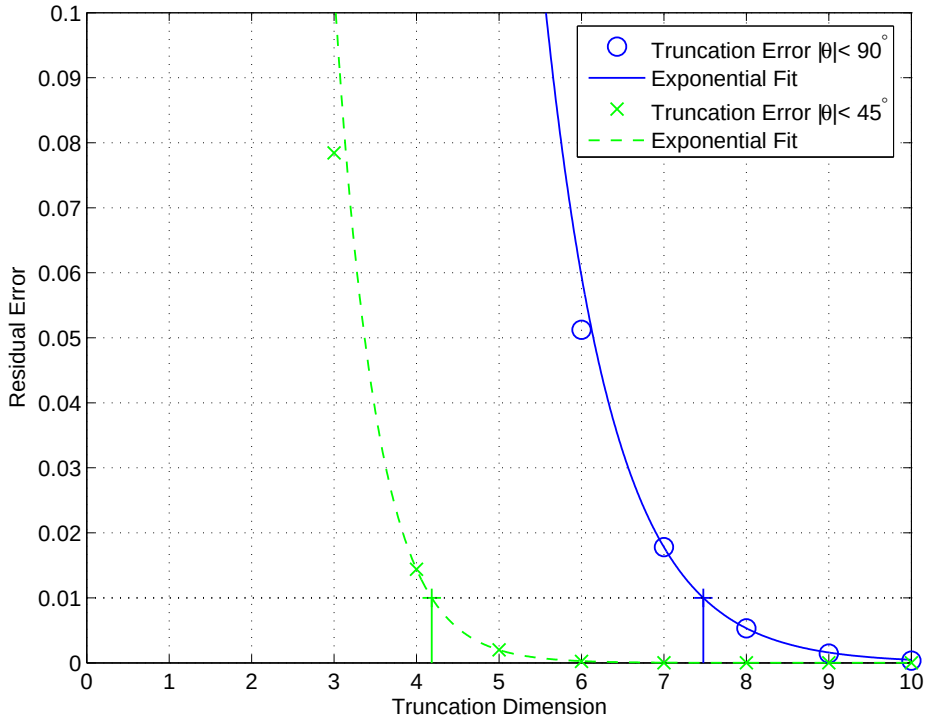

(a) Linear scale

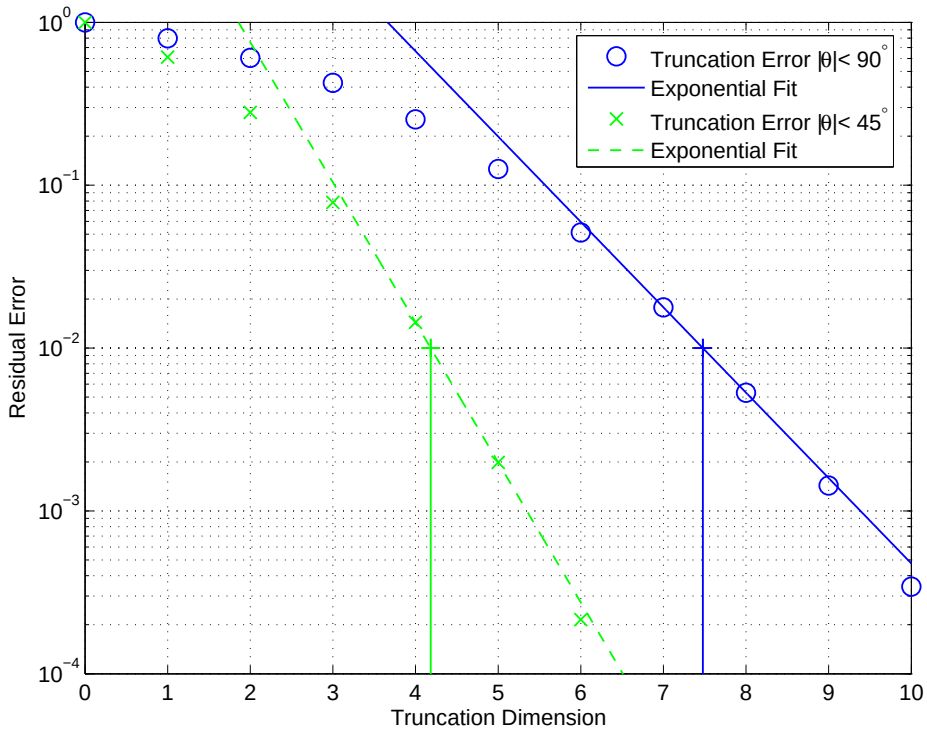

(b) Logarithmic scale

Figure A.2: Error for truncation of two sets of solutions to the eigenequation (A.1). An exponential fit to the sequence is made around the threshold of 0.01. This fit is then used to determine the fractional dimensionality of the solution.

Appendix B

Derivation of the Cramér-Rao Bound

This appendix presents the derivation of the Cramér-Rao Bound (CRB) for the estimation of direction of arrival using the continuous sensor framework developed in Chapter 5.

B.1 Key Bessel Identities

The derivations make extensive use of some identities for the Bessel functions. These are stated and reformulated here for use in the following proofs. The Bessel recurrence relationship [160, 9.1.27],

$$nJ_n(z) = \frac{z}{2}J_{n-1}(z) + \frac{z}{2}J_{n+1}(z). \tag{B.1}$$

Sum of second order Bessel terms, from Neumann's addition theorem [160, 9.1.75 p. 363]

$$\sum_{n=-\infty}^{\infty} J_n^2(z) = 1 \qquad \sum_{n=-\infty}^{\infty} J_n(z)J_{n+k}(z) = 0, \quad k \neq 0 \qquad . \tag{B.2}$$

Variants of Graf's addition theorem with some basic trigonometric manipulation [160, 9.1.79],

$$\sum_{n=-\infty}^{\infty} J_n^2(z)e^{jn\theta} = J_0\left(z\sin\frac{\theta}{2}\right) \tag{B.3}$$

$$\sum_{n=-\infty}^{\infty} J_n(z)J_{n+1}(z)e^{jn\theta} = jJ_1\left(z\sin\frac{\theta}{2}\right)e^{-j\theta/2} \tag{B.4}$$

$$\sum_{n=-\infty}^{\infty} J_n(z)J_{n+2}(z)e^{jn\theta} = -J_2\left(z\sin\frac{\theta}{2}\right)e^{-j\theta} \tag{B.5}$$

$$\sum_{n=-\infty}^{\infty} J_n(z) J_{n+3}(z) e^{jn\theta} = -j J_3\left(z \sin\frac{\theta}{2}\right) e^{-j3\theta/2}. \tag{B.6}$$

B.2 Derivation Overview

We are interested in the Cramér-Rao bound for a deterministic source model, as this will provide a lower bound for the variance of any unbiased estimate. From [260], the deterministic CRB is

$$\text{CRB} = \frac{\sigma^2}{2N}\left\{\text{Re}\left[\left(\mathbf{D}^H\mathbf{D} - \mathbf{D}^H\mathbf{A}\left(\mathbf{A}^H\mathbf{A}\right)^{-1}\mathbf{A}^H\mathbf{D}\right) \odot \mathbf{R}_{\boldsymbol{s}}{}^T\right]\right\}^{-1}, \tag{B.7}$$

where σ^2 is the noise variance, N is the number of data samples,

$$\mathbf{A} \triangleq \left[\begin{array}{ccc} \boldsymbol{a}(\theta_1) & \ldots & \boldsymbol{a}(\theta_P) \end{array}\right] \tag{B.8}$$

$$\mathbf{D} \triangleq \left[\frac{\partial}{\partial\theta_1}\boldsymbol{a}(\theta_1), \ldots, \frac{\partial}{\partial\theta_P}\boldsymbol{a}(\theta_P)\right] \tag{B.9}$$

with $\boldsymbol{a}(\theta)$ the sensor array steering vector for direction θ. The matrix $\mathbf{R}_{\boldsymbol{s}}$ is the sample covariance matrix for the signals $\boldsymbol{s}$ and $\odot$ represents the elementwise Schur-Hadamard product of the matrices.

The matrices $\mathbf{A} \equiv \mathbf{A}(\boldsymbol{\theta})$ and $\mathbf{D} \equiv \mathbf{D}(\boldsymbol{\theta})$ are dependent on the source directions.

Three main terms are required to compute the Cramér-Rao bound from (B.7). These are $\mathbf{A}^H\mathbf{A}$, $\mathbf{D}^H\mathbf{D}$ and $\mathbf{D}^H\mathbf{A}$. To evaluate these, we will use the continuous sensor model, which for a circularly symmetric region has the form

$$\boldsymbol{a}(\theta) = \left[\ldots, \sqrt{C_{-m}}e^{jm\theta}, \ldots, \sqrt{C_m}e^{-jm\theta}, \ldots\right]^T \tag{B.10}$$

with $C_m = \|\beta_m\|_\Lambda^2 \, Q/|\Lambda|$ being a normalisation constant dependent on the region shape. The details of the continuous model framework can be found in Section 5.4.3.

From this we can derive the Cramér-Rao bound for the case of a circular and disc shaped region with one and two uncorrelated sources.

B.3 Circular Array, One Source

The signal scaling, C_n, for the circular array from Section 5.5 equation (5.16)

$$C_n = \frac{Q}{2\pi R}\int_0^{2\pi} |\beta_n(\boldsymbol{x})|^2 \, R d\theta = Q J_n^2(kR). \tag{B.11}$$

For the circular array with a single source, the array steering matrix and derivative will be the vectors

$$\mathbf{A} = [\boldsymbol{a}(\theta)] = \left[\ldots \ \sqrt{C_{-n}} e^{jn\theta} \ \ldots \ \sqrt{C_n} e^{-jn\theta} \ \ldots\right]^T \tag{B.12}$$

$$\mathbf{D} = \left[\frac{\partial}{\partial\theta}\boldsymbol{a}(\theta)\right] = \left[\ldots \ n\sqrt{C_{-n}} e^{jn\theta} \ \ldots \ -n\sqrt{C_n} e^{-jn\theta} \ \ldots\right]^T. \tag{B.13}$$

The term $\mathbf{A}^H\mathbf{A}$ is related to the signal energy. Using identity (B.2) we obtain

$$\mathbf{A}^H\mathbf{A} = \sum_{n=-\infty}^{\infty} C_n = Q \sum_{n=-\infty}^{\infty} J_n^2(kR) = Q. \tag{B.14}$$

The term $\mathbf{D}^H\mathbf{D}$ is evaluated using the recurrence relationship (B.1) to expand the two terms $nJ_n(kR)$ followed by the use of identity (B.2),

$$\begin{aligned}
\mathbf{D}^H\mathbf{D} &= \sum_{n=-\infty}^{\infty} n^2 C_n = Q \sum_{n=-\infty}^{\infty} n^2 J_n^2(kR) \\
&= Q \sum_{n=-\infty}^{\infty} \left(\frac{kR}{2} J_{n-1}(kR) + \frac{kR}{2} J_{n+1}(kR)\right)^2 \\
&= \frac{Qk^2R^2}{4} \sum_{n=-\infty}^{\infty} J_{n-1}^2(kR) + J_{n-1}(kR)J_{n+1}(kR) + J_{n+1}^2(kR) \\
&= \frac{Qk^2R^2}{2}.
\end{aligned} \tag{B.15}$$

The term $\mathbf{D}^H\mathbf{A}$ is evaluated using the recurrence relationship (B.1) for $nJ_n(kR)$. Noting that no Bessel terms of equal index are in the infinite sum, using (B.2) the result is zero.

$$\begin{aligned}
\mathbf{D}^H\mathbf{A} &= \sum_{n=-\infty}^{\infty} -nC_n = Q \sum_{n=-\infty}^{\infty} -nJ_n^2(kR) \\
&= Q \sum_{n=-\infty}^{\infty} -\left(\frac{kR}{2} J_{n-1}(kR) + \frac{kR}{2} J_{n+1}(kR)\right) J_n(kR) \\
&= \frac{QkR}{2} \sum_{n=-\infty}^{\infty} J_{n-1}(kR)J_n(kR) + J_{n+1}(kR)J_n(kR) = 0.
\end{aligned} \tag{B.16}$$

Using the results from (B.14), (B.15) and (B.16) in the bound expression (B.7)

$$\begin{aligned}\mathrm{CRB}_{P=1} &= \frac{\sigma^2}{2N}\left\{\mathrm{Re}\left[\left(\mathbf{D}^H\mathbf{D} - \mathbf{D}^H\mathbf{A}\left(\mathbf{A}^H\mathbf{A}\right)^{-1}\mathbf{A}^H\mathbf{D}\right)\odot \mathbf{R_s}^T\right]\right\}^{-1} \\ &= \frac{\sigma^2}{2N}\left\{\left(\frac{Qk^2R^2}{2} - 0.\frac{1}{Q}.0\right)\odot 1\right\}^{-1} \\ &= \frac{\sigma^2}{QN}\frac{1}{k^2R^2}. \end{aligned} \tag{B.17}$$

B.4 Circular Array, Two Sources

The signal scaling for the circular array is $C_n = QJ_n^2(kR)$. For two sources located with directions θ_1 and θ_2, the array response matrix and derivative are

$$\mathbf{A} = \left[\begin{array}{cc} \boldsymbol{a}(\theta_1) & \boldsymbol{a}(\theta_2)\end{array}\right] = \left[\begin{array}{ccccc} \dots & \sqrt{C_{-n}}e^{jn\theta_1} & \dots & \sqrt{C_n}e^{-jn\theta_1} & \dots \\ \dots & \sqrt{C_{-n}}e^{jn\theta_2} & \dots & \sqrt{C_n}e^{-jn\theta_2} & \dots \end{array}\right]^T \tag{B.18}$$

$$\mathbf{D} = \left[\begin{array}{cc} \frac{\partial}{\partial\theta_1}\boldsymbol{a}(\theta_1) & \frac{\partial}{\partial\theta_2}\boldsymbol{a}(\theta_2)\end{array}\right] = \left[\begin{array}{ccccc} \dots & n\sqrt{C_{-n}}e^{jn\theta_1} & \dots & -n\sqrt{C_n}e^{-jn\theta_1} & \dots \\ \dots & n\sqrt{C_{-n}}e^{jn\theta_2} & \dots & -n\sqrt{C_n}e^{-jn\theta_2} & \dots \end{array}\right]^T. \tag{B.19}$$

The self adjoint product of the array response matrix is

$$\mathbf{A}^H\mathbf{A} = \left[\begin{array}{cc} \sum_{n=-\infty}^{\infty} C_n & \sum_{n=-\infty}^{\infty} C_n e^{jn(\theta_1-\theta_2)} \\ \sum_{n=-\infty}^{\infty} C_n e^{jn(\theta_2-\theta_1)} & \sum_{n=-\infty}^{\infty} C_n \end{array}\right] \tag{B.20}$$

$$= Q\left[\begin{array}{cc} 1 & \overline{\mu} \\ \mu & 1 \end{array}\right] \tag{B.21}$$

where the diagonal entries follow directly from (B.14). Defining $\Delta\theta = \theta_2 - \theta_1$ and using the identity (B.4) the off diagonal entries are

$$\begin{aligned}\mu &= \sum_{n=-\infty}^{\infty} C_n e^{jn\Delta\theta} = \sum_{n=-\infty}^{\infty} J_n^2(kR)e^{jn\Delta\theta} \\ &= J_0\left(2kR\sin\frac{\Delta\theta}{2}\right) \\ &= J_0\left(kR\Delta\theta\right) + O\left((\Delta\theta)^4\right) \end{aligned} \tag{B.22}$$

where the final approximation can be obtained by noting $\sin(\Delta\theta/2) = \Delta\theta/2 + O((\Delta\theta)^3)$ and using a linear approximation for $J_0(kR\Delta\theta)$.

For the two uncorrelated sources $\mathbf{R}_{\boldsymbol{s}} = \mathbf{I}$ and from the elementwise product in (B.7), the off diagonal entries in $\mathbf{D}^H\mathbf{D}$ are not required for the final result. Using the result from (B.15) for the diagonal entries, we obtain

$$\begin{aligned}\mathbf{D}^H\mathbf{D} &= \begin{bmatrix} \sum_{n=-\infty}^{\infty} n^2 C_n & \sum_{n=-\infty}^{\infty} n^2 C_n e^{jn(\theta_1-\theta_2)} \\ \sum_{n=-\infty}^{\infty} n^2 C_n e^{jn(\theta_2-\theta_1)} & \sum_{n=-\infty}^{\infty} n^2 C_n \end{bmatrix} \\ &= \begin{bmatrix} \frac{Qk^2R^2}{2} & \cdots \\ \cdots & \frac{Qk^2R^2}{2} \end{bmatrix}. \end{aligned} \tag{B.23}$$

Using the result (B.16) for the diagonal entries of the final term, we obtain

$$\begin{aligned}\mathbf{D}^H\mathbf{A} &= \begin{bmatrix} \sum_{n=-\infty}^{\infty} -nC_n & \sum_{n=-\infty}^{\infty} -nC_n e^{jn(\theta_1-\theta_2)} \\ \sum_{n=-\infty}^{\infty} -nC_n e^{jn(\theta_2-\theta_1)} & \sum_{n=-\infty}^{\infty} -nC_n \end{bmatrix} \\ &= Q \begin{bmatrix} 0 & \overline{\nu} \\ \nu & 0 \end{bmatrix}. \end{aligned} \tag{B.24}$$

The off diagonal entries can be evaluated and simplified using the recurrence identity $B.1$ for $nJ_n(kR)$, followed by some manipulation and the application of the identity (B.4),

$$\begin{aligned}\nu &= \sum_{n=-\infty}^{\infty} -nC_n e^{jn\Delta\theta} = \sum_{n=-\infty}^{\infty} -nJ_n^2(kR)e^{jn\Delta\theta} \\ &= -\frac{kR}{2} \sum_{n=-\infty}^{\infty} \left(J_{n-1}(kR) + J_{n+1}(kR)\right) J_n(kR) e^{jn\Delta\theta} \\ &= -\frac{kR}{2} \sum_{n=-\infty}^{\infty} J_{n-1}(kR)J_n(kR)e^{jn\Delta\theta} - \frac{kR}{2} \sum_{n=-\infty}^{\infty} J_n(kR)J_{n+1}(kR)e^{jn\Delta\theta} \\ &= -\frac{kR}{2} e^{j\Delta\theta} \sum_{n=-\infty}^{\infty} J_n(kR)J_{n+1}(kR)e^{jn\Delta\theta} - \frac{kR}{2} \sum_{n=-\infty}^{\infty} J_n(kR)J_{n+1}(kR)e^{jn\Delta\theta} \\ &= -\frac{jkR}{2} \left(e^{j\Delta\theta/2} + e^{-j\Delta\theta/2}\right) J_1\left(2kR\sin\frac{\Delta\theta}{2}\right) \\ &= -jkR\cos\left(\frac{\Delta\theta}{2}\right) J_1\left(2kR\sin\frac{\Delta\theta}{2}\right) \\ &= -jkRJ_1\left(kR\Delta\theta\right) + O\left((\Delta\theta)^3\right) \end{aligned} \tag{B.25}$$

where the final approximation is based on small arguments $\Delta\theta$ where $\cos(\Delta\theta/2) \approx 1$ and $\sin(\Delta\theta/2) \approx \Delta\theta/2$.

To evaluate the CRB from (B.7), first consider the term using the results from (B.24) and (B.21)

$$\begin{aligned}\mathbf{D}^H\mathbf{A}(\mathbf{A}^H\mathbf{A})^{-1}\mathbf{A}^H\mathbf{D} &= Q\begin{bmatrix} 0 & \nu \\ -\nu & 0 \end{bmatrix}\frac{1}{Q}\frac{1}{1-\mu^2}\begin{bmatrix} 1 & -\mu \\ -\mu & 1 \end{bmatrix}Q\begin{bmatrix} 0 & \nu \\ -\nu & 0 \end{bmatrix} \\ &= \frac{-Q\nu^2}{1-\mu^2}\begin{bmatrix} 1 & \mu \\ \mu & 1 \end{bmatrix}. \end{aligned} \tag{B.26}$$

Substituting (B.26) and (B.23) into (B.7) we obtain

$$\begin{aligned}\mathrm{CRB}_{P=2} &= \frac{\sigma^2}{2N}\left\{\mathrm{Re}\left[\left(\mathbf{D}^H\mathbf{D} - \mathbf{D}^H\mathbf{A}\left(\mathbf{A}^H\mathbf{A}\right)^{-1}\mathbf{A}^H\mathbf{D}\right)\odot \mathbf{R}_{\boldsymbol{s}}{}^T\right]\right\}^{-1} \\ &= \frac{\sigma^2}{2N}\left\{\left(\begin{bmatrix} \frac{Qk^2R^2}{2} & \dots \\ \dots & \frac{Qk^2R^2}{2} \end{bmatrix} + \frac{Q\nu^2}{1-\mu^2}\begin{bmatrix} 1 & \mu \\ \mu & 1 \end{bmatrix}\right)\odot\begin{bmatrix} 1 & 0 \\ 0 & 1 \end{bmatrix}\right\}^{-1} \\ &= \frac{\sigma^2}{QN}\frac{1}{k^2R^2}\left(1+\frac{2\nu^2}{1-\mu^2}\right)^{-1}\begin{bmatrix} 1 & 0 \\ 0 & 1 \end{bmatrix}. \end{aligned} \tag{B.27}$$

Using the expressions for μ (B.22) and ν (B.25)

$$\begin{aligned}\mathrm{CRB}_{P=2} &= QN\frac{1}{k^2R^2}\left(1-\frac{2J_1^2\left(2kR\sin\frac{\Delta\theta}{2}\right)\cos^2\left(\frac{\Delta\theta}{2}\right)}{1-J_0^2\left(2kR\sin\frac{\Delta\theta}{2}\right)}\right)^{-1} \\ &\approx \frac{\sigma^2}{QN}\frac{1}{k^2R^2}\left(1-\frac{2J_1^2\left(kR\Delta\theta\right)}{1-J_0^2\left(kR\Delta\theta\right)}\right)^{-1} \end{aligned} \tag{B.28}$$

where the approximation uses the approximations for μ and ν previously stated for small angular separations $\Delta\theta$.

B.5 Filled Disc Array, One Source

The derivation for the filled disc array is similar with the signal scaling,

$$C_n = \frac{Q}{\pi R^2}\int_0^R\int_0^{2\pi} J_n^2(kr)rd\theta dr = Q\left(J_n^2(kR) - J_{n-1}(kR)J_{n+1}(kR)\right) \tag{B.29}$$

For a single source, the array response vector and derivative to a source at θ are

$$\mathbf{A} = [\boldsymbol{a}(\theta)] = \left[\ldots\ \sqrt{C_{-n}}e^{jn\theta}\ \ldots\ \sqrt{C_n}e^{-jn\theta}\ \ldots\right]^T \tag{B.30}$$

$$\mathbf{D} = \left[\frac{\partial}{\partial\theta}\boldsymbol{a}(\theta)\right] = \left[\ldots\ n\sqrt{C_{-n}}e^{jn\theta}\ \ldots\ -n\sqrt{C_n}e^{-jn\theta}\ \ldots\right]^T. \tag{B.31}$$

Using the identities from (B.2) the self adjoint of the response vector is unchanged,

$$\mathbf{A}^H\mathbf{A} = \sum_{n=-\infty}^{\infty} C_n = Q\sum_{n=-\infty}^{\infty} J_n^2(kR) - J_{n-1}(kR)J_{n+1}(kR) = Q. \tag{B.32}$$

The additional term in (B.29) reduces the value of $\mathbf{D}^H\mathbf{D}$. Using the result from (B.15), some basic manipulations, and the identities from (B.2)

$$\begin{aligned}
\mathbf{D}^H\mathbf{D} &= \sum_{n=-\infty}^{\infty} n^2C_n = Q\sum_{n=-\infty}^{\infty} n^2\left(J_n^2(kR) - J_{n-1}(kR)J_{n+1}(kR)\right)\\
&= \frac{Qk^2R^2}{2} - Q\sum_{n=-\infty}^{\infty}\left(n^2-1\right)J_{n-1}(kR)J_{n+1} - Q\sum_{n=-\infty}^{\infty} J_{n-1}(kR)J_{n+1}\\
&= \frac{Qk^2R^2}{2} - Q\sum_{n=-\infty}^{\infty}(n-1)J_{n-1}(kR)(n+1)J_{n+1}\\
&= \frac{Qk^2R^2}{2} - \frac{Qk^2R^2}{4}\sum_{n=-\infty}^{\infty}\left(J_{n-2}(kR) + J_n(kR)\right)\left(J_n(kR) + J_{n+2}(kR)\right)\\
&= \frac{Qk^2R^2}{4}.
\end{aligned} \tag{B.33}$$

The third term remains unchanged.

$$\begin{aligned}
\mathbf{D}^H\mathbf{A} &= \sum_{n=-\infty}^{\infty} -nC_n = Q\sum_{n=-\infty}^{\infty} -n\left(J_n^2(kR) - J_{n-1}(kR)J_{n+1}(kR)\right)\\
&= 0 + Q\sum_{n=-\infty}^{\infty}(n-1)J_{n-1}(kR)J_{n+1}(kR) + Q\sum_{n=-\infty}^{\infty} J_{n-1}(kR)J_{n+1}(kR)\\
&= \frac{QkR}{2}\sum_{n=-\infty}^{\infty}\left(J_{n-2}(kR) + J_n(kR)\right)J_{n+1}(kR) = 0.
\end{aligned} \tag{B.34}$$

Substituting the results from (B.32), (B.33) and (B.34) into the bound expression (B.7)

$$\begin{aligned}\text{CRB}_{P=1} &= \frac{\sigma^2}{2N}\left\{\text{Re}\left[\left(\mathbf{D}^H\mathbf{D} - \mathbf{D}^H\mathbf{A}\left(\mathbf{A}^H\mathbf{A}\right)^{-1}\mathbf{A}^H\mathbf{D}\right)\odot \mathbf{R}_{\boldsymbol{s}}{}^T\right]\right\}^{-1} \\ &= \frac{\sigma^2}{2N}\left\{\left(\frac{Qk^2R^2}{4} - 0.\frac{1}{Q}.0\right)\odot 1\right\}^{-1} \\ &= \frac{\sigma^2}{QN}\frac{2}{k^2R^2}. \end{aligned} \tag{B.35}$$

.

B.6 Filled Disc Array, Two Sources

The signal scaling for the disc array is $C_n = Q(J_n^2(kR) - J_{n-1}(kR)J_{n+1}(kR))$. For two sources located with directions θ_1 and θ_2, the array response matrix and derivative are

$$\mathbf{A} = \left[\begin{array}{cc} \boldsymbol{a}(\theta_1) & \boldsymbol{a}(\theta_2)\end{array}\right] = \left[\begin{array}{ccccc} \dots & \sqrt{C_{-n}}e^{jn\theta_1} & \dots & \sqrt{C_n}e^{-jn\theta_1} & \dots \\ \dots & \sqrt{C_{-n}}e^{jn\theta_2} & \dots & \sqrt{C_n}e^{-jn\theta_2} & \dots \end{array}\right]^T \tag{B.36}$$

$$\mathbf{D} = \left[\begin{array}{cc} \frac{\partial}{\partial\theta_1}\boldsymbol{a}(\theta_1) & \frac{\partial}{\partial\theta_2}\boldsymbol{a}(\theta_2)\end{array}\right] = \left[\begin{array}{ccccc} \dots & n\sqrt{C_{-n}}e^{jn\theta_1} & \dots & -n\sqrt{C_n}e^{-jn\theta_1} & \dots \\ \dots & n\sqrt{C_{-n}}e^{jn\theta_2} & \dots & -n\sqrt{C_n}e^{-jn\theta_2} & \dots \end{array}\right]^T. \tag{B.37}$$

The self adjoint product of the array response matrix is

$$\begin{aligned}\mathbf{A}^H\mathbf{A} &= \left[\begin{array}{cc} \sum_{n=-\infty}^{\infty} C_n & \sum_{n=-\infty}^{\infty} C_n e^{jn(\theta_1-\theta_2)} \\ \sum_{n=-\infty}^{\infty} C_n e^{jn(\theta_2-\theta_1)} & \sum_{n=-\infty}^{\infty} C_n\end{array}\right] \\ &= Q\left[\begin{array}{cc} 1 & \overline{\mu'} \\ \mu' & 1\end{array}\right] \end{aligned} \tag{B.38}$$

where the diagonal entries follow directly from (B.32) and the off diagonal entries can be evaluated using the previous result (B.22) and the identity (B.5)

$$\begin{aligned}\mu' &= \sum_{n=-\infty}^{\infty} C_n e^{jn\Delta\theta} = \sum_{n=-\infty}^{\infty}\left(J_n^2(kR) - J_{n-1}(kR)J_{n+1}(kR)\right)e^{jn\Delta\theta} \\ &= \mu - \sum_{n=-\infty}^{\infty} J_{n-1}(kR)J_{n+1}(kR)e^{jn\Delta\theta} \\ &= \mu - e^{j\Delta\theta}\sum_{n=-\infty}^{\infty} J_n(kR)J_{n+2}(kR)e^{jn\Delta\theta}\end{aligned}$$

$$
\begin{aligned}
&= \mu + e^{j\Delta\theta} J_2\left(2kR\sin\frac{\Delta\theta}{2}\right) e^{-j\Delta\theta} \\
&= J_0\left(2kR\sin\frac{\Delta\theta}{2}\right) + J_2\left(2kR\sin\frac{\Delta\theta}{2}\right) \\
&\approx J_0\left(kR\Delta\theta\right) + J_2\left(kR\Delta\theta\right) \qquad \text{(B.39)}
\end{aligned}
$$

where the final approximation is for small angular separations $\Delta\theta$.

As before, the off diagonal entries of $\mathbf{D}^H\mathbf{D}$ are not required. Using the previous result (B.33 for the diagonal entries,

$$
\begin{aligned}
\mathbf{D}^H\mathbf{D} &= \begin{bmatrix} \sum_{n=-\infty}^{\infty} n^2 C_n & \sum_{n=-\infty}^{\infty} n^2 C_n e^{jn(\theta_1-\theta_2)} \\ \sum_{n=-\infty}^{\infty} n^2 C_n e^{jn(\theta_2-\theta_1)} & \sum_{n=-\infty}^{\infty} n^2 C_n \end{bmatrix} \\
&= \begin{bmatrix} \frac{Qk^2R^2}{4} & \cdots \\ \cdots & \frac{Qk^2R^2}{4} \end{bmatrix}. \qquad \text{(B.40)}
\end{aligned}
$$

The diagonal entries of the final term $\mathbf{D}^H\mathbf{A}$ are obtained from (B.34)

$$
\begin{aligned}
\mathbf{D}^H\mathbf{A} &= \begin{bmatrix} \sum_{n=-\infty}^{\infty} -nC_n & \sum_{n=-\infty}^{\infty} -nC_n e^{jn(\theta_1-\theta_2)} \\ \sum_{n=-\infty}^{\infty} -nC_n e^{jn(\theta_2-\theta_1)} & \sum_{n=-\infty}^{\infty} -nC_n \end{bmatrix} \\
&= Q\begin{bmatrix} 0 & \overline{\nu'} \\ \nu' & 0 \end{bmatrix} \qquad \text{using (B.24).} \qquad \text{(B.41)}
\end{aligned}
$$

A lengthy manipulation and the use of identities (B.4) and (B.6) provides an expression for the off diagonal terms,

$$
\begin{aligned}
\nu' &= \sum_{n=-\infty}^{\infty} -nC_n e^{jn\Delta\theta} = \sum_{n=-\infty}^{\infty} -n\left(J_n^2(kR) - J_{n-1}(kR)J_{n+1}(kR)\right) e^{jn\Delta\theta} \\
&= \nu + \sum_{n=-\infty}^{\infty} nJ_{n-1}(kR)J_{n+1}(kR)e^{jn\Delta\theta} \\
&= \nu + \frac{1}{2}\sum_{n=-\infty}^{\infty} (n+1)J_{n-1}(kR)J_{n+1}(kR)e^{jn\Delta\theta} + \frac{1}{2}\sum_{n=-\infty}^{\infty} (n-1)J_{n-1}(kR)J_{n+1}(kR)e^{jn\Delta\theta} \\
&= \nu + \frac{kR}{4}\sum_{n=-\infty}^{\infty} J_{n-1}(\cdot)\left(J_n(\cdot) + J_{n+2}(\cdot)\right)e^{jn\Delta\theta} + \frac{kR}{4}\sum_{n=-\infty}^{\infty} \left(J_{n-2}(\cdot) + J_n(\cdot)\right)J_{n+1}(\cdot)e^{jn\Delta\theta} \\
&= \nu + \frac{kR}{4}\sum_{n=-\infty}^{\infty} \begin{matrix} e^{j\Delta\theta}J_n(kR)J_{n+1}(kR)e^{jn\Delta\theta} + & e^{j\Delta\theta}J_n(kR)J_{n+3}(kR)e^{jn\Delta\theta} + \\ e^{j2\Delta\theta}J_n(kR)J_{n+3}(kR)e^{jn\Delta\theta} + & J_n(kR)J_{n+1}(kR)e^{jn\Delta\theta} \end{matrix} \\
&= \nu + \frac{jkR}{4}\begin{pmatrix} e^{j\Delta\theta}J_1\left(2kR\sin\frac{\Delta\theta}{2}\right)e^{-j\Delta\theta/2} & - & e^{j\Delta\theta}J_3\left(2kR\sin\frac{\Delta\theta}{2}\right)e^{-j3\Delta\theta/2} + \\ -e^{j2\Delta\theta}J_3\left(2kR\sin\frac{\Delta\theta}{2}\right)e^{-j3\Delta\theta/2} + & & J_1\left(2kR\sin\frac{\Delta\theta}{2}\right)e^{-j\Delta\theta/2} \end{pmatrix}
\end{aligned}
$$

$$
\begin{aligned}
&= \nu - \frac{jkR}{2}\cos\left(\frac{\Delta\theta}{2}\right)\left(J_1\left(2kR\sin\frac{\Delta\theta}{2}\right) - J_3\left(2kR\sin\frac{\Delta\theta}{2}\right)\right) \\
&= -\frac{jkR}{2}\cos\left(\frac{\Delta\theta}{2}\right)\left(J_1\left(2kR\sin\frac{\Delta\theta}{2}\right) + J_3\left(2kR\sin\frac{\Delta\theta}{2}\right)\right) \\
&\approx -\frac{jkR}{2}J_1\left(kR\Delta\theta\right) - \frac{jkR}{2}J_3\left(kR\Delta\theta\right) \qquad \text{(B.42)}
\end{aligned}
$$

where the final approximation is for small angular separations $\Delta\theta$.

Using the matrix result previously computed (B.26) and substituting (B.40) into (B.7)

$$
\begin{aligned}
\text{CRB}_{P=2} &= \frac{\sigma^2}{2N}\left\{\text{Re}\left[\left(\mathbf{D}^H\mathbf{D} - \mathbf{D}^H\mathbf{A}\left(\mathbf{A}^H\mathbf{A}\right)^{-1}\mathbf{A}^H\mathbf{D}\right)\odot\mathbf{R}_{\boldsymbol{s}}{}^T\right]\right\}^{-1} \\
&= \frac{\sigma^2}{2N}\left\{\left(\begin{bmatrix} \frac{Qk^2R^2}{4} & \dots \\ \dots & \frac{Qk^2R^2}{4}\end{bmatrix} + \frac{Q\nu'^2}{1-\mu'^2}\begin{bmatrix} 1 & \mu' \\ \mu' & 1\end{bmatrix}\right)\odot\begin{bmatrix} 1 & 0 \\ 0 & 1\end{bmatrix}\right\}^{-1} \\
&= \frac{\sigma^2}{QN}\frac{2}{k^2R^2}\left(1 + \frac{4\nu'^2}{1-\mu'^2}\right)^{-1}\begin{bmatrix} 1 & 0 \\ 0 & 1\end{bmatrix}. \qquad \text{(B.43)}
\end{aligned}
$$

Finally, substituting the expressions for μ' (B.39) and ν' (B.42)

$$
\begin{aligned}
\text{CRB}_{P=2} &= \frac{\sigma^2}{QN}\frac{2}{k^2R^2}\left(1 - \frac{\cos^2\left(\frac{\Delta\theta}{2}\right)\left(J_1\left(2kR\sin\frac{\Delta\theta}{2}\right) + J_3\left(2kR\sin\frac{\Delta\theta}{2}\right)\right)^2}{1 - \left(J_0\left(2kR\sin\frac{\Delta\theta}{2}\right) + J_2\left(2kR\sin\frac{\Delta\theta}{2}\right)\right)^2}\right)^{-1} \\
&\approx \frac{\sigma^2}{QN}\frac{2}{k^2R^2}\left(1 - \frac{\left(J_1\left(kR\Delta\theta\right) + J_3\left(kR\Delta\theta\right)\right)^2}{1 - \left(J_0\left(kR\Delta\theta\right) + J_2\left(kR\Delta\theta\right)\right)^2}\right)^{-1} \qquad \text{(B.44)}
\end{aligned}
$$

with the approximation valid for small angular separations $\Delta\theta$.

Bibliography

[1] J. C. Maxwell, "A dynamical theory of the electromagnetic field," *Philosophical Trans. of the Royal Society of London*, vol. 155, pp. 459–512, 1865.

[2] Wikipedia contributors, "Mobile phone. from Wikipedia, the free encyclopedia," 2007. `http://en.wikipedia.org/wiki/Mobile_phone`.

[3] C. E. Shannon, "A mathematical theory of communication," *Bell System Technical Journal*, vol. 27, pp. 379–423,623–656, 1948.

[4] W. C. Jakes, *Microwave Mobile Communications*. New York: Wiley, 1974.

[5] J. Winters, "On the capacity of radio communication systems with diversity in a Rayleigh fading environment," *IEEE Journal on Selected Areas in Communications*, vol. 5, no. 5, pp. 871–878, 1987.

[6] I. E. Telatar, "Capacity of multi-antenna Gaussian channels," Technical Report, AT&T-Bell Labs, June 1995.

[7] G. J. Foschini, "Layered space-time architecture for wireless communication in a fading environment when using multi-element antennas," *Bell Labs Technical Journal*, vol. 1, no. 2, pp. 41–59, 1996.

[8] P. Wolniansky, G. Foschini, G. Golden, and R. Valenzuela, "V-BLAST: An architecture for realizing very high data rates over the rich-scattering wireless channel," in *IEEE International Symposium of Signals, Systems and Electronics (ISSSE 1998)*, (Pisa, Italy), pp. 295–300, 1998.

[9] G. Golden, C. Foschini, R. Valenzuela, and P. Wolniansky, "Detection algorithm and initial laboratory results using V-BLAST space-time communication architecture," *Electronics Letters*, vol. 35, no. 1, pp. 14–16, 1999.

[10] T. Marzetta and B. Hochwald, "Capacity of a mobile multiple-antenna communication link in Rayleigh flat fading," *IEEE Trans. Information Theory*, vol. 45, no. 1, pp. 139–157, 1999.

[11] R. Gallager, *Information Theory and Reliable Communication*. New York, USA: Wiley, 1968.

[12] G. Raleigh and J. Cioffi, "Spatio-temporal coding for wireless communications," in *Global Telecommunications Conference (GLOBECOM 1996)*, vol. 3, (London, UK), pp. 1809–1814, 1996.

[13] G. J. Foschini and M. J. Gans, "On limits of wireless communications in a fading environment when using multiple antennas," *Wireless Personal Communications*, vol. 6, no. 3, 1998.

[14] G. Raleigh and J. Cioffi, "Spatio-temporal coding for wireless communication," *IEEE Trans. Communications*, vol. 46, no. 3, pp. 357–366, 1998.

[15] A. Goldsmith, S. Jafar, N. Jindal, and S. Vishwanath, "Capacity limits of MIMO channels," *IEEE Journal on Selected Areas in Communications*, vol. 21, no. 5, pp. 684–702, 2003.

[16] D. A. Miller and R. Pietsum, "Electromagnetic degrees of freedom of an optical system," *Journal of the Optical Society of America*, vol. 17, no. 6, pp. 892–902, 2000.

[17] D. A. Miller, "Communicating with waves between volumes: evaluating orthogonal spatial channels and limits on coupling strengths," *Applied Optics*, vol. 39, no. 11, pp. 1681–1699, 2000.

[18] L. Hanlen, *Channel Modelling and Capacity Analysis for Multi-input, Multi-output, Wireless Communication Systems*. PhD thesis, University of Newcastle, Australia, 2003.

[19] D. Chizhik, F. Rashid-Farrokhi, J. Ling, and A. Lozano, "Effect of antenna separation on the capacity of blast in correlated channels," *IEEE Communications Letters*, vol. 4, no. 11, pp. 337–339, 2000.

[20] S. L. Loyka, "Channel capacity of MIMO architecture using the exponential correlation matrix," *IEEE Communications Letters*, vol. 5, no. 9, pp. 369–371, 2001.

[21] C. N. Chuah, D. S. E. Tse, J. M. Kahn, and R. A. Valenzuela, "Capacity scaling in MIMO wireless systems under correlated fading," *IEEE Trans. Information Theory*, vol. 48, no. 3, pp. 637–650, 2002.

[22] D. Gesbert, H. Bolcskei, D. Gore, and A. Paulraj, "Outdoor MIMO wireless channels: models and performance prediction," *IEEE Trans. Communications*, vol. 50, no. 12, pp. 1926–1934, 2002.

[23] J. Kermoal, L. Schumacher, K. Pedersen, P. Mogensen, and F. Frederiksen, "A stochastic MIMO radio channel model with experimental validation," *IEEE Journal on Selected Areas in Communications*, vol. 20, no. 6, pp. 1211–1226, 2002.

[24] H. Shin and J. H. Lee, "Capacity of multiple-antenna fading channels: spatial fading correlation, double scattering, and keyhole," *IEEE Trans. Information Theory*, vol. 49, no. 10, pp. 2636–2647, 2003.

[25] N. Chiurtu, B. Rimoldi, E. Telatar, and V. Pauli, "Impact of correlation and coupling on the capacity of MIMO systems," in *IEEE Symposium on Signal Processing and Information Technology (ISSPIT 2003)*, (Darmstadt, Germany), 2003.

[26] K. Yu, M. Bengtsson, B. Ottersten, D. McNamara, P. Karlsson, and M. Beach, "Second order statistics of NLOS indoor MIMO channels based on 5.2 GHz measurements," in *IEEE Global Telecommunications Conference (GLOBECOM 2001)*, vol. 1, pp. 156–160, 2001.

[27] J. Wallace and M. Jensen, "Modeling the indoor MIMO wireless channel," *IEEE Trans. Antennas and Propagation*, vol. 50, no. 5, pp. 591–599, 2002.

[28] A. Molisch, M. Steinbauer, M. Toeltsch, E. Bonek, and R. Thoma, "Capacity of MIMO systems based on measured wireless channels," *IEEE Journal on Selected Areas in Communications*, vol. 20, no. 3, pp. 561–569, 2002.

[29] J. Wallace, M. Jensen, A. Swindlehurst, and B. Jeffs, "Experimental characterization of the mimo wireless channel: data acquisition and analysis," *IEEE Trans. Wireless Communications*, vol. 2, no. 2, pp. 335–343, 2003.

[30] D. Shiu, G. J. Foschini, M. J. Gans, and J. M. Kans, "Fading correlation and its effect on the capacity of multielement antenna systems," *IEEE Trans. Communications*, vol. 48, no. 3, pp. 502–513, 2000.

[31] A. Abdi, J. Barger, and M. Kaveh, "A parametric model for the distribution of the angle of arrival and the associated correlation function and power spectrum at the mobile station," *IEEE Trans. Vehicular Technology*, vol. 51, no. 3, pp. 425–434, 2002.

[32] M. Kang and M. S. Alouini, "Largest eigenvalue of complex Wishart matrices and performance analysis of MIMO MRC systems," *IEEE Journal on Selected Areas in Communications*, vol. 21, no. 3, pp. 418–426, 2003.

[33] I. E. Telatar and D. N. C. Tse, "Capacity and mutual information of wideband multipath fading channels," *IEEE Trans. Information Theory*, vol. 46, no. 4, pp. 1384–1400, 2000.

[34] S. Loyka and A. Kouki, "New compound upper bound on MIMO channel capacity," *IEEE Communications Letters*, vol. 6, no. 3, pp. 96–98, 2002.

[35] M. Chiani, M. Z. Win, and A. Zanella, "On the capacity of spatially correlated MIMO Rayleigh-fading channels," *IEEE Trans. Information Theory*, vol. 49, no. 10, pp. 2363–2371, 2003.

[36] S. Jafar and A. Goldsmith, "Multiple-antenna capacity in correlated Rayleigh fading with channel covariance information," *IEEE Trans. Wireless Communications*, vol. 4, no. 3, pp. 990–997, 2005.

[37] D. Chizhik, G. Foschini, M. Gans, and R. Valenzuela, "Keyholes, correlations, and capacities of multielement transmit and receive antennas," *IEEE Trans. Wireless Communications*, vol. 1, no. 2, pp. 361–368, 2002.

[38] S. Loyka and A. Kouki, "On MIMO channel capacity, correlations, and keyholes: analysis of degenerate channels," *IEEE Trans. Communications*, vol. 50, no. 12, pp. 1886–1888, 2002.

[39] E. Bonek, M. Herdin, W. Weichselberger, and H. Ozcelik, "MIMO - study propagation first!," in *IEEE International Symposium on Signal Processing and Information Technology (ISSPIT 2003)*, pp. 150–153, 2003.

[40] P. Almers, F. Tufvesson, and A. Molisch, "Measurement of keyhole effect in a wireless multiple-input multiple-output (MIMO) channel," *IEEE Communications Letters*, vol. 7, no. 8, pp. 373–375, 2003.

[41] H. M. Jones, R. A. Kennedy, and T. D. Abhayapala, "On dimensionality of multipath fields: Spatial extent and richness," in *IEEE Conference on Acoustics, Speech and Signal Processing (ICASSP 2002)*, (Orlando, Florida), 2002.

[42] R. A. Kennedy, T. D. Abhayapala, and H. M. Jones, "Bounds on the spatial richness of multipath," in *Proc. 3rd Australian Communications Theory Workshop (AusCTW 2002)*, (Canberra, Australia), pp. 76–80, 2002.

[43] S. Poon, R. Brodersen, and N. Tse, "The signal dimensions in multiple-antenna channels," in *IEEE Global Telecommunications Conference (GLOBECOM 2003)*, vol. 3, (San Fransisco), pp. 1247–1251, 2003.

[44] T. D. Abhayapala, T. S. Pollock, and R. A. Kennedy, "Spatial decomposition of MIMO wireless channels," in *International Symposium on Signal Processing and its Applications (ISSPA 2003)*, vol. 1, (Paris), pp. 309–312, 2003.

[45] A. L. Moustakas, H. U. Baranger, L. Balents, A. M. Sengupta, and S. H. Simon, "Communication through a diffusive medium: coherence and capacity," *Science*, vol. 287, no. 1, pp. 287–290, 2000.

[46] J. Hui, C. Bi, and H. Sun, "Spatial communication capacity based on electromagnetic wave equations," in *IEEE International Symposium on Information Theory (ISIT 2001)*, (Washington), p. 342, 2001.

[47] T. S. Pollock, T. D. Abhayapala, and R. A. Kennedy, "Introducing space into MIMO capacity calculations," *Telecommunications Systems*, vol. 24, no. 2, pp. 415–436, 2003.

[48] T. S. Pollock, T. D. Abhayapala, and R. A. Kennedy, "Spatial characterization of multiple antenna channels," in *Signal Processing for Telecommunications and Multimedia* (T. A. Wysocki, B. Honary, and B. J. Wysocki, eds.), pp. 145–158, Kluwer Academic Publishers, 2004.

[49] A. Naguib, N. Seshadri, and A. Calderbank, "Increasing data rate over wireless channels," *IEEE Signal Processing Magazine*, vol. 17, no. 3, pp. 76–92, 2000.

[50] D. Gesbert, M. Shafi, D. Shiu, P. Smith, and A. Naguib, "From theory to practice: an overview of MIMO space-time coded wireless systems," *IEEE Journal on Selected Areas in Communications*, vol. 21, no. 3, pp. 281–302, 2003.

[51] A. Paulraj, D. Gore, R. Nabar, and H. Bolcskei, "An overview of MIMO communications - a key to gigabit wireless," *Proceedings of the IEEE*, vol. 92, no. 2, pp. 198–218, 2004.

[52] R. W. Heath, E. G. Larsson, R. Murch, A. Nehorai, and M. Uysal, "Special issue: Multiple-input multiple-output MIMO communications," *Wireless Communications and Mobile Computing*, vol. 4, no. 7, pp. 693–696, 2004.

[53] M. S. Alouini, A. Molisch, and R. Valenzuela, "Special issue: Adaptive antennas and MIMO systems," *Wireless Communications and Mobile Computing*, vol. 2, no. 7, pp. 651–652, 2002.

[54] S. Barbarossa, C. Papadias, H. Vincent-Poor, and X. Wang, "Special issue: MIMO communications and signal processing," *EURASIP Journal on Applied Signal Processing*, vol. 2004, no. 5, pp. 587–590, 2004.

[55] R. Blum, H. Bolcskei, M. Fitz, B. Hughes, and A. Paulraj, "Guest editorial special issue on mimo wireless communications," *IEEE Trans. Signal Processing*, vol. 51, no. 11, p. 2709, 2003.

[56] M. Shafi, D. Gesbert, D. Shiu, P. Smith, and W. Tranter, "Guest editorial: MIMO systems and applications. I," *Selected Areas in Communications, IEEE Journal on*, vol. 21, no. 3, pp. 277–280, 2003.

[57] M. Shafi, D. Gesbert, D. Shiu, P. Smith, and W. Tranter, "Guest editorial: MIMO systems and applications. II," *Selected Areas in Communications, IEEE Journal on*, vol. 21, no. 5, pp. 681–683, 2003.

[58] G. D. Durgin, *Space-time wireless channels*. Prentice Hall communications engineering and emerging technologies series., Upper Saddle River, NJ: Prentice Hall PTR, 2003.

[59] M. Jankiraman, *Space-time codes and MIMO systems*. Artech House universal personal communications series., Boston: Artech House, 2004.

[60] A. Paulraj, R. Nabar, and D. Gore, *Introduction to space-time wireless communications*. Cambridge ; New York: Cambridge University Press, 2005.

[61] A. Gershman and N. Sidiropoulos, *Space-Time Processing for MIMO Communications*. West Sussex, England: John Wiley and Sons, 2005.

[62] G. V. Tsoulos, *MIMO System Technology for Wireless Communciations*. Boca Raton: Taylor and Francis, 2006.

[63] H. Ozcelik, N. Czink, and E. Bonek, "What makes a good MIMO channel model?," in *IEEE Vehicular Technology Conference (VTC 2005 Spring)*, vol. 1, (Stockholm), pp. 156–160, 2005.

[64] K. Yu and B. Ottersen, "Models for MIMO propagation channels: a review," *Wireless Communications and Mobile Computing*, vol. 2, pp. 653–666, 2002.

[65] M. A. Jensen and J. W. Wallace, "MIMO wireless channel modeling and experimental characterization," in *Space-Time Processing for MIMO Communications* (A. B. Gersham and N. D. Sidropoukos, eds.), John Wiley and Sons, 2005.

[66] A. Sayeed, "Deconstructing multiantenna fading channels," *IEEE Trans. Signal Processing*, vol. 50, no. 10, pp. 2563–2579, 2002.

[67] W. Weichselberger, M. Herdin, H. Ozcelik, and E. Bonek, "A stochastic MIMO channel model with joint correlation of both link ends," *IEEE Trans. Wireless Communications*, vol. 5, no. 1, pp. 90–100, 2006.

[68] H. Ozcelik, M. Herdin, W. Weichselberger, J. Wallace, and E. Bonek, "Deficiencies of 'Kronecker' MIMO radio channel model," *Electronics Letters*, vol. 39, no. 16, pp. 1209–1210, 2003.

[69] T. S. Pollock, "Correlation modelling in MIMO systems: When can we Kronecker?," in *Australian Communications Theory Workshop (AusCTS 2004)*, (Newcastle), pp. 149–153, 2004.

[70] M. Steinbauer, A. Molisch, and E. Bonek, "The double-directional radio channel," *IEEE Antennas and Propagation Magazine*, vol. 43, no. 4, pp. 51–63, 2001.

[71] A. Saleh and R. Valenzuela, "A statistical model for indoor multipath propagation," *IEEE Journal on Selected Areas in Communications*, vol. 5, no. 2, pp. 128–137, 1987.

[72] A. Abdi and M. Kaveh, "A space-time correlation model for multielement antenna systems in mobile fading channels," *IEEE Journal on Selected Areas in Communications*, vol. 20, no. 3, pp. 550–560, 2002.

[73] R. Ertel, P. Cardieri, K. Sowerby, T. Rappaport, and J. Reed, "Overview of spatial channel models for antenna array communication systems," *IEEE Personal Communications*, vol. 5, no. 1, pp. 10–22, 1998.

[74] K. Pedersen, P. Mogensen, and B. Fleury, "Power azimuth spectrum in outdoor environments," *Electronics Letters*, vol. 33, no. 18, pp. 1583–1584, 1997.

[75] T. Zwick, C. Fischer, D. Didascalou, and W. Wiesbeck, "A stochastic spatial channel model based on wave-propagation modeling," *IEEE Journal on Selected Areas in Communications*, vol. 18, no. 1, pp. 6–15, 2000.

[76] T. Fgen, J. Maurer, T. Kayser, and W. Wiesbeck, "Verification of 3D ray-tracing with non-directional and directional measurements in urban macrocellular environments," in *IEEE Vehicular Technology Conference (VTC 2006 Spring)*, (Melbourne, Australia), 2006.

[77] "Spatial channel model for MIMO simulations," tech. rep., 3GPP Organizational Partners, September 2003. 3GPP-TR-25.996 Release 6 `http://www.3gpp.org`.

[78] T. D. Abhayapala, T. S. Pollock, and R. A. Kennedy, "Characterization of 3D spatial wireless channels," in *Proc. IEEE Vehicular Technology Conference (VTC 2006 Fall)*, vol. 1, (Orlando), pp. 123–127, 2003.

[79] T. S. Pollock, *On Limits of Multi-Antenna Wireless Communications in Spatially Selective Channels*. Phd, The Australian National University, 2003.

[80] R. A. Kennedy and T. D. Abhayapala, "Spatial concentration of wave-fields: Towards spatial information content in arbitrary multipath scattering," in *Proc. 4th Australian Communications Theory Workshop (AusCTW 2003)*, (Melbourne, Australia), pp. 38–45, 2003.

[81] R. A. Kennedy, P. Sadeghi, T. D. Abhayapala, and H. M. Jones, "Intrinsic limits of dimensionality and richness in random multipath fields," *IEEE Trans. Signal Processing*, vol. 55, no. 6, pp. 2542–2556, 2007.

[82] T. S. Pollock, T. D. Abhayapala, and R. A. Kennedy, "Fundamental limits of MIMO capacity for spatially constrained arrays," in *Proc. 4th Australian Communications Theory Workshop (AusCTW 2003)*, (Melbourne, Australia), pp. 7–12, 2003.

[83] T. S. Pollock, M. I. Y. Williams, and T. D. Abhayapala, "Spatial limits to mutual information scaling in multi-antenna systems," in *IEEE ICASP*, (Pennsylvania, PA), 2005.

[84] A. Poon, R. Brodersen, and D. Tse, "Degrees of freedom in multiple-antenna channels: a signal space approach," *IEEE Trans. Information Theory*, vol. 51, no. 2, pp. 523–536, 2005.

[85] D. Slepian, "On bandwidth," *Proceedings of the IEEE*, vol. 64, no. 3, pp. 292–300, 1976.

[86] M. Jensen and J. Wallace, "A review of antennas and propagation for MIMO wireless communications," *IEEE Trans. Antennas and Propagation*, vol. 52, no. 11, pp. 2810–2824, 2004.

[87] C. A. Coulson, *Waves: A mathematical account of the common types of wave motion*. London: Longman Group Ltd., 1977.

[88] G. R. Baldock and T. Bridgeman, *Mathematical theory of wave motion*. Chichester: Ellis Horwood, 1981.

[89] E. Kreyszig, *Advanced engineering mathematics*. New York: John Wiley, 8th ed., 1999.

[90] W. C. Elmore and M. A. Heald, *Physics of waves*. New York: Dover Publications, 1985.

[91] D. L. Colton and R. Kress, *Inverse acoustic and electromagnetic scattering theory*. Berlin: Springer, 1998.

[92] P. M. Morse and K. U. Ingard, *Theoretical Acoustics*. New York: McGraw-Hill, 1968.

[93] A. S. Y. Poon, *Use of Spatial Dimension for Spectrum Sharing*. Phd, University of California, Berkeley, 2004.

[94] R. Vaughan, "Polarization diversity in mobile communications," *IEEE Trans. Vehicular Technology*, vol. 39, no. 3, pp. 177–186, 1990.

[95] M. R. Andrews, P. P. Mitra, and R. deCarvalho, "Tripling the capacity of wireless communications using electromagnetic polarization," *Nature*, vol. 409, pp. 316–318, 2001.

[96] S. Krishnamurthy, A. Konanur, G. Lazzi, and B. Hughes, "On the capacity of vector antenna MIMO systems," in *International Symposium on Information Theory (ISIT 2004)*, (Chicago, Illinois), p. 240, 2004.

[97] T. Svantesson, M. Jensen, and J. Wallace, "Analysis of electromagnetic field polarizations in multiantenna systems," *IEEE Trans. Wireless Communications*, vol. 3, no. 2, pp. 641–646, 2004.

[98] R. Nabar, H. Bolcskei, V. Erceg, D. Gesbert, and A. Paulraj, "Performance of multiantenna signaling techniques in the presence of polarization diversity," *IEEE Trans. Signal Processing*, vol. 50, no. 10, pp. 2553–2562, 2002.

[99] N. Das, T. Inoue, T. Taniguchi, and Y. Karasawa, "An experiment on MIMO system having three orthogonal polarization diversity branches in multipath-rich environment," in *IEEE Vehicular Technology Conference (VTC 2004 Fall)*, vol. 2, (Los Angeles), pp. 1528–1532, 2004.

[100] L. Dong, H. Choo, J. Heath, R.W., and H. Ling, "Simulation of MIMO channel capacity with antenna polarization diversity," *IEEE Trans. Wireless Communications*, vol. 4, no. 4, pp. 1869–1873, 2005.

[101] A. Konanur, K. Gosalia, S. Krishnamurthy, B. Hughes, and G. Lazzi, "Increasing wireless channel capacity through MIMO systems employing co-located antennas," *IEEE Trans. Microwave Theory and Techniques*, vol. 53, no. 6, pp. 1837–1844, 2005.

[102] T. Svantesson, "Multimode based direction finding," in *Asilomar Conference on Signals, Systems and Computers*, vol. 1, (Pacific Grove, California), pp. 595–599, 2000.

[103] M. Shafi, M. Zhang, A. Moustakas, P. Smith, A. Molisch, F. Tufvesson, and S. Simon, "Polarized MIMO channels in 3-D: models, measurements and mutual information," *IEEE Journal on Selected Areas in Communications*, vol. 24, no. 3, pp. 514–527, 2006.

[104] T. Svantesson and A. Ranheim, "Mutual coupling effects on the capacity of multielement antenna systems," in *IEEE International Converence on Acoustics, Speech, and Signal Processing (ICASSP 2001)*, vol. 4, (Salt Lake City, Utah), pp. 2485–2488, 2001.

[105] C. Borja, A. Algans, M. Royo, J. Anguera, and C. Puente, "Impact of the antenna technology and the antenna parameters on the performance of MIMO systems," in *IEEE Antennas and Propagation Society International Symposium*, vol. 2, (Columbus, Ohio), pp. 507–510, 2003.

[106] J. Wallace and M. Jensen, "The capacity of MIMO wireless systems with mutual coupling," in *IEEE Vehicular Technology Conference (VTC 2002 Spring)*, vol. 2, (Vancouver), pp. 696–700, 2002.

[107] V. Jungnickel, V. Pohl, and C. von Helmolt, "Capacity of MIMO systems with closely spaced antennas," *IEEE Communications Letters*, vol. 7, no. 8, pp. 361–363, 2003.

[108] P. Fletcher, M. Dean, and A. Nix, "Mutual coupling in multi-element array antennas and its influence on MIMO channel capacity," *Electronics Letters*, vol. 39, no. 4, pp. 342–344, 2003.

[109] R. Janaswamy, "Effect of element mutual coupling on the capacity of fixed length linear arrays," *Antennas and Wireless Propagation Letters*, vol. 1, pp. 157–160, 2002.

[110] P.-S. Kildal and K. Rosengren, "Correlation and capacity of MIMO systems and mutual coupling, radiation efficiency, and diversity gain of their antennas: simulations and measurements in a reverberation chamber," *IEEE Communications Magazine*, vol. 42, no. 12, pp. 104–112, 2004.

[111] B. Lau, S. Ow, G. Kristensson, and A. Molisch, "Capacity analysis for compact MIMO systems," in *IEEE Vehicular Technology Conference VTC 2005 Spring)*, vol. 1, (Stockholm, Sweden), pp. 165–170, 2005.

[112] X. Li and Z.-P. Nie, "Mutual coupling effects on the performance of MIMO wireless channels," *Antennas and Wireless Propagation Letters*, vol. 3, pp. 344–347, 2004.

[113] M. Ozdemir, H. Arslan, and E. Arvas, "Mutual coupling effect in multiantenna wireless communication systems," in *IEEE Global Telecommunications Conference (GLOBECOM 2003)*, vol. 2, (San Fransisco), pp. 829–833, 2003.

[114] C. Waldschmidt, S. Schulteis, and W. Wiesbeck, "Complete RF system model for analysis of compact MIMO arrays," *IEEE Trans. Vehicular Technology*, vol. 53, no. 3, pp. 579–586, 2004.

[115] J. Wallace and M. Jensen, "Mutual coupling in MIMO wireless systems: a rigorous network theory analysis," *IEEE Trans. Wireless Communications*, vol. 3, no. 4, pp. 1317–1325, 2004.

[116] H. Chaloupka and X. Wang, "Novel approach for diversity and MIMO antennas at small mobile platforms," in *IEEE International Symposium on Personal, Indoor and Mobile Radio Communications (PIMRC 2004)*, vol. 1, (Barcelona), pp. 637–642, 2004.

[117] M. Morris, M. Jensen, and J. Wallace, "Superdirectivity in MIMO systems," *IEEE Trans. Antennas and Propagation*, vol. 53, no. 9, pp. 2850–2857, 2005.

[118] R. Q. Twiss, "Nyquists's and Thevenin's theorems generalized for nonreciprocal linear networks," *Journal of Applied Physics*, vol. 26, no. 5, pp. 599–602, 1955.

[119] S. Krusevac, P. Rapajic, R. Kennedy, and P. Sadeghi, "Mutual coupling effect on thermal noise in multi-antenna wireless communication systems," in *Proceedings of the 6th Australian Communications Theory Workshop (AusCTW 2005)*, (Brisbane, Australia), pp. 209–214, 2005.

[120] S. Krusevac, P. Rapajic, and R. Kennedy, "Channel capacity estimation for MIMO systems with correlated noise," in *IEEE Global Telecommunications Conference (GLOBECOM 2005)*, vol. 5, (St Louise, Missouri), pp. 2812–2816, 2005.

[121] I. P. Kovalyov, *SDMA for Multipath Wireless Channels, Limiting Characteristics and Stochastic Models*. Berlin: Springer-Verlag, 2004.

[122] T. S. Pollock, T. D. Abhayapala, and R. A. Kennedy, "Antenna saturation effects on MIMO capacity," in *IEEE International Conference on Communications (ICC 2003)*, vol. 4, (Anchorage, Alaska), pp. 2301–2305, 2003.

[123] T. S. Pollock, T. D. Abhayapala, and R. A. Kennedy, "Antenna saturation effects on dense array mimo capacity," in *IEEE Conference on Acoustics, Speech, and Signal Processing (ICASSP 2003)*, vol. 4, (Hong Kong), pp. 361–364, 2003.

[124] T. S. Pollock, T. D. Abhayapala, and R. A. Kennedy, "Limits to multiantenna capacity of spatially selective channels," in *IEEE International Symposium on Information Theory (ISIT 2004)*, (Chicago), p. 244, 2004.

[125] G. Dickins, T. Betlehem, and L. W. Hanlen, "A stochastic MIMO model utilising spatial dimensionality and modes," in *IEEE Vehicular Technology Conference (VTC 2006 Spring)*, (Melbourne, Australia), 2006.

[126] P. Teal and R. Kennedy, "Bounds on extrapolation of field knowledge for long-range prediction of mobile signals," *IEEE Trans. Wireless Communications*, vol. 3, no. 2, pp. 672–676, 2004.

[127] M. Williams, G. Dickins, R. Kennedy, T. Pollock, and T. Abhayapala, "Novel scheme for spatial extrapolation of multipath," in *2005 Asia-Pacific Conference on Communications (APCC 2005)*, pp. 784–787, 2005.

[128] O. Birkenes, R. A. Kennedy, and T. S. Pollock, "Spatial limits for direction of arrival estimation for narrowband wireless communication," in *Nordic Signal Processing Conference*, (Bergen, Norway), 2003.

[129] M. I. Y. Williams, G. Dickins, R. A. Kennedy, and T. D. Abhayapala, "Spatial limits on the performance of direction of arrival estimation," in *Proceedings of the 6th Australian Communications Theory Workshop (AusCTW 2005)*, (Brisbane, Australia), pp. 189–194, 2005.

[130] A. Poon, D. Tse, and R. Brodersen, "Impact of scattering on the capacity, diversity, and propagation range of multiple-antenna channels," *IEEE Trans. Information Theory*, vol. 52, no. 3, pp. 1087–1100, 2006.

[131] O. M. Bucci and G. Franceschetti, "On the spatial bandwidth of scattered fields," *IEEE Trans. Antennas and Propagation*, vol. 35, no. 12, pp. 1445–1455, 1987.

[132] O. M. Bucci and G. Franceschetti, "On the degrees of freedom of scattered fields," *IEEE Trans. Antennas and Propagation*, vol. 37, no. 7, pp. 918–926, 1989.

[133] O. M. Bucci, C. Gennarelli, and C. Savarese, "Representation of electromagnetic fields over arbitrary surfaces by a finite and nonredundant number of samples," *IEEE Trans. Antennas and Propagation*, vol. 46, no. 3, pp. 351–359, 1998.

[134] N. Chiurtu, B. Rimoldi, and I. E. Telatar, "Dense multiple antenna systems," in *IEEE Information Theory Workshop (ITW 2001)*, (Cairns, Australia), 2001.

[135] L. Hanlen, A. J. Grant, and R. Kennedy, "On the capacity of operator channels," in *Autralian Communications Theory Workshop (AusCTW 04)*, (Newcastle, Australia), IEEE, 2004.

[136] S. Loyka, "On MIMO channel capacity, spatial sampling and the laws of electromagnetism," in *IASTED International Conference on Wireless and Optical Communications*, (Banff, Canada), pp. 132–137, 2003.

[137] S. Loyka, "Information theory and electromagnetism: Are they related?," in *International Symposium on Antenna Technology and Applied Electromagnetics*, (Ottowa), 2004.

[138] J. Wallace and M. Jensen, "Intrinsic capacity of the MIMO wireless channel," in *IEEE Vehicular Technology Conference (VTC 2002 Fall)*, vol. 2, (Chicago), pp. 701–705, 2002.

[139] J. Wallace and M. Jensen, "Intrinsic capacity of the MIMO wireless channel," in *IEEE Antennas and Propagation Society International Symposium*, vol. 3, p. 198, 2002.

[140] L. Hanlen and M. Fu, "On point-wise models for MIMO wireless systems," in *IEEE Global Telecommunications Conference (GLOBECOM 2004)*, vol. 1, (Dallas, Texas), pp. 76–80, 2004.

[141] M. Jensen and J. Wallace, "Antenna-independent capacity bound of electromagnetic channels," in *IEEE Antennas and Propagation Society International Symposium*, vol. 2A, (Washington DC), pp. 317–320, 2005.

[142] D. Slepian and H. O. Pollak, "Prolate spheroidal wave functions, fourier analysis and uncertainty - I," *Bell Systems Technical Journal*, vol. 40, pp. 45–63, 1961.

[143] H. J. Landau and H. O. Pollak, "Prolate spheroidal wave functions, fourier analysis and uncertainty - II," *Bell Systems Technical Journal*, vol. 40, pp. 65–84, 1961.

[144] H. J. Landau and H. O. Pollak, "Prolate spheroidal wave functions, fourier analysis and uncertainty - III," *Bell Systems Technical Journal*, pp. 1295–1336, 1962.

[145] D. Slepian, "Some asymptotic expansions for prolate spheroidal wave functions," *Journal of Mathematical Physics*, vol. 44, pp. 99–143, 1965.

[146] L. Hanlen and M. Fu, "Wireless communications systems with spatial diversity: a volumetric approach," in *IEEE International Conference on Communications (ICC 2003)*, vol. 4, (Seattle), pp. 2673–2677, 2003.

[147] D. E. N. Davies, "A transformation between the phasing techniques required for linear and circular aerial arrays," *Proc. Institute of Electrical Engineers*, vol. 112, pp. 2041—2045, 1966.

[148] R. E. Collin and F. J. Zucker, *Antenna theory*, vol. 1. New York: McGraw-Hill, 1969.

[149] J. N. Maksym, "Directional accuracy of small ring arrays," *Journal of the Acoustical Society of America*, vol. 61, no. 1, pp. 105–109, 1977.

[150] M. Wax and J. Sheinvald, "Direction finding of coherent signals via spatial smoothing for uniform circular arrays," *IEEE Trans. Antennas and Propagation*, vol. 42, no. 5, pp. 613–620, 1994.

[151] C. Mathews and M. Zoltowski, "Eigenstructure techniques for 2D angle estimation with uniform circular arrays," *IEEE Trans. Signal Processing*, vol. 42, no. 9, pp. 2395–2407, 1994.

[152] C. Ma, Y. Peng, and L. Tian, "An improved MODE algorithm for DOA estimation based on UCA," in *IEEE Region 10 Annual Conference on Speech and Image Technologies for Computing and Telecommunications*, vol. 2, (Brisbane, Australia), pp. 811–814, 1997.

[153] J. Rossi, J.-P. Barbot, and A. Levy, "Theory and measurement of the angle of arrival and time delay of UHF radiowaves using a ring array," *IEEE Trans. Antennas and Propagation*, vol. 45, no. 5, pp. 876–884, 1997.

[154] D. Swingler and S. Davies, "Spatial harmonic interpolation and extrapolation for use with circular arrays," in *IEEE Pacific Rim Conference on Communications, Computers and Signal Processing*, (Victoria, Canada), pp. 138–141, 1991.

[155] A. Tewfik and W. Hong, "On the application of uniform linear array bearing estimation techniques to uniform circular arrays," *IEEE Trans. Signal Processing*, vol. 40, no. 4, pp. 1008–1011, 1992.

[156] G. Dickins and L. Hanlen, "Fast calculation of singular values for MIMO wireless systems," in *Proceedings 5th Australian Communications Theory Workshop (AusCTW 2004)* (R. A. Kennedy and A. J. Grant, eds.), (Canberra, Australia), pp. 185–190, 2004.

[157] G. Dickins, M. Williams, and L. W. Hanlen, "On the dimensionality of spatial fields with restricted angle of arrival," in *IEEE International Symposium on Information Theory (ISIT 2005)*, (Adelaide), pp. 1033–1037, 2005.

[158] G. Dickins and L. Hanlen, "On finite dimensional approximation in MIMO," in *2005 Asia-Pacific Conference on Communications (APCC 2005)*, (Perth, Australia), pp. 710–714, 2005.

[159] L. E. Franks, *Signal Theory*. Prentice-Hall, 1969.

[160] M. Abramowitz and I. A. Stegun, *Handbook of mathematical functions with formulas, graphs, and mathematical tables*. Washington: U.S. Govt. Print. Off., 1970.

[161] G. Arfken and H. J. Weber, *Mathematical Methods for Physicists*. New York: Academic Press, 4th ed., 1995.

[162] M. Abramowitz and Y. L. Luke, *Mathematical functions and their approximations*. New York: Academic Press, 1975.

[163] N. W. McLachlan, *Bessel functions for engineers*. Oxford engineering science series., Clarendon Press, 1961.

[164] I. S. Gradshteyn, I. M. Ryzhik, A. Jeffrey, and D. Zwillinger, *Table of Integrals, Series, and Products*. San Diego: Academic Press, 2000.

[165] R. A. Kennedy, T. D. Abhayapala, and T. S. Pollock, "Modeling multipath scattering environments using generalized Herglotz wave functions," in *Proc. 4th Australian Communications Theory Workshop (AusCTW 2003)*, (Melbourne, Australia), pp. 87–92, 2003.

[166] B. Carl and I. Stephani, *Entropy, compactness, and the approximation of operators*. Cambridge tracts in mathematics ; 98., Cambridge ; New York: Cambridge University Press, 1990.

[167] D. Slepian, "Prolate spheroidal wave functions, fourier analysis, and uncertainty - V: The discrete case," *Bell Systems Technical Journal*, vol. 57, no. 5, pp. 1371–1430, 1978.

[168] S. Dharanipragada and K. S. Arun, "Bandlimited extrapolation using time-bandwidth dimension," *IEEE Trans. Signal Processing*, vol. 45, no. 12, pp. 2951–2966, 1997.

[169] T. Zemen and C. F. Mecklenbruker, "Doppler diversity in MC-CDMA using the Slepian basis expansion model," in *European Signal Processing Conference (EUSIPCO 2004)*, (Vienna, Austria), 2004.

[170] H. Hofstetter, T. Zemen, J. Wehinger, and G. Steinbck, "Iterative MIMO multi-user detection: Performance evaluation with COST 259 channel model," in *Wireless Personal Multimedia Communications (WPMC 2004)*, (Abano Terme, Italy), 2004.

[171] I. C. Moore and M. Cada, "Prolate spheroidal wave functions, an introduction to the Slepian series and its properties," *Applied Computational Harmonic Analysis*, vol. 16, pp. 208–230, 2004.

[172] T. Fulghum and K. Molnar, "The Jakes fading model incorporating angular spread for a disk of scatterers," in *IEEE Vehicular Technology Conference (VTC 1998 Spring)*, vol. 1, (Ottawa, Canata), pp. 489–493, 1998.

[173] T. Fulghum, K. Molnar, and A. Duel-Hallen, "The Jakes fading model for antenna arrays incorporating azimuth spread," *IEEE Trans. Vehicular Technology*, vol. 51, no. 5, pp. 968–977, 2002.

[174] P. D. Teal, T. D. Abhayapala, and R. A. Kennedy, "Spatial correlation for general distributions of scatterers," *IEEE Signal Processing Letters*, vol. 9, no. 10, pp. 305–308, 2002.

[175] H. Rad and S. Gazor, "A 3D correlation model for MIMO non-isotropic scattering with arbitrary antenna arrays," in *IEEE Wireless Communications and Networking Conference (WCNC 2005)*, vol. 2, pp. 938–943, 2005.

[176] G. Dickins and R. A. Kennedy, "Angular domain representation of a random multipath field," *Submitted 2007*, 2007.

[177] E. G. Williams, *Fourier Acoustics - Sound Radiation and Nearfield Acoustical Holography*. London: Academic Press, 1999.

[178] P. Bello, "Characterization of randomly time-variant linear channels," *IEEE Trans. on Communications*, vol. 11, no. 4, pp. 360–393, 1963.

[179] R. K. Cook, R. V. Waterhouse, R. D. Berendt, S. Edelman, and J. M. D. Tompson, "Measurement of correlation coefficients in reverberant sound fields," *Acoustical Society of America*, vol. 27, no. 6, pp. 1072–1077, 1955.

[180] A. Papoulis, *Probability, random variables, and stochastic processes*. New York: Mcgraw-hill, 1984.

[181] R. E. Mortensen, *Random signals and systems*. New York: Wiley, 1987.

[182] W. B. Davenport and W. L. Root, *An introduction to the theory of random signals and noise*. Lincoln Laboratory Publications, McGraw-Hill, 1958.

[183] W. Rudin, *Functional analysis*. Boston, Mass.: McGraw-Hill, 1991.

[184] A. V. Balakrishnan, *Applied functional analysis*. New York: Springer-verlag, 1976.

[185] Wolfram, "The wolfram functions site," 2006. http://functions.wolfram.com/.

[186] P. Courmontagne, "A new formulation for the Karhunen-Loeve expansion," *Signal Processing*, vol. 79, no. 3, pp. 235–249, 1999.

[187] J. A. Stratton, P. M. Morse, L. J. Chu, J. D. C. Little, and J. Corbato, *Spheroidal Wave Functions*. MIT Press, 1959.

[188] P. M. Morse and H. Feshback, *Methods of Theoretical Physics*. 1953.

[189] C. Flammer, *Spheroidal wave functions*. 1957.

[190] F. M. Kahnert, "Numerical methods in electromagnetic scattering theory," *Journal of Quantitative Spectroscopy and Radiative Transfer*, vol. 79, pp. 775–824, 2003.

[191] K. E. Atkinson, *A survey of numerical methods for the solution of Fredholm integral equations of the second kind*. Philadelphia: Society For Industrial And Applied Mathematics, 1976.

[192] L. M. Delves and J. L. Mohamed, *Computational methods for integral equations*. Cambridge ; New York: Cambridge University Press, 1985.

[193] W. H. Press, B. P. Flannery, S. A. Teukolsky, and W. T. Vetterling., *Numerical recipes in C: the art of scientific computing*. Cambridge: Cambridge University Press., 1992.

[194] A. J. Jerri, *Introduction to integral equations with applications*. New York: Dekker, 1985.

[195] A. C. Pipkin, *A course on integral equations*. New York: Springer-verlag, 1991.

[196] I. H. Sloan and R. S. Womersley, "Extremal systems of points and numerical integration on the sphere," *Advances in Computational Mathematics*, vol. 21, pp. 107–125, 2004.

[197] S. Kunis and D. Potts, "Fast spherical Fourier algorithms," *Journal of Computational and Applied Mathematics*, vol. 161, no. 1, pp. 75–98, 2003.

[198] J. Fliege and U. Maier, "The distribution of points on the sphere and corresponding cubature formulae," *IMA Journal of Numerical Analysis*, vol. 19, pp. 317–334, 1999.

[199] J. R. Driscoll and D. M. Healy, "Computing fourier transforms and convolutions on the 2-sphere," *Advances in Applied Mathematics*, vol. 15, no. 2, pp. 202–250, 1994.

[200] V. I. Lebedev and D. N. Laikov, "A quadrature formula for the sphere of the 131st algebraic order of accuracy," *Doklady Mathematics*, vol. 58, no. 3, pp. 477–481, 1999.

[201] V. I. Lebedev, "Quadratures on a sphere," *Computational Mathematics and Mathematical Physics*, vol. 16, pp. 10–24, 1976.

[202] R. Buehrer, "The impact of angular energy distribution on spatial correlation," in *IEEE Vehicular Technology Conference (VTC 2002 Fall)*, vol. 2, pp. 1173–1177, 2002.

[203] L. Chan and S. Loyka, "Impact of multipath angular distribution on performance of MIMO systems," in *Canadian Conference on Electrical and Computer Engineering*, vol. 2, pp. 853–857, 2004.

[204] G. Dickins, M. I. Y. Williams, and R. A. Kennedy, "Spatial limits to direction of arrival estimation," *Submitted 2007*, 2007.

[205] S. Chandran, *Advances in direction-of-arrival estimation*. Boston: Artech House, 2006.

[206] M. Landmann, A. Richter, and R. Thoma, "DOA resolution limits in MIMO channel sounding," in *IEEE International Symposium on Antennas and Propagation*, vol. 2, (Monterey, California, USA), pp. 1708–1711, 2004.

[207] H. Krim and M. Viberg, "Two decades of array signal processing research: the parametric approach," *IEEE Signal Processing Magazine*, vol. 13, no. 4, pp. 67–94, 1996.

[208] M. Bartlett, "Smoothing periodograms from time series with continuous spectra," *Nature*, vol. 161, no. 8, pp. 686–687, 1948.

[209] J. Capon, "High-resolution frequency-wavenumber spectrum analysis," *Proceedings of the IEEE*, vol. 57, no. 8, pp. 1408–1418, 1969.

[210] D. Johnson, "The application of spectral estimation methods to bearing estimation problems," *Proceedings of the IEEE*, vol. 70, no. 9, pp. 1018–1028, 1982.

[211] R. Schmidt, "Multiple emitter location and signal parameter estimation," *IEEE Trans. Antennas and Propagation*, vol. 34, no. 3, pp. 276–280, 1986.

[212] M. Viberg and B. Ottersten, "Sensor array processing based on subspace fitting," *IEEE Trans. Signal Processing*, vol. 39, no. 5, pp. 1110–1121, 1991.

[213] A. Barabell, "Improving the resolution performance of eigenstructure-based direction-finding algorithms," in *IEEE International Conference on Acoustics, Speech, and Signal Processing (ICASSP 1983)*, vol. 8, (Boston), pp. 336–339, 1983.

[214] R. Roy, A. Paulraj, and T. Kailath, "ESPRIT – A subspace rotation approach to estimation of parameters of cisoids in noise," *IEEE Trans. Acoustics, Speech, and Signal Processing*, vol. 34, no. 5, pp. 1340–1342, 1986.

[215] Y. Bresler and A. Macovski, "Exact maximum likelihood parameter estimation of superimposed exponential signals in noise," *IEEE Trans. Acoustics, Speech, and Signal Processing*, vol. 34, no. 5, pp. 1081–1089, 1986.

[216] A. Jaffer, "Maximum likelihood direction finding of stochastic sources: a separable solution," in *International Conference on Acoustics, Speech, and Signal Processing (ICASSP 1988)*, vol. 5, (New York), pp. 2893–2896, 1988.

[217] B. Friedlander, "Sensitivity analysis of the maximum likelihood direction-finding algorithm," *IEEE Trans. Aerospace and Electronic Systems*, vol. 26, no. 6, pp. 953–968, 1990.

[218] A. Zeira and B. Friedlander, "Direction of arrival estimation using parametric signal models," *IEEE Trans. Signal Processing*, vol. 44, no. 2, pp. 339–350, 1996.

[219] P. Stoica and A. Nehorai, "Music, maximum likelihood, and Cramer-Rao bound: further results and comparisons," *IEEE Trans. Acoustics, Speech, and Signal Processing*, vol. 38, no. 12, pp. 2140–2150, 1990.

[220] B. Porat and B. Friedlander, "Analysis of the asymptotic relative efficiency of the MUSIC algorithm," *IEEE Trans. Acoustics, Speech, and Signal Processing*, vol. 36, no. 4, pp. 532–544, 1988.

[221] J. Le Cadre and O. Zugmeyer, "Temporal integration for array processing," in *International Conference on Acoustics, Speech, and Signal Processing (ICASSP 1991)*, vol. 2, (Toronto, Canada), pp. 1441–1444, 1991.

[222] C. Sword, M. Simaan, and E. Kamen, "Multiple target angle tracking using sensor array outputs," *IEEE Trans. Aerospace and Electronic Systems*, vol. 26, no. 2, pp. 367–373, 1990.

[223] C. Rao, C. Sastry, and B. Zhou, "Tracking the direction of arrival of multiple moving targets," *IEEE Trans. on Signal Processing*, vol. 42, no. 5, pp. 1133–1144, 1994.

[224] T. Wigren and A. Eriksson, "Accuracy aspects of DOA and angular velocity estimation in sensor array processing," *IEEE Signal Processing Letters*, vol. 2, no. 4, pp. 60–62, 1995.

[225] Y. Zhou, P. Yip, and H. Leung, "Tracking the direction-of-arrival of multiple moving targets by passive arrays: algorithm," *IEEE Trans. Signal Processing*, vol. 47, no. 10, pp. 2655–2666, 1999.

[226] H. Cramer, *Mathematical methods of statistics*. Princeton: Princeton University Press, 1946.

[227] P. Stoica and A. Nehorai, "Music, maximum likelihood, and Cramer-Rao bound," *IEEE Trans. Acoustics, Speech, and Signal Processing*, vol. 37, no. 5, pp. 720–741, 1989.

[228] H. Ye and D. DeGroat, "Maximum likelihood DOA estimation and asymptotic Cramer-Rao bounds for additive unknown colored noise," *IEEE Trans. Signal Processing*, vol. 43, no. 4, pp. 938–949, 1995.

[229] M. Pesavento and A. Gershman, "Maximum-likelihood direction-of-arrival estimation in the presence of unknown nonuniform noise," *IEEE Trans. Signal Processing*, vol. 49, no. 7, pp. 1310–1324, 2001.

[230] H. L. Van Trees, *Detection, estimation, and modulation theory: IV Optimum Array Processing*. New York: Wiley, 2002.

[231] L. Scharf and L. McWhorter, "Geometry of the Cramer-Rao bound," in *IEEE Workshop on Statistical Signal and Array Processing*, pp. 5–8, 1992.

[232] P. Stoica, E. Larsson, and A. Gershman, "The stochastic CRB for array processing: a textbook derivation," *IEEE Signal Processing Letters*, vol. 8, no. 5, pp. 148–150, 2001.

[233] D. Swingler, "Simple approximations to the Cramer-Rao lower bound on direction of arrival for closely spaced sources," *IEEE Trans. Signal Processingon]*, vol. 41, no. 4, pp. 1668–1672, 1993.

[234] B. Hochwald and A. Nehorai, "Concentrated Cramer-Rao bound expressions," *IEEE Trans. Information Theory*, vol. 40, no. 2, pp. 363–371, 1994.

[235] A. Satish and R. Kashyap, "Maximum likelihood estimation and Cramer-Rao bounds for direction of arrival parameters of a large sensor array," *IEEE Trans. Antennas and Propagation*, vol. 44, no. 4, pp. 478–491, 1996.

[236] C. Proukakis and A. Manikas, "Study of ambiguities of linear arrays," in *IEEE International Conference on Acoustics, Speech, and Signal Processing (ICASSP 1994)*, vol. 4, (Adelaide, Australia), pp. 549–552, 1994.

[237] M. Wax and I. Ziskind, "On unique localization of multiple sources by passive sensor arrays," *IEEE Trans. Acoustics, Speech, and Signal Processing*, vol. 37, no. 7, pp. 996–1000, 1989.

[238] A. Moffet, "Minimum-redundancy linear arrays," *IEEE Trans. Antennas and Propagation*, vol. 16, no. 2, pp. 172–175, 1968.

[239] S. Pillai, Y. Bar-Ness, and F. Haber, "A new approach to array geometry for improved spatial spectrum estimation," *Proceedings of the IEEE*, vol. 73, no. 10, pp. 1522–1524, 1985.

[240] Y. Abramovich, N. Spencer, and A. Gorokhov, "DOA estimation for noninteger linear antenna arrays with more uncorrelated sources than sensors," *IEEE Trans. on Signal Processing*, vol. 48, no. 4, pp. 943–955, 2000.

[241] Y. Abramovich, D. Gray, A. Gorokhov, and N. Spencer, "Positive-definite Toeplitz completion in DOA estimation for nonuniform linear antenna arrays. I. Fully augmentable arrays," *IEEE Trans. on Signal Processing*, vol. 46, no. 9, pp. 2458–2471, 1998.

[242] Y. Abramovich, N. Spencer, and A. Gorokhov, "Positive-definite Toeplitz completion in DOA estimation for nonuniform linear antenna arrays. II. Partially augmentable arrays," *IEEE Trans. on Signal Processing*, vol. 47, no. 6, pp. 1502–1521, 1999.

[243] B. Friedlander and A. Weiss, "On the number of signals whose directions can be estimated by an array," *IEEE Trans. Signal Processing*, vol. 39, no. 7, pp. 1686–1689, 1991.

[244] M. Ghogho, O. Besson, and A. Swami, "Estimation of directions of arrival of multiple scattered sources," *IEEE Trans. Signal Processing*, vol. 49, no. 11, pp. 2467–2480, 2001.

[245] M. Wax and A. Leshem, "Joint estimation of time delays and directions of arrival of multiple reflections of a known signal," *IEEE Trans. Signal Processing*, vol. 45, no. 10, pp. 2477–2484, 1997.

[246] D. Pearson, S. Pillai, and Y. Lee, "An algorithm for near-optimal placement of sensor elements," *IEEE Trans. Information Theory*, vol. 36, no. 6, pp. 1280–1284, 1990.

[247] E. Vertatschitsch and S. Haykin, "Impact of linear array geometry on direction-of-arrival estimation for a single source," *IEEE Trans. Antennas and Propagation*, vol. 39, no. 5, pp. 576–584, 1991.

[248] M. Gavish and A. Weiss, "Array geometry for ambiguity resolution in direction finding," *IEEE Trans. Antennas and Propagation*, vol. 44, no. 6, pp. 889–895, 1996.

[249] Y. Abramovich, N. Spencer, and A. Gorokhov, "Resolving manifold ambiguities in direction-of-arrival estimation for nonuniform linear antenna arrays," *IEEE Trans. Signal Processingon]*, vol. 47, no. 10, pp. 2629–2643, 1999.

[250] H. Gazzah and S. Marcos, "Cramer-Rao bounds for antenna array design," *IEEE Trans. Signal Processing*, vol. 54, no. 1, pp. 336–345, 2006.

[251] U. Baysal and R. Moses, "On the geometry of isotropic arrays," *IEEE Trans. Signal Processing*, vol. 51, no. 6, pp. 1469–1478, 2003.

[252] M. Hawkes and A. Nehorai, "Effects of sensor placement on acoustic vector-sensor array performance," *IEEE Journal of Oceanic Engineering*, vol. 24, no. 1, pp. 33–40, 1999.

[253] A. Dogandzic and A. Nehorai, "Cramer-rao bounds for estimating range, velocity, and direction with an active array," *IEEE Trans. Signal Processing*, vol. 49, no. 6, pp. 1122–1137, 2001.

[254] A. Nehorai and E. Paldi, "Vector-sensor array processing for electromagnetic source localization," *IEEE Trans. Signal Processing*, vol. 42, no. 2, pp. 376–398, 1994.

[255] J. Tabrikian, R. Shavit, and D. Rahamim, "An efficient vector sensor configuration for source localization," *IEEE Signal Processing Letters*, vol. 11, no. 8, pp. 690–693, 2004.

[256] T. Svantesson, "Direction finding in the presence of mutual coupling," Technical Report, Chalmers University of Technology, 1999. No. 307L.

[257] B. Friedlander and A. Weiss, "Direction finding in the presence of mutual coupling," *IEEE Trans. Antennas and Propagation*, vol. 39, no. 3, pp. 273–284, 1991.

[258] O. Birkenes, *On the Limits to Determining the Direction of Arrival for Narrowband Communication*. Diploma, Australian National University, 2002.

[259] H. L. Van Trees, *Detection, estimation, and modulation theory*. New York: Wiley, 2001.

[260] P. Stoica and A. Nehorai, "Performance study of conditional and unconditional direction-of-arrival estimation," *IEEE Trans. Acoustics, Speech, and Signal Processing*, vol. 38, no. 10, pp. 1783–1795, 1990.

[261] M. Viberg, B. Ottersten, and A. Nehorai, "Performance analysis of direction finding with large arrays and finite data," *IEEE Trans. on Signal Processing*, vol. 43, no. 2, pp. 469–477, 1995.

[262] Y. Hua and T. Sarkar, "A note on the cramer-rao bound for 2-D direction finding based on 2-D array," *IEEE Trans. Signal Processing*, vol. 39, no. 5, pp. 1215–1218, 1991.

[263] S. Anderson and A. Nehorai, "Optimal dimension reduction for array processing-generalized," *IEEE Trans. Signal Processing*, vol. 43, no. 8, pp. 2025–2027, 1995.

[264] S. Smith, "Statistical resolution limits and the complexified Cramer-Rao bound," *IEEE Trans. Signal Processing*, vol. 53, no. 5, pp. 1597–1609, 2005.

[265] F. Athley, "Threshold region performance of maximum likelihood direction of arrival estimators," *IEEE Trans. Signal Processing*, vol. 53, no. 4, pp. 1359–1373, 2005.

[266] B. Hochwald and A. Nehorai, "Identifiability in array processing models with vector-sensor applications," *IEEE Trans. Signal Processing*, vol. 44, no. 1, pp. 83–95, 1996.

[267] A. Manikas and C. Proukakis, "Modeling and estimation of ambiguities in linear arrays," *IEEE Trans. Signal Processing*, vol. 46, no. 8, pp. 2166–2179, 1998.

[268] W. Xiao, X.-C. Xiao, and H.-M. Tai, "Rank-1 ambiguity DOA estimation of circular array with fewer sensors," in *Midwest Symposium on Circuits and Systems*, vol. 3, (Tulsa, Oklahoma), pp. 29–32, 2002.

[269] A. Manikas and C. Proukakis, "Investigative study of planar array ambiguities based on hyperhelical parameterization," *IEEE Trans. Signal Processing*, vol. 47, no. 6, pp. 1532–1541, 1999.

[270] W. Weichselberger, H. Ozcelik, and M. Herdin, "A novel stochastic MIMO channel model and its physical interpretation," in *6th International Symposium on Wireless Personal Multimedia Communications (WPMC 2003)*, (Japan), 2003.

[271] T. Lamahewa, R. Kennedy, T. Abhayapala, and T. Betlehem, "MIMO channel correlation in general scattering environments," in *Australian Communications Theory Workshop, (AusCTW 2006)*, (Perth, Australia), pp. 93–98, 2006.

[272] T. A. Lamahewa, T. D. Abhayapala, R. A. Kennedy, T. Betlehem, and J. T. Y. Ho, "Space-time channel modelling in general scattering environments," *IEEE Trans. Signal Processing*, 2006 (Submitted).

[273] T. Betlehem, T. A. Lamahewa, and T. D. Abhayapala, "Dependence of MIMO system performance on the joint properties of angular power," in *IEEE International Symposium on Information Theory (ISIT 2006)*, (Seattle, Washington), 2006.

[274] A. Graham, *Kronecker products and matrix calculus : with applications*. Chichester, New York: Halsted Press, 1981.

[275] B. Fleury, P. Jourdan, and A. Stucki, "High-resolution channel parameter estimation for MIMO applications using the SAGE algorithm," in *International Seminar on Broadband Communications*, (Zurich), pp. 30.1–30.9, 2002.

[276] K. Haneda and J. Takada, "High-resolution estimation of NLOS indoor MIMO channel with network analyzer based system," in *IEEE Conference on Personal, Indoor and Mobile Radio Communications (PIMRC 2003)*, vol. 1, (Beijing, China), pp. 675–679, 2003.

[277] S. Wyne, A. Molisch, P. Almers, G. Eriksson, J. Karedal, and F. Tufvesson, "Statistical evaluation of outdoor-to-indoor office MIMO measurements at 5.2 ghz," in *IEEE Vehicular Technology Conference (VTC 2005 Spring)*, vol. 1, (Stockholm), pp. 146–150, 2005.

[278] Brigham Young University, "Wideband MIMO measurements 2.4 GHz - 4th floor clyde building, hall to room, moving, 80MHz BW," January 2005. `http://www.ece.byu.edu/wireless/`.

[279] P. Beckmann, *Orthogonal polynomials for engineers and physicists*. Boulder, Colorado: Golem Press, 1973.

[280] A. Swindlehurst and T. Kailath, "Passive direction-of-arrival and range estimation for near-field sources," in *Fourth Annual ASSP Workshop on Spectrum Estimation and Modeling*, (Minneapolis, Minnesota), pp. 123–128, 1988.

[281] R. Kouyoumjian and J. Peters, L., "Range requirements in radar cross-section measurements," *Proceedings of the IEEE*, vol. 53, no. 8, pp. 920–928, 1965.

[282] E. Knott and T. Senior, "How far is far?," *IEEE Trans. Antennas and Propagation*, vol. 22, no. 5, pp. 732–734, 1974.

[283] R. Jeffers, B. Breed, and B. Gallemore, "Passive range estimation and range rate detection," in *IEEE Sensor Array and Multichannel Signal Processing Workshop*, (Cambridge, MA), pp. 112–116, 2000. TY - CONF.

[284] L. J. Landau, "Bessel functions: Monotonicity and bounds," *Journal of the London Mathematical Society*, vol. 61, no. 2, pp. 197–215, 2000.

[285] I. H. Sloan and R. S. Womersley, "Good approximation on the sphere, with application to geodesy and the scattering of sound," *Journal of Computational and Applied Mathematics*, vol. 149, 2002.

[286] I. H. Sloan, "Polynomial interpolation and hyperinterpolation over general regions," *Journal of Approximation Theory*, vol. 83, pp. 238–254, 1995.

[287] R. S. Womersley and I. H. Sloan, "How good can polynomial interpolation on the sphere be?," *Advances in Computational Mathematics*, vol. 14, pp. 195–226, 2001.

[288] M. Reimer, "Quadrature rules for the surface integral of the unit sphere based on extremal fundamental systems," *Mathematische Nachrichten*, vol. 169, pp. 235–241, 1994.

[289] R. S. Womersley, "Interplolation and cubature on the sphere," Tech. Rep. http://web.maths.unsw.edu.au/ rsw/Sphere/, University of New South Wales, 2004.

[290] B. Rafaely, "Analysis and design of spherical microphone arrays," *IEEE Transactions on Speech and Audio Processing*, vol. 13, no. 1, pp. 135–143, 2005. Design of the spherical microphone array. Should include the scattering formula. Interesting analysis of whitenoise gain due to aliasing and HF and modal extrapolation error at LF.

[291] S. Krusevac, R. Kennedy, and P. Rapajic, "Effect of signal and noise coupling on mimo channel capacity," *Wireless Personal Communications*, vol. 40, no. 3, pp. 317–328, 2007.

Index